Polyelectrolyte Multilayer Capsules for Medical Applications

Dissertation

zur

Erlangung des Doktorgrades

der Naturwissenschaften

(Dr. rer. nat.)

dem

Fachbereich Physik

der Philipps-Universität Marburg

vorgelegt von

Moritz Julian Nazarenus

aus

Friedberg

Marburg/Lahn, 2014

Vom Fachbereich Physik der Philipps-Universität (Hochschulkennziffer 1180)
als Dissertation angenommen am: 01.12.2014

Erstgutachter: Prof. Dr. Wolfgang J. Parak
Zweitgutachter: Prof. Dr. Martin Koch
Prüfer: Prof. Dr. Florian Gebhard
Prüfer: Prof. Dr. Pilar Rivera Gil

Tag der mündlichen Prüfung: 17.12.2014

Die vorliegende Arbeit wurde am Fachbereich Physik
der Philipps-Universität Marburg unter der Anleitung von

Herrn Prof. Dr. Wolfgang J. Parak

in der Zeit von November 2010 bis Oktober 2014 angefertigt.

Zusammenfassung

Die vorliegende Arbeit hat die Anwendung von Polymerkapseln in diagnostischen und therapeutischen Fragestellungen in Säugerzellen zum Thema. Die Kapseln bestehen aus einer Kavität umhüllt von mehrern gegensätzlich geladenen Polyelektrolytschichten und haben eine Größe von zwei bis fünf Mikrometern. Für die diagnostischen Anwendungen wurden Kapseln für die Beobachtung des lysosomalen pH-Wertes von Krebszellen synthetisiert. Die Kavitäten der Kapseln wurde dafür mit einem fluoreszenten, pH-abhängigen Farbstoff gefüllt, um das Signal optisch auszulesen. Die Dynamik des lysosomalen pH-Wertes unter äußerlicher Beeinflussung wurde vermessen. Aus den Ergebnissen ging hervor, dass die Kapseln für die intrazelluläre Langzeitmessung geeignet waren und Änderungen des pH-Wertes verfolgt werden konnten. Für therapeutische Aufgaben wurden bioabbaubare Kapseln mit biologisch aktiven Molekülen beladen. Zwei verschiedene Strategien wurden verwendet. Im ersten Fall wurde die Kavität der Kapseln mit Polyplexen aus DNA oder RNA und Polyetylenimin gefüllt, die weithin für die Einbringung von fremden Genmaterial in Zellen eingesetzt werden. Dies ist ein Beispiel für Gentherapie. Die Ergebnisse zeigten, dass die Integration des fremden Genmaterials mithilfe von Kapseln sehr effizient war und die eingekapselten Polyplexe weniger toxisch für die Zellen waren als freie Polyplexe. Die zweite Strategie war, funktionale Enzyme direkt zu integrieren. Dafür wurden Modelle für lysosomale Speicherkrankheiten eingesetzt. Patienten mit Morbus Fabry expremieren das Enzym α-Galactosidase A nicht oder nur unzureichend. Im Versuch wurden bioabbaubare Kapsel mit dem Enzym synthetisiert und den Modellzellen verabreicht. Diese Therapieform nennt man Enzymersatztherapie. Die intrazelluläre Enzymaktivität wurde mithilfe eines fluoreszenten Substrats von α-Galactosidase A bestimmt. Da das Produkt der Enzymreaktion nichtfluoreszierend ist, kann aus der intrazellulären Fluoreszenz auf die Aktivität des Enzyms geschlossen werden. Zuletzt wurden Diagnose und Therapie in einem Modell für Morbus Krabbe, einer weiteren lysosomalen Speicherkrankheit, vereint. Bei Krabbe-Patienten sammeln sich Sphingolipide und Cerebroside in den oligodendritischen Glia-Zellen an, da das Enzym Galactocerebrosidase, das diese Stoffe normalerweise abbaut, aufgrund eines Gendefekts nicht expremiert wird. Im Modell wurden die Zellen mit dem Sphingolipid Psychosin inkubiert, um die Krankheit zu simulieren. Galactocerebrosidase wurde den Zellen mithilfe bioabbaubarer Kapseln verabreicht. Die Funktionalität des Enzyms wurde mit einem Viabilitätstest verifiziert. Zwei Typen von Zellen, der Wildtyp, der das Enzym expremierte, und Knockout-Zellen, die das Enzym nicht expremierten, wurden verwendet. Die Viabilität der Zellen bei Zugabe verschiedener Konzentrationen von Psychosin wurde mit und ohne Kapselzugabe bestimmt. Es zeigte sich, dass die Kapseln einen gegensätzlichen Effekt auf die zwei Typen von Zellen ausübten. Knockout-Zellen erreichten eine höhere Viabilität nach Zugabe der Enzym-Kapseln, wohingegen Wildtyp-Zellen eine leicht geringere hatten. Der diagnostische Part des Modells bestand in der Messung des lysosomalen pH-Wertes während der Inkubation mit Psychosin. Das zeitaufgelöste pH-Profil der beiden Zelltypen unterschied sich dabei. Daher kann die Entscheidung, ob Kapseln zur Therapie verabreicht werden sollten, von der Diagnose durch die pH-Messung abhängig gemacht werden. Dies kann man als *in-vitro*-Beispiel für Theranostik betrachten, der Kombination aus Therapie und Diagnose.

Summary

This thesis deals with the application of polymer capsules for diagnostic and therapeutic purposes in mammalian cells. The capsules comprise a multilayer shell of oppositely charged polyelectrolytes surrounding a cavity and have a size of two to five microns. Concerning diagnostics, capsules were produced to monitor the dynamics of the lysosomal pH in cancer cells. The cavities of the capsules were filled with a fluorescent, pH-sensitive dye for optical readout of the signal. The cells were monitored under physiological conditions upon induced pH imbalances. The results showed that the capsules were appropriate for intracellular long-term measurements and could monitor changes of the pH. For therapy, biodegradable capsules filled with biologically active molecules were synthesized. Two strategies were employed. In one approach, the cavity was filled with polyplexes of DNA or RNA and polyethylenimine, which are used regularly for the delivery of foreign genetic material into host cells. This approach is an example for gene therapy. The results showed that delivery by the capsules was very efficient and the encapsulated polyplexes were less toxic for the cells than their free counterparts. The other strategy was to directly deliver functional enzymes into cells. For this approach, cell models representing lysosomal storage diseases were employed. One of these diseases is Fabry. Patients with Fabry disease are deficient of the enzyme α-galactosidase A. The enzyme was encapsulated in biodegradable capsules and given to the cells. This therapy form is called enzyme replacement therapy. The intracellular enzyme activity was determined by quantification of the intracellular level of a fluorescently labeled substrate of α-galactosidase A. As the products of the reaction were non-fluorescent, the intracellular fluorescence could be used to quantify the intracellular activity of the encapsulated enzyme. Finally, therapy and diagnostics were combined in a model of Krabbe disease, another lysosomal storage disorder. In Krabbe patients, sphingolipids and cerebrosides accumulate in the oligodendritic glia cells of the patients, as due to a gene defect the enzyme galactocerebrosidase usually converting these agents is not expressed. In the model, the cause of the disease was simulated by incubation of oligodendritic cells with psychosine, which belongs to the group of sphingolipids. Galactocerebrosidase was encapsulated in biodegradable capsules and delivered to the cells. The functionality was tested by a viability assay. Two types of cells were used, wild-type cells expressing galactocerebrosidase and knockout cells, which did not express the enzyme. The viability of the cells in the presence of psychosine was determined with and without addition of galactocerebrosidase-filled capsules. The results showed that the effect of the capsules on the viability of the two different cell types was contrary. Whereas knockout cells gained higher viability when capsules were administered, wild-type cells suffered a loss in viability. The diagnostic part was characterized by monitoring the lysosomal pH upon incubation with psychosine. The dynamics of the lysosomal pH of the two types of cells turned out to be different. Each of the cell types could therefore be identified with a specific pH profile and the decision to treat cells with the enzyme-filled capsules can be based on the measured pH profile. This is considered an *in vitro*-example of theranostics, the combination of therapy and diagnostics.

Contents

1 Introduction

1.1 Polyelectrolyte Multilayer Capsules in Biomedical Fields

Polyelectrolyte multilayer capsules were first introduced in 1998 by the group of Helmuth Möhwald and since then gained increasing interest over the years, especially in biomedical fields.[1, 2] These capsules are fabricated using template particles, onto which polymers of alternating charge are deposited.[2] After dissolution of the template, stable hollow capsules remain. Capsules can be produced with a great variety of different polymers, including the possibility to produce both biodegradable and bio-stable capsules.[3-7] Biodegradable capsules are made of polymers that can be degraded inside living cells, for example by enzymes in the lysosomes.[3, 5] Furthermore, the capsules can be tuned in size from 30 nm up to several microns, opening the way for customization of the capsules according to the problem of interest.[8] In cell culture models, for example, a larg size of the capsules can be of advantage as they are easily observable with optical techniques. Small capsules in the size of nanometers are of interest for *in vivo*-experiments, where large capsules cannot be used as they may block capillaries. Capsules are taken up by almost all mammalian cells, both immortal cell lines and primary cells.[9-11] The uptake is triggered by phagocytosis and lipid-rafts-mediated macropinocytosis and the final location of the capsules is in the heterophagolysosomes of the cells.[10] After cell division, the capsules are passed to the daughter cells.[3] The distribution, however, is asymmetric, *i.e.* they are not passed on in a fifty-fifty manner.[12, 13] Applications of capsules in biomedical fields are diverse and can generally be divided into delivery and sensing applications.[14, 15] Capsules can be filled with various cargoes for delivery, among them drugs, genetic material like DNA or RNA, or proteins.[4, 16-21] The experimental challenges lie in the difficulties to encapsulate certain cargoes in a sufficient way, but also in problems to release the cargo at the desired target site. Concerning release, one major challenge is to free the capsule content from the lysosome so that it becomes available to reach targets outside this vesicle. For sensing applications the capsules are filled with a sensor. This can be an ion-sensitive dye,[6, 22-24] but also more complex systems have been described, such as enzymes that convert a metabolite and a component that gives a signal quantifying the conversion.[25, 26] Finally, it should be mentioned that many other ways of synthesizing capsules apart from the LbL method are widespread. The reader is referred to recent reviews on capsules as biological carriers.[8, 21, 27]

1.2 Theranostics

One of the future goals in medical treatment is so-called personalized medicine.[28] This term describes the idea to customize treatment of different patients based on their individual condition. The treatment should involve the identification of the molecular factors of the disease and from this the appropriate treatment and medication should be chosen. Moreover, this approach is expected to reduce unnecessary treatment, as ineffective drugs and therapies are to be prevented by the identification of the specific disease markers. In a further step, the outcome of the treatment should be monitored, so to be able to respond to side effects.[29] The major example where personalized medicine is expected to improve treatment is cancer.[30, 31] Theranostics is the term to describe the combination of therapy and diagnostics in one treatment.[32, 33]

1.3 Scope of this Thesis

In this thesis, the goal was to combine the needs of diagnostics and therapy using polymer capsules as carriers. Towards this goal, the starting point was the diagnostic tool. The intracellular ion homeostasis plays a crucial role for the cells and disturbances of it are often associated with diseases or with apoptosis of the affected cells.[34-37] Diagnosis here was based on capsules as intracellular optical pH sensors. There are numerous publications on optical sensors for intracellular ion sensing. However, very often there are also numerous shortcomings included.[38, 39] In many articles sensor systems are presented that show very good behavior in defined environment, for example buffers with varying concentration of the targeted ion. Yet, the claim that these sensors will work the same way intracellularly is often too strong as the intracellular environment is in many aspects different from a simple buffer solution. Hence, a study presenting a sensor system but no proof that the sensors work inside cells is incomplete and should be taken with a grain of salt. Studies including cell experiments often focus only on the proof that intracellular measurements are possible. Monitoring the behavior of the targeted ion concentration, however, is often excluded or only done over very short times.[40, 41] In the work described in section 3.1, the focus lay on the long-term monitoring of the dynamics of the lysosomal pH upon induced ion deregulation. pH was chosen for two reasons. First, pH is a ubiquitous quantity and relevant for many cellular processes. Second, optical sensing of other ions is not as easy and straightforward as might be expected. The fluorescent dyes available for intracellular sensing are usually pH-dependent in addition to their specific ion-sensitivity.[38] This problem is addressed in section 3.1, where the pH dependency of four commercial dyes is examined. Considering this, monitoring intracellular ion concentrations should be accompanied by observation of the local pH. The second objective of theranostics is therapy. For this purpose, the integration of genetic material, *i.e.* DNA and RNA, into eukaryotic cells was chosen as exemplary application, the so-called gene therapy. Transfection of cells with genetic material like DNA or RNA is a typical application in biological laboratories and for medical treatment purposes. Examples are transfection with green fluorescent protein (GFP) to mark cells,[42] but also knockout of genes such as in manuscript [A9] (*cf.* section 6.3),

where V-ATPases, which regulate the pH in vesicles like the lysosome, are knocked out or enhanced and the effect on the lysosomal acidification is measured. For the work described in section 3.2 and publication [A7][4], siRNA for knockout of GFP was used. By using capsules as carriers, certain advantages over the established methods can be obtained. These involve the protection of the nucleic acids against degradation before they reach their action site, the protection of the cell from adverse effects that can occur due to the transfection agent,[43] and also the possibility to perform transfection in serum-supplemented media.[44] In all cases, the advantages lie in the protective shield in form of the capsules. For the experiments, polyplexes with polyethyleneimine (PEI) and the nucleic acids, either DNA or siRNA, were synthesized and encapsulated in biodegradable capsules. By using this method, the properties of PEI for facilitating lysosomal escape of the nucleic acids could be utilized, while the toxic effects of PEI were diminished. The lysosomal escape is often ascribed to the so-called proton sponge effect,[45, 46] although this effect is still under debate. The proton sponge effect is stated to take place when polycations with buffering capacity, such as PEI, which at slightly acidic pH contains many deprotonated amine groups, buffer the pH in the lysosomes. The lysosomal pH hence does not decrease when proton pumps transfer protons from the outside into the lysosomes and thus influx of further protons takes place.[47] To ensure the charge and ion activity equilibrium across the lysosomal membrane, also chloride and water enter the lysosomes. This leads to swelling of the lysosomes and if the pressure rises high enough, the vesicles finally burst releasing their content to the cytosol.[48] In a first step for characterizing the delivery of genetic material, fluorescently labeled DNA was delivered to MDA-MB-231 cells and the distribution in the cells over time was observed. In a second step, silencing RNA (siRNA) was used to knock out GFP in GFP-transfected HeLa cells. The siRNA was also fluorescently labeled so it could be observed with the microscope. The quantification, however, was based on the GFP fluorescence of the cells. It could be shown that DNA and siRNA were set free from the capsules within a reasonable timeframe of less than 48 hours and that the knockout of GFP by siRNA was very efficient. Furthermore, the silencing could be performed in serum-containing media, which is a big advantage over standard protocols where transfection is done in serum-free medium,[44] which puts a lot of stress on the cells. In further experiments, another way of treatment, so-called enzyme replacement therapy (ERT) was employed. As mentioned already, the capsules are trafficked to the lysosomes of the cells after uptake. This paves the way for applications of capsules as carriers for the introduction of biologically active cargo into the lysosomes. There is a large family of diseases called lysosomal storage disorders (also lysosomal storage diseases, LSDs), which are characterized by defective enzymes in the lysosomes of one or more types of cells in the body.[49-51] Two diseases were picked for the treatment with enzyme-delivering capsules, Fabry disease and Krabbe disease. In case of Fabry, the enzyme α-galactosidase A (GLA) is defective throughout the body, mainly in the endothelial cells of blood vessels. For the *in vitro*-experiments, primary cells from mouse aorta of GLA-defective mice were used.[52, 53] The intracellular activity of the enzyme was determined. For this purpose, the cells were co-incubated with the encapsulated enzyme and a substrate. After 48 h of incubation, the substrate level inside the cells was measured and from this the efficacy of the delivery was obtained. The amount of substrate degradation was put into relation to the amount of delivered enzyme. In Krabbe disease, the enzyme galactocerebrosidase (GALC) is

defective in the oligodendrocytes of the patients, a type of glia cells in the brain. The experiments were performed with an oligodendritic cell line, MO3.13.[54, 55] In these cells, the enzyme GALC is still expressed in small amounts. Therefore, also knockout cells were used, where GALC was not expressed anymore. The cells are thus referred to as MO3.13 wild-type (MO3.13 WT) and MO3.13 knockout (MO3.13 KO) cells. GALC is responsible for the degradation of sphingolipids and galactosphingolipids. In Krabbe patients, these substances, especially psychosine and galactocerebroside, accumulate in the cells. Both are toxic for the oligodendrocytes. In the cell culture model, MO3.13 cells were incubated with psychosine to simulate the accumulation that happens in patients. The cytotoxicity of psychosine was also quantified with a viability assay to verify this. In this model, both diagnosis and therapy were performed to take the next step to theranostics. A time-resolved profile of the lysosomal pH during the accumulation of psychosine in the lysosomes was recorded for KO and WT cells for diagnosis of the effect of psychosine on the lysosomal pH. For therapy, the defective enzyme was delivered to the cells by capsules to inhibit the accumulation of psychosine. The effectivity of the delivery was quantified by a viability test by scrutinizing if cells suffered from psychosine also when GALC was provided by capsules.

1.4 Goals

In short, the following goals for this thesis can be defined: goal one was to establish a sensor system that was capable of diagnostic purposes in living cells. As the pH is a very important and furthermore a ubiquitous quantity in cells, it was chosen as parameter of interest. More specifically, the lysosomal pH was observed and the effect of external stimuli was quantified. Goal two addressed the applicability of capsules for therapy, *i.e.* the delivery of biologically active materials into living cells. Two different approaches were employed. One was to introduce siRNA into the cells to down-regulate the expression of the protein GFP, the other one was to directly deliver functional enzymes to the cells. The third goal was to perform diagnosis and therapy in one model and correlate the results. This was done in the Krabbe model, where the lysosomal pH was monitored in WT and KO cells, and the enzyme GALC was delivered to the cells.

2 Materials and Methods

2.1 List of Chemicals

Product (Abbreviation)	Supplier	Product Number
0.05 % Trypsin-EDTA	Lifetech	25300-054
BAC-SE	Emp Biotech	AF-0406-5
2-*N*-(morpholino) ethansulfonic acid (MES)	Sigma-Aldrich	M8250
Antibiotic-antimicotic (aa)	Lifetech	15240-096
Bovine Serum Albumin (BSA)	Sigma-Aldrich	A8806
$Ca(NO_3)_2 \cdot 4H_2O$	Sigma-Aldrich	C1396
$CaCl_2 \cdot 2H_2O$	Sigma-Aldrich	223506
Calcium-Green-1	Lifetech	C-3714
$Cd(C_2H_3O_2)_2 \cdot 2\ H_2O$	Sigma-Aldrich	229490
$CoCl_2 \cdot 6\ H_2O$	Alfa Aesar	10692
Commercial buffers pH 3 to 10	Sigma-Aldrich	38742 to 38749
D-(+)-Glucose	Sigma-Aldrich	G8270
Dextran sulfate sodium salt (6.5-10 kDa) (DexS)	Sigma-Aldrich	D4911
Dimethyl sulfoxide (DMSO)	Sigma-Aldrich	D4540
Dulbecco's Modified Eagle's Medium (DMEM)	Sigma-Aldrich	D5030
Dy-634-NHS-ester	Dyomics	634-01
Eagle's Minimum Essential Medium (EMEM)	Sigma-Aldrich	M2279
Ethylendiaminetetraacetic acid (EDTA)	Sigma-Aldrich	E5134
Endothelial cell growth supplement (ECGS)	Becton Dickinson	356006
$FeCl_3 \cdot 6\ H_2O$	Sigma-Aldrich	236489

Product (Abbreviation)	Supplier	Product Number
Fetal Bovine Serum (FBS)	Biochrom	S0615
Fetal Bovine Serum (FBS)	Lonza	DE14-801F
HCl (37 %)	Roth	7476
Heparin sodium salt	Sigma-Aldrich	H3149
Hydrocortisone	Sigma-Aldrich	H0888
KCl	Sigma-Aldrich	P9541
L-Glutamine (L-Glu)	Lifetech	25030-024
L-Glutamine (L-Glu)	Lonza	17-605E
Mag-Indo-1	Setareh Biotech	6519
$MgCl_2$	Sigma-Aldrich	M8266
$MgSO_4$	Sigma-Aldrich	M2643
N-(Ethoxycarbonylmethyl)-6-Methoxyquinolinium Bromide (MQAE)	Synthesized by Fabian Dommershausen, Koert Lab, FB Chemie, Philipps-Universität Marburg, Germany	
Na_2CO_3	Sigma-Aldrich	S7795
NaCl	Roth	HN00
NaOH	Roth	6771
N-dodecanoyl-NBD-ceramide trihexoside (NBD-Gb3)	Matreya	1631
Non-essential amino acid solution (NE AA)	Lonza	13-114E
Penicillin/Streptomycin (P/S)	Sigma-Aldrich	P4333
Phosphate buffered saline (PBS)	Biochrom	L1825
Phosphate buffered saline (PBS)	Lonza	17-516F
Poly(allylamine hydrochloride) (56 kDa) (PAH)	Sigma-Aldrich	283223
Poly(sodium 4-styrenesulfonate) (70 kDa) (PSS)	Sigma-Aldrich	243051
Poly-L-Arginine hydrochloride (70 kDa) (pArg)	Sigma-Aldrich	P3892
Potassium acetate	Sigma-Aldrich	32309

Product (Abbreviation)	Supplier	Product Number
$PrCl_3 \cdot x\ H_2O$	Sigma-Aldrich	205141
Psychosine	Santa Cruz Biotechnology	sc-202781
Recombinant Human Galactosylceramidase/GALC, CF (Galactocerebrosidase, GALC)	R&D Systems	7310-GH-005
Replagal®	Shire	
(drug containing α-galactosidase A as active ingredient)	obtained from Abasolo Lab, Vall d'Hebron Institut de Recerca, Barcelona, Spain	
Resazurin Toxicity Assay	Sigma-Aldrich	TOX8-1KT
RPMI medium	HyClone	SH30255.01
SNARF® dextran (70 kDa)	Lifetech	D-3304
$SrCl_2 \cdot 6\ H_2O$	Sigma-Aldrich	255521
Tris (hydromethyl) aminomethane (Tris)	Sigma-Aldrich	154563

Table 2.1 List of chemicals, suppliers, and order numbers.

All chemicals were used as received. Water for experiments was purified with a *Milli-Q Academic* water purification system from Millipore (now Merck Millipore) and had a resistivity of 18 MΩ·cm.

2.2 Capsule Synthesis

2.2.1 Template Synthesis

Polyelectrolyte multilayer capsules were synthesized by the co-precipitation method to form sacrificial $CaCO_3$ templates followed by the LbL method to adsorb alternating layers of oppositely charged polyelectrolytes onto the templates.[2] Depending on the type of cargo, either Na_2CO_3 was mixed with the cargo solution first and then precipitated with $CaCl_2$ to obtain $CaCO_3$ particles containing cargo or *vice versa*, as can be found in the description of the different capsule syntheses. For the template formation, the first solution was mixed for 30 seconds with the cargo solution prior to adding the second solution and mixing for 30 seconds at a speed of 1000 rotations per minute (rpm) with a magnet stirrer. After formation of $CaCO_3$ particles with entrapped cargo, the particles were spun down at 1000 rpm with a centrifuge, the supernatant was removed and fresh Milli-Q water was added to rinse the particles from unreacted ions and cargo twice or three times.

2.2.2 Layer-by-Layer Adsorption of Polyelectrolytes

Two different pairs of polyelectrolytes were used; for non-degradable capsules, polystyrene sulfonate (PSS, negatively charged, solutions of 2 mg/mL in NaCl (0.5 M), pH=6.5) and polyallanyl hydrochloride (PAH, positively charged, solutions of 2 mg/mL in NaCl (0.5 M), pH=6.5)) were used. For biodegradable capsules, dextran sulfate (DexS, negatively charged, solutions of 2 mg/mL in NaCl (0.5 M), pH=6.5)) and poly-L-arginine (pArg, positively charged, solutions of 1 or 2 mg/mL in NaCl (0.5 M), pH=6.5)) were adsorbed onto the templates. After the templates had been washed, they were resuspended in 1 mL of the positively charged polyelectrolyte solution and vortexed continuously for 15 minutes. Subsequently, the solution was centrifuged at 1000 rpm and washed twice or three times with Milli-Q water. Then, 1 mL of the negatively charged polyelectrolytes was added and the suspension was vortexed as before. This was repeated until the desired number of bilayers was adsorbed onto the templates. The $CaCO_3$ core was removed with EDTA and the resulting hollow capsules were washed and re-suspended in water or buffer until further use.

2.2.3 Synthesis of SNARF® Capsules

SNARF® capsules were synthesized according to the procedure explained above. 615 µL of $CaCl_2$ (0.33 M) in NaCl solution (0.5 M) were mixed with 770 µL of SNARF®-1 dextran (70 kDa, 1 mg/mL in DMSO) for 30 seconds. Subsequently, 615 µL of Na_2CO_3 (0.33 M) in NaCl solution (0.5 M) were added quickly, and the solution was mixed for 30 seconds on a magnet stirrer at 1000 rpm. After resting for 2 minutes at room temperature, the resulting $CaCO_3$ particles with entrapped SNARF® were washed twice with Milli-Q water. For the experiments with MCF-7 cells (*cf.* section 2.6), five bilayers of PSS and PAH were adsorbed to the cores, for the experiments with MO3.13 cells (*cf.* section 2.6), two bilayers were added. The template cores were removed with EDTA (0.2 M, pH=5 adjusted with HCl) by adding 1 mL EDTA solution to the particles and sonicating for 30 to 60 seconds until no further production of CO_2 in form of gas bubbles could be observed. The capsules were washed three times with Milli-Q water and stored in water at 4 °C until use in experiments.

2.2.4 Synthesis of α-Galactosidase A Capsules

For the experiments, the Fabry drug Replagal®, which is a solution containing GLA as active ingredient, was used. Therefore, Replagal® is used as synonym for GLA in this thesis. The capsules were prepared as follows: 1 mL of Na_2CO_3 (0.33 M) in NaCl solution (0.5 M) was mixed with 1 mL of Replagal® solution (1 mg/mL) for 30 seconds prior to addition of 1 mL of $CaCl_2$ (0.33 M) in NaCl solution (0.5 M) and mixing for 30 seconds at 1000 rpm. The resulting $CaCO_3$ particles were washed and coated with 2 bilayers of DexS and pArg. After removal of the cores, the capsules were stored in water at 4 °C until use in experiments.

2.2.5 Synthesis of Galactocerebrosidase Capsules

The synthesis of the cores was done with 50 µL of Na_2CO_3 (0.33 M) in NaCl solution (0.5 M), 50 µL GALC (0.05 mg/mL in water), and 50 µL of $CaCl_2$ (0.33 M) in NaCl solution (0.5 M). The templates were coated with 2 bilayers of DexS and pArg. After removal of the core the capsules were washed with Milli-Q water and kept in water at 4 °C until use in experiments.

2.3 Cell Culture

All cell lines used throughout the work for this thesis were of mammalian origin. With the exception of mouse aorta endothelial cells (MAEC, provided by Simo Schwartz and Ibane Abasolo from Vall d'Hebron Hospital, Barcelona, Spain), which are primary cells, all cell lines were immortalized commercial cell lines. MDA-MB-231 and MCF-7 cells were obtained from ATCC. Vero cells were provided by Jesús de la Fuente from the University of Zaragoza, Spain. Furthermore, for some experiments, genetically modified cells were used, in which certain proteins were expressed or silenced. This was the case for MO3.13 cells, where the enzyme GALC was silenced (referred to as MO3.13 KO cells then), and GFP-transfected HeLa cells. MO3.13 WT and MO3.13 KO cells were a gift from Marco Cecchini from Instituto Nanoscienze in Pisa, Italy. GFP-expressing HeLa cells were a gift from Christian Plank from Technische Universität München, Germany. All cells were kept in standard cell culture flasks or plates at 37 °C and 5 % CO_2 and split twice or three times a week. For sub-culturing, the old medium was aspirated, the cells were rinsed with PBS, and Trypsin-EDTA 0.05 % was added for an appropriate time, which ranged from 1 to 10 minutes depending on the cell line, to detach the cells from the flasks. Then, two or three times the volume of Trypsin-EDTA of complete growth medium was added in order to stop the effect of Trypsin-EDTA. The cell suspension was transferred into a centrifuge tube and centrifuged at a speed of 1000 rpm for 5 minutes. The supernatant was decanted and the cells were re-suspended in fresh medium. The cells were then seeded in appropriate numbers in new flasks, or in cell culture dishes for experiments. MAEC, being primary cells, were more sensitive and therefore needed a slightly different treatment. The content of FBS was higher for low passages and the medium was supplemented with more additives to ensure healthy conditions for MAEC. In Table 2.2 the formulations of the cell media for the different cell lines used for this thesis are summarized.

Cell Line	Basal Medium	Additives (v/v)
MAEC	RPMI	1st and 2nd passage: 20 % hiFBS 3rd and 4th passage: 15 % hiFBS 5th and higher: 10 % hiFBS To all passages: 1 % L-glutamine, 1 % aa, 1 % NE AA, 0.1 mg/mL heparin, 0.5 mg/mL ECGS, 0.001 mg/mL hydrocortisone
HeLa GFP	EMEM	10 % FBS, 1 % L-glutamine, 1 % P/S
MCF-7	DMEM	10 % FBS, 1 % L-glutamine, 0.1% Insulin 1 % P/S
MDA-MB-231	DMEM	10 % FBS, 1 % P/S
Vero	DMEM	10 % FBS, 1 % L-glutamine, 1 % P/S
MO3.13	DMEM	10 % FBS, 1 % L-glutamine, 1 % P/S
MO3.13 differentiated	DMEM	0.02 % FBS, 1 % L-glutamine, 1 % P/S

Table 2.2 Media for the different cell lines.

2.4 Viability Tests

2.4.1 MTT Viability Tests of Psychosine in MO3.13 Cells

For this test, help was obtained from Joanna Rejman.

MO3.13 cells and MO3.13 KO cells were seeded in 96-well plates at a density of 5,000 cells *per* well. The cells were starved in culture medium with 0.2 % (v/v) FBS for 24 hours for differentiation. After that, the cells for capsule tests were incubated with 5 or 10 GALC capsules *per* cell or with 10 capsules only filled with amino dextran (70 kDa) for 24 hours. Then the cells were incubated with psychosine in starvation medium at various concentrations and incubated for 24 hours. The viability was scrutinized with the MTT test.

2.4.2 Resazurin-Based Viability Tests of PEI and PEI Capsules

MDA-MB-231 cells were seeded in 96-well plates at a density of 15,000 cells *per* well. The next day, the medium was aspirated and the cells were rinsed with PBS and incubated with PEI or PEI capsules at different concentrations, as described in the results, for 48 hours. Afterwards, the cells were rinsed with PBS and fresh medium containing 10 % (v/v) resazurin was added to the cells for 3 hours. At last, the fluorescence of each well was recorded with the plate reader of a fluorospectrometer. In the appendix, the test is described in detail at the example of metallic nanotubes and the corresponding metal ions, *cf.* section 5.3. The test with capsules was performed in the same way with the parameters mentioned above. The values for the PEI experiments were normalized with a linear function $f(x) = ax + b$

between the minimum m and the maximum M of all experiments, *i.e.* data of capsules and free PEI. With the side conditions $f(m) = 0$ and $f(M) = 1$, the two equations $aM + b = 1$ and $am + b = 0$ are obtained, from which the values of a and b were calculated. With the inverse of the function *f,* the values were normalized.

2.5 pH Response Curves of Fluorescent Dyes

The following is a slightly shortened version of the description presented in the supporting information of manuscript [A3][38] (*cf.* section 6.1).

For the experiments with Mag-Indo-1 and Calcium-Green-1, Ca^{2+}- and Mg^{2+}-free buffers from Sigma-Aldrich were used and fine-adjusted with HCl or NaOH, respectively. 50 µg Mag-Indo-1 were dissolved in 100 µL DMSO to prepare a stock solution of 0.5 mg/mL or 684 µM. Calcium-green-1 dextran was dissolved in water at a concentration of 1 mg/mL. From this, the molar concentration was calculated as $c_{Dextran} = n/V = m/(M_w V)$ = 1 mg/(70 kDa·1 mL) with the molar mass M_w. Taking into account that to each dextran molecule (70 kDa) 3.5 Calcium-Green-1 fluorophores are bound, the concentration of Calcium-Green-1 in the solution is $c_{CG1} = 3.5 \cdot c_{Dextran}$ =3.5 mg/(70 kDa·mL) = 50 µM. 1 M stock solutions of $MgCl_2$ and $CaCl_2$ were prepared in MilliQ water. Chloride-free buffers for experiments with MQAE and BAC-SE were prepared as follows: an alkaline buffer was prepared with 140 mM potassium acetate, 1 mM $Ca(NO_3)_2$, 2 mM $MgSO_4$, 5 mM Glucose, and 20 mM tris(hydroxymethyl)aminomethane) (Tris). In parallel an acidic buffer was prepared similar to the alkaline buffer, but in which Tris was exchanged for 2-(*N*-morpholino)ethanesulfonic acid (MES) buffer. Buffers with different pH values were adjusted by mixing the acidic and alkaline buffers upon monitoring with a pH-meter (Satorius Professional Meter PP-50). 1 M KCl solution was prepared in Milli-Q water. 5 mg BAC-SE were dissolved in 1 mL DMSO to obtain a stock solution of 23 mM. This was further diluted in Milli-Q water for experiments. MQAE was dissolved in Milli-Q water to obtain a stock solution of 5 mM. Solutions of different pH and ion concentrations were filled into 96-well plates and fluorescence was recorded. The concentrations of the dyes and the corresponding ions are shown in Table 2.3. Solutions for the measurement were prepared by mixing 70 µL of buffer with 20 µL of salt solution of 5-fold concentration as stated in Table 2.3 and 10 µL of the dye at 10-fold concentration as stated in Table 2.3 directly in the 96-well plates.

c(Calcium-Green-1)	c(Mag-Indo-1)	c(MQAE)	c(BAC-SE)
5 µM	68.4 µM	0.5 mM	100 µM
c(Ca^{2+})[µM]	**c(Mg^{2+})[mM]**	**c(Cl^-)[mM]**	**c(Cl^-)[mM]**
0	0	0	0
0.05	0.1	5	5
0.1	0.25	10	10
0.15	0.5	20	15
0.5	1	40	20
1	2	60	25
5	4	80	30
10	6	100	40
25	8	150	50
50	10	300	100
100	50	500	150
250	100		200

Table 2.3 Concentrations of the dyes and the corresponding ions.

2.6 pH Sensing in Living Cells with SNARF® Capsules

2.6.1 pH Calibration Curves of SNARF® Capsules

The calibration curves of the SNARF® capsules were obtained by taking images of the capsules in commercial buffers from pH 3 to pH 10 (*cf.* list of chemicals, Table 2.1), measuring the ratio of the fluorescence intensities in the green and the red channel, and fitting the values with a sigmoidal function (*cf.* Figure 2.1 and section 3.1.3)

$$f(\mathrm{pH}) = \frac{a-b}{1+exp\left(\frac{\mathrm{pH}-c}{d}\right)} + b$$

with fit constants a, b, c, and d. The batch of capsules for the experiments with MCF-7 cells was imaged with a widefield microscope, the batch for the experiments with MO3.13 cells with a confocal laser scanning microscope (CLSM).

2.6.2 pH Sensing in MCF-7 Cells upon Addition of Monensin

Course of Experiments

MCF-7 cells were seeded in 8-well plates (Ibidi µ-slides) at a density of 15,000 to 25,000 cells *per* cm^2 in culture medium and incubated overnight at 37 °C and 5% CO_2. After 24 hours, the medium was exchanged and SNARF® capsules were added to the cells at a concentration of 20 to 40 capsules *per* seeded cell. The cells were observed with a widefield microscope equipped with an automated stage in time intervals of two to four hours. 15 to 30 positions were chosen and observed during the whole experiment. After at least 12 hours of

incubation with capsules, the medium was aspirated, the cells were rinsed with PBS, and fresh medium containing 20 µM monensin was added to the cells. The cells then were observed for four hours in time intervals of one hour. Subsequently, the monensin-containing medium was aspirated, the cells were rinsed with PBS, and fresh medium was added. The cells were then observed again in intervals of 2 to 4 hours until the end of the experiment.

Image Processing and Data Presentation

The goal was to obtain a time series of the lysosomal pH of the cells. For each experiment the capsules in each image were detected and a region of interest (ROI) was drawn around the area of the capsule in the image of the overlay of the transmission and the fluorescence channels. The fluorescence intensity of both channels was measured and the ratio was plotted *versus* time.

2.6.3 pH Sensing in MO3.13 Cells upon Addition of Psychosine

Course of Experiments

These experiments were carried out on a CLSM with automated stage and autofocus and an incubation chamber to keep the cells at 37 °C and 5 % CO_2 over the course of the experiments. This made it possible to take time series of a number of positions of the sample automatically, typically 8 to 16. Additionally, tile scans were performed which means that neighboring squares of 512 x 512 pixels were imaged automatically. Usually images of 4 tiles were taken for each position. MO3.13 WT or MO3.13 KO cells were seeded in 8-well plates at a density of $1.5 \cdot 10^4$ cells *per* cm^2. After 24 hours, five capsules *per* seeded cell were added and the cells were deprived of serum for 24 hours yielding differentiated cells. Then, the cells were incubated with psychosine-containing, serum-free medium at a concentration of 2 or 10 µM, or no psychosine in case of the controls. The acquisition time varied between 15 and 24 hours with time intervals of 10 or 15 minutes between the points in time.

Image Processing and Data Presentation

The ratio of the green and the red channel was obtained as described above. This time, the intensity ratio was converted into a pH value by use of the inverse function of the calibration curve of the capsules. The average of the pH values of all internalized capsules of one experiment was built for every point in time. As the curves obtained in this manner show large variations among neighboring points in time, a lowpass filter in form of the “moving mean” of the time series was calculated and plotted instead. For the moving mean, instead of the value of the point in time t_n, the average of the value t_n and the neighboring values, in this case t_{n-2}, t_{n-1}, t_{n+1}, and t_{n+2}, was calculated and plotted. To obtain a complete curve the first value is the same as in the mean curve, and the second value was calculated as average of the first three values. Similarly, the last two values were obtained. Figure 2.1 shows the calibration curve and, as example, the mean and moving mean of one experiment with MO3.13 KO cells and 10 µM psychosine.

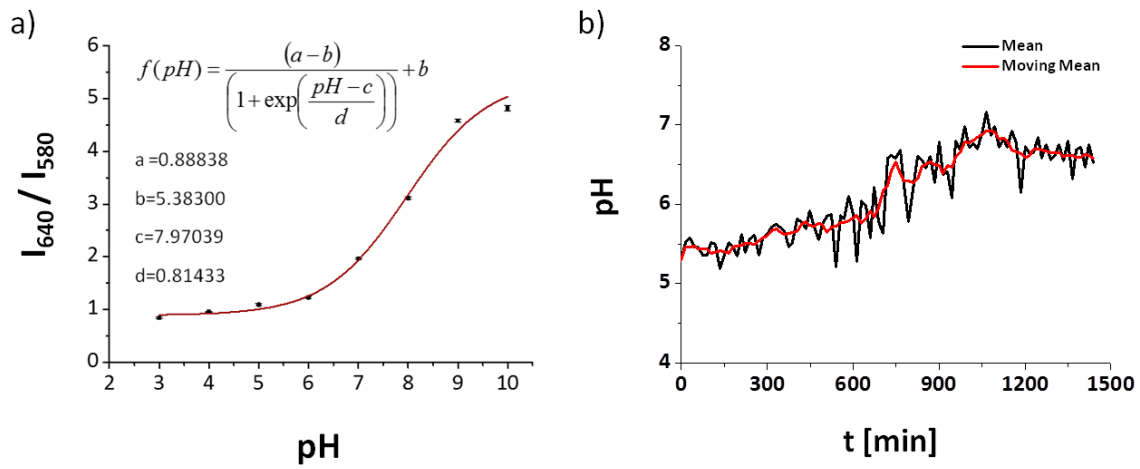

Figure 2.1 Evaluation of capsule pH values. a) Calibration curve of the SNARF® capsules. The fit was done with the function *f* and revealed the values a-d. b) Mean and moving mean for one experiment with psychosine. The ratio values of the fluorescence channels (indicated as I_{640} for the red fluorescence peak of SNARF® and I_{580} for the yellow-green fluorescence peak of SNARF® in the calibration curve) are converted into pH values using the inverse function of the calibration curve.

2.6.4 Determination of Intracellular α-Galactosidase A Activity

These experiments were conducted at Vall d'Hebron Institut de Recerca, Barcelona, Spain, under guidance of Maria-Eugenia López Sánchez. The amount of Replagal® in capsules was determined by Western Blot by Natalia García Aranda.

2.6.4.1 Isolation of Endothelial Cells from Mouse Aorta

This was not part of the work for this thesis. The cells were already obtained and frozen in the past by the group of Ibane Abasolo and could be used directly for the experiments. However, the procedure of isolation is summarized shortly here for completeness.

Mice bearing the Fabry enzyme defect are sacrificed and the aorta is removed, cleaned, and cut into rings of 2 mm thickness. These rings are placed onto collagen-coated culture dishes and supplemented with MAEC growth medium containing 20 % FBS (*cf.* Table 2.2). The cells now detach from the rings and spread in the dishes automatically. After 5 to 10 days the ring is removed and cells can be collected for experiments or grown further until confluence is reached. The procedure is explained by Shu *et al.* in their publication "An *in vitro* model of Fabry disease".[53]

2.6.4.2 Preparation of NBD-Gb3 Medium

The substrate for Replagal® in the MAEC assays was the fluorescent N-dedecanoyl-NBD-ceramide trihexoside (NBD-Gb3) as depicted in Figure 2.2. The sugar rings are removed by Replagal® and the remaining molecule can be further processed until the fluorescence is lost. This fluorescence loss is quantified and used as measure for the intracellular activity of Replagal®.

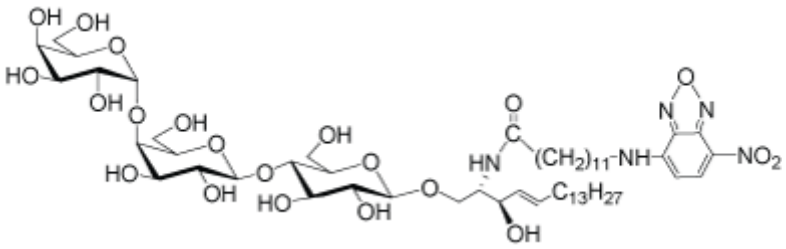

Figure 2.2 NBD-Gb3 structure formula. NBD-Gb3 is a fluorescent molecule. Replagal® removes the sugar rings and inhibits the accumulation of NBD-Gb3 in the lysosomes. The remaining molecule can be further processed and fluorescence is lost.

To make the substrate available to the enzymes in the lysosomes, it needed to be prepared in order to make uptake possible. NBD-Gb3 needs a carrier to enter the cells which here was bovine serum albumin (BSA). The medium with the substrate was prepared as follows. A 2 % solution of BSA in NaCl solution (9 $mg \cdot mL^{-1}$) was prepared. NBD-Gb3 was dissolved in DMSO at a concentration of 4 mM. 10 µL of the solution was heated 10 minutes at 60 °C and vortexed from time to time. 130 µL of the 2 % BSA solution was added dropwise and the solution was shaken at 37 °C for 20 minutes. Afterwards, another 140 µL of 2 % BSA solution were added and the solution was mixed. The solution was filtered through a column (Sephadex G25, VWR) to remove unreacted NBD-Gb3. For cell experiments, the solution was diluted 500-fold in complete growth medium. As the reaction yield may differ among batches of NBD-Gb3 medium, the results of the cytometry experiments were always compared to a positive control, which represented the maximum fluorescence possible for the respective batch.

2.6.4.3 Conduction of Cell Experiments

MAEC were seeded in standard 24-well cell culture plates. 10^5 cells were seeded in 0.5 mL of growth medium appropriate for the given cell passage for 24 hours. Then the medium was exchanged for medium containing NDB-Gb3 and Replagal® or Replagal®-containing capsules, respectively. 48 hours later, the cells were rinsed with PBS and trypsinized. The trypsin was removed by centrifugation and the cells were re-suspended in 350 µL of ice-cold PBS and stored at 0°C until use for cytometry.

2.6.4.4 Evaluation

The events were plotted as scatter plot with side scattering (SCC) versus forward scattering (FSC). From this plot the cells were gated for the first time to exclude events of small size which were too small to be cells, *cf.* Figure 2.1. From these events, only those were chosen where the fluorescence signal was within gate 2. This gate was adjusted from the negative control, *i.e.* cells neither incubated with NBD-Gb3 nor Replagal® or Replagal® capsules. The gate was set in such a way that 2 % of the control cells were inside gate 2.

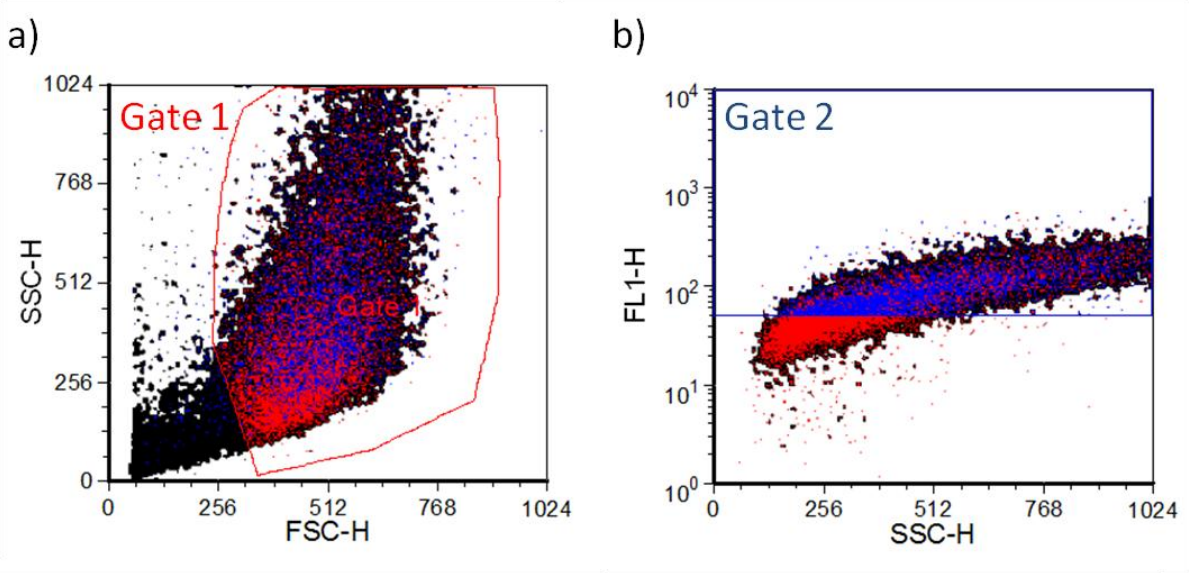

Figure 2.1 Example plots of the gating for the evaluation of the flow cytometry experiment. a) Events are plotted as scatter plot with side scattering versus forward scattering. Gate 1 excludes events of elements which are smaller than cells. b) The gated cells are plotted as scatter plot with the collected fluorescene *versus* side scattering. Cells are gated again, this time according to their fluorescence signal.

The positive control was done with cells incubated with NBD-Gb3, but without Replagal® or Replagal® capsules. Cells without Replagal® treatment cannot metabolize NBD-Gb3, and therefore, they set the maximum percentage of fluorescent cells. The results of the cells treated with Replagal® or Replagal® capsules are put in relation to the positive control to determine the efficacy of the treatment (*cf.* section 2.6.4.2). The efficacy was finally plotted against the mass concentration of the administered Replagal® either as solution or in capsules.

3 Results

3.1 Ion Sensing with Fluorophores, Stimulation and Sensing of pH in Cells

Work described in this section was used for the manuscript of [A3][38] and publication [A6][6] (*cf.* section 6). The data showing pH dependences of fluorescent dyes were recorded and evaluated by the author. Data in publication [A6] were obtained by more than one person. All data described in this thesis, however, was recorded and evaluated by the author as well as additional data used for [A6] although not presented here.

3.1.1 pH Sensing with Fluorescent Dyes

In the context of medical or pharmaceutical purposes, monitoring the internal properties of a cell is of highest interest, as many diseases are triggered by malfunctions of cells. In many cases, the homeostasis of the cells is influenced and alterations of intracellular properties can occur. One of the most fundamental properties in this manner is the pH. The activity of enzymes, for example, is dependent on the pH value and deviations from the appropriate pH lead to low activity and can in the worst case harm the enzyme irreversibly. Furthermore, pH gradients across cellular membranes play an important role as they ensure that the cell can extract energy from transport processes across membranes. pH monitoring in living cells can help to study proliferation, apoptosis, and endocytosis, among others.[56-59] Moreover, there are many examples of diseases where the pH regulation in the affected cells or tissue is disturbed.[60, 61] Monitoring pH can therefore be used to identify affected cells or *vice versa* tell, if a certain drug is capable of stopping the pH regulation disturbance. A straightforward way is to use cell-permeant forms of a dye, *e.g.* acetoxymethyl ester derivates. These dyes are electrically neutral and are taken up by cells *via* osmosis. Either they show a spectral shift upon change of pH or the emission intensity alters. As the cellular fluids are very complex, there are many ways in which the dye can be influenced, *e.g.* by binding to proteins.[62] Therefore, to measure accurate pH values, the dye must be calibrated intracellularly. The most common way to do this is the use of nigericin, a K^+/H^+ ionophore.[63] After treatment with nigericin, the intra- and extracellular pH value equilibrate and the intracellular pH can be adjusted by change of the extracellular pH. However, there are some problems associated with these kinds of measurements. During long-time measurements, the cells sequester parts of the dye, which leads to lower signal although no actual change of pH may have happened. Fading, also called photobleaching, is another problem in long-time experiments. In this case, repeated illumination leads to lower signal due to reaction of the dye with radicals, *e.g.* reactive oxygen species, into non-fluorescent molecules.[64, 65] Furthermore, a ratiometric measurement is preferred as it excludes sources of errors such as local gradients of the concentration of the dye, fluctuations of the illumination intensity over time, different exposure times, *etc*.[66, 67] For ratiometric measurements, however, a second

dye is needed as a reference where the ratio of the local concentrations of the two dyes is constant and the ratio of the intensities is pH-dependent, at least in the interesting pH range, which is around 4.5 to 8 for cells.

3.1.2 pH Dependence of Organic Fluorophores

Apart from protons, the most critical ions in cells are Na^+, K^+, Ca^{2+}, Mg^{2+}, and Cl^-. The concentrations of Na^+, K^+, and Cl^- are, for example, of special importance for muscle cells and neurons as the formation of action potentials is dependent on them. Ca^{2+} is important for the release of neurotransmitters and muscle contraction and can serve as cofactor for enzymes. Mg^{2+} also is a cofactor for many enzymes. The use of ATP as energy source for the cell is, for example, only possible if magnesium is bound to the ATP. There are many organic fluorophores available to sense and measure intracellular concentrations of the mentioned ions. However, many of the dyes available tend to be pH-sensitive in addition to their specific ion and may be sensitive to other ions.[68] For example, the potassium- and sodium-sensitive dyes PBFI and SBFI, respectively, show crosstalk with the correspondent other ion,[23, 38] and the Mg^{2+}-sensitive dye Mag-Indo-1 can also be used for sensing Ca^{2+}. In Figure 3.1, the pH dependence of the chloride-sensitive dyes MQAE and BAC, the calcium sensor dye Calcium Green-1, and the magnesium sensor dye Mag-Indo-1 are depicted. In all cases, the fluorescence intensity is clearly dependent on pH. In the plots of the chloride-sensitive dyes, intensity values rise especially for low pH values, whereas for higher values, from pH 6 to 10, the profile only slightly changes for constant chloride concentration. For the other two dyes, the fluorescence intensity is clearly dependent on pH as well. This means in principle that measurements with all these dyes need to be supported also by pH measurements to obtain clear results on changes of concentrations of the desired ions.

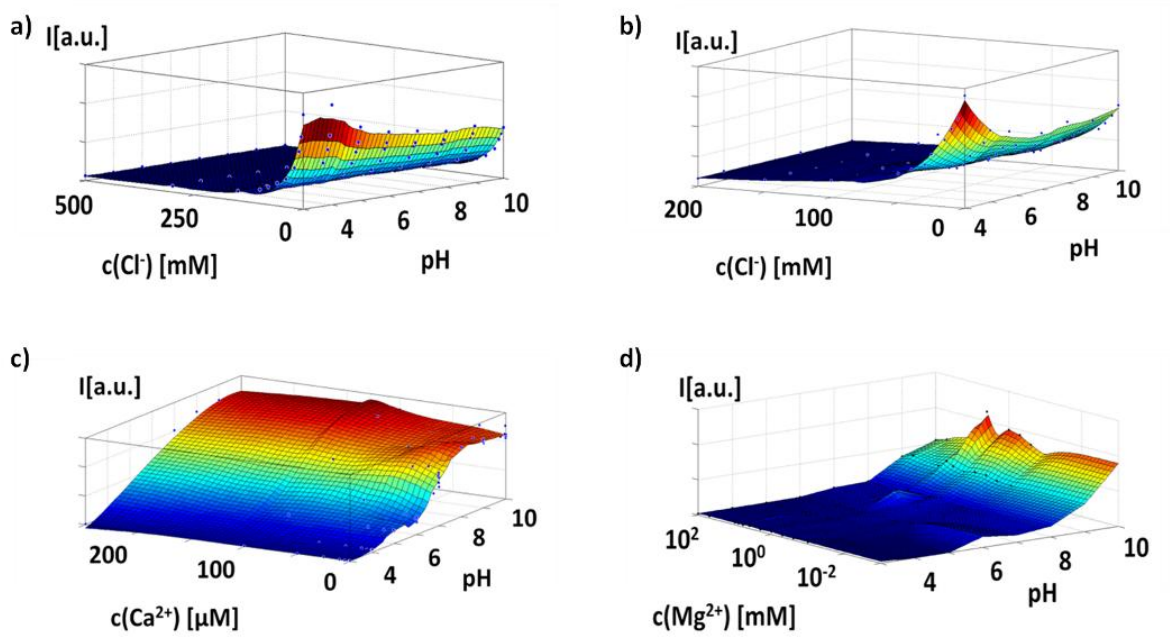

Figure 3.1 Response curves of ion-sensitives dyes to the respective ion and pH. a) Fluorescence intensity of MQAE against Cl^- and pH. b) Fluorescence intensity of BAC in dependence of Cl^- and pH. c) Fluorescence intensity of Calcium-green-1 against Ca^{2+} and pH. d) Fluorescence intensity of Mag-Indo-1 in dependence of Mg^{2+} and pH. In all cases the fluorescence intensity is dependent on pH in addition to the respective ion. The figure has been taken from publication [A3].[38]

3.1.3 Intracellular pH Sensing with Capsules

One application of capsules is their use as intracellular sensors. Thereby, advantage is taken of the porosity of the capsules, as small ions can freely diffuse through the capsule walls,[69] whereas the dye can be bound to bigger molecules such as dextran to keep it trapped inside the cavity. The use of capsules or other carriers has some advantages over the free dye. As the probe is confined to a small volume, the local concentration of the dye does not influence the measurement. For the free dye, problems can occur when the concentration of the dye is not evenly distributed as then the signal obtained is dependent on the concentration of the dye and on the concentration of the analyte.[70] Moreover, the capsules protect the dye from unspecific binding, sequestering, and degradation inside the cells.[22] *Vice versa*, the capsule also protects the cell from the dye. This opens the possibility to use molecules, which intrinsically are toxic for the cells or have other undesired effects. To perform intracellular sensing with capsules, they were filled with the pH-sensitive dye SNARF® bound to dextran. This dye has two emission maxima, one at 580 nm, and one at 640 nm. The maximum at 580 nm grows with smaller pH, whereas the one at 640 nm grows with higher pH. The ratio of both maxima can be used to obtain a calibration curve of the dye. In Figure 3.2, the calibration curve for one batch of SNARF® capsules is depicted. The capsules can be used as sensors roughly from pH 6 to 9, as above and below the slope vanishes and hence the ratios cannot be related to a specific pH value anymore.

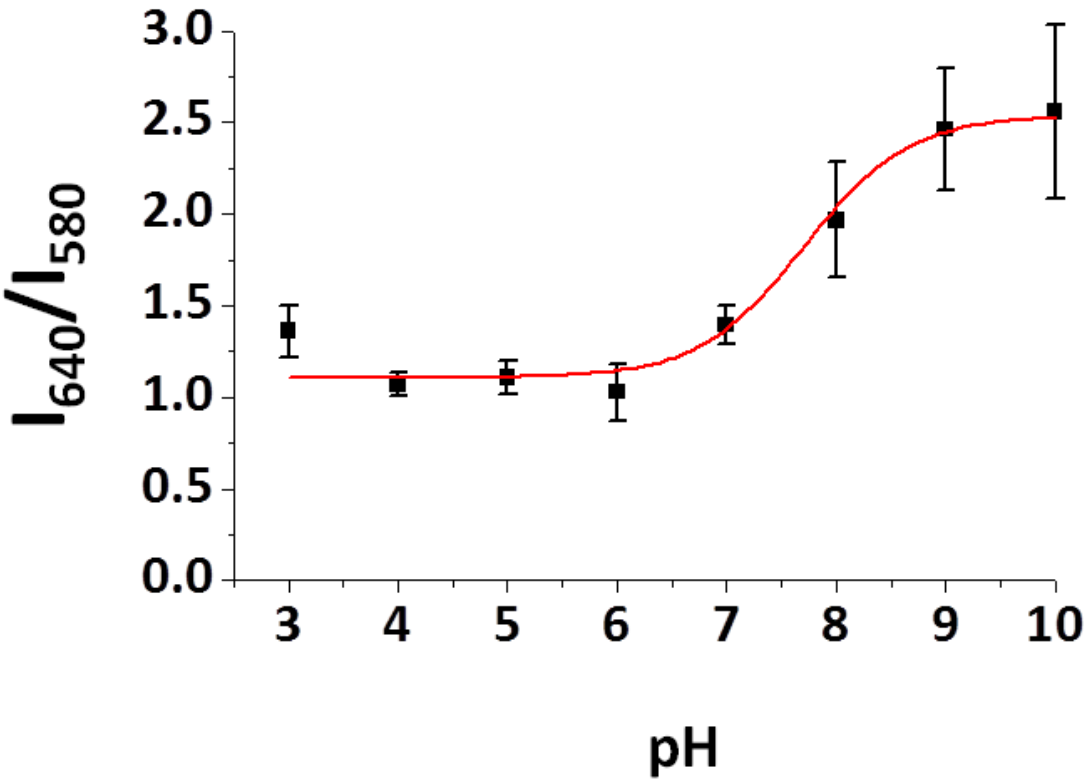

Figure 3.2 Calibration curve of SNARF® capsules from widefield microscopy images. Capsules were suspended in commercial buffers from pH 3 to 10 and the ratio of the fluorescence intensities was measured. The figure has been adapted from publication [A6].[6]

3.1.3.1 Lysosomal pH Measurement in MCF-7 Cells with SNARF® Capsules

The SNARF® capsules were used as intracellular reporters for the lysosomal pH of MCF-7 breast cancer cells. Capsules in the extracellular medium served as control capsules to confirm that changes of the color of the capsules did not take place automatically as an intrinsic feature of the capsules. In Figure 3.3, curves of intra- and extracellular capsules are plotted as function of time. The red line displays extracellular capsules and the green one internalized capsules. The ratio of the red and green intensity is plotted, which means that higher values correspond to higher pH. The green line stays constant throughout the measurements. The red one starts from a higher value, but after 10 hours, the value reaches its baseline, although the pH in the extracellular medium is kept constant throughout the experiment. The drop of the ratio of the red curve can be ascribed to photobleaching. After 10 hours, the bleaching does not influence the ratio anymore. In the green curve, no sign of photobleaching is observable. The reason is that SNARF® bleaches stronger in alkaline than in acidic conditions.[71, 72]

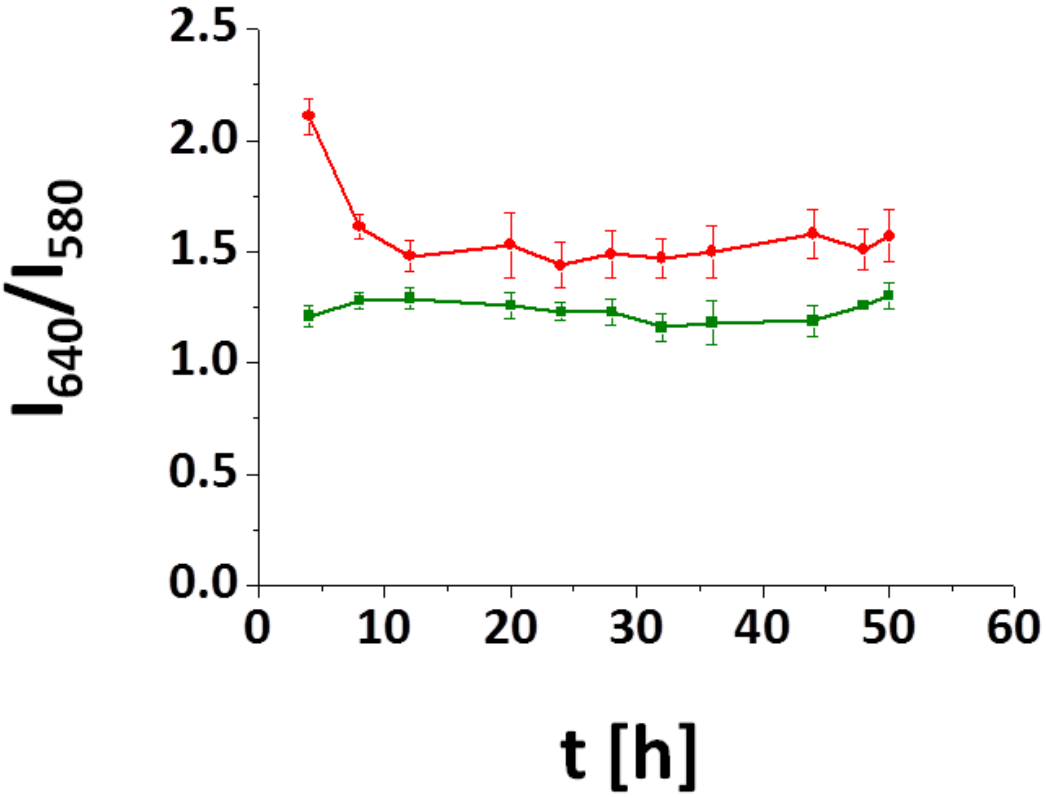

Figure 3.3 MCF-7 cells were incubated with SNARF® capsules and the fluorescence intensity ratio was monitored over a period of 50 hours. Intracellular capsules (green curve) show that the intracellular pH does not change during that time. Extracellular capsules start from a high value but then tend to be constant. The drop within the first 10 hours is ascribed to photobleaching. Error bars indicate standard deviations. The figure has been adapted from publication [A6].[6]

3.1.3.2 Stimulation of the Lysosomal pH of MCF-7 Cells and Detection with SNARF® Capsules

The capsules were used now to monitor the lysosomal pH under influence of substances that are reported in the literature to influence the lysosomal or generally the cellular pH. The substances tested were amiloride, bafilomycin A_1, chloroquine, and monensin. The mechanisms influencing the pH were of different nature. In this section, only the example of monensin will be described. Details for the other substances can be found in the publication and its supporting information.[6] Monensin is a Na^+ ionophore, which means that it can bind to sodium ions and transport them through cell membranes. It is not specific to sodium ions but can bind also to potassium and other monovalent cations.[73] However, in cells it plays an important role as Na^+/H^+ antiporter. This means that it transports sodium ions through membranes in one direction and protons in the other direction. Thereby, it abolishes sodium and pH gradients in the cells.[74] In Figure 3.4, the plot of one monensin experiment is displayed. The yellow bar indicates the period when monensin was added. The red curve again shows photobleaching in the beginning (*cf.* Figure 3.3). The green curve has a baseline slightly above one, but when monensin is added the ratio rises to that of the extracellular capsules very fast, meaning that the lysosomal and the extracellular pH equilibrate during the presence of monensin. The peak keeps a high level during the presence of monensin. As

soon as there is equilibrium of pH and sodium ions across a membrane, a further increase of the pH value is not possible. This means that the equilibrium was reached within one hour. The fast decrease of the green curve after the washing supports this. By rinsing the cells, the effect of monensin is completely diminished within one hour.

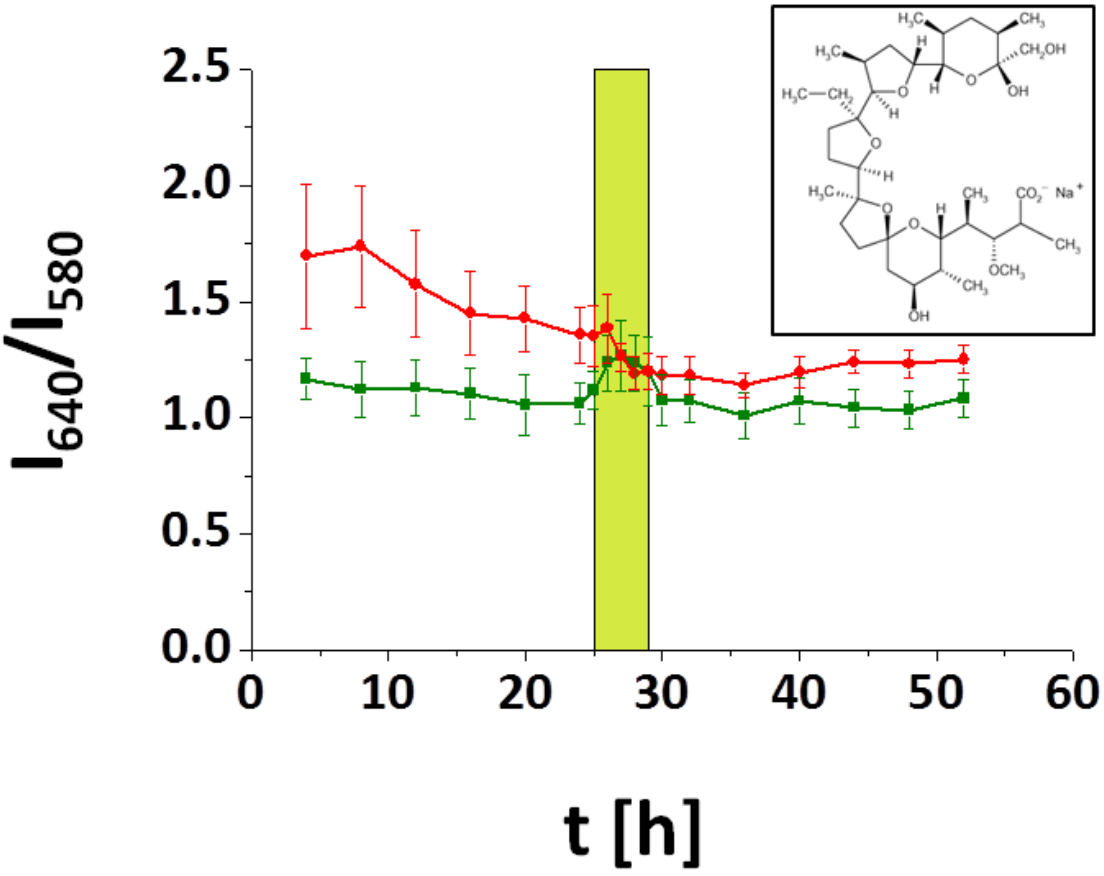

Figure 3.4 Fluorescence ratio of internalized (green curve) and extracellular (red curve) capsules over time. The yellow bar indicates the time when monensin was present. The intracellular values clearly rise during the presence of monensin showing a rise in pH. After the cells have been rinsed the ratio and thus the pH drops to its normal value. The inset shows the structure formula of monensin. Error bars indicate standard deviation. The figure has been adapted from publication [A6].[6]

3.2 Capsules for Intracellular Delivery of Genetic Material

The results were used for publication [A7][4] (*cf.*section 6). The author did all quantitative evaluation of images leading to the results depicted in Figure 3.6, Figure 3.8, and Figure 5.2 as well as the cytotoxicity assays shown in Figure 3.9.

3.2.1 Introduction

Despite the established methods, there is need for other or improved means of delivery of the genetic material to cells. Viral vectors usually show a high transfection rate and are therefore the preferred vectors. They, however, raise concerns because of mutagenesis, *i.e.* the possibility that the viral vectors trigger mutations of the genome, and immunogenicity, *i.e.* the possibility that viral vectors induce an unwanted immune response.[75-77] This is the reason why, so far, only one gene therapy has been approved in Europe, namely Glybera® from uniQure.[78, 79] Non-viral vectors such as lipoplexes and polyplexes, in contrast, show only small transfection rates. Microinjection does not allow for high numbers of transfected cells, as the transfection is very time-consuming and not automatable. Furthermore, it does not allow for *in vivo*-transfection, which is also true for electroporation. Thus, other carries are of interest both for *in vitro*- and *in vivo*-transfection. A bio-compatible carrier is desired, which protects the genetic material against degradation before it reaches its target, facilitates cell internalization, and enables controlled release of the genetic material.[80] Biocompatible capsules have been synthesized by many groups and subsequent release into the cytoplasm has been achieved for different cargo, such as proteins, DNA, or RNA.[3, 9, 17, 18, 81, 82]

3.2.2 Delivery of DNA

This study was a comparative study where the delivered amount of DNA was quantified for different delivery systems. Cells were incubated with plain DNA, PEI/DNA polyplexes, PEI/DNA polyplexes encapsulated in biodegradable capsules, and PEI/DNA polyplexes encapsulated in non-degradable capsules. Standard transfection protocols with polyplexes are performed in serum-free growth medium.[44] Here, a comparison for media with and without serum was performed. The amount of DNA for each of the experiments was equalized so that a comparison based on the administered amount of DNA was possible. In Figure 3.5, images of HeLa cells at different points in time and for the different ways of delivery are shown. The images show cells incubated without serum. The DNA was labeled with the fluorophore Cy5 and is colored in violet and PEI was labeled with FITC and is colored in green. The result of the overlay of violet and green is white. In the images, one can see that cells with plain DNA and PEI/DNA polyplexes show no fluorescence signal at any point in time. With both capsule types, the cells show fluorescence signal but only cells incubated with biodegradable capsules show fluorescence in the cytosol, whereas in non-degradable capsules the signal is confined to the area of the capsules. The PEI, however, is distributed in the cytosol also in case of non-degradable capsules. Note that the amount of PEI/DNA polyplexes is very small compared to what is stated in standard protocols. This was due to

the small amounts needed for the delivery by capsules and the fact that the comparison was based on the amount of DNA added to the cells. Furthermore, the cells begin to become round at later times as the serum-free medium stresses them.

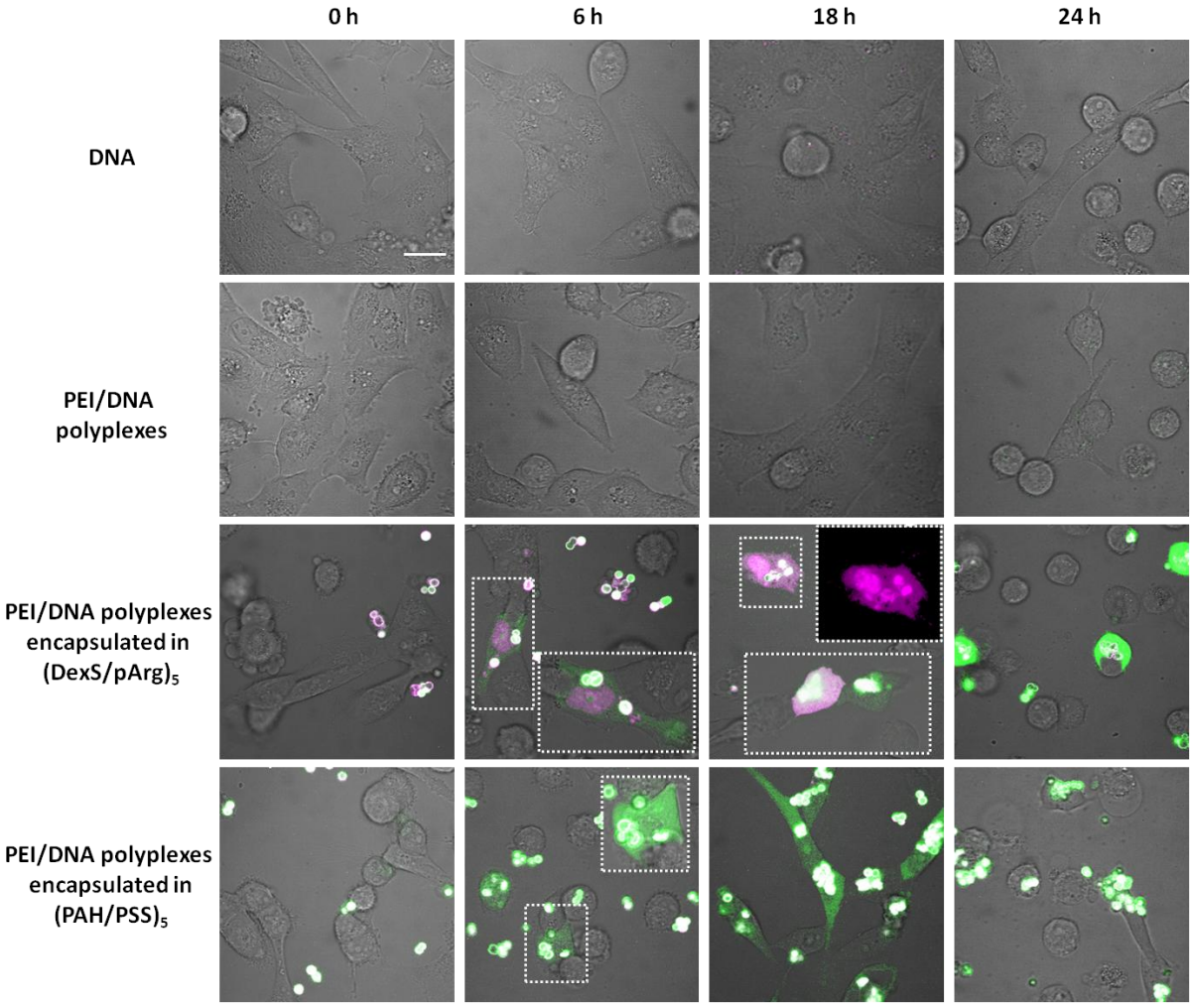

Figure 3.5 MDA-MB-231 cells were incubated with free DNA, DNA/PEI polyplexes, biodegradable $(DexS/pArg)_5$ capsules with embedded PEI/DNA, and non-degradable $(PSS/PAH)_5$ capsules with embedded PEI/DNA. After different incubation times t, as indicated in the top panel, cells were imaged. The transmission channel shows the cells, and the green and violet channels show the emission of the FITC labels and Cy5 labels of PEI and DNA, respectively. Images from serum-free experiments are shown. The scale bar corresponds to 20 µm. The figure has been taken from publication [A7].[4]

The delivery efficacy was quantified by image analysis. The area of each cell was determined from the transmission channel and the mean fluorescence intensity in that area was measured. Fluorescence from the area of the capsules was not included. The mean fluorescence of the cells was averaged and plotted as column diagrams in Figure 3.6. The left graph corresponds to serum-free incubation and the right graph to cells in serum-containing medium. The amount of DNA delivered was highest for biodegradable capsules and already took place within less than 24 hours of incubation. DNA transport was not observable for free DNA or PEI/DNA polyplexes in serum-free medium, which is also visible in the images in Figure 3.5. However, non-degradable capsules could deliver a small but observable amount in serum-free medium. In serum-containing medium, free DNA and PEI/DNA polyplexes show a small effect. Nevertheless, here, as well as in serum-free medium, the biodegradable capsules have a much higher efficacy. Moreover, the amount delivered DNA with

biodegradable capsules is clearly higher in serum-containing medium than in serum-free medium.

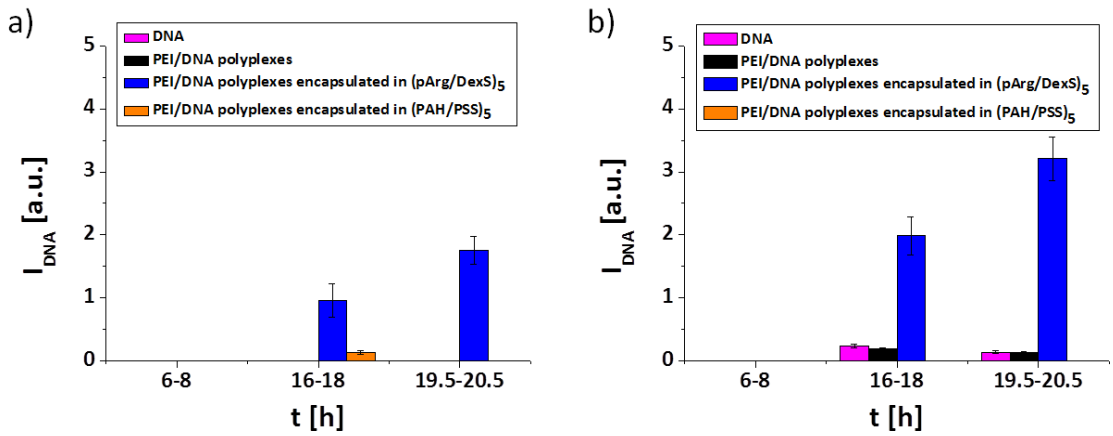

Figure 3.6 From the microscopy data as presented in Figure 3.5, for each cell in each recorded image the integrated fluorescence intensity I_{DNA} was determined. The integrated fluorescence intensity corresponds to the area of the cell (determined from the transmission channel) times the mean fluorescence intensity from the Cy5 channel in that area. Fluorescence originating from the capsules was not considered, but only fluorescence located in the cytosol. The mean fluorescence intensities, as observed for the different ways of delivery, are displayed for incubation in a) serum-free and in b) serum-containing media together with the corresponding standard deviations. For each data point at least 30 cells were analyzed. The figure has been taken from publication [A7].[4]

Cells deprived of serum will suffer from stress, which in turn influences the metabolism. Therefore, transfection in serum-containing medium is clearly preferred. Here, it could be shown that transfection with biodegradable capsules offers a possibility to do that and the capsules provide protection for the DNA in the extracellular medium.

3.2.3 Delivery of siRNA with Capsules for Knockout of GFP

In the section above, the amount of delivered DNA was measured and quantified. In a further step, silencing RNA (siRNA) was used to transfect cells and to determine the efficacy of transfection with biodegradable capsules. For this purpose, GFP-expressing HeLa cells and siRNA capable of knocking out GFP were used. The cells were kept in serum-free medium for these experiments. The comparison here was made only between cells incubated with biodegradable siRNA-containing capsules and polyplexes. In Figure 3.7, images of the cells are shown. In this case, PEI was labeled with Dy-651 and colored in violet and siRNA was labeled with AF-546 and colored in red. GFP is depicted in green. The left panel shows cells incubated with polyplexes and the right one cells incubated with polyplex-containing biodegradable capsules. The cells incubated with polyplexes keep their green fluorescence over the entire time, while in the images of cells incubated with capsules the fluorescence is lost after 30 hours in the cells marked with asterisks. After 20 hours, the cells with capsules clearly show distribution of PEI (violet) in the cytosol. The insets labeled with the number sign (#) in the polyplex panel show that there is siRNA present in the cells (red label). These images were enhanced in contrast to make the red fluorescence visible.

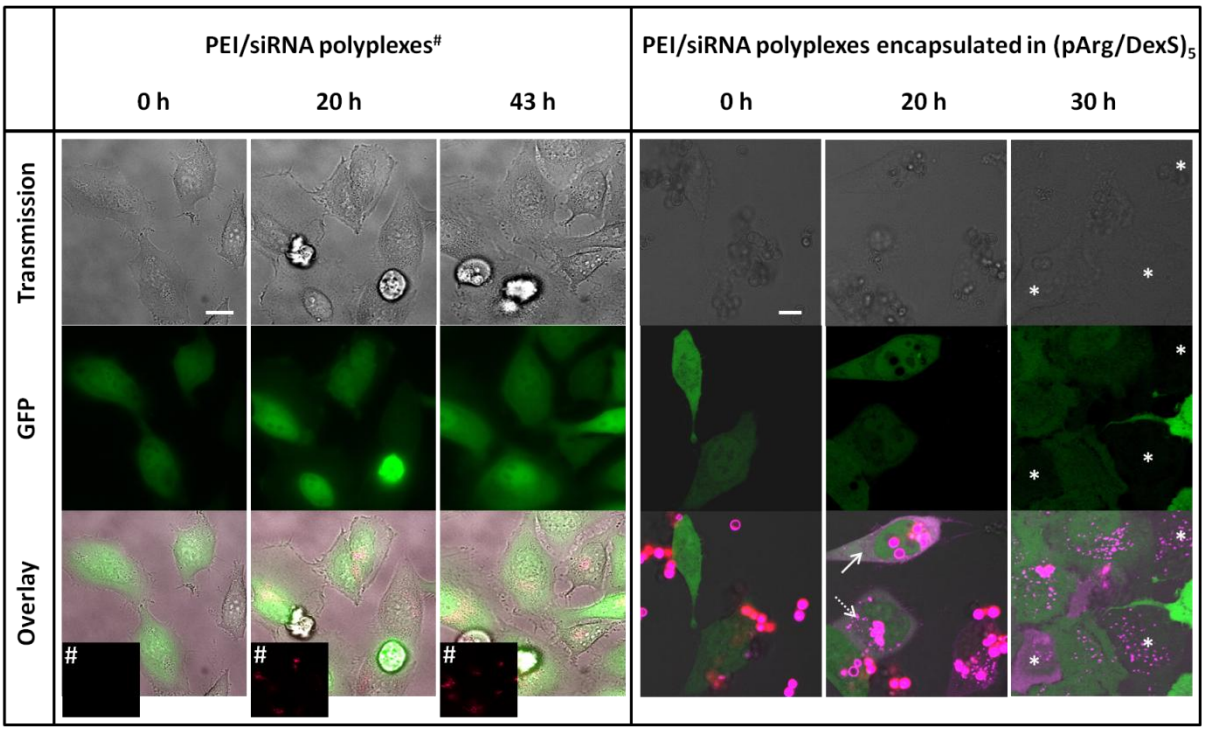

Figure 3.7 GFP-expressing HeLa cells were incubated with free (left column) and encapsulated (right column) PEI/siRNA polyplexes. Live images of the same cells were taken over time t. Besides the transmission channel showing the cells, also GFP (green), AF-546 labeled siRNA (red), and DY-651 (violet) labeled PEI are displayed. The straight arrow indicates a homogenous cytosolic distribution of PEI, whereas the dashed arrow shows a punctuate distribution. Cells marked with asterisks have clearly lost their GFP fluorescence. The insets (#) correspond to images of the polyplexes. For clarity, these insets were enhanced in contrast in order to show the presence of the siRNA inside the cells. The scale bars correspond to 10 µm. The figure has been taken from publication [A7].[4]

From images as presented in Figure 3.7, the fluorescence intensity in the cells was measured. In the transmission channel, the area of each cell was determined and the mean GFP intensity was measured. To calculate the mean of these cells, only cells in between the 0.25- and the 0.75-quantile were used to exclude outliers. Cells dividing, for example, have a much higher mean intensity as the cell contracts to a spherical form. In Figure 3.8, the mean intensity was plotted against time for cells incubated with polyplexes, cells incubated with capsules, and untreated control cells. The amounts of siRNA added to the cells were comparable, $6.4 \cdot 10^{-3}$ µg *via* capsules and $10 \cdot 10^{-3}$ µg *via* polyplexes added to $2 \cdot 10^{4}$ seeded cells in 300 µL of medium. The graph clearly shows that encapsulated polyplexes decrease the GFP fluorescence after 30 hours of incubation. On the contrary, both polyplexes and control cells do not show any effect. It has to be noted that an amount of $400 \cdot 10^{-3}$ µg under the same conditions was sufficient to knock out GFP successfully. This can be found in the appendix in section 5.1.

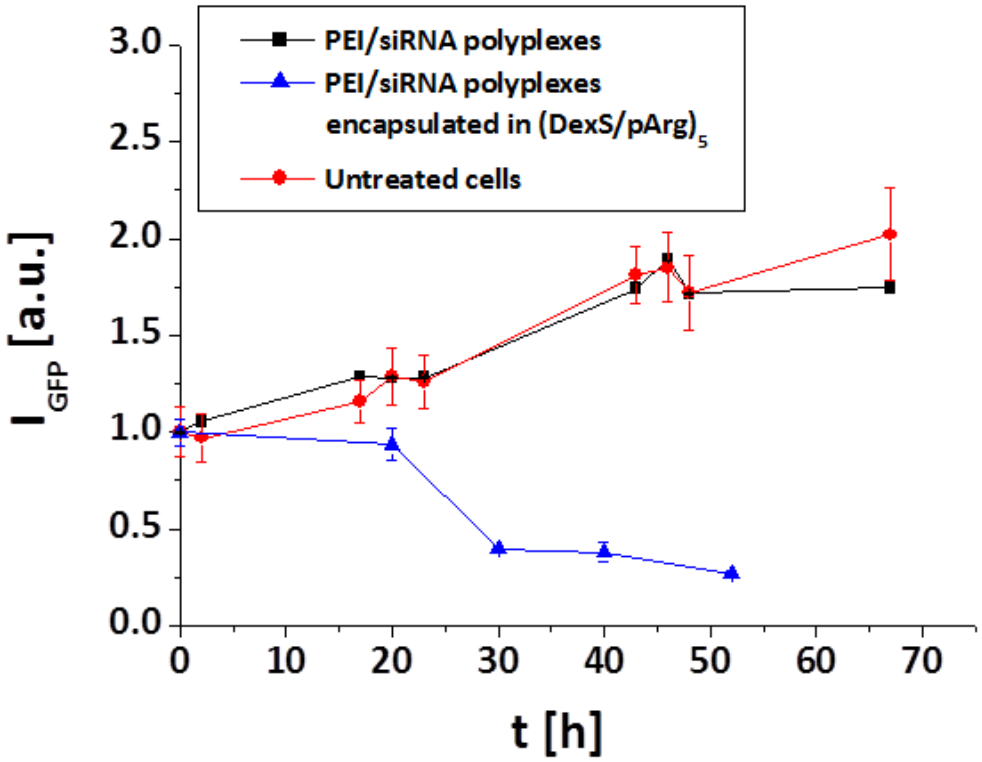

Figure 3.8 GFP-expressing HeLa cells were incubated with free encapsulated PEI/siRNA polyplexes. The total amount of siRNA and PEI was $6.4 \cdot 10^{-3}$ µg and $25 \cdot 10^{-3}$ µg for capsules and $10 \cdot 10^{-3}$ µg and $12.5 \cdot 10^{-3}$ µg for polyplexes, respectively. Images were taken at different points in time t (*cf.* Figure 3.7) and the mean integrated fluorescence density of GFP, i.e. the area of each cell times its mean fluorescence intensity, is displayed. The error bars represent standard deviations of the mean. The figure has been taken from publication [A7].[4]

These results mean that encapsulated polyplexes are much more efficient for the delivery of siRNA into cells than plain polyplexes. Furthermore, the advantages mentioned in the beginning of the section, protection of the siRNA against degradation, high biocompatibility, and controlled release of the cargo can be utilized.

3.2.4 Cytotoxicity of PEI Polyplexes and Encapsulated PEI

One concern not dealt with yet is the toxicity of PEI for cells, which has been described regularly for PEI polyplexes.[43, 46, 83] The capsules offer a way to circumvent this problem as they not only facilitate protection of siRNA against degradation but also protection for the cells from PEI. This was verified by a resazurin-based toxicity assay. The toxicity of PEI and PEI in biodegradable capsules as tested. The results are depicted as a function of added mass of PEI to make the experiments comparable. A linear function between the minimum and the maximum value was used to normalize the values (*cf.* section 2.4.2). Note that the value for zero PEI could not be plotted due to the logarithmic scale but lies in the same range as the smallest plotted value.

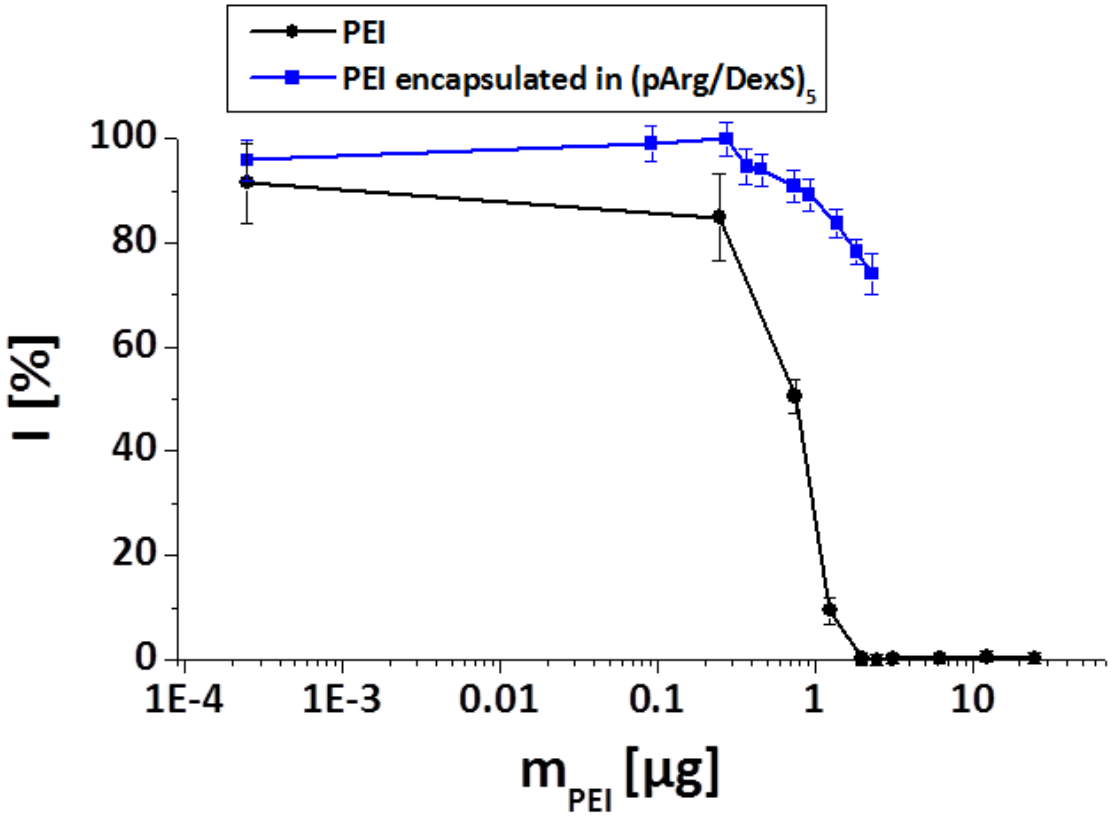

Figure 3.9 Reduction of cell viability caused by encapsulated and non-encapsulated PEI. The normalized cell viability in terms of resorufin fluorescence intensity I versus the amount of added PEI m_{PEI} is displayed. The average of six (PEI capsules) and three (PEI solution) independent measurements is displayed. Higher amounts of encapsulated PEI could not be measured as there is a threshold at which the capsules themselves can induce toxicity if added in too high quantities to the cells[84]. The error bars represent standard deviations of the mean. The figure has been taken from publication [A7].[4]

The value where 50 % of the cells had died was (0.80 ± 0.02) µg, as obtained from fitting with the sigmoidal function

$$\mathrm{I(c)} = \frac{I_{max}-I_{min}}{1+\left(\frac{c}{c_0}\right)^{p}} + I_{min}.$$

For the capsules, larger amounts of PEI than plotted were not added to the cells because at some point the capsules themselves may introduce adverse effects,[85] and also the cells do not have the capability to take up arbitrarily high numbers of capsules. Nonetheless, the graphs show that the toxicity of encapsulated PEI is much less than that of free PEI. The number of capsules added to the experiments corresponding to Figure 3.7 and Figure 3.8, respectively, was 20 capsules *per* seeded cell, which accords to 25 ng in the whole well. In the toxicity test, this accords to 0.1875 ng, as only $1.5 \cdot 10^4$ instead of $2 \cdot 10^4$ cells were seeded *per* well. At this amount, however, the viability of the cells is not affected. This means that the capsules protect the cells from the PEI of the encapsulated polyplexes.

3.3 Capsules for Sensing and Enzyme Delivery in Lysosomal Storage Disease Models

The work presented in this section was used for the preparation of the manuscript [A8] (*cf.* section 6). Work done by the author includes all capsule preparations, all pH time series from the experiments to the evaluations, preparation of cells for cytometry measurements, and parts of the cytotoxicity experiments. Cytometry runs and processing of the data were done under guidance of Maria-Eugenia López Sánchez. Western Blots were taken out by Natalia García Aranda. Help for MTT-assays was obtained from Joanna Rejman.

3.3.1 Introduction

Lysosomal storage diseases result from the deficiency of certain enzymes in the lysosomes of cells. So far, round about 50 LSDs are known. Each single disease is very rare in the population, but taken together make for a rate of 1 in 4000-8000 live births.[51] Approved treatment is only available for six of these diseases so far and relies on so-called enzyme replacement therapy, in which the patients are administered the defective enzyme *via* infusion.

3.3.2 Fabry Disease

One of these six diseases where treatment is available is Fabry disease. Patients with Fabry lack the enzyme GLA. This enzyme is responsible for the degradation of globotriaosylceramide (Gb3). There are two drugs approved for treatment, Replagal® from Shire and Fabrazyme® from Genzyme. However, there is need for improvement of these treatments for several reasons: first, so far the defective enzyme is injected as solution into the blood stream, which means that the enzyme is unprotected against degradation. This degradation already can happen in the body outside the cells, but also inside the cells the enzyme can be degraded before it begins its work in the lysosome.[86] The advantage of capsules is therefore the protection of the drug against degradation in the body. Second, Replagal® enters the cells through receptor-mediated uptake by mannose-6-phosphate receptors. These receptors, however, may not be expressed homogeneously in all relevant organs of the patient, leading to imbalanced distribution of Replagal® in the body and thus ineffective treatment of the patient.[49] This can be evaded by use of capsules as shell, as their uptake is independent of receptors. Third, many patients begin to express antibodies against Replagal® and treatment becomes ineffective or inefficient.[49, 87] The mechanism behind the immune response is the production of antibodies binding to Replagal® which can influence, among others, receptor binding and subcellular trafficking, which means that the enzymes might not reach the lysosomes anymore.[87]

3.3.2.1 Determination of Replagal® Content of Capsules by Western Blot

Determination of capsule content is, in general, a difficult task. Absorption spectroscopy, for example, does not work properly as the capsules themselves usually absorb and scatter light much stronger than the cargo. Measuring the content of all washing solutions and

subtracting the value from the amount used for synthesis is also highly error-prone. As the cargo in this case is a protein, Western Blot was used to determine the content of the capsules. The capsules were put in a vertical gel and an electric field was applied. In the electric field, the enzyme was released from the capsules and ran in the gel. The exact mechanism why the capsules break and release their content is not clarified yet and to the best of the author's knowledge Western Blots with polyelectrolyte capsules to determine the loading level have not been published so far. As the polyelectrolytes of the capsules are not covalently bound to each other, the electric field might rupture the capsules and subsequently, the content could be released. After gel electrophoresis, the proteins were transferred to a membrane where antibodies to mark the protein could be applied. In Figure 3.10 b) the calibration curve of one Western Blot is depicted, as obtained from the Replagal® standards in a). The area of the bands was measured as shown below the bands. From the calibration curve, the amount of Replagal® in the capsules could be obtained through the area of the Western Blot bands of the capsules. The amount of Replagal® in the capsule suspension found in case of the depicted data was 161.7 µg·mL^{-1}. The concentration of the capsule suspension was 4·10^{8} capsules *per* mL. Therefore, the average amount *per* capsule was approximately 400 fg.

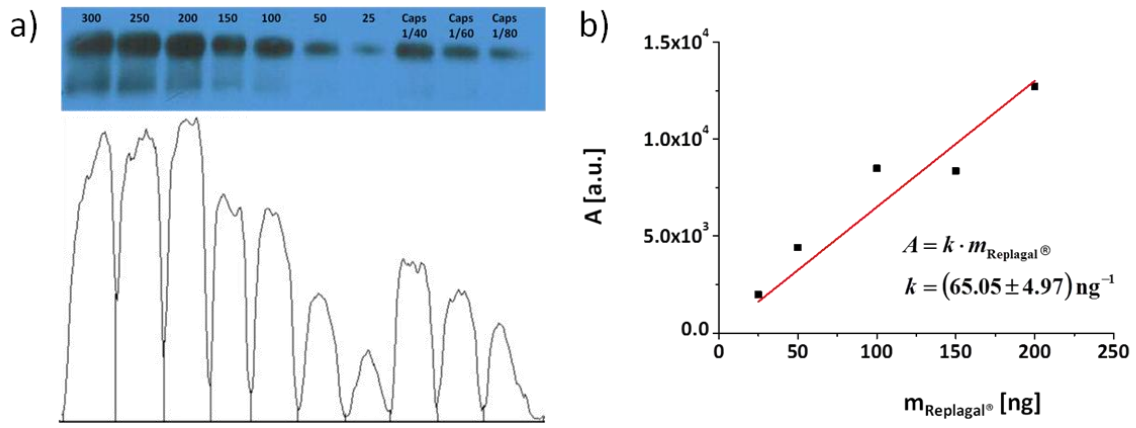

Figure 3.10 Results of the Western Blot. The bands as obtained for Replagal® from 300 ng down to 25 ng and from the capsule solution diluted 1/40, 1/60, or 1/80 can be seen in a) From the area of the bands of the Western Blot in a) (arbitrary units), the data points for the plot in b) were obtained. The data for 250 ng and 300 ng was neglected, as the values were too small due to saturation of the camera. The data was fitted with a line $A=k \cdot m_{Replagal®}$ of intercept zero and slope *k*. From this line the amount of Replagal® in the capsules was determined.

3.3.2.2 Intracellular Effect of Replagal® and Replagal® Capsules

The Replagal® capsules were tested for their intracellular effectivity with MAEC. GLA was knocked out in these mice to simulate Fabry disease. To determine the intracellular activity of the Replagal® capsules, the cells were co-incubated with the capsules and the Replagal® substrate NBD-Gb3. The substrate is fluorescent while the product after conversion by Replagal® is non-fluorescent. Therefore, the intracellular activity of the capsules or free Replagal® can be obtained from the fluorescence of NBD-Gb3 in the cells. Concerns that the substrate is converted already in the cell medium before take-up by the cells can be ruled out as the enzyme only works well at acidic pH and thus only when it has reached the late

endosomes or lysosomes in the cells. The efficiency of the capsules compared with Replagal® was determined by the fluorescence loss of NBD-Gb3. In Figure 3.11, the fluorescence loss is plotted against the mass concentration of Replagal®, which was calculated from the amount of Replagal® determined by Western Blot. The amount administered with capsules was higher than that of the Replagal® solution. The curves show that the Replagal® solution has a higher efficacy, since already with a concentration of 1 $mg \cdot mL^{-1}$ a fluorescence reduction of more than 90 % was obtained, while the capsules do not reach such a high level, but only about 80 %. Furthermore, the Replagal® concentrations needed in case of capsules are higher than those in case of the Replagal® solution.

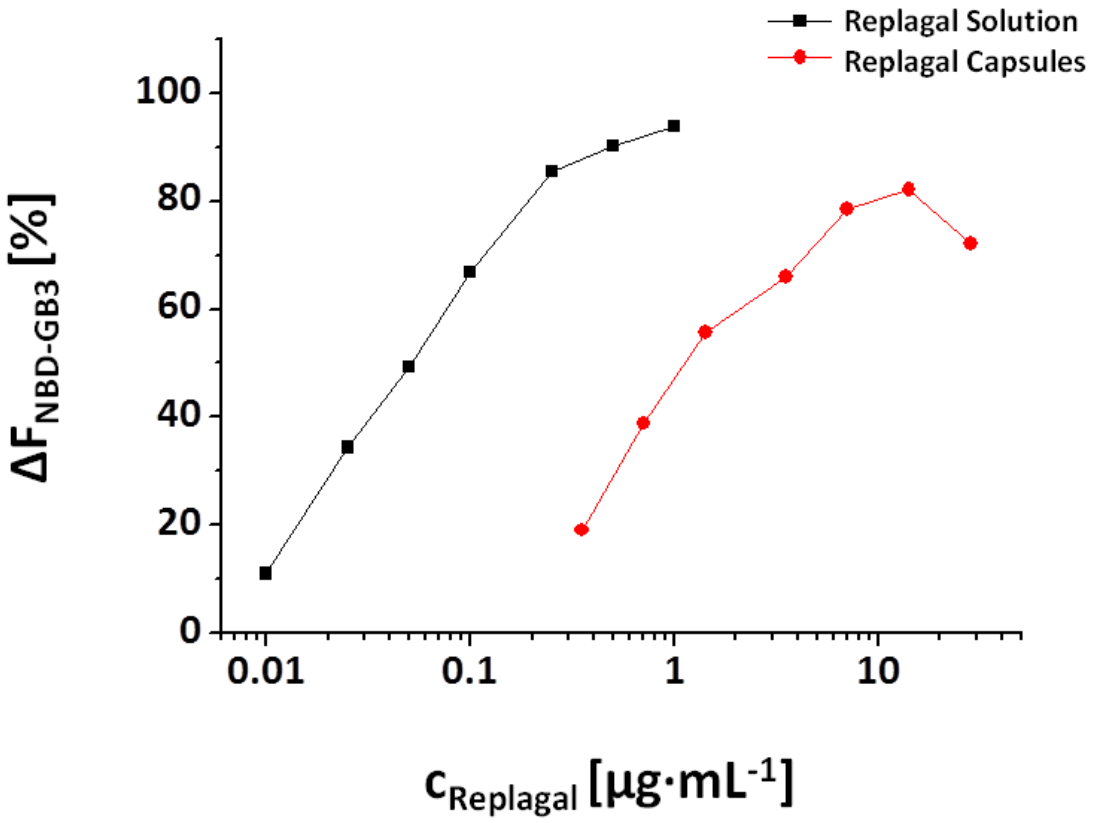

Figure 3.11 Fluorescence reduction of NBD-Gb3 in MAEC as determined with flow cytometry. The plot depicts the loss of fluorescence as function of the administered concentration of Replagal®, either as solution or as capsule suspension. The figure has been adapted from manuscript [A8].

3.3.3 Krabbe Disease

Krabbe disease, also called globoid cell leukodystrophy, is an inherited neurological disorder. Knowledge about the disease is limited and so far no cure but only palliative and symptom-related treatment is available. Symptoms occur at the age of 3 to 6 months and involve fevers, limp stiffness, and decelerated mental and motor development among others. Later blindness and deafness can appear. The disease is triggered by a dysfunction of the oligodendrocytes of the patients. Oligodendrocytes are a type of brain cells, which provide the axons of neurons with an electrically insulating myelin sheath that also serves as scaffold. When the oligodendrocytes produce myelin, side products such as psychosine or

other sphingolipids, and galactosylceramides are produced, which are metabolized by GALC. This enzyme is located in the lysosomes of the cells. In Krabbe disease, however, the oligodendrocytes lack this enzyme, and therefore, sphingolipids and galactosylceramides accumulate in the lysosomes. This accumulation leads to cell death, and subsequently, the axons are not provided their myelin sheath. The lack of insulation leads to slower signaling which can be measured in a nerve conduction study.[88] A simple model of Krabbe disease can be obtained from the MO3.13 cell line.[54, 55] These cells are immortalized oligodendrocytes. When incubated with psychosine they internalize and store it in lysosomes. For the studies, the wild-type (MO3.13 WT) was used as well as cells where the enzyme GALC was knocked out (MO3.13 KO). The KO cells represent dysfunctional oligodendrocytes in the brain of Krabbe patients whereas the WT serve as control.

3.3.3.1 pH Sensing in MO3.13 Cells

So far, there is not much knowledge about the influence of psychosine and other sphingolipids on the pH of oligodendrocytic cells and especially on cells lacking GALC. In this work, SNARF® capsules were used to monitor the pH to obtain a time-resolved pH-profile of the lysosomes during the accumulation of psychosine in both KO and WT MO3.13 cells. In Figure 3.12, images of cells incubated with 2 µM psychosine are shown. The capsules have already been taken up and appear in yellow due to the acidic environment. Images of both WT and KO cells are depicted and “PSY” indicates cells incubated with psychosine whereas “Control” shows cells kept in psychosine- and serum-free media. After 20 h of incubation, the cells in all the four conformations appear healthy and no sign of apoptosis is visible.

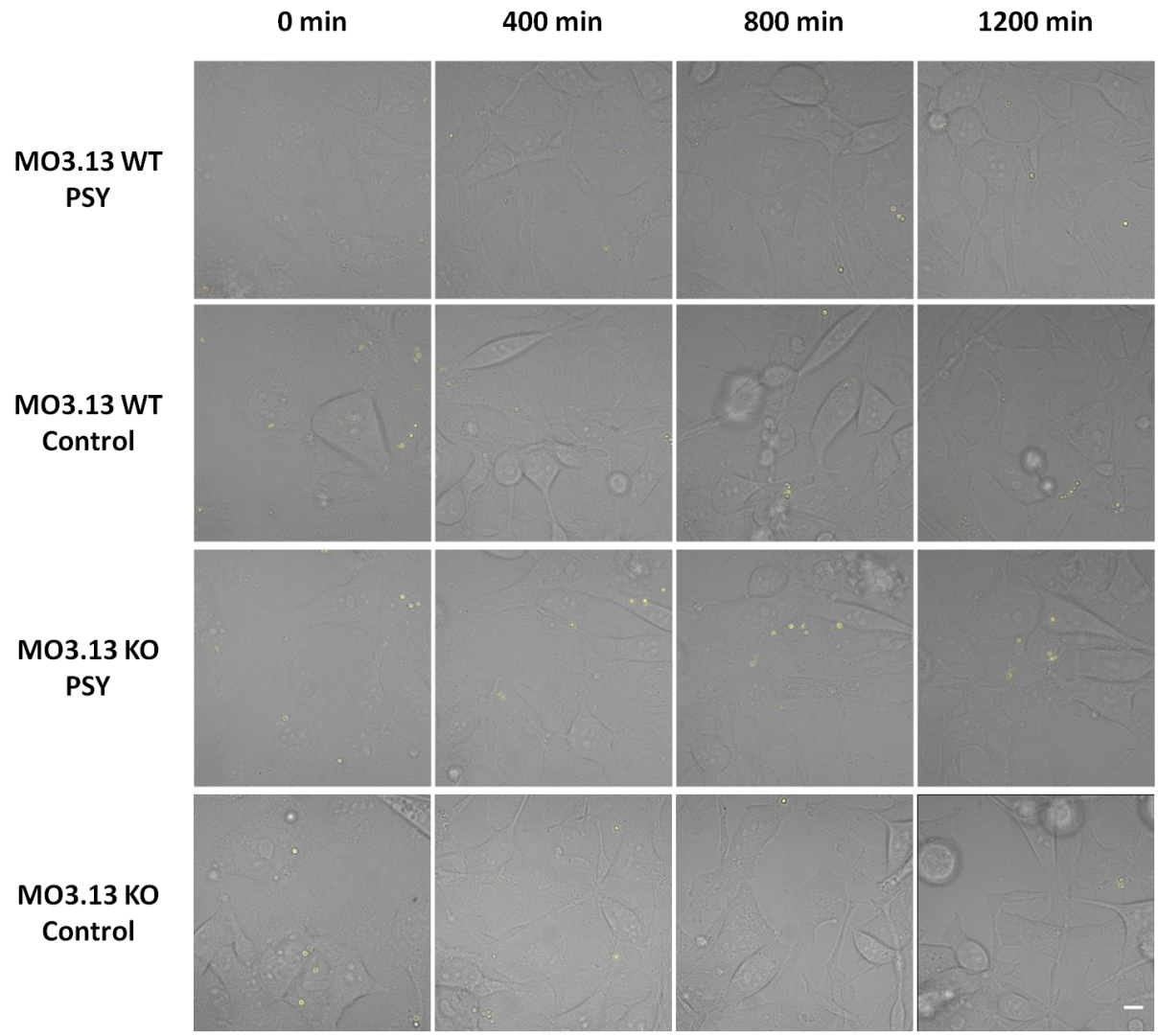

Figure 3.12 MO3.13 cells incubated with psychosine at a concentration of 2 µM. Images of the points in time indicated at the top are shown. "PSY" indicates the panels with cells incubated with psychosine, whereas "Control" indicates the cells in medium not supplemented with psychosine. From the images it can be seen that the cells are viable and healthy throughout the experiment whether psychosine had been added or omitted. SNARF® capsules in all images are yellow indicating the acidic pH-environment of the lysosomes. The scale bar represents 10 µm.

Images like these were evaluated to obtain the time-resolved pH profile of the cells during the presence of psychosine. In Figure 3.13, the results are plotted as "moving mean" of a value and its four next neighbors. The blue lines represent the cells incubated with psychosine, the red lines the controls without psychosine. The graphs show that both the wild-type cells in a) as well as the knockout cells in b) show small variations but no significant changes of pH during the presence of psychosine.

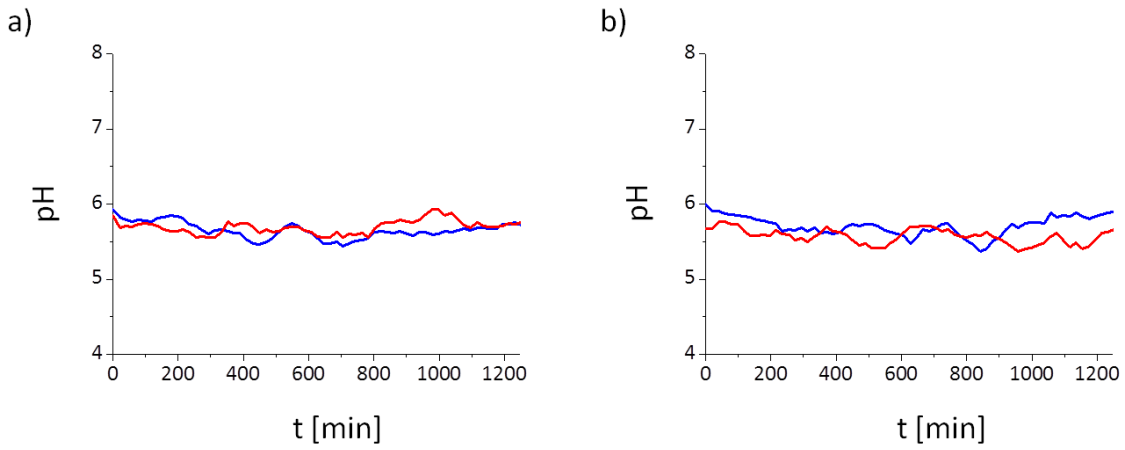

Figure 3.13 MO3.13 cells treated with 2 µM psychosine (blue line) and controls without treatment (red line). a) Wild-type cells as well as b) knockout cells do not show significant response in the lysosomal pH during incubation with 2 µM of psychosine. The figure is taken from manuscript [A8].

Figure 3.14 contains images of MO3.13 cells incubated with 10 µM of psychosine at different points in time. The marking is similar to the images above. Cells incubated with psychosine show round shapes after 600 minutes, which is a sign of apoptosis. Both WT and KO cells show this behavior. In the KO cells, no significant color change is detectable, which is also true for both WT and KO controls.

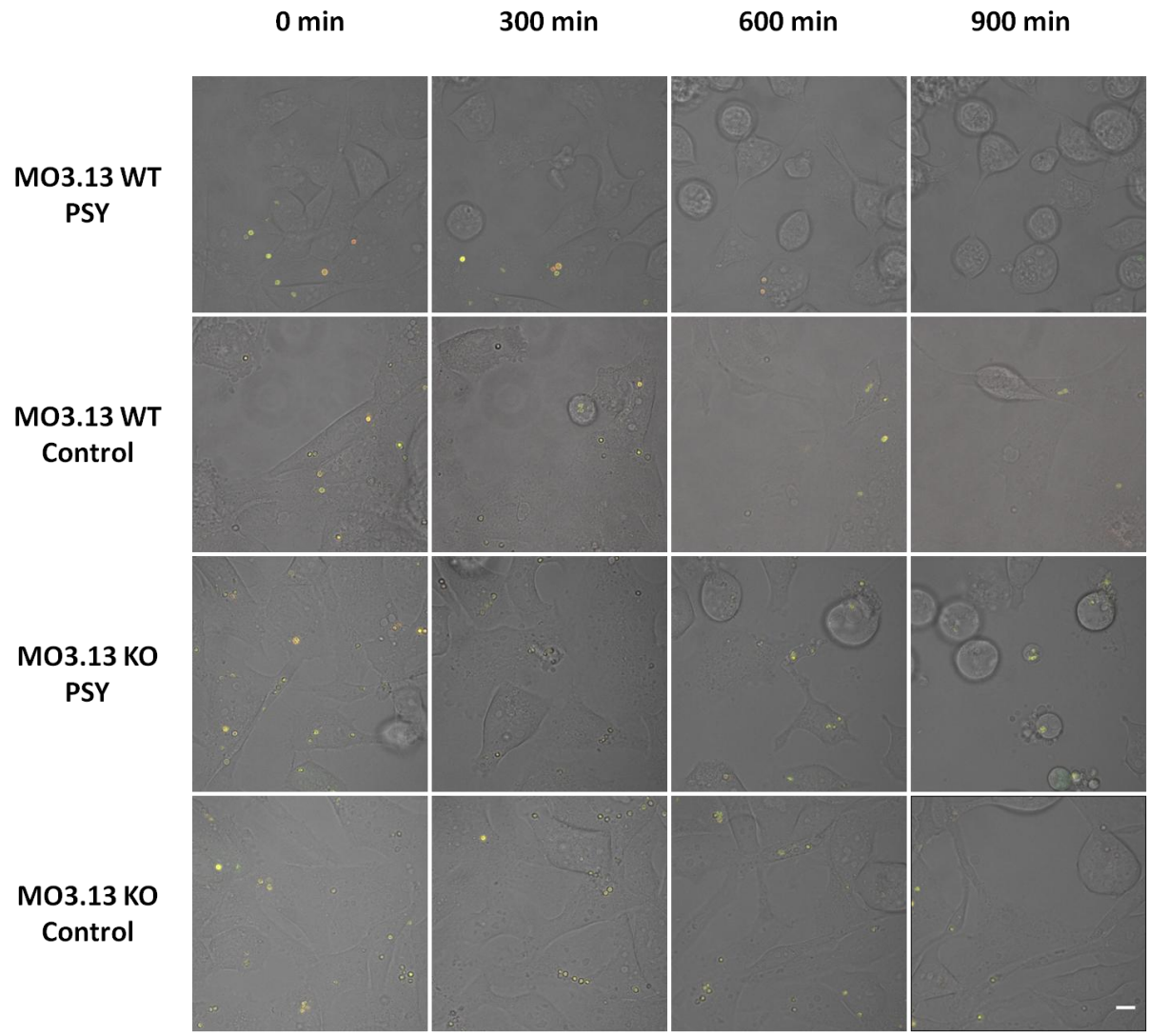

Figure 3.14 MO3.13 cells incubated with psychosine at a concentration of 10 µM. Images of the points in time indicated at the top are shown. "PSY" indicates the panels with cells incubated with psychosine, whereas "Control" indicates the cells in medium not supplemented with psychosine. From the images it can be seen that both the wild-type and the knockout cells suffer from psychosine as cells become round, which is a sign of apoptosis. SNARF® capsules in all images are yellow indicating the acidic pH-environment of the lysosomes. The scale bar represents 10 µm.

Again, the moving mean of a value and its four next neighbors was plotted *versus* time. As before, the blue lines in Figure 3.15 represent the psychosine-treated cells and the red ones the control cells. In the graphs, a significant difference between WT and KO cells is observable. While the KO cells in b) do not show pH changes, the WT cells in a) show a clear rise in pH during the presence and accumulation of psychosine. Note that the images for the two graphs in a) were not taken at the same time and therefore with cells of a different passage, which explains the difference of the 0 hours value. In the other experiments, the psychosine-treated and the control cells were taken from the same culture flask and therefore show no difference in their respective 0 hours value. In c) the color change of one capsule in a WT cell is shown. The two images were taken within a period of 20 minutes. The color changes from green to red, which means that the local pH rose between those two images.

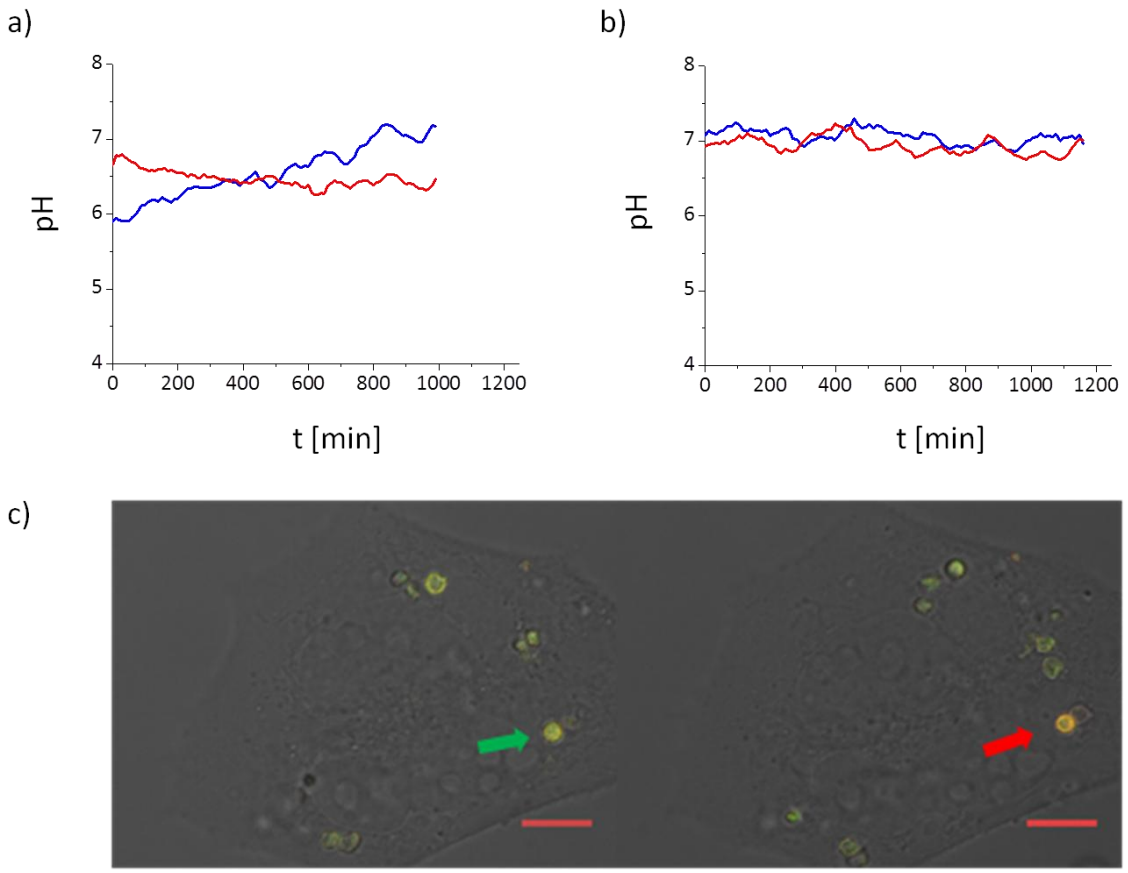

Figure 3.15 MO3.13 cells MO3.13 cells treated with 10 µM psychosine (blue line) and controls without treatment (red line). a) Wild type cells show a significant rise of lysosomal pH during treatment with 10 µM psychosine whereas the control cells keep the lysosomal pH constant. b) In contrary, knockout cells show no significant difference in lysosomal pH whether treated with psychosine or not. c) Example of a capsule, where the color changes from green to red in a MO3.13 wild-type cell. The scale bar corresponds to 10 µm. The figures in a) and b) are taken from publication [A8].

3.3.3.2 Delivery of Galactocerebrosidase to MO3.13 Cells

Krabbe disease arises due to lack of GALC and so far, there is no drug to cure the disease. Other LSDs like Fabry or Gaucher can be treated by enzyme replacement therapy where the missing enzyme is delivered to the patients by infusion. Here the idea was to introduce the lacking enzyme GALC into the cells by capsules and scrutinize if the delivered enzyme could reduce the toxic effects of psychosine. As seen from the images in section 3.3.3.1, cells of the wild type as well as KO cells treated with 10 µM of psychosine show signs of apoptosis after longer incubation times, *i.e.* the cells appear spherical. This was quantified further by MTT cytotoxicity assays. 5 or 10 GALC capsules, and in case of KO cells also 10 empty capsules *per* seeded cell were added to the cells together with the serum-free medium. Control cells without capsules were treated similarly. Afterwards, psychosine was added in serum-free medium at different concentrations from 0 to 20 µM. The results are found in Figure 3.16. The blue and black curves show the cells treated with capsules, the red curves the cells without capsules. The 100 % value was always assigned to cells without capsules and without psychosine, *i.e.* the 0 µM value of the red curves. In KO cells, the red curves show the same trend in both diagrams, and the black curve in b), which represents empty capsules, shows the same behavior. KO cells incubated with GALC-containing capsules show

high viability both with 5 and with 10 GALC capsules *per* seeded cell. The viability, however, is higher for cells treated with 5 capsules. With 10 capsules, the cells show a small loss in viability with rising psychosine concentration and generally lower viability. In WT cells, a contradictory behavior is observed, as shown in c). The untreated cells show high viability independent of the concentration of psychosine, whereas cells incubated with capsules show clearly reduced viability, which means that the capsules have an adverse effect on the WT cells.

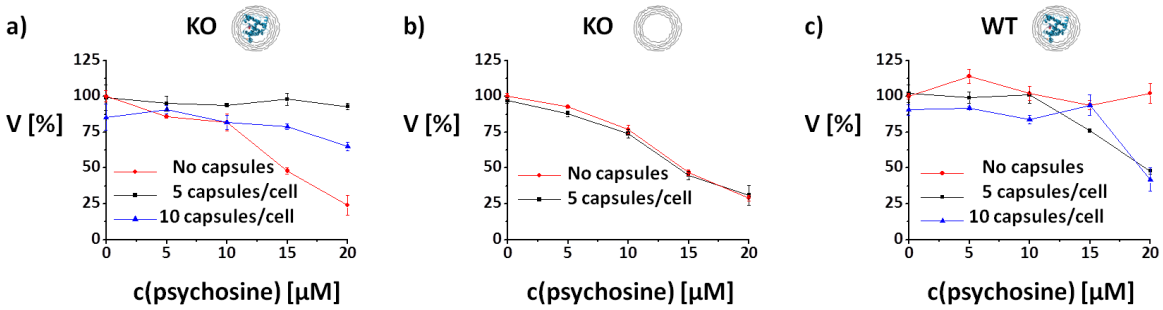

Figure 3.16 MTT assays of MO3.13 KO cells. The viability V after 24 hours is plotted versus the concentration of psychosine. The red curves represent cells without capsules whereas the black curves represent cells treated with a) 5 GALC capsules *per* cell, b) 10 GALC capsules *per* cell, and c) 10 empty capsules *per* cell. The error bars represent standard deviations. The figure has been taken from publication [A8].

Note that values larger than 100 % are a phenomenon often observed in cells treated with substances that do not harm them at these concentrations. The reason is the enhanced metabolism due to stress because of the added substance. The second thing to note is that the viability of WT cells at 10 µM is not reduced although the images of WT cells treated with psychosine show signs of apoptosis, *i.e.* the round shape, *cf.* Figure 3.14. This can be explained because the cells are still viable although they began with apoptotic behavior and therefore the MTT test does not detect reduced metabolism.

4 Discussion

The topic of this thesis was the application of polymer capsules in mammalian cells for diagnosis and therapy, the combination of which is called theranostics. The goal was to have a sensor, which reads out the condition of a certain type of cell, and to apply an appropriate treatment based on the diagnosis. In a first step a diagnostic capsule was synthesized and tested. Knowledge of intracellular ion distributions and concentrations is of high value for the diagnosis of diseases. Especially pH plays a prominent role, and was thus chosen as parameter for the experiments. In general, the analysis of the entire intracellular ion milieu is of relevance for the health condition of cells. However, the intracellular measurements of other ions such as sodium, potassium, chloride, calcium, or magnesium, which are the most important ions for the cells, are problematic. The available ion-sensitive dyes usually are not only sensitive to the specific ion of interest but also show sensitivity to other ions. Problems, for example, occur for dyes used to measure potassium or sodium, as they are usually sensitive to the respective other ion.[22] The same is true for calcium and magnesium. However, in cells, the concentrations of potassium and sodium, or calcium and magnesium, are usually very different, so that the crosstalk between these ions can often be neglected. For Na^+, K^+, and Cl^-, capsules have been produced by encapsulation of the dyes SBFI, PBFI, and MQAE.[22] Another severe problem though is crosstalk with pH. As shown in section 3.1.2, the optical signal of the dyes considered there is influenced massively by pH. This means in principle that determination of ion concentrations with these sorts of dyes is pointless unless the local pH is measured in addition. The first step towards theranostics was to prove the applicability of pH sensitive capsules for diagnosis. This was done in the experiments for publication [A6].[6] The intracellular pH was influenced externally by addition of pH-active substances. SNARF® capsules were used as lysosomal sensors to monitor changes of pH upon stimulation with these substances. In the results section, only monensin was presented. The reader is referred to the paper for detailed information about the other substances, amiloride, bafilomycin A_1, and chloroquine. Monensin caused the lysosomal pH to rise to a level comparable to that of the extracellular medium. This was explained by the H^+/Na^+ antiporter property of monensin that leads to dispelling of pH gradients across membranes. The effect was highly reversible as the pH dropped to the previous level when monensin was removed again. The effects of the other substances showed different pH profiles, as can be found in Figure 5.1 in the appendix. Bafilomycin A_1 showed a slower increase and the pH level was staying high upon removal of the external stimulus. Chloroquine induced a fast rise of the pH comparable to monensin, but after removal of chloroquine from the extracellular medium, the pH kept an elevated level as in the treatment with bafilomycin A_1. This means that the measurement of the pH can be used to discriminate which of the substances was added, in other words, the reason for the pH changes can be diagnosed in this way. Amiloride, though, did not show influence on the lysosomal pH, and therefore amiloride treatment cannot be detected through the pH profile, as it is not different from untreated cells. For the therapeutic task, two systems were employed. The first was to introduce siRNA into the cells to knock down GFP. The second

system was the direct integration of functional enzymes. The first belongs to the spectrum of gene therapy, whereas the second one constitutes an example of enzyme replacement therapy. The challenge thereby was the encapsulation of the biologically active molecules into the capsules and the save delivery into the cells, *i.e.* after uptake, the cargo needed to still be functional. Starting with the delivery of genetic material into cells, biodegradable capsules were used as carriers for fluorescently labeled DNA to examine the efficiency of delivery, and for siRNA to perform transfection. The DNA experiments showed the potential of capsules to introduce DNA into cells and subsequently release it to the cytosol. The results were compared to standard PEI/DNA polyplexes often used for transfection experiments. It could be shown that the capsules had a higher delivery rate than PEI/DNA polyplexes, and furthermore, the delivery could be performed in serum-supplemented medium. This is a big advantage over standard protocols, as deprivation of serum results in stress for the cells. Especially, if the cells are not very robust, for example in case of primary cells, the possibility to transfect cells in serum-containing medium is of importance. The release of DNA or siRNA to the cytosol happened automatically instead of having to be triggered by an external stimulus. Compared to non-encapsulated PEI/siRNA polyplexes, the transfection efficacy in terms of time needed for transfection was enhanced; the effect of siRNA was observable already after 20 hours rather than 48 hours, which is the time normally stated for transfection in standard protocols.[44] Another point addressed in this work was cytotoxicity. Polyplexes made of PEI are known to be toxic for cells, and hence, the PEI concentration has to be kept low, which, however, is a limiting factor for applications of PEI polyplexes. The PEI-filled capsules had reduced adverse effects compared to the same amount of PEI added in non-encapsulated way. PEI was used for the synthesis of polyplexes as it facilitates lysosomal escape of the genetic material. This feature is ascribed to the proton sponge effect. The capsules therefore have the advantage that higher amounts of PEI can be used without the adverse effects, while at the same time offering enhanced proton sponge effect and subsequently increased transfection efficacy. Taken together, it could be shown that the capsules have a great potential for gene therapy as they facilitate enhanced uptake and thus enhanced delivery rates compared to standard transfection agents, and furthermore, the cells do not need to suffer from low serum levels. This feature is especially important for *in vivo*-experiments, where the serum levels cannot be regulated externally. Concerning the delivery of functional enzymes to cells, one problem occurs which is the so-called lysosomal escape dilemma. This term describes the difficulties to make cargo in the lysosome available outside of this vesicle.[89] Therefore, delivery of enzymes was performed in models of LSDs to make use of the fact that capsules are automatically trafficked to the organelle of interest, the lysosome. The challenge of delivery of enzymes to the cells was to deliver functional enzymes and to verify the effectivity and to quantify the efficacy. The experiments were performed with cells representing models of the diseases Krabbe and Fabry. Two different ways of verification of the functionality of delivered enzymes were employed. In case of Fabry, the goal was to measure the intracellular activity of Replagal® delivered to the cells. To do so, the cells were co-incubated with the encapsulated enzyme and the fluorescently labeled substrate Gb3. The activity of the delivered enzyme was determined in terms of fluorescence reduction of the substrate. The capsules used for these experiments were biodegradable, so the enzyme could be released inside the lysosomes. The results clearly

showed that the enzyme delivered by capsules had activity inside the cells. Furthermore, a reduction of about 80 % of fluorescence of NBD-Gb3 could be obtained. The optimum of 100 % was hereby defined by a negative control where no substrate was added before. Compared to Replagal® solution, however, the efficiency was smaller, *i.e.* the amount of Replagal® needed when capsules were used was higher than in the free enzyme solution. Nonetheless, the results can be seen as proof of concept for the delivery of defective enzymes to the lysosomes of cells and future research might lead to better results. Concerning Krabbe disease, the MO3.13 cell line can be used as simple model to study basic features of the disease. With the use of KO cells, the absence of the enzyme GALC can be modeled. Incubation with psychosine simulates the condition of accumulation of sphingolipids and cerebrosides in the oligodendrocytes of Krabbe patients. MO3.13 cells incubated with high concentrations of psychosine showed apoptosis as the internalized psychosine is toxic for them. Therefore, the effectivity of delivery of GALC by biodegradable capsules could be verified by viability assays. The test was performed both with WT cells and KO cells. The findings of the MTT cytotoxicity assays showed that the delivery of GALC to KO cells by capsules was successful and that psychosine did not have an adverse effect on cells provided with the enzyme. On WT cells, psychosine did have less adverse effect due to the presence of intrinsic GALC. Once the cells were treated with capsules though, psychosine induced an adverse effect on them. This means that treatment with capsules only makes sense in case of KO cells. This is an example where theranostics plays an important role; with a preliminary diagnosis test verifying total absence of the enzyme, the applicability of enzyme replacement therapy can be assured. One possibility for diagnosis can be obtained from pH measurements. The pH of the MO3.13 WT and MO3.13 KO cells was measured in the presence of psychosine and two different effects were found. In the WT cells, *i.e.* the cells containing a fraction of GALC, the pH rose in the presence of psychosine. On the contrary, the pH in KO cells did not change in the presence of psychosine. With help of these findings, it is possible to decide if a given sample of MO3.13 cells is of WT or KO type and based on this, one can decide if treatment of the cells with GALC capsules is possible or not. Concerning the goals of the thesis, the following could be achieved. The usefulness of capsules as diagnostic tool could be shown. When the pH profile of the lysosomal pH is known, the substances bafilomycin A_1, chloroquine, and monensin can be distinguished, *i.e.* a diagnosis which of them has been added to the cells is possible. The applicability of capsules as carrier of therapeutics, either in form of nucleic acids or in form of enzymes, was demonstrated. In case of siRNA, the successful knockout of GFP was obtained and moreover the capsules were more efficient compared to the standard protocol. The delivery of functional Replagal® by capsules was also successful, as intracellular activity could be observed. However, the results of Replagal® solution showed a higher metabolic rate for the conversion of Gb3 and smaller amounts of Replagal® were needed than in the assays with encapsulated Replagal®. The capsule treatment is therefore less efficient than Replagal® solution. The combination of diagnostics and therapy was undertaken in the Krabbe model. It could be shown that the pH profile can be employed to determine if cells are of KO type or WT. The decision whether to treat cells with GALC-filled capsules or not therefore can be made based on the diagnosis obtained by the pH capsules. This can be seen as an *in vitro*-example for theranostics.

Outlook

So far, capsules and other carriers are used individually, *i.e.* only one type of capsule or carrier is employed. With the possibility to modify the capsules in various ways and label them differently, the next step is to use different capsules simultaneously to monitor different analytes in the cells or to sense and deliver at the same time. Ultimately, the goal is to produce multifunctional capsules for sensing of different analytes or even capsules for both delivery and sensing. Cystic fibrosis (CF), also called mucoviscidosis, is a disease that could serve as model for this research. In CF the cystic fibrosis transmembrane conductance regulator (CFTR) gene responsible for the expression of a chloride channel is expressed wrongly. The most common dysfunctional version of the gene leads to the misfolding mutation ΔF 508. This misfolding results in low chloride levels inside endothelial cells. The possibility to introduce RNA into cells by capsules as shown in this thesis, but also in other publications[19, 81] paves the way to deliver messenger RNA (mRNA) of the chloride channel into cells to trigger the correct expression of the channel. A chloride-sensitive capsule could then be employed to monitor the changes of chloride levels in the cells to verify the expression of the chloride-channels. Other methods to verify the expression of the ion channel like Western Blot require disrupting the cells to detect the protein of interest in the resulting suspension. In the way described here, the protein could be detected non-invasively in living cells. Another possibility to make use of the results obtained in this thesis is to make the step from *in vitro*- to *in vivo*-experiments. For this purpose, the capsules should have a size of some 100 nm as otherwise capillaries may be blocked. The fabrication of nanocapsules as small as 100 nm or less has been demonstrated already although the synthesis is different from the one used in this thesis. Current methods to produce enzyme nanocapsules can be found in a recent reviews by Shimanovich *et al.*[27] and Cui *et al.*[8] Animal models for Krabbe and for Fabry disease are readily available. A similar disease as Krabbe is found in the twitcher mouse.[90] In this mouse, the deficiency of GALC and subsequent accumulation of sphingolipids and cerebrosides in the oligodendrocytes occurs naturally. Similarly, a mouse model of Fabry disease can be employed.[52, 91] Difficulties of Replagal® treatment, as already outlined in section 3.3.2, include degradation of the drug in the blood stream, imbalanced distribution within the body and hence inefficient treatment, and immune responses. Capsules serve as protective shield for the drug in the blood stream as proteins and big molecules cannot pass through the capsule walls. Uptake of free Replagal® by cells is mediated by mannose-6-phosphate receptors. As these receptors are distributed unevenly among cells in the body, the treatment can be affected as Replagal® will accumulate in cells where there are receptors, whereas cells without receptors will not be targeted. Capsules, however, are taken up receptor-independently, and thus also cells without these receptors will be targeted. Moreover, if capsules are modified by magnetic nanoparticles in their walls, the distribution of the carriers can be controlled by magnetic field gradients.[92, 93] Finally, also the combination of the hitherto Replagal® treatment with magnetic carriers may improve the treatment, as the carriers could be directed to organs where receptors are not sufficiently expressed, whereas free Replagal® will be internalized by receptor-expressing cells as before.

5 Appendix

5.1 Results of Bafilomycin A_1, Chloroquine, and Amiloride

For completeness, the results of the other agents used for publication [A6] are depicted in Figure 5.1. The figure of monensin in b) and the control in e) were shown in section 3.1.3. Bafilomycin A_1 (a) induces a rapid increase of pH and the pH level stays high after rinsing. Monensin induces a rapid increase, but after rinsing, the pH drops to the starting level. After incubation with chloroquine (c), the pH rises quickly to high levels, and after rinsing, the pH drops slowly to the starting level before addition of chloroquine. Amiloride (d) does not influence the lysosomal pH.

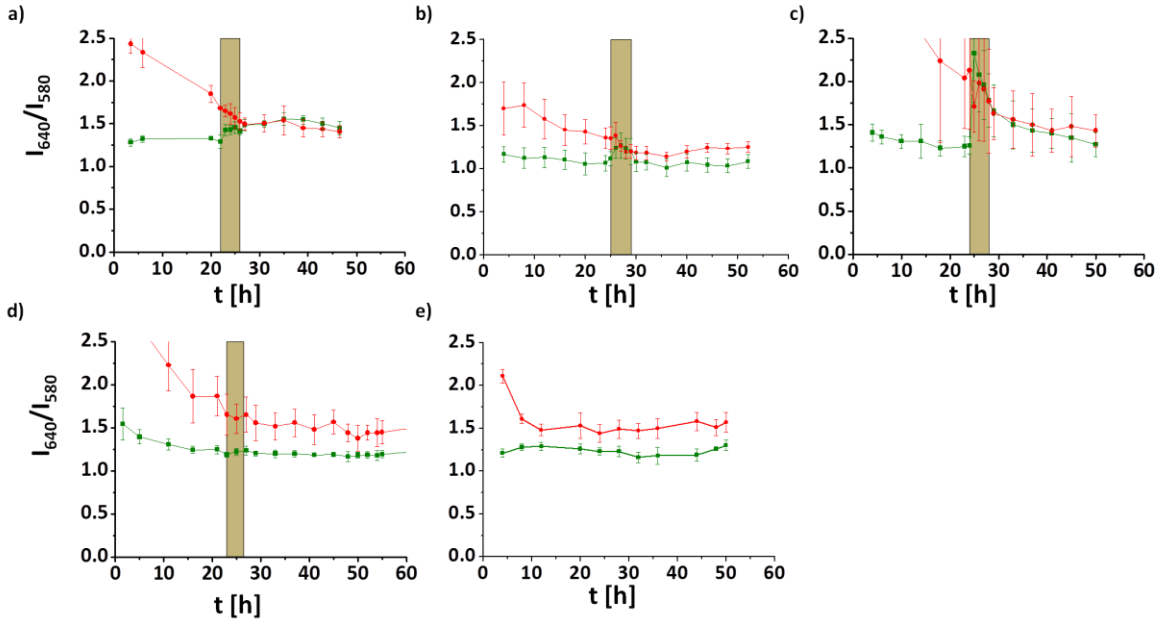

Figure 5.1 Results of the treatment of MCF-7 cells with different agents. a) Bafilomycin A1 (600 nM), b) Monensin (20 µM), c) Chloroquine (100 µM), d) Amiloride (1 mM). In e) no agent was added. The ratio of red to yellow fluorescence (I_{640}/I_{580}) origination from capules inside the lysosome (drawn in green) and control capsules in the extracellular medium (drawn in red) is plotted versus time. Error bars represent standard deviations. The figure has been adapted from publication [A6].

5.2 GFP Knockout with PEI/siRNA Polyplexes

In the knockout experiments, a comparison of polyplexes and capsule-embedded polyplexes was performed based on the amount of siRNA. Here, the results of an experiment with a high amount of siRNA delivered with polyplexes are shown for completeness to prove the possibility to knock out GFP with PEI/siRNA polyplexes. In Figure 5.2, the curves from section 3.2.3 are shown together with data of an experiment of PEI/siRNA polyplexes with a much higher amount of siRNA, namely $400 \cdot 10^{-3}$ µg instead of $10 \cdot 10^{-3}$ µg. The decrease of GFP intensity is clearly visible showing that the polyplexes work in principle.

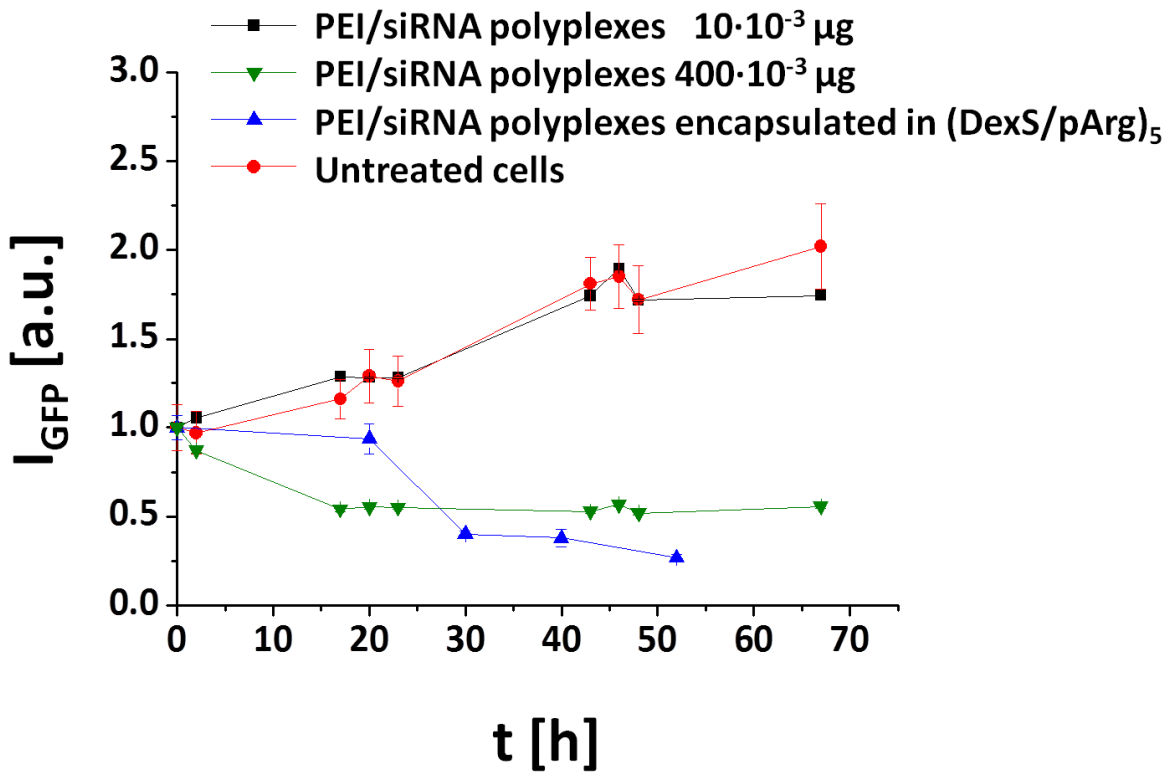

Figure 5.2 Normalized GFP intensity I_{GFP} against time. The time-dependent change of GFP for PEI/siRNA polyplexes containing $10 \cdot 10^{-3}$ µg or $400 \cdot 10^{-3}$ µg siRNA *per* experiment, as well as for encapsulated PEI/siRNA with a final amount of $6.4 \cdot 10^{-3}$ µg siRNA *per* experiment are depicted. Intensities are normalized to their respective 0 hours value. Error bars represent standard deviations of the mean. The figure has been taken from the supporting information of publication [A7].[4]

5.3 Cytotoxicity of Metallic Nanotubes

The author did this work for a co-operation with a group from the University of the Basque Country. Ricardo Sanchéz Pinedo from the Spanish group synthesized the nanotubes, whereas the author did all cytotoxicity measurements described in this section. The results were published in the PhD thesis of Ricardo Sanchéz Pinedo.[94] For details of the nanotube synthesis, the reader is referred to this PhD thesis.

Conduction of the Experiments

Cytotoxicity of nanotubes (NTs) and ions was measured according to the following protocol: Vero cells were seeded in 96-well plates at a density of 10,000 cells per well and were grown for 24 hours in cell growth medium. Then, the cells were rinsed with PBS and medium containing NTs or ions at appropriate concentrations was added to the wells. Concentrations were adjusted in a way that a wide range of concentrations was covered. The cells were incubated at 37 °C and 5% CO_2 atmosphere for 24 hours. After that, the cells were rinsed with PBS and a freshly prepared solution of medium containing 10% resazurin was added to the wells. The cells were incubated for 3 hours at 37°C and 5% CO_2. Non-fluorescent resazurin is oxidized by living cells to fluorescent resorufin. Therefore, the fluorescence intensity is a measure of the viability of the cells. After incubation, the fluorescence emission spectrum of the solution was recorded. Hereby, the wells were excited at 560 nm and fluorescence emission was recorded from 572 nm to 650 or 700 nm. The recorded spectra I(c,λ) for cells incubated with Cd^{2+} ions at different concentration are shown as example in Figure 5.3. The intensities of 685 to 700 nm (or 640 nm to 650 nm) were averaged and subtracted as background from the average of 580 to 585 nm, which was the maximum of the emission spectrum. The background-corrected, averaged intensities I(c) were plotted *versus* the concentration, as shown as example in Figure 5.3b. The concentration-dependent fluorescence intensities I(c) were then fitted with the sigmoidal function

$$\mathrm{I(c)} = \frac{I_{max} - I_{min}}{1 + \left(\frac{c}{c_0}\right)^p} + I_{min}.$$

c_0 is the concentration, at which the viability of the cells was reduced to half of its activity. In Figure 5.3, the fluorescence spectra of cells incubated with Cd ions is shown, which serves as positive control of the resazurin assay. In a) the entire spectra are displayed, whereas in b) the background-corrected averages of the maxima are plotted. From the fit, the concentration c_0 at which half of the cells have died was obtained.

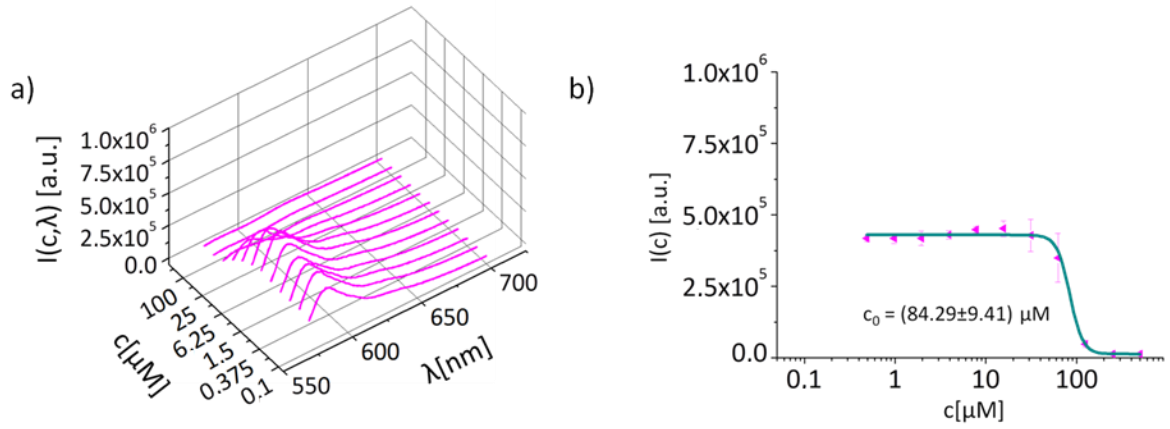

Figure 5.3 Fluorescence spectra of cells incubated with different concentrations of Cd^{2+} ions and the resazurin assay. a) Raw data given as recorded fluorescence spectra I(c, λ). b) Background-corrected average intensities I(c) as derived from the raw data. A fit and the derived c_0 value are shown.

As sample, $Pr_{0.6}Sr_{0.4}Fe_{0.8}Co_{0.2}O_3$ NTs and, as control, salts containing the metal ions out of which the NTs were composed were used. Three different methods for the synthesis of the NTs were used, which were named LiO 10, LiO 80, and Sg 80. NTs were mixed with medium at a concentration of 1 $mg \cdot mL^{-1}$ and stirred overnight at room temperature with a magnet stirrer to obtain a homogenous suspension. It has to be noted that the NTs did not dissolve in aqueous solution. Besides this procedure over 1 day, the NTs were also left for 8 days or 3 weeks, respectively, in growth medium, before the suspensions were added to the cells. In this way, leaching of ions from the NPs over time was investigated. Salts containing Co^{2+}, Fe^{3+}, Pr^{3+}, Sr^{2+}, and Cd^{2+} were directly dissolved in cell growth medium. In case of Pr^{3+}, the concentrations were estimated, as the manufacturer did not provide the water content of the salt $PrCl_3 \cdot xH_2O$. The fluorescence spectra I(c) obtained for the salt solutions are displayed in Figure 5.4. The fluorescence spectra I(c) obtained for NTs are displayed in Figure 5.5.

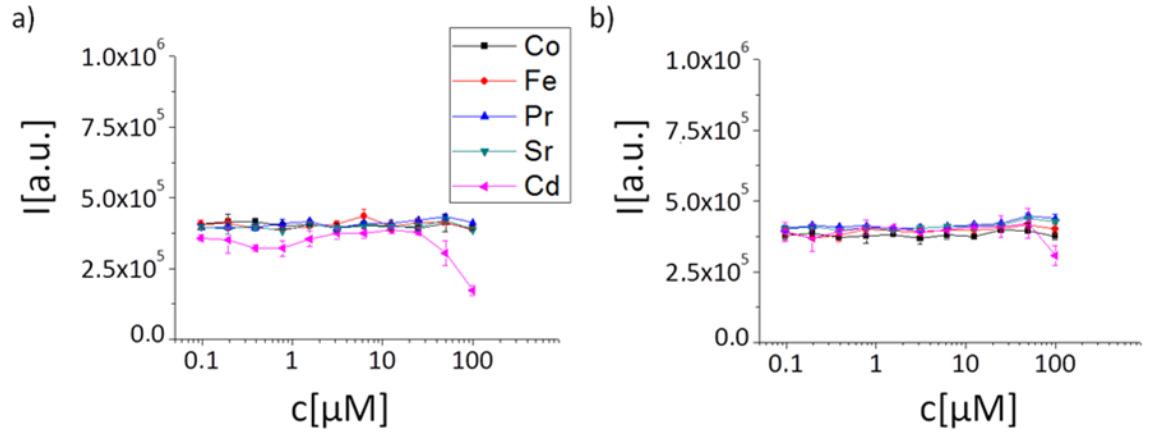

Figure 5.4 Background-corrected average fluorescence intensities I(c) of cells incubated with different metal salts and the resazurin assay. a) and b) display 2 sets of experiments. The mean values are based on 8 values.

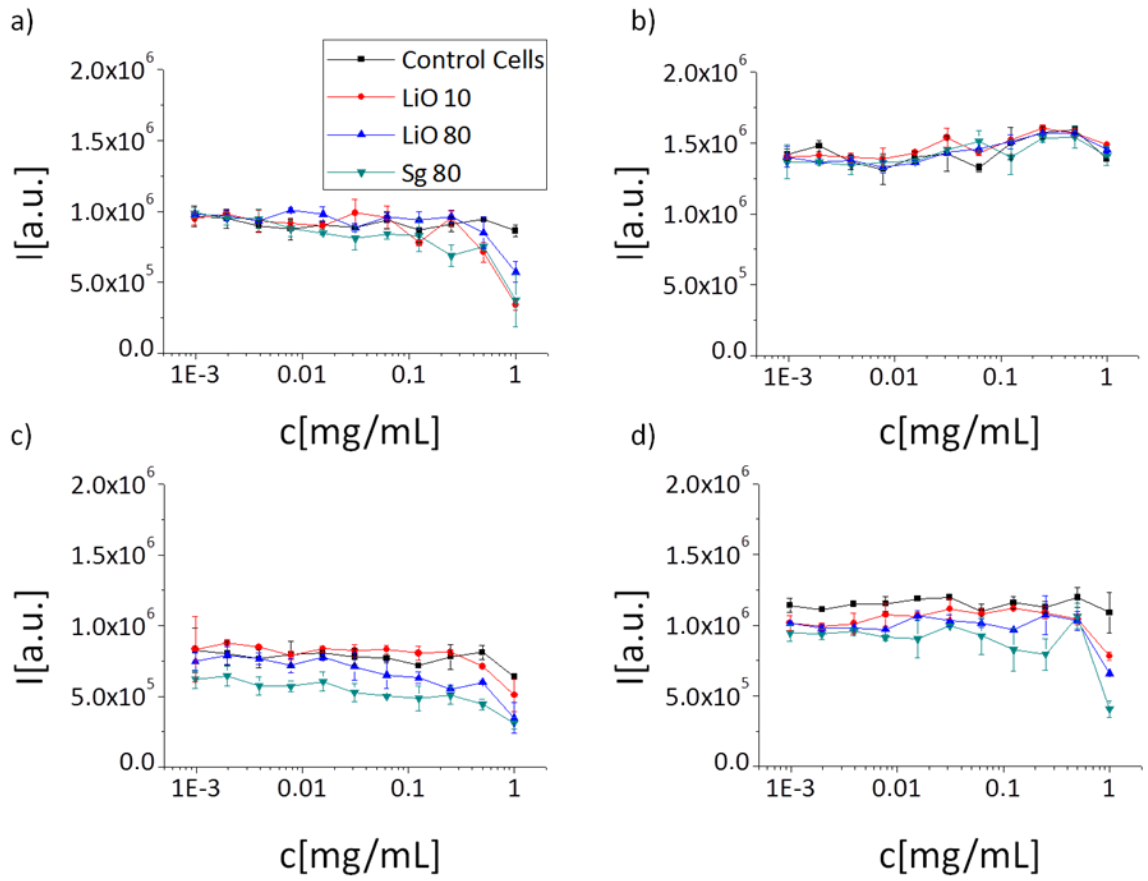

Figure 5.5 Background-corrected average fluorescence intensities I(c) of cells incubated with and without nanotubes (batches LiO10, LiO80, Sg80) and the resazurin assay. a) Nanotubes were suspended in medium 1 day prior to addition to the cells. b) Repetition of experiment as described in a). c) Nanotubes were suspended in medium 8 days prior to addition to the cells. d) Nanotubes were suspended in medium 3 weeks prior to addition to the cells. The error bars are the standard deviations. The mean values are based on 2 values.

Except for Cd^{2+} at high concentrations, none of the metal ions showed reduced cell viability under the used conditions (*cf.* Figure 5.4). For the NTs, some reduced viability was observed at high concentrations (*cf.* Figure 5.5). In case NTs were longer incubated in medium (before addition of cells), there is a tendency that the NTs cause more cytotoxic effects to cells. This is likely to be due to increased leaching of ions from the NTs to the solution. In order to compare the effects of NTs and free ions, the data was normalized. Normalization, as displayed in Figure 5.6, was done by calculating the amount of each ion in one NT and converting all concentrations to $mg \cdot mL^{-1}$. The molecular weight M_W of $Pr_{0.6}Sr_{0.4}Fe_{0.8}Co_{0.2}O_3$ NTs is 224 $g \cdot mol^{-1}$. The molar masses of O, Pr, Sr, Fe, and Co are 16, 141, 88, 56, and 59 $g \cdot mol^{-1}$, respectively. Thus, x = 21 %, 38%, 16%, 20%, and 5% of the mass of NTs is composed out of O, Pr, Sr, Fe, and Co, respectively. In order to calculate the effective mass concentration $c^*[mg \cdot mL^{-1}]$ of ions in reference to the NTs, the content x of ions *per* NT was used as $c^*[mg \cdot mL^{-1}] = c[\mu M] \cdot M_W/x$. In this way, an ion, which is only present at fraction x in the NTs, accounts for an x-fold higher effective NT concentration. To give an example, for Pr^{3+} the concentration c = 100 µM corresponds to c* = 37 $mg \cdot mL^{-1}$ as calculated in the following: $c^* \left[\frac{mg}{mL}\right] = c[\mu M] \cdot \frac{M_W}{x} = \frac{100\ \mu M \cdot 141 \frac{g}{mol}}{38\ \%} = 37\ {}^{\mu g}/_{mL}$.

The normalized concentrations of the ions are plotted in Figure 5.6, which allows for comparison with the viability results obtained with the NTs. In the overlap of both graphs, which reaches up to 0.1 mg·mL^{-1} depending on the specific ion, the data consistently does not show reduced viability of cells. Only for NT-concentrations of 1 mg·mL^{-1}, the intensity values decrease significantly. The contents of Pr, Sr, Fe, and Co in 1 mg NTs are 377, 156, 199, and 53 µg, respectively. Note, that these amounts are only set free, if the NTs were fully disintegrated.

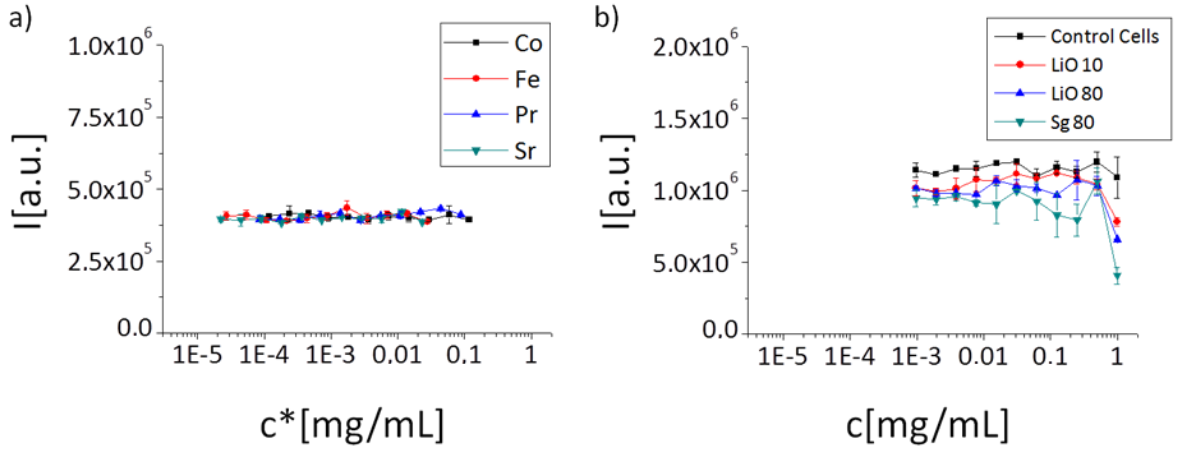

Figure 5.6 Background-corrected average fluorescence intensities I(c*) and I(c) of cells incubated with different metal salts and NTs and the resazurin assay. a) Normalized ion data from Figure 5.4 a) (without Cd^{2+}) b) NTs in suspension for 3 weeks (data from Figure 5.5 d)).

5.4 List of Abbreviations

ATCC	American Type Culture Collection
CCD	Charge-Coupled Device
CF	Cystic Fibrosis
CFTR	Cystic Fibrosis Transmembrane Conductance Regulator
CLSM	Confocal Laser Scanning Microscope
Cy5	A fluorescent dye
DNA	Desoxyribonucleic Acid
ERT	Enzyme Replacement Therapy
FITC	Fluorescein isothiocyanate
FSC	Forward Scattering
GALC	Galactocerebrosidase
GFP	Green Fluorescent Protein
GLA	α-Galactosidase A
KO	Knockout
LbL	Layer-by-Layer
LSD	Lysosomal Storage Disease (Disorder)
MAEC	Mouse Aorta Endothelial Cells
mRNA	Messenger RNA
MTT assay	Viability Test based on the chemical MTT
NT	Nanotube
PBFI	A fluorescent potassium-sensitive indicator
RNA	Ribonucleic Acid
ROI	Region of Interest
rpm	Rotations per Minute
SBFI	A fluorescent sodium-sensitive indicator
SCC	Side Scattering
siRNA	Silencing RNA
WT	Wild-Type
ΔF508	A gene mutation responsible for occurrence of Cystic Fibrosis

6 Publications

This thesis is a cumulative dissertation and therefore the publications constituting it are shortly summarized here and the contribution of the author is described. The contributions of the author to the research papers used for this thesis are also described in the results part at the beginning of each section.

6.1 Reviews

[A1][95] C. Carillo-Carrion, **M. Nazarenus**, S. Sánchez Paradinas, S. Carregal-Romero, M. Jesús Almendral, M. Fuentes, B. Pelaz, P. del Pino, I. Hussain, M.J.D. Clift, B. Rothen-Rutishauser, X. Liang., W.J. Parak, Metal ions in the context of nanoparticles towards biological applications, *Curr. Opin. Chem. Eng.* **2014**, *4*, 88 (Paper attached)

In this review, the interactions of nanoparticles and ions in biological context are discussed. Three major topics are pointed out; unintended modification of the particles such as corrosion and dissolution of the particles, intended modification of the particles with certain ions for new applications, and nanoparticles for the detection of ions, for example inside cells.

The author did literature research, corrections and amendments of the text, and the editoring of the manuscript before final submission.

[A2][39] **M. Nazarenus**, Q. Zhang, M.G. Soliman, P. del Pino, B. Pelaz, S. Carregal-Romero, J. Rejman, B. Rothen-Rutishauser, M.J.D. Clift, R. Zellner, G.U. Nienhaus, J.B. Delehanty, I.L. Medintz, W.J. Parak, Interaction of Colloidal Nanoparticles with Mammalian Cells: What Have We Learned Thus Far? *Beilstein J. Nanotechnol.* **2014**, *5*, 1477 (Paper attached)

In this review, the principles of interaction between cells and colloidal nanoparticles are outlined. The focus is put on the fundamentals of interactions rather than special phenomena. Critical assessment of effects on colloidal particles taking place in biological media, such as agglomeration and formation of a protein corona on the particles, and the consequences for uptake by cells is presented. The problem how to compare the results of studies with different methodologies is addressed.

The author did a large part of the literature research, included the contributions of the different authors into coherent text and did the editing before submission. He as well did part of the revision before final acceptance.

[A3][38] K. Kantner, S. Ashraf[#], S. Carregal-Romero, C. Carrillo-Carrion, M. Collot, P. del Pino, W. Heimbrodt, D. Jimenez de Aberasturi, U. Kaiser, L. I. Kazakova, M. Lelle, N. Martinez de Baroja, J. Montenegro, **M. Nazarenus**, B. Pelaz, K. Peneva, P. Rivera Gil, N. Sabir, L.M. Schneider, L. I. Shabarchina, G.B. Sukhorukov, M. Vazquez, F. Yang, W.J. Parak,

Particle-Based Optical Sensing of Intracellular Ions at the Example of Calcium - What are the Experimental Pitfalls?, *Small.* DOI: 10.1002/smll.201402110 (paper attached)

[#] alphabetical order

This review deals with intracellular ion sensing. The intracellular location and trafficking of colloidal nanoparticles are discussed. The difficulties arising due to crosstalk of emission of different fluorophores as well as the influence of pH on fluorophores are addressed. Experimental data is shown to underline the problematic.

The author recorded and evaluated the data of crosstalk of ion-sensitive dyes with pH and wrote the part of the supporting information describing these experiments in detail.

[A4][96] P. del Pino, X. Jiang, D. Valdeperez, **M. Nazarenus**, Z. Wang, F. Stellacci, W.J. Parak, Nanomaterials for Smart Food Packaging and Quality Control, *Part. Part. Syst. Charact.* **2014**, DOI: 10.1002/ppsc.201400192 (paper attached)

Future perspectives for the use of nanomaterials in food science, especially for smart ways of packaging, are presented in this review. Possible ways of quality control and enhancing sustainability of food utilizing nanotechnology are described.

The author did literature research, wrote the part of the manuscript describing dual-readout particles, and did the editing before the first submission.

6.2 Book Chapters

[A5][97] P. Rivera Gil, **M. Nazarenus**, W.J. Parak, Composite Colloidal Nanosystems for Targeted Delivery and Sensing, in Bioinspired and Biomimetic Systems for Drug and Gene Delivery, Gu, Z., Ed.; Wiley-VCH: Weinheim, **2015**; p.61-81 (galley proofs attached)

In the chapter of this book, the applicability of capsules in drug delivery and sensing, which are the main topics also of this thesis, is presented. In the part about sensing, the data for the chapter includes the main results of publication [A6]. Furthermore the internalization and intracellular location of capsules are shown and an outlook on delivery of genetic material is given and ways of release inside the cells are described.

The author's contribution was part of the data for pH sensing and proofreading of the manuscript.

6.3 Research Papers

[A6][6] P. Rivera Gil, **M. Nazarenus**, S. Ashraf, W.J. Parak, pH-sensitive capsules as intracellular optical reporters for monitoring lysosomal pH changes upon stimulation, *Small* **2012**, *8*, 943 (paper attached)

This paper showed the applicability of capsules as intracellular long-term pH probes. The cells were stimulated with four different substances, amiloride, bafilomycin A_1, chloroquine, and monensin. The effect on the lysosomal pH was examined. The results of monensin are presented in this thesis as it was the author's suggestion to examine the effect of monensin.

The author did a major part of the experiments and evaluations of all the different substances. Furthermore he wrote part of the supporting information, and established the evaluation method.

[A7][4] C. Ganas, A. Weiß, **M. Nazarenus**, S. Rösler, T. Kissel, P. Rivera Gil, W.J. Parak, Biodegradable capsules as non-viral vectors for *in vitro* delivery of PEI/siRNA polyplexes for efficient gene silencing, *J. Control. Release* **2014**, *196*, 132 (paper attached)

In this paper, biodegradable capsules were used to deliver siRNA into living cells to perform down-regulation of GFP. The results showed a better efficacy for delivery of genetic material with capsules compared to that of the polyplexes used regularly. Furthermore, the toxicity of the capsules was scrutinized and compared to that of standard PEI polyplexes.

The author did all evaluations of the experimental data presented in the paper, *i.e.* image processing and quantification of the data. The cytotoxicity experiments were performed by the author. The author helped with the manuscript and wrote part of the supporting information and did part of the revision after the peer-review process.

[A8] M. Nazarenus, M. López Sánchez, N. García, J. Rejman, I. Abasolo, P. Rivera Gil, W.J. Parak, Polymer capsules as theranostic delivery and analysis vehicle for universal *in vitro* screening assays in the case of lysosomal storage diseases, in preparation (draft attached)

In this paper, capsules were used for pH sensing and enzyme delivery. Cell culture models of the lysosomal storage diseases Krabbe and Fabry were employed to show the applicability of capsules as carrier for enzyme delivery. In these diseases, certain enzymes are deficient. The capsules were used to deliver the deficient enzymes to the cells and intracellular activity could be verified. In case of Krabbe disease, also the lysosomal pH was monitored in a long-term manner. A difference was found between cells expressing the enzyme and enzyme-deficient cells.

The author did all capsule syntheses and recorded and evaluated all pH sensing experiments. Furthermore, part of the flow cytometry experiments was done by the author under guidance. Help was obtained for MTT cytotoxicity assays and Western Blots. The author wrote part of the manuscript and the major part of the supporting information, and did the editing.

[A9] M.M. Ferraro, M. De Luca, R. Hartmann, P. Rivera Gil, A. Klingl, **M. Nazarenus**, A. Ramirez, W.J. Parak, C. Bucci, R. Rinaldi, L.L. del Mercato, pH-sensitive Capsules as Intracellular Optical Reporters for Studying the Role of the V1G1 Subunit of Vacuolar ATPase, in preparation. (draft not attached)

In this paper, the expression of the vacuolar ATPase in cells was modified and the effect on the lysosomal pH was measured with capsules. The pH signal of the capsules was recorded

from the first contact to the membrane of the cells until the final location in the lysosomes was reached. Different results were obtained whether vacuolar ATPases were enhanced or diminished. Transmission electron microscopy (TEM) images of the cells with capsules were obtained to show the intracellular location of the capsules.

The author helped with the cell culture and capsule preparation for TEM images, and did TEM imaging.

7 Bibliography

[1] F. Caruso, R. A. Caruso, H. Möhwald, *Science* **1998**, *282*, 1111.

[2] E. Donath, G. B. Sukhorukov, F. Caruso, S. A. Davis, H. Möhwald, *Angew. Chem. Int. Edit.* **1998**, *37*, 2202.

[3] P. Rivera_Gil, S. D. Koker, B. G. De_Geest, W. J. Parak, *Nano Lett.* **2009**, *9*, 4398.

[4] C. Ganas, A. Weiß, M. Nazarenus, S. Rösler, T. Kissel, P. Rivera_Gil, W. J. Parak, *J. Control. Release* **2014**, *196*, 132.

[5] S. De Koker, T. Naessens, B. G. De Geest, P. Bogaert, J. Demeester, S. De Smedt, J. Grooten, *J. .Immunol.* **2010**, *184*, 203.

[6] P. Rivera Gil, M. Nazarenus, S. Ashraf, W. J. Parak, *Small* **2012**, *8*, 943.

[7] M. Ochs, S. Carregal-Romero, J. Rejman, K. Braeckmans, S. C. De Smedt, W. J. Parak, *Angew. Chem. Int. Edit.* **2013**, *52*, 695.

[8] J. W. Cui, M. P. van Koeverden, M. Mullner, K. Kempe, F. Caruso, *Adv. Colloid Interfac.* **2014**, *207*, 14.

[9] S. De Koker, B. G. De Geest, S. K. Singh, R. De Rycke, T. Naessens, Y. Van Kooyk, J. Demeester, S. C. De Smedt, J. Grooten, *Angew. Chem. Int. Edit.* **2009**, *48*, 8485.

[10] L. Kastl, D. Sasse, V. Wulf, R. Hartmann, J. Mircheski, C. Ranke, S. Carregal-Romero, J. A. Martínez-López, R. Fernández-Chacón, W. J. Parak, H.-P. Elsaesser, P. Rivera_Gil, *ACS Nano* **2013**, *7*, 6605.

[11] S. De Koker, B. G. De Geest, C. Cuvelier, L. Ferdinande, W. Deckers, W. E. Hennink, S. De Smedt, N. Mertens, *Adv. Funct. Mater.* **2007**, *17*, 3754.

[12] Y. Yan, M. Bjornmalm, F. Caruso, *Chem. Mater.* **2014**, *26*, 452.

[13] Y. Yan, Z. W. Lai, R. J. A. Goode, J. Cui, T. Bacic, M. M. J. Kamphuis, E. C. Nice, F. Caruso, *ACS Nano* **2013**, *7*, 5558.

[14] L. L. del Mercato, M. M. Ferraro, F. Baldassarre, S. Mancarella, V. Greco, R. Rinaldi, S. Leporatti, *Adv. Colloid Interfac.* **2014**, *207*, 139.

[15] S. Carregal-Romero, M. Ochs, W. J. Parak, *Nanophotonics* **2012**, *1*, 171.

[16] Z. J. Wang, L. Qian, X. L. Wang, H. Zhu, F. Yang, X. R. Yang, *Colloid. Surface. A* **2009**, *332*, 164.

[17] T. Borodina, E. Markvicheva, S. Kunizhev, H. Moehwald, G. B. Sukhorukov, O. Kreft, *Macromol. Rapid Comm.* **2007**, *28*, 1894.

[18] O. E. Selina, S. Y. Belov, N. N. Vlasova, V. I. Balysheva, A. I. Churin, A. Bartkoviak, G. B. Sukhorukov, E. A. Markvicheva, *Russ. J. Bioorg. Chem+* **2009**, *35*, 103.

[19] J. Ruesing, O. Rotan, C. Gross-Heitfeld, C. Mayer, M. Epple, *J. Mater. Chem. B* **2014**, *2*, 4625.

[20] S. De Koker, R. Hoogenboom, B. G. De Geest, *Chem. Soc. Rev.* **2012**, *41*, 2867.

[21] A. Musyanovych, K. Landfester, *Macromol. Biosci.* **2014**, *14*, 458.

[22] L. L. del Mercato, A. Z. Abbasi, W. J. Parak, *Small* **2011**, *7*, 351.

[23] L. L. del Mercato, A. Z. Abbasi, M. Ochs, W. J. Parak, *ACS Nano* **2011**, *5*, 9668.

[24] O. Kreft, A. Muñoz Javier, G. B. Sukhorukov, W. J. Parak, *J. Mater. Chem.* **2007**, *17*, 4471.

[25] L. I. Kazakova, L. I. Shabarchina, G. B. Sukhorukov, *Phys. Chem. Chem. Phys.* **2011**, *13*, 11110.

[26] T. Saxl, F. Khan, D. R. Matthews, Z. L. Zhi, O. Rolinski, S. Ameer-Beg, J. Pickup, *Biosens. Bioelectron.* **2009**, *24*, 3229.
[27] U. Shimanovich, G. J. L. Bernardes, T. P. J. Knowles, A. Cavaco-Paulo, *Chem. Soc. Rev.* **2014**, *43*, 1361.
[28] L. Hood, J. R. Heath, M. E. Phelps, B. Y. Lin, *Science* **2004**, *306*, 640.
[29] F. Pene, E. Courtine, A. Cariou, J. P. Mira, *Crit. Care Med.* **2009**, *37*, 50.
[30] J. K. Kim, K. J. Choi, M. Lee, M. H. Jo, S. Kim, *Biomaterials* **2012**, *33*, 207.
[31] V. I. Shubayev, T. R. Pisanic Ii, S. Jin, *Adv. Drug Deliver. Rev.* **2009**, *61*, 467.
[32] P. Prabhu, V. Patravale, *J. Biomed. Nanotechnol.* **2012**, *8*, 859.
[33] R. Kumar, A. Kulkarni, D. K. Nagesha, S. Sridhar, *Theranostics* **2012**, *2*, 714.
[34] K. Lawson, N. G. McKay, *Curr. Pharm. Design* **2006**, *12*, 459.
[35] F. Lang, *J. Am. Coll. Nutr.* **2007**, *26*, 613.
[36] H. Matsui, B. R. Grubb, R. Tarran, S. H. Randell, J. T. Gatzy, C. W. Davis, R. C. Boucher, *Cell* **1998**, *95*, 1005.
[37] G. K. Darbha, A. Ray, P. C. Ray, *ACS Nano* **2007**, *1*, 208.
[38] K. Kantner, S. Ashraf, S. Carregal-Romero, C. Carrillo-Carrion, M. Collot, P. del Pino, W. Heimbrodt, D. Jimenez de Aberasturi, U. Kaiser, L. I. Kazakova, M. Lelle, N. Martinez de Baroja, J.-M. Montenegro, M. Nazarenus, B. Pelaz, K. Peneva, P. Rivera Gil, N. Sabir, L. M. Schneider, L. I. Shabarchina, G. B. Sukhorukov, M. Vazquez, F. Yang, W. J. Parak, *Small* **2014,** accepted.
[39] M. Nazarenus, Q. Zhang, M. G. Soliman, P. del Pino, B. Pelaz, S. Carregal_Romero, J. Rejman, B. Rothen-Ruthishauser, M. J. D. Clift, R. Zellner, G. U. Nienhaus, J. B. Delehanty, I. L. Medintz, W. J. Parak, *Beilstein J. Nanotechnol.* **2014**, *5*, 1477.
[40] A. M. Dennis, W. J. Rhee, D. Sotto, S. N. Dublin, G. Bao, *ACS Nano* **2012**, *6*, 2917.
[41] A. Orte, J. M. Alvarez-Pez, M. J. Ruedas-Rama, *ACS Nano* **2013**, *7*, 6387.
[42] J. S. Donner, S. A. Thompson, M. P. Kreuzer, G. Baffou, R. Quidant, *Nano Lett.* **2012**, *12*, 2107.
[43] O. M. Merkel, A. Beyerle, B. M. Beckmann, M. Y. Zheng, R. K. Hartmann, T. Stoger, T. H. Kissel, *Biomaterials* **2011**, *32*, 2388.
[44] Invitrogen, **2006**, http://www.lifetechnologies.com/de/de/home/references/protocols/cell-culture/transfection-protocol/stealth-sirna-transfection-lipofectamine.html, last accessed 08 May 2014
[45] G. Creusat, A. S. Rinaldi, E. Weiss, R. Elbaghdadi, J. S. Remy, R. Mulherkar, G. Zuber, *Bioconjug. Chem.* **2010**, *21*, 994.
[46] A. Zintchenko, A. Philipp, A. Dehshahri, E. Wagner, *Bioconjug. Chem.* **2008**, *19*, 1448.
[47] J. P. Behr, *Chimia* **1997**, *51*, 34.
[48] N. D. Sonawane, F. C. Szoka, Jr., A. S. Verkman, *J. Biol. Chem.* **2003**, *278*, 44826.
[49] S. Muro, *WIREs Nanomed. Nanobiotechnol.* **2010**, *2*, 189.
[50] R. M. N. Boustany, *Nat. Rev. Neurol.* **2013**, *9*, 583.
[51] S. Ortolano, I. Vieitez, C. Navarro, C. Spuch, *Recent. Pat. Endocr. Metab. Immune Drug Discov.* **2014**, *8*, 9.
[52] T. Ohshima, G. J. Murray, W. D. Swaim, G. Longenecker, J. M. Quirk, C. O. Cardarelli, Y. Sugimoto, I. Pastan, M. M. Gottesman, R. O. Brady, A. B. Kulkarni, *P. Natl. Acad. Sci. U.S.A.* **1997**, *94*, 2540.
[53] L. M. Shu, H. S. Murphy, L. Cooling, J. A. Shayman, *J. Am. Soc. Nephrol.* **2005**, *16*, 2636.
[54] S. Giri, M. Khan, R. Rattan, I. Singh, A. K. Singh, *J. Lipid Res.* **2006**, *47*, 1478.

[55] E. Haq, S. Giri, I. Singh, A. K. Singh, *J. Neurochem.* **2003**, *86*, 1428.
[56] D. Lagadic-Gossmann, L. Huc, V. Lecureur, *Cell Death Differ.* **2004**, *11*, 953.
[57] H. Sakai, G. Li, Y. Hino, Y. Moriura, J. Kawawaki, M. Sawada, M. Kuno, *J. Physiol.-London* **2013**, *591*, 5851.
[58] S. D. Freedman, H. F. Kern, G. A. Scheele, *Eur. J. Cell Biol.* **1998**, *75*, 153.
[59] P. Cosson, I. Decurtis, J. Pouyssegur, G. Griffiths, J. Davoust, *J. Cell Biol.* **1989**, *108*, 377.
[60] P. Swietach, R. D. Vaughan-Jones, A. L. Harris, A. Hulikova, *Philos. T. Roy. Soc. B* **2014**, *369,* 20130099.
[61] A. Rivinoja, F. M. Pujol, A. Hassinen, S. Kellokumpu, *Ann. Med.* **2012**, *44*, 542.
[62] O. Seksek, N. Henrytoulme, F. Sureau, J. Bolard, *Anal. Biochem.* **1991**, *193*, 49.
[63] J. Bond, J. Varley, *Cytom. Part A* **2005**, *64A*, 43.
[64] A. Longin, C. Souchier, M. Ffrench, P. A. Bryon, *J. Histochem. Cytochem.* **1993**, *41*, 1833.
[65] L. L. Song, E. J. Hennink, I. T. Young, H. J. Tanke, *Biophys. J.* **1995**, *68*, 2588.
[66] M. J. Marin, F. Galindo, P. Thomas, D. A. Russell, *Angew. Chem. Int. Edit.* **2012**, *51*, 9657.
[67] E. S. Childress, C. A. Roberts, D. Y. Sherwood, C. L. M. LeGuyader, E. J. Harbron, *Anal. Chem.* **2012**, *84*, 1235.
[68] F. A. Lattanzio, D. K. Bartschat, *Biochem. Biophys. Res. Comm.* **1991**, *177*, 184.
[69] S. Carregal-Romero, P. Rinklin, S. Schulze, M. Schäfer, A. Ott, D. Hühn, X. Yu, B. Wolfrum, K.-M. Weitzel, W. J. Parak, *Macromol. Rapid Comm.* **2013**, *34*, 1820–1826.
[70] J. Y. Han, K. Burgess, *Chem. Rev.* **2010**, *110*, 2709.
[71] S. Bassnett, L. Reinisch, D. C. Beebe, *Am. J. Physiol.* **1990**, *258*, C171.
[72] R. C. Hunter, T. J. Beveridge, *Appl. Environ. Microb.* **2005**, *71*, 2501.
[73] Pinkerton.M, Steinrau.Lk, *J. Mol. Biol.* **1970**, *49*, 533.
[74] K. A. Schmitz, D. L. Holcomb-Wygle, D. J. Oberski, C. B. Lindemann, *Biophys. J.* **2000**, *79*, 468.
[75] K. Pike-Overzet, M. van der Burg, G. Wagemaker, J. J. van Dongen, F. J. Staal, *Mol. Ther.* **2007**, *15*, 1910.
[76] S. Han, R. I. Mahato, Y. K. Sung, S. W. Kim, *Mol. Ther.* **2000**, *2*, 302.
[77] A. Schambach, D. Zychlinski, B. Ehrnstroem, C. Baum, *Hum. Gene Ther.* **2013**, *24*, 132.
[78] A. Flemming, *Nat. Rev. Drug Discov.* **2012**, *11*, 664.
[79] D. Melchiorri, L. Pani, P. Gasparini, G. Cossu, J. Ancans, J. J. Borg, C. Drai, P. Fiedor, E. Flory, I. Hudson, H. G. Leufkens, J. Muller-Berghaus, G. Narayanan, B. Neugebauer, J. Pokrotnieks, J. L. Robert, T. Salmonson, C. K. Schneider, *Nat. Rev. Drug Discov.* **2013**, *12*, 719.
[80] S. De Koker, L. J. De Cock, P. Rivera_Gil, W. J. Parak, R. A. Velty, C. Vervaet, J. P. Remon, J. Grooten, B. G. De Geest, *Adv. Drug Deliver. Rev.* **2011**, *63*, 748.
[81] A. L. Becker, N. I. Orlotti, M. Folini, F. Cavalieri, A. N. Zelikin, A. P. R. Johnston, N. Zaffaroni, F. Caruso, *ACS Nano* **2011**, *5*, 1335.
[82] N. Toub, J. R. Bertrand, A. Tamaddon, H. Elhamess, H. Hillaireau, A. Maksimenko, J. Maccario, C. Malvy, E. Fattal, P. Couvreur, *Pharm. Res.* **2006**, *23*, 892.
[83] S. M. Sparks, C. L. Waite, A. M. Harmon, L. M. Nusblat, C. M. Roth, K. E. Uhrich, *Macromol. Biosci.* **2011**, *11*, 1192.
[84] C. Kirchner, A. M. Javier, A. S. Susha, A. L. Rogach, O. Kreft, G. B. Sukhorukov, W. J. Parak, *Talanta* **2005**, *67*, 486.
[85] B. G. De_Geest, G. B. Sukhorukov, H. Mohwald, *Expert Opin. Drug Del.* **2009**, *6*, 613.

[86] S. Mumtaz, B. K. Bachhawat, *BBA-Gen. Subjects* **1994**, *1199*, 175.
[87] P. B. Deegan, *J. Inherit. Metab. Dis.* **2012**, *35*, 227.
[88] M. B. Weimer, A. Gutierrez, G. B. Baskin, J. T. Borda, R. S. Veazey, L. Myers, K. M. Phillippi-Falkenstein, B. A. Bunnell, M. S. Ratterree, J. D. England, *Muscle Nerve* **2005**, *32*, 185.
[89] J. Panyam, W. Z. Zhou, S. Prabha, S. K. Sahoo, V. Labhasetwar, *FASEB J.* **2002**, *16*, 1217.
[90] Y. Li, M. S. Sands, *Pediatr. Neurol.* **2014**, *51,* 595.
[91] M.A. Haskins, U. Giger, D.F. Patterson in *Fabry Disease: Perspectives from 5 Years of FOS* (Eds.: A. Mehta, M. Beck, G. Sunder-Plassman), Oxford PharmaGenesis™, Oxford, **2006**, http://www.ncbi.nlm.nih.gov/books/NBK11586/, last accessed 27 Oct. 2014
[92] P. Rivera Gil, L. L. del Mercato, P. del Pino, A. Muñoz-Javier, W. J. Parak, *Nano Today* **2008**, *3*, 12.
[93] B. Zebli, A. S. Susha, G. B. Sukhorukov, A. L. Rogach, W. J. Parak, *Langmuir* **2005**, *21*, 4262.
[94] R. Pinedo, PhD thesis, University of the Basque Country (Spain) **2013**.
[95] C. Carrillo-Carrion, M. Nazarenus, S. Sánchez Paradinas, S. Carregal-Romero, M. J. Almendral, M. Fuentes, B. Pelaz, P. del Pino, I. Hussain, M. J. D. Clift, B. Rothen-Rutishauser, X.-J. Liang, W. J. Parak, *Curr. Opin. Chem. Eng.* **2014**, *4*, 88.
[96] X. Jiang, D. Valdeperez, M. Nazarenus, Z. Wang, F. Stellacci, W. J. Parak, P. del Pino, Part. Part. Syst. Charact. **2014**. doi: 10.1002/ppsc.201400192
[97] P. Rivera Gil, M. Nazarenus, W. J. Parak, in *Bioinspired and Biomimetic Systems for Drug and Gene Delivery* (Ed.: Z. Gu), Wiley-VCH, Weinheim, **2015**, pp. 61.

Erklärung

Hiermit versichere ich, dass ich meine Dissertation

Polyelectrolyte Multilayer Capsules for Medical Applications

selbständig, ohne unerlaubte Hilfe angefertigt und mich dabei keiner anderen als der von mir ausdrücklich bezeichneten Quellen und Hilfen bedient habe.

Die Dissertation wurde in der jetzigen oder einer ähnlichen Form noch bei keiner Hochschule eingereicht und hat noch keinem sonstigen Prüfungszweck gedient.

Name, Vorname: Nazarenus, Moritz Julian

Marburg, 28.10.2014 .....

(Unterschrift)

Available online at www.sciencedirect.com

ScienceDirect

Current Opinion in Chemical Engineering

Metal ions in the context of nanoparticles toward biological applications

Carolina Carrillo-Carrión[1], Moritz Nazarenus[1], Sara Sánchez Paradinas[1,2], Susana Carregal-Romero[1], María Jesús Almendral[2], Manuel Fuentes[2], Beatriz Pelaz[1], Pablo del Pino[1,3], Irshad Hussain[4], Martin JD Clift[5], Barbara Rothen-Rutishauser[5], Xing-Jie Liang[6,7] and Wolfgang J Parak[1,3]

In this review the relation of inorganic colloidal nanoparticles with metal ions in biological media is discussed. Metal ions in the context of nanoparticles are relevant because of completely different reasons. First, considering unwanted effects, upon corrosion/dissolution some particular inorganic nanoparticles can release metal ions and cause toxicity, such as in the case of Cd^{2+}, Zn^{2+}, and Ag^{+}. Second, intentional modification of nanoparticles with particular metal ions can provide contrast for imaging applications, such as Gd^{3+} ions for magnetic resonance imaging. Third, nanoparticles themselves can be used for the detection of metal ions, even inside cells. Thus, there are several unwanted/intended scenarios where the interplay between nanoparticles, metal ions, and biological systems is of paramount importance.

Addresses
[1] Fachbereich Physik, Philipps Universität Marburg, 35037 Marburg, Germany
[2] Department of Analytical Chemistry, Nutrition and Food Science, Faculty of Chemistry, University of Salamanca, 37008 Salamanca, Spain
[3] CIC Biomagune, San Sebastian, Spain
[4] Department of Chemistry, SBA School of Science & Engineering, Lahore University of Management Sciences (LUMS), DHA, Lahore, Pakistan
[5] BioNanomaterials, Adolphe Merkle Institute, University of Fribourg, Route de l'Ancienne Papeterie CP 209, 1723 Marly, Switzerland
[6] Laboratory of Nanomedicine and Nanosafety, Division of Nanomedicine and Nanobiology, National Center for Nanoscience and Technology, China
[7] CAS Key Laboratory for Biomedical Effects of Nanomaterials and Nanosafety, Chinese Academy of Sciences, Beijing 100190, China

Corresponding author:
Parak, Wolfgang J (wolfgang.parak@physik.uni-marburg.de)

Current Opinion in Chemical Engineering 2014, **4**:88–96

This review comes from a themed issue on **Nanotechnology**

Edited by **Hong Yang** and **Hua Chun Zeng**

2211-3398/$ – see front matter,

http://dx.doi.org/10.1016/j.coche.2013.11.006

Introduction

Most inorganic nanoparticles (NPs) contain metals, be they in the form of elemental metals (*e.g.* Au [1,2•,3], Ag [4], Pt [5], Pd [6], Co [7,8]), metal alloys (*e.g.* FePt [6], CoPt [9]), metal oxides (*e.g.* Fe_2O_3 [10], Fe_3O_4 [11], $CoFe_2O_4$ [12], TiO_2 [13]), or other metal compounds (*e.g.* CdSe [14•], PbS [15], InP [15]). Such NPs are being explored for their potential use in life science due to their functional properties, which can be very different from those of typical organic molecules [16]. The functional properties are defined by the material of the NPs, as well as their size and shape. Important classes of functional NPs comprise fluorescent NPs, plasmonic NPs, and magnetic NPs. (i) Fluorescent NPs can be made of semiconductor materials such as CdS and CdSe, so-called quantum dots (QDs) [14•]. In comparison to organic fluorophores, QDs suffer less from photobleaching and thus can be observed over extended periods of time. Fluorescence has also been reported for ultra small metal NPs (Au, Ag), so-called metal clusters [17,18•,19,20•,21], which, however, concerning the physical origin of their fluorescence, must not be confused with QDs. Lanthanide-containing NPs are another newly emerging system, which also promise better and more stable optical properties [22]. (ii) Plasmonic NPs have been widely used for optical read-out [23••], photothermal heating, and other related applications [24•]. Most often, plasmonic NPs are composed of noble metals (in particular Au and Ag), but recently also plasmonic semiconductors have been reported [25–27]. (iii) Magnetic NPs can be used for directing NPs *via* magnetic field gradients, for imaging applications, or for the creation of heat (hyperthermia), just to give a few examples [28•,29•,30,31•]. They can be composed of elemental metals (*e.g.* Co), metal alloys (*e.g.* CoPt), or metal oxides (*e.g.* Fe_2O_3).

In case such NPs (partly) dissolve upon corrosion/oxidation, metal ions are released into the surrounding medium. Biological media, however, also contain metal ions. Ions such as Na^{+}, K^{+}, Ca^{2+}, and Mg^{2+} are basis of cell culture media (in particular Na^{+} at physiological concentrations of about 150 mM NaCl). Dynamic differences in intracellular and extracellular Na^{+}, K^{+}, Ca^{2+} concentrations regulate cellular communication, such as the formation of action potentials in neurons or muscles [32]. In addition, a gradient of metallic ions is directly related to cell migration and/or transportation. Biological media may also contain contaminants, such as Hg^{2+}, which are uptaken unintendedly by organisms. In the

following sections, we will discuss three scenarios describing the mutual interaction of these metal ions with NPs, which all have implications on life-science motivated experiments involving NPs.

Nanoparticles can release metal ions and thus cause toxic effects

Metal-containing NPs can corrode/oxidize in biological media, which results in release of metal ions to the solution, *cf.* Figure 1. While this effect is negligible for Au, it plays an important role for less stable NP materials such as Ag and CdSe [33••,34,35••]. NPs present in cell culture are internalized by cells, typically through endocytosis upon multipoint contact with the cell membrane [36,37]. Even though one can distinguish clearly between different pathways [38] NPs generally end up in lysosomal compartments [39], which are highly acidic. Acidic media enhances oxidation of NPs [40] and thus, it is assumed that in those compartments the release of metal ions from NPs internalized by cells is increased. Although ion-release from NPs in biological media can be partly reduced by appropriate surface coatings [41•], for many types of NPs release of ions to their environment is a matter of fact. While NPs clearly have potential for use in medical applications, diagnosis, and treatment, their potential toxicity to the environment upon chemical or biochemical conversion has to be considered [42,43•,44••]. One might easily be mistaken by ascribing toxicity of certain NP materials only to the metal ions released from them. Surely, for example Ag^+ (as released from Ag NPs) and Cd^{2+} (as released from CdSe NPs) can be toxic depending on the exposure route and the concentration [45•,46,47]. But is toxicity induced by Ag and CdSe NPs only caused by their released ions? Unfortunately, it is complicated to strictly address this question, as the NPs and their released metal ions cannot be separated experimentally. Whenever there are NPs prone to corrosion inside biological media, there automatically will be released ions around. While naturally one can assess toxicity of ''only'' metal ions (most trivial by incubating cells with the respective salt), one has to take into account that in these experiments biodistribution will be different from ions released from NPs [48]. While the cellular membrane is more or less impermeable to certain metal ions (in case there are no specific ion transporters) NPs are generally incorporated into intracellular vesicular compartments (in particular the lysosome), where, due to acidic conditions, ions are released. Thus, ions released from NPs are in general located at different locations than ions added as salts to the cell culture medium. Even when there is no doubt about the relevance of the dissolution and shedding of toxic ions to the toxicity of metal-containing NPs, there are also several studies in which NP toxicity could not be completely explained by their liberation of ions [49,50]. Thus, in general, both the NPs themselves, and ions released from them can contribute to toxic effects. Nel *et al.* [51] demonstrated for 24 different metal oxide NPs that their toxicological potential at cellular and animal level depends on their conduction band energy levels. Among the materials, the overlap of the conduction band energy levels with the cellular redox potential (−4.12 to −4.84 eV) was strongly correlated to the ability of Co_3O_4, Cr_2O_3, Ni_2O_3, Mn_2O_3, and CoO NPs to induce oxygen radicals, oxidative stress, and (pro-) inflammation. As the band gap is in general a bulk property these toxic effects can be ascribed to the NPs as an intact entity. In contrast, for other particles such as Ag, CuO, ZnO, or CdSe NPs, their solubility and subsequent release of ions upon oxidation has been found to be a major contribution to their toxicity [51]. Metal ions (*i.e.* Zn^{2+}, Cu^{2+}, Cd^{2+} or Ag^+) shedding during intracellular dissolution induces lysosomal damage, calcium flux, mitochondrial perturbation, generation of reactive oxygen species (ROS), alteration of the cytoskeleton, oxidative stress, excitation of pro-inflammatory responses, and cell death [52–54]. Because nanosized particles have a large specific surface area to interact with solvent molecules, NPs show faster dissolution than their respective bulk materials. This higher solubility (*i.e.* ion release) is a possible reason to explain the higher toxicity observed for ZnO and CuO NPs compared to microparticles or bulk materials of the same composition [54]. Still, more studies are required for investigating the respective contributions of NPs and their released ions to toxic effects, though, as mentioned above, it is experimentally complicated to separate both entities.

Figure 1

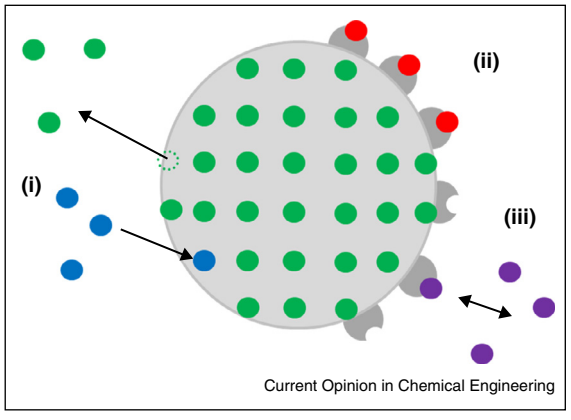

Scheme of the interrelations between metal-containing NPs and metal ions in solution. **(i)** Metal ions (depicted in green) can be released from the NP to the medium upon corrosion/oxidation of the NP. Metal ions from solution (depicted in blue) can enter into the NP and substitute the original ions. **(ii)** Metal ions (depicted in red) can be attached *via* chelators to the surface of NPs. **(iii)** Upon binding of metal ions from the solution (depicted in violet) to the NP a signal is generated, which can be used to sense the ions.

Further understanding of the mechanisms would allow for synthesizing more biocompatible NPs. This concept has been called ''safe-by-design'' strategy and has been pioneered by Nel et al. [55••]. Four ''safe-by-design'' strategies have been proposed: (i) covering the NPs with

polymers to prevent direct interaction with biomolecules, (ii) doping metal or metal oxide NPs to change the electronic structure and prevent dissolution of toxic constituents [56,57•], (iii) covering the NPs with a shell to prevent dissolution and release of metal ions from the core [35••,41•,58], and (iv) passivation of surface defects to prevent the generation of reactive oxygen species. We conclude that contamination of biological liquids by the release of metal-ions from NPs is at least partly responsible for certain toxic effects of metal-containing NPs, and is thus an undesired effect. Though this is typically true for most envisaged medical (*in vivo*) applications, such as controlled delivery, imaging, or diagnosis, the antibacterial properties of certain inorganic NPs, like those made of silver, and the corresponding ions (*e.g.* silver nitrate) have been widely employed for thousands of years. One of the pathways typically associated with the antibacterial properties of inorganic NPs is indeed release of toxic ions [59] and thus, for certain applications, corrosion of the inorganic core may turn into an asset. It is therefore mandatory to understand the chemical and biochemical behavior of metal-containing NPs in biological environments to make correct interpretations of observed effects [60].

We just briefly want to mention that, *vice versa*, also metal ions in media can contaminate NPs. Hg^{2+} ions present in media can contaminate CdTe NPs by forming an alloy ($Cd_xHg_{1-x}Te$ NPs) with optical properties different from those of the original CdTe NPs [61]. Exchange of metal ions in NPs by metal ions in solution has also been used intentionally to create new NP materials. Inorganic NPs can act as templates which upon mixing with atomic ions from different elements, can be used to produce new materials of great potential for biological applications [62]. Processes such as Kirkendall effect and the galvanic replacement can be used for producing materials of superior complexity (*e.g.* porous, hollow, multicomponent materials, *etc.*) which can be used for specific purposes [63,64]. For example, incubation of CdSe NPs in a solution of Ag^+ ions results in substitution of Cd^{2+} in the NPs *via* a cation exchange reaction and thus in the formation of Ag_2Se NPs [65]. Moreover, in addition to corrosion, these processes might play an important role in the fate of inorganic NPs inside living animals, or even in the environment.

Metal ions attached to nanoparticles as contrast agents

Whilst in the previous section the presence of metal ions released from the NP material was in general considered a drawback (except for antibacterial properties), in certain cases it can be also beneficial to link metal ions to the surface of NPs, *cf.* Figure 1. Several metal ions are useful for providing contrast in *in vitro* and *in vivo* imaging. Gd^{3+}-based complexes such as Gd–DTPA (Gd^{3+} chelated by diethylenetriaminepentaacetic acid) and Gd–DOTA (Gd^{3+} chelated by 1,4,7,10-tetraazacyclododecane-1,4,7,10 tetraacetic acid) are, for example, widely used as alternative magnetic resonance imaging (MRI) contrast agents to generate the unambiguous positive contrast (hyper-intensity) [66]. Even though various paramagnetic ions (*e.g.*, Mn^{2+}, Fe^{3+}, Eu^{3+}) were considered as paramagnetic centers for MRI, Gd^{3+} has received the most attention due to its unique features. It has a very high value of magnetic moment because of the seven unpaired electrons in the ''+3'' oxidation state and a much longer electronic relaxation time ($\sim10^{-9}$ s) than other lanthanides such as Dy^{3+}, Eu^{3+}, and Ho^{3+} ($\sim10^{-13}$ s) [67]. However, Gd-based complexes have short residence time and cannot pass easily through the cell membrane, which leave them residing within the extracellular space where they usually interact with blood so that they have some limitations as molecular probes for longer time tracking. To overcome these limitations, a new strategy of linking Gd^{3+} ions to NPs has recently been introduced and is nowadays under intense study [68]. The attachment of Gd^{3+} ions to the surface of NPs offers several advantages for MRI: (i) The relaxivity of Gd^{3+} is enhanced by increasing the molecular weight of the agent by attaching them to larger molecules such as proteins or NP scaffolds, giving rise to higher sensitivity as contrast agents [66]. For example, Gd^{3+} ions encapsulated in single-walled carbon nanotubes showed a surprising increase in the relaxivity of the Gd^{3+} ions by nearly 40-fold [69]. (ii) Longer circulation times and different biodistribution according to their size [68]. The size of NPs is the main factor controlling their physiological characteristics, such as blood half-life and biodistribution. Small NPs with an effective size in the range of ≈10–100 nm have a longer plasma-circulation time, because they are small enough to slow down activation of the mononuclear phagocyte system, mostly evade the reticuloendothelial system (RES), and reduce immediate opsonization. Studies carried out with ultrasmall superparamagnetic iron oxide (USPIO; less than 50 nm) showed that, unfortunately, they are yet big enough to slow down the excretion by the liver [68]. (iii) Improved cellular uptake either *via* active or passive targeting [70]. Passive targeting leads to enhanced accumulation of NPs in tumor sites *via* the enhanced permeability and retention (EPR) effect, as result of the combination of an increased permeability of tumor blood vessels and a decreased rate of clearance caused by the lack of functional lymphatic vessels in the tumor [71,72]. These findings support the use of NPs in tumor diagnosis and therapy as carriers, because they passively accumulate in solid tumors after their intravenous administration. In addition, the uptake can be modulated by controlling the size and surface chemistry (charge and specific ligands) of the NPs. Concerning attachment strategies, Gd^{3+} ions have been linked to different kinds of NPs, such as silica NPs [73•,74], dendrimer-based NPs [75,76], lipid-based NPs [77•,78], chitosan NPs [79], iron oxide NPs [80,81,82•], gold NPs [82•,83,84], nanodiamonds [85], and QDs [82•,86–90]. Linkage is often realized by means of chelators such as

DOTA or DTPA, which both have a high binding affinity to Gd^{3+}. The chelator then is linked to the NPs through either covalent linkage, such as amide bonds [79,82•], sulfide bonds [83,84], streptavidin–biotin interaction [89], or by non-covalent linkages, for example by incorporating the chelator into micelles [86,87,89,90], lipid bilayers [78], or polyelectrolyte cappings [83,84]. In similar strategies the linkage of metal ions to the surface of NPs can also provide contrast for other imaging modalities, such as single photon emission computed tomography (SPECT). In this case, radioactive isotopes of certain ions, such as $^{111}In^{3+}$ can be added to the surface of the NPs [82•]. Also, lanthanides such as Eu^{3+} and Tb^{3+} have been linked to the surface of QDs in order to achieve particular optical properties [91••]. These examples demonstrate that it is useful to chemically link certain metal ions to the surface of NPs, in order to provide them with additional functionality. Naturally this linkage should be stable, thus preventing release of the metal ions from the chelators.

Detection of metal ions with nanoparticles

While so far the origin of the discussed metal ions was the NPs themselves (corrosion of NP materials and linkage of metal ions to the NP surface), NPs also can be used to detect metal ions in solution: in test tube, *in vitro*, and *in vivo*. The NP-based sensors can be divided into two main categories, depending on the role of the NP. (i) NPs can act merely as a chemically inert platform (carrier), which is loaded with the actual sensing components, or (ii) NPs can act as active sensing unit. At any rate, the sensing mechanism requires some kind of interaction (preferably selective) between the metal ions and the NPs, resulting in measurable signal changes, *cf.* Figure 1. For intracellular detection, optical read-out is a frequent choice since alternative techniques such as electrochemical electrodes are more cumbersome to apply inside cells [92]. In case of charged surface NPs, it is also important to note that the conditions at the NPs surface are different from bulk, as there will be a higher and lower concentration of ions with the opposite and the same sign of charge around the nanoparticles compared to bulk, respectively [93–95]. This fact has profound effect on ion-sensitive NPs, and therefore, it has to be taken into account in the design of the sensing systems by using appropriate calibration curves. Several analytical strategies for NP-based ion-sensing are used. (i) Plasmonic NPs (in particular Au) have been widely used for the development of colorimetric sensors for metal ions detection *via* an ion-chelation induced agglomeration process. Upon NP agglomeration, color changes (in the case of Au NPs from red to blue) can be employed for visual sensing of the ions. This method has been used, for example, for the detection of Pb^{2+}, Cd^{2+} and Hg^{2+} [96–98]. (ii) Fluorescent NPs such as QDs and nanoclusters (NCs) can report metal ions *via* changes in their fluorescence. The simplest ion sensing strategy is based on fluorescence quenching when the ions are electrostatically adsorbed on the surface of the QDs/NCs, or by means of a specific ligand (*e.g.* ion chelators, peptides). The detection of different metal ions such as Hg^{2+}, Cu^{2+}, Zn^{2+}, Ag^{+}, has been reported following this strategy [99•,100]. However, the maximum potential of QDs relies on the development of multiplexing assays for the simultaneous determination of several ions by using different-sized QDs. A multiplexed analysis of Hg^{2+} and Ag^{+} ions by nucleic acid functionalized CdSe/ZnS QDs has been reported [101]. Besides QDs and NCs, other NP-based sensors are being used as well, such as the PEBBLE (probes encapsulated by biologically localized embedding) system, in which ion-sensitive dyes are linked to a carrier matrix. PEBBLE sensors have been developed for example for the detection of Ca^{2+}, K^{+}, Na^{+}, Mg^{2+}, Zn^{2+}, Cu^{2+}, and Fe^{3+} [102•,103–110]. In these systems, the readout involves mainly optical detection, absorption, or fluorescence, depending on the ion-sensitive dye used. There are several advantages of PEBBLE sensors as follows: (i) The matrix protects the cell from the dye and the dye from the cell components. In other words, the matrix provides a protective coating for the indicator dyes, avoiding responses of interferences such as protein binding and/or membrane/organelle sequestration in the biological sample. The nanosensor matrix also provides protection to the cellular contents, enabling the use of dyes that would usually be toxic. (ii) The PEBBLE creates a separate sensing phase (the PEBBLE matrix) distinct from the cellular environment which allows that multiple dyes and ionophores can be combined within this sensing phase to create complex sensing schemes. These complex sensing schemes can include reference dyes for allowing ratiometric sensing/imaging, or ionophore/chromoionophore combinations for the use of highly selective, non-fluorescent ionophores. However, there are still several challenges for NP-based sensing of metal ions. One major problem is that the selectivity of many ligands or fluorophores to the target ion is sometimes not as high as required. Another problem for the application of NP-based sensors, in particular in cells, is that colloidal stability needs to be provided. This problem is particularly evident for the detection principles in which read-out depends on direct binding of ions to the NP surface, which limits employing coating strategies for enhanced colloidal stability. Most difficult to solve is that, in theory, NP-based sensors should be ''silent observers'', measuring the ion concentrations without interfering with normal cell behavior. However, as we have discussed in the first part, the NPs can cause toxic effects, for example by the release of toxic ions, as happens with QDs, and thus, the ions release influences the cellular environment.

Conclusions

In this review we have discussed three different topics, which at first glance seem to be unrelated: (i) Toxic effects upon corrosion of metal-containing NPs, (ii) modification of NPs with metal-ions for improved contrast properties concerning imaging applications, and (iii) detection of metal ions with NPs. However, as we have

demonstrated, these three topics are conceptually linked, involving metal ions either in the NPs or in solution. The ideal metal-containing NP should preserve its integrity even under the harsh conditions of biological environments (*e.g.* presence of binding ligands, low pH, and proteases in the lysosome), preventing release of metal ions both from the NP material (corrosion/oxidation) and from the surface (*e.g.* from chelators). In case metal ions from solution are to be detected, however, these ions should bind only reversibly to the NP surface in order to warrant multiple uses.

Acknowledgements

Parts of this work we supported by DAAD (Projekt ID 54372132 to IH and WJP), the SPP1313 program of the DFG (grant to WJP and BRR), and the Chinese Academy of Science (visiting professorship for senior international scientists grant no. 2012T1J0021). CC and BP acknowledge the Alexander von Humboldt Foundation for a PostDoc fellowship.

References and recommended reading

Papers of particular interest, published within the period of review, have been highlighted as:

- • of special interest
- •• of outstanding interest

1. Chanana M, Rivera_Gil P, Correa-Duarte MA, Parak WJ, Liz-Marzán LM: **Physicochemical properties of protein-coated gold nanoparticles in biological fluids and cells before and after proteolytic digestion**. *Angew Chem Int Ed Engl* 2013, **52**:4179-4183.

2. • Dreaden EC, Alkilany AM, Huang X, Murphy CJ, El-Sayed MA: **The golden age: gold nanoparticles for biomedicine**. *Chem Soc Rev* 2012, **41**:2740-2779.
This *critical review* provides insights into the design, synthesis, functionalization, and applications of gold nanoparticles in biomedicine and discusses their tailored interactions with biological systems. Through a survey of the rapidly expanding body of literature on this topic, it argues that a new 'Golden Age' of biomedical nanotechnology is truly upon us.

3. Boisselier E, Astruc D: **Gold nanoparticles in nanomedicine: preparations, imaging, diagnostics, therapies and toxicity**. *Chem Soc Rev* 2009, **38**:1759-1782.

4. Yang J, Yin H, Jia J, Wei Y: **Facile synthesis of high-concentration. Stable aqueous dispersions of uniform silver nanoparticles using aniline as a reductant**. *Langmuir* 2011, **27**:5047-5053.

5. Podsiadlo P, Paternel S, Rouillard J-M, Zhang Z, Lee J, Lee J-W, Gulari E, Kotov NA: **Layer-by-layer assembly of nacre-like nanostructured composites with antimicrobial properties**. *Langmuir* 2005, **21**:11915-11921.

6. Ramakrishnan A, Dumbuya K, Ofili J, Steinruck HP, Gottfried JM, Schwieger W: **Highly dispersed Pd nanoparticles within silica: synthesis and characterization**. *Appl Clay Sci* 2011, **51**:8-14.

7. Ung D, Tung LD, Caruntu G, Delaportas D, Alexandrou I, Prior IA, Thanh NTK: **Variant shape growth of nanoparticles of metallic Fe–Pt, Fe–Pd and Fe–Pt–Pd alloys**. *Cryst Eng Comm* 2009, **11**:1309-1316.

8. Lu LT, Tung LD, Robinson I, Ung D, Tan B, Long J, Cooper AI, Fernig DG, Thanh NTK: **Size and shape control for water-soluble magnetic cobalt nanoparticles using polymer ligands**. *J Mater Chem* 2008, **18**:2453-2458.

9. Bao Y, Beerman M, Krishnan KM: **Controlled self-assembly of colloidal cobalt nanocrystals**. *J Magn Magn Mater* 2003, **266**:L245-L249.

10. Ni Y, Ge X, Zhang Z, Ye Q: **Fabrication and characterization of the plate-shaped g-Fe_2O_3 nanocrystals**. *Chem Mater* 2002, **14**:1048-1052.

11. Maji SK, Mukherjee N, Mondal A, Adhikary B: **Synthesis, characterization and photocatalytic activity of alpha-Fe_2O_3 nanoparticles**. *Polyhedron* 2012, **33**:145-149.

12. Wagner J, Autenrieth T, Hempelmann R: **Core shell particles consisting of cobalt ferrite and silica as model ferrofluids [$CoFe_2O_4$-SiO_2 core shell particles]**. *J Magn Magn Mater* 2002, **252**:4-6.

13. Drbohlavova J, Adam V, Kizek R, Hubalek J: **Quantum dots – characterization. Preparation and usage in biological systems**. *Int J Mol Sci* 2009, **10**:656-673.

14. • Alivisatos AP, Gu WW, Larabell C: **Quantum dots as cellular probes**. *Annu Rev Biomed Eng* 2005, **7**:55-76.
The great potential of using quantum dots as new probes in vitro and in vivo is pointed out, summarizing the recent advances of quantum dot usage at the cellular level, including immunolabeling, cell tracking, in situ hybridization, FRET, in vivo imaging, and other related technologies.

15. Rogach AL, Eychmüller A, Hickey SG, Kershaw SV: **Infrared-emitting colloidal nanocrystals: synthesis, assembly spectroscopy, and applications**. *Small* 2007, **3**:536-557.

16. Parak WJ, Gerion D, Pellegrino T, Zanchet D, Micheel C, Williams SC, Boudreau R, Le Gros MA, Larabell CA, Alivisatos AP: **Biological applications of colloidal nanocrystals**. *Nanotechnology* 2003, **14**:R15-R27.

17. Yeh H-C, Sharma J, Han JJ, Martinez JS, Werner JH: **A DNA-silver nanocluster probe that fluoresces upon hybridization**. *Nano Lett* 2010, **10**:3106-3110.

18. • Lin CA, Yang TY, Lee CH, Huang SH, Sperling RA, Zanella M, Li JK, Shen JL, Wang HH, Yeh HI, Parak WJ, Chang WH: **Synthesis, characterization, and bioconjugation of fluorescent gold nanoclusters toward biological labeling applications**. *ACS Nano* 2009, **3**:395-401.
Ultrasmall water-soluble fluorescent gold nanoclusters are synthesised and conjugated with biological molecules. Specific staining of cells and nonspecific uptake by living cells is demonstrated.

19. Shang L, Azadfar N, Stockmar F, Send W, Trouillet V, Bruns M, Gerthsen D, Nienhaus GU: **One-pot synthesis of near-infrared fluorescent gold clusters for cellular fluorescence lifetime imaging**. *Small* 2011, **7**:2614-2620.

20. • Shang L, Dorlich RM, Trouillet V, Bruns M, Nienhaus GU: **Ultrasmall fluorescent silver nanoclusters: protein adsorption and its effects on cellular responses**. *Nano Res.* 2012, **5**:531-542.
Interactions of ultrasmall silver nanoclusters (AgNCs) with a model protein, human serum albumin (HSA), have been systematically investigated by using a variety of techniques including absorption spectroscopy, steady-state and time-resolved fluorescence, as well as circular dichroism spectroscopy. The results showed that the physicochemical properties of both proteins and AgNCs undergo changes upon their interactions. Furthermore, biological implications of protein adsorption were quantitatively explored by evaluating responses of HeLa cells to AgNC exposure through live-cell fluorescence microscopy and a cytotoxicity test, revealing that protein adsorption has a significant effect on the biological response to AgNC exposure.

21. Huang S, Pfeiffer C, Hollmann J, Friede S, Chen JJ-C, Beyer A, Volz K, Heimbrodt W, Montenegro Martos JM, Chang W, Parak WJ: **Synthesis and characterization of colloidal fluorescent silver nanoclusters**. *Langmuir* 2012, **28**:8915-8919.

22. Wilhelm S, Hirsch T, Patterson WM, Scheucher E, Mayr T, Wolfbeis OS: **Multicolor upconversion nanoparticles for protein conjugation**. *Theranostics* 2013, **13**:239-248.

23. •• Elghanian R, Storhoff JJ, Mucic RC, Letsinger RL, Mirkin CA: **Selective colorimetric detection of polynucleotides based on the distance-dependent optical properties of gold nanoparticles**. *Science* 1997, **277**:1078-1081.
A highly selective, colorimetric polynucleotide detection method based on mercaptoalkyloligonucleotide-modified gold nanoparticle probes was reported. With the use of a single-stranded target oligonucleotide (30 bases), the unoptimized system could detect about 10 femtomoles of an oligonucleotide.

24. • Sperling RA, Rivera_Gil P, Zhang F, Zanella M, Parak WJ: **Biological applications of gold nanoparticles**. *Chem Soc Rev* 2008, **37**:1896-1908.

This critical review gives a short overview of the widespread use of gold nanoparticles in biology. Four classes of applications in which gold nanoparticles have been used so far are discussed: labelling, delivering, heating, and sensing. For each of these applications the underlying mechanisms and concepts, the specific features of the gold nanoparticles needed for this application, as well as several examples are described.

25. Scotognella F, Della Valle G, Kandada ARS, Dorfs D, Zavelani-Rossi M, Conforti M, Miszta K, Comin A, Korobcheyskaya K, Lanzani G, Manna L, Tassone F: **Plasmon dynamics in colloidal Cu_2-xSe nanocrystals**. *Nano Lett* 2011, **11**:4711-4717.

26. Dorfs D, Hartling T, Miszta K, Bigall NC, Kim MR, Genovese A, Falqui A, Povia M, Manna L: **Reversible tunability of the near-infrared valence band plasmon resonance in Cu_2-xSe nanocrystals**. *J Am Chem Soc* 2011, **133**:11175-11180.

27. Li WH, Zamani R, Rivera_Gil P, Pelaz B, Ibanez M, Cadavid D, Shavel A, Alvarez-Puebla RA, Parak WJ, Arbiol J, Cabot A: **CuTe nanocrystals: shape and size control, plasmonic properties, and use as SERS probes and photothermal agents**. *J Am Chem Soc* 2013, **135**:7098-7101.

28. • Pankhurst QA, Connolly J, Jones SK, Dobson J: **Applications of magnetic nanoparticles in biomedicine**. *J Phys D: Appl Phys* 2003, **36**:R167-R181.
The physical principles underlying some current biomedical applications of magnetic nanoparticles are reviewed. The way these properties are controlled and used is illustrated with reference to (i) magnetic separation of labelled cells and other biological entities; (ii) therapeutic drug, gene and radionuclide delivery; (iii) radio frequency methods for the catabolism of tumours via hyperthermia; and (iv) contrast enhancement agents for magnetic resonance imaging applications.

29. • Colombo M, Carregal-Romero S, Casula MF, Gutiérrez L, Morales MP, Böhm IB, Heverhagen JT, Prosperi D, Parak WJ: **Biological applications of magnetic nanoparticles**. *Chem Soc Rev* 2012, **41**:4306-4334.
An overview about biological applications of magnetic colloidal nanoparticles is given, which comprises their synthesis, characterization, and in vitro and in vivo applications. The potential future role of magnetic nanoparticles compared to other functional nanoparticles is discussed. Besides, current limitations in the fabrication process and issues related with the outcome of the particles in the body are pointed out in order to address the remaining challenges for an extended application of magnetic nanoparticles in medicine.

30. del Pino P, Munoz-Javier A, Vlaskou D, Rivera Gil P, Plank C, Parak WJ: **Gene silencing mediated by magnetic lipospheres tagged with small interfering RNA**. *Nano Lett* 2010, **10**:3914-3921.

31. • Dias JT, Moros M, del Pino P, Rivera S, Grazú V, de la Fuente JM: **DNA as a molecular local thermal probe for the analysis of magnetic hyperthermia**. *Angew Chem Int Ed Engl* 2013, **52**:11526-11529.
Polymer-coated magnetic nanoparticles were functionalized with single-stranded DNA molecules and further hybridized with DNA modified with different fluorophores. By correlating the denaturation profiles of the DNA with the local temperature, temperature gradients for the vicinity of the excited nanoparticles were determined.

32. Hille B: *Ionic Channels of Excitable Membranes*. 2nd ed. Sunderland, MA: Sinauer Associates Inc.; 1992.

33. •• Kittler S, Greulich C, Diendorf J, Koller M, Epple M: **Toxicity of silver nanoparticles increases during storage because of slow dissolution under release of silver ions**. *Chem Mater* 2010, **22**:4548-4554.
The dissolution of citrate-stabilized and poly(vinylpyrrolidone)-stabilized silver nanoparticles in water was studied by dialysis for up to 125 days at 5, 25, and 37 °C. The results showed that the rate and degree of dissolution depended on the functionalization as well as on the storage temperature. The release of silver led to a considerably increased toxicity of silver nanoparticles which had been stored in dispersion for several weeks toward human mesenchymal stem cells due to the increased concentration of silver ions.

34. Chernousova S, Epple M: **Silver as antibacterial agent: ion, nanoparticle, and metal**. *Angew Chem Int Ed Engl* 2013, **52**:1636-1653.

35. •• Derfus AM, Chan WCW, Bhatia SN: **Probing the cytotoxicity of semiconductor quantum dots**. *Nano Lett* 2004, **4**:11-18.
CdSe-core QDs were found to be toxic under certain conditions. The results showed that the cytotoxicity of QDs can be modulated by processing parameters during synthesis, exposure to ultraviolet light, and surface coatings. The data suggested that cytotoxicity correlates with the liberation of free Cd^{2+} ions due to deterioration of the CdSe lattice. When appropriately coated, CdSe-core QDs can be rendered nontoxic and used to track cell migration and reorganization in vitro.

36. Iversen TG, Skotland T, Sandvig K: **Endocytosis and intracellular transport of nanoparticles: present knowledge and need for future studies**. *Nano Today* 2011, **6**:176-185.

37. Zhao F, Zhao Y, Liu Y, Chang X, Chen C, Zhao Y: **Cellular uptake, intracellular trafficking, and cytotoxicity of nanomaterials**. *Small* 2011, **7**:1322-1337.

38. Conner SD, Schmid LS: **Regulated portals of entry into the cell**. *Nature* 2003, **422**:37-41.

39. Brandenberger C, Mühlfeld C, Ali Z, Lenz A-G, Schmid O, Parak WJ, Gehr P, Rothen-Rutishauser B: **Quantitative evaluation of cellular uptake and trafficking of plain and polyethylene glycol-coated gold nanoparticles**. *Small* 2010, **6**:1669-1678.

40. Caballero-Díaz E, Pfeiffer C, Kastl L, Rivera_Gil P, Simonet B, Valcárcel M, Jiménez-Lamana J, Laborda F, Parak WJ: **The toxicity of silver nanoparticles depends on their uptake by cells and thus on their surface chemistry**. *Part Part Syst Charact* 2013, **30**:1079-1085.

41. • Kirchner C, Kudera TL, Pellegrino S, Muñoz Javier T, Gaub A, Stölzle HE, Fertig S, Parak NWJ: **Cytotoxicity of colloidal CdSe and CdSe/ZnS nanoparticles**. *Nano Lett* 2005, **5**:331-338.
Cytotoxicity of CdSe and CdSe/ZnS nanoparticles was investigated for different surface modifications such as coating with mercaptopropionic acid, silanization, and polymer coating. The data showed that in addition to the release of toxic Cd^{2+} ions from the particles also their surface chemistry, in particular their stability toward aggregation, plays an important role for cytotoxic effects.

42. Doane TL, Burda C: **The unique role of nanoparticles in nanomedicine: imaging, drug delivery and therapy**. *Chem Soc Rev* 2012, **41**:2885-2911.

43. • Stark WJ: **Nanoparticles in biological systems**. *Angew Chem Int Ed* 2011, **50**:1242-1258.
This review discusses molecules and nanoparticles when in contact with cells or whole organisms. The interaction of particles with biology unravels a series of new mechanisms not found for molecules: altered biodistribution, chemically reactive interfaces, and the combination of solid-state properties and mobility. Externally guided movement of medicaments by using functional nanomagnets brings mechanics into drug design. The role of inertness and bioaccumulation is discussed in regard to the long-term safety of nanoparticles.

44. •• Rivera_Gil P, Oberdorster G, Elder A, Puntes VF, Parak WJ: **Correlating physico-chemical with toxicological properties of nanoparticles: the present and the future**. *ACS Nano* 2010, **4**:5527-5531.
The origins of the Nanotoxicology as a new discipline and its future trends are discussed. The important issues to be considered in this field are discussed.

45. • Beer C, Foldbjerg R, Hayashi Y, Sutherland DS, Autrup H: **Toxicity of silver nanoparticles – nanoparticle or silver ion?** *Toxicol Lett* 2012, **208**:286-292.
Since the toxicity of silver nanoparticles (AgNPs) has been shown in many publications, this paper investigates to which degree the silver ion fraction of AgNP suspensions contributes to the toxicity of AgNPs in A549 lung cells. The data showed that at high silver ion fractions ($\geq$5.5%) the AgNPs did not add measurable additional toxicity to the AgNP suspension, whereas at low silver ion fractions ($\leq$2.6%) AgNP suspensions are more toxic than their supernatant.

46. Priester JH, Stoimenov PK, Mielke RE, Webb SM, Ehrhardt C, Zhang JP, Stucky GD, Holden PA: **Effects of soluble cadmium salts versus CdSe quantum dots on the growth of planktonic *Pseudomonas aeruginosa***. *Environ Sci Technol* 2009, **43**:2589-2594.

47. Galeone A, Vecchio G, Malvindi MA, Brunetti V, Cingolanib R, Pompa PP: **In vivo assessment of CdSe–ZnS quantum dots: coating dependent bioaccumulation and genotoxicity**. *Nanoscale* 2012, **4**:6401-6407.

48. Herzog F, Clift MJD, Piccapietra F, Behra R, Schmid O, Petri-Fink A, Rothen-Rutishauser B: **Exposure of silver-nanoparticles and silver-ions to lung cells in vitro at the air–liquid interface**. *Part Fibre Toxicol* 2013, **10**:11.

49. Stampoulis D, Sinha SK, White JC: **Assay-dependent phytotoxicity of nanoparticles to plants**. *Environ Sci Technol* 2009, **43**:9473-9479.

50. Carlson C, Hussain SM, Schrand AM, Braydich-Stolle LK, Hess KL, Jones RL, Schlager JJ: **Unique cellular interaction of silver nanoparticles: size-dependent generation of reactive oxygen species**. *J Phys Chem B* 2008, **112**:13608-13619.

51. Zhang HY, Ji ZX, Xia T, Meng H, Low-Kam C, Liu R, Pokhrel S, Lin SJ, Wang X, Liao YP, Wang M, Li L, Rallo R, Damoiseaux R, Telesca D, Mädler L, Cohen Y, Zink JI, Nel AE: **Use of metal oxide nanoparticle band gap to develop a predictive paradigm for oxidative stress and acute pulmonary inflammation**. *ACS Nano* 2012, **6**:4349-4368.

52. Sharifi S, Behzadi S, Laurent S, Laird Forrest M, Stroeve P, Mahmoudi M: **Toxicity of nanomaterials**. *Chem Soc Rev* 2012, **41**:2323-2343.

53. Huang CC, Aronstam RS, Chen DR, Huang YW: **Oxidative stress, calcium homeostasis, and altered gene expression in human lung epithelial cells exposed to ZnO nanoparticles**. *Toxicol In Vitro* 2010, **24**:45-55.

54. Chang YN, Zhang MY, Xia L, Zhang J, Xing GM: **The toxic effects and mechanisms of CuO and ZnO nanoparticles**. *Materials* 2012, **5**:2850-2871.

55. •• Pokhrel S, Nel AE, Mädler L: **Custom-designed nanomaterial libraries for testing metal oxide toxicity**. *Acc Chem Res* 2013 Mar, **46**:632-641.

A strategy for creating nanoparticlelibraries (pure or Fedoped ZnO or TiO_2) utilizing flame spray pyrolysis (FSP) and using these libraries to test hypotheses related to the particles' toxicity has been described. This paper summarizes the last advances in (1) synthesizing nanomaterials to address specific hypotheses, (2) demonstrating the electronic properties that cause the material toxicity, (3) understanding the reaction mechanisms causing the toxicity, and (4) extracting from in vitro testing and in vivo testing in terrestrial and marine organisms the essential properties of safe nanomaterials. On the basis of this acquired knowledge, it was described how the dissolved metal ion from these materials (Zn^{2+}) can effectively bind with different cell constituents, causing toxicity.

56. George S, Pokhrel S, Xia T, Gilbert B, Ji Z, Schowalter M, Rosenauer A, Damoiseaux R, Bradley KA, Mädler L, Nel AE: **Use of a rapid cytotoxicity screening approach to engineer a safer zinc oxide nanoparticle through iron doping**. *ACS Nano* 2010, **4**:15-29.

57. • Xia T, Zhao Y, Sager T, George S, Pokhrel S, Li N, Schoenfeld D, Meng H, Lin S, Wang X, Wang M, Ji Z, Zink JI, Mädler L, Castranova V, Lin S, Nel AE: **Decreased dissolution of ZnO by iron doping yields nanoparticles with reduced toxicity in the rodent lung and zebrafish embryos**. *ACS Nano* 2011, **5**:1223-1235.

The dissolution of ZnO nanoparticles and Zn(2+) shedding leads to a series of sublethal and lethal toxicological responses at the cellular level that can be alleviated by iron doping. To determine whether iron doping of ZnO also leads to lesser toxic effects in vivo, toxicity studies were performed in rodent and zebrafish models. Studies compared the effects of undoped to doped particles in the rat lung, mouse lung, and the zebrafish embryo. The data showed that Fe doping is a possible safe design strategy for preventing ZnO toxicity in animals and the environment.

58. Selvan ST, Tan TT, Ying JY: **Robust, non-cytotoxic, silica-coated CdSe quantum dots with efficient photoluminescence**. *Adv Mater* 2005, **17**:1620-1625.

59. Hajipour MJ, Fromm KM, Akbar Ashkarran A, Jimenez de Aberasturi D, Larramendi IRd, Rojo T, Serpooshan V, Parak WJ, Mahmoudi M: **Antibacterial properties of nanoparticles**. *Trends Biotechnol* 2012, **30**:499-511.

60. Behra R, Sigg L, Clift MJ, Herzog F, Minghetti M, Johnston B, Petri-Fink A, Rothen-Rutishauser B: **Bioavailability of silver nanoparticles and ions: from a chemical and biochemical**. *J R Soc Interface* 2013, **10**:20130396.

61. Susha AS, Javier AM, Parak WJ, Rogach AL: **Luminescent CdTe nanocrystals as ion probes and pH sensors in aqueous solutions**. *Colloid Surf A* 2006, **281**:40-43.

62. Skrabalak SE, Chen J, Sun Y, Lu X, Au L, Cobley CM, Xia Y: **Gold Nanocages: synthesis, properties, and applications**. *Acc Chem Res* 2008, **41**:1587-1595.

63. Oh MH, Yu T, Yu SH, Lim B, Ko KT, Willinger MG, Seo DH, Kim BH, Cho MG, Park JH, Kang K, Sung YE, Pinna N, Hyeon T: **Galvanic replacement reactions in metal oxide nanocrystals**. *Science* 2013, **340**:964-968.

64. Gonzalez E, Arbiol J, Puntes VF: **Carving at the nanoscale: sequential galvanic exchange and kirkendall growth at room temperature**. *Science* 2011, **334**:1377-1380.

65. Son DH, Hughes SM, Yin Y, Alivisatos AP: **Cation exchange reactions in ionic nanocrystals**. *Science* 2004, **306**:1009-1012.

66. Xu C, Mu L, Roes I, Miranda-Nieves D, Nahrendorf M, Ankrum JA, Zhao W, Karp JM: **Nanoparticle-based monitoring of cell therapy**. *Nanotechnology* 2011, **22**:494001.

67. Warsi MF: *Lanthanide Functionalised Gold Nanoparticles as MRI Contrast Agent*. York, UK: The University of York; 2010.

68. Na HB, Song IC, Hyeon T: **Inorganic nanoparticles for MRI contrast agents**. *Adv Mater* 2009, **21**:2133-2148.

69. Tran LA, Krishnamurthy R, Muthupillai R, Cabreira-Hansen Mda G, Willerson JT, Perin EC, Wilson LJ: **Gadonanotubes as magnetic nanolabels for stem cell detection**. *Biomaterials* 2010, **31**:9482-9491.

70. Rivera_Gil P, Parak WJ: **Composite nanoparticles take aim at cancer**. *ACS Nano* 2008, **2**:2200-2205.

71. Maeda H, Wu J, Sawa T, Matsumura Y, Hori K: **Tumor vascular permeability and the EPR effect in macromolecular therapeutics: a review**. *J Control Release* 2000, **65**:271-284.

72. Iyer AK, Khaled G, Fang J, Maeda H: **Exploiting the enhanced permeability and retention effect for tumor targeting**. *Drug Discov Today* 2006, **11**:812-818.

73. • Rieter WJ, Kim JS, Taylor KML, An HY, Lin WL, Tarrant T, Lin WB: **Hybrid silica nanoparticles for multimodal Imaging**. *Angew Chem Int Ed* 2007, **46**:3680-3682.

Multifunctional silica nanoparticles containing a luminescent core and a paramagnetic coat are prepared, and their utility as multimodal imaging probes is demonstrated in vitro. Monocyte cells can be labeled with the hybrid nanoparticles with greater than 98% efficiency and do not experience measurable toxicity even at a high loading of 0.123 mg per 5000 cells.

74. Hsiao JK, Tsai CP, Chung TH, Hung Y, Yao M, Liu HM, Mou CY, Yang CS, Chen YC, Huang DM: **Mesoporous silica nanoparticles as a delivery system of gadolinium for effective human stem cell tracking**. *Small* 2008, **4**:1445-1452.

75. Kobayashi H, Kawamoto S, Bernardo M, Brechbiel MW, Knopp MV, Choyke PL: **Delivery of gadolinium-labeled nanoparticles to the sentinel lymph node: comparison of the sentinel node visualization and estimations of intra-nodal gadolinium concentration by the magnetic resonance imaging**. *J Control Release* 2006, **111**:343-351.

76. Cheng ZL, Thorek DLJ, Tsourkas A: **Gadolinium-conjugated dendrimer nanoclusters as a tumor-targeted T-1 magnetic resonance imaging contrast agent**. *Angew Chem Int Ed* 2010, **49**:346-350.

77. • Mulder WJM, Strijkers GJ, van Tilborg GAF, Griffioen AW, Nicolay K: **Lipid-based nanoparticles for contrast-enhanced MRI and molecular imaging**. *NMR Biomed* 2006, **19**:142-164.

A relatively new and promising application of lipid-based nanoparticles, such as liposomes or micelles, is their use as multimodal MR contrast agents. An overview of different lipidic nanoparticles for use in MRI is given, with the main emphasis on Gd-based contrast agents. The mechanisms of particle formation, conjugation strategies and applications in the field of contrast-enhanced, cellular and molecular MRI are discussed.

78. Bui T, Stevenson J, Hoekman J, Zhang SR, Maravilla K, Ho RJY: **Novel Gd nanoparticles enhance vascular contrast for high-resolution magnetic resonance imaging**. *PLoS One* 2010, **5(9)**:e13082.

79. Tallury P, Santra S, Sharma P, Matos BMD, Bengtsson N, Biswas S, Saha AK, Walter GA, Scott EA, Moudgil BM: **Fluorescent and paramagnetic chitosan nanoparticles that exhibit high magnetic resonance relaxivity: synthesis, characterization and in vitro studies**. *J Biomed Nanotechnol* 2011, **7**:724-729.

80. Bae KH, Kim YB, Lee Y, Hwang J, Park H, Park TG: **Bioinspired synthesis and characterization of gadolinium-labeled magnetite nanoparticles for dual contrast T-1- and T-2-weighted magnetic resonance imaging**. *Bioconjugate Chem* 2010, **21**:505-512.

81. Yang H, Zhuang YM, Sun Y, Dai AT, Shi XY, Wu DM, Li FY, Hu H, Yang SP: **Targeted dual-contrast T-1- and T-2-weighted magnetic resonance imaging of tumors using multifunctional gadolinium-labeled superparamagnetic iron oxide nanoparticles**. *Biomaterials* 2011, **32**:4584-4593.

82. • Ali Z, Abbasi AZ, Zhang F, Arosio P, Lascialfari A, Casula MF, Wenk A, Kreyling W, Plapper R, Seidel M *et al.*: **Multifunctional nanoparticles for dual imaging**. *Anal Chem* 2011, **83**:2877-2882.

Colloidal nanoparticles composed out of an inorganic core and a polymer shell offer progress for imaging with different modalities. When different cores are combined with different polymer shells, different types of particles for dual imaging can be obtained, as for example, fluorescent cores with radioactive polymer shells. Properties and perspectives of such nanoparticles for multimodal imaging are discussed.

83. Alric C, Taleb J, Le Duc G, Mandon C, Billotey C, Le Meur-Herland A, Brochard T, Vocanson F, Janier M, Perriat P, Roux S, Tillement O: **Gadolinium chelate coated gold nanoparticles as contrast agents for both X-ray computed tomography and magnetic resonance imaging**. *J Am Chem Soc* 2008, **130**:5908-5915.

84. Warsi MF, Adams RW, Duckett SB, Chechik V: **Gd-functionalised Au nanoparticles as targeted contrast agents in MRI: relaxivity enhancement by polyelectrolyte coating**. *Chem Commun* 2010, **46**:451-453.

85. Manus LM, Mastarone DJ, Waters EA, Zhang X-Q, Schultz-Sikma EA, MacRenaris KW, Ho D, Meade TJ: **Gd(III)-nanodiamond conjugates for MRI contrast enhancement**. *Nano Lett* 2010, **10**:484-489.

86. Gopalakrishnan G, Danelon C, Izewska P, Prummer M, Bolinger PY, Geissbuhler I, Demurtas D, Dubochet J, Vogel H: **Multifunctional lipid/quantum dot hybrid nanocontainers for controlled targeting of live cells**. *Angew Chem Int Ed* 2006, **45**:5478-5483.

87. Jin T, Yoshioka Y, Fujii F, Komai Y, Seki J, Seiyama A: **Gd^{3+}-functionalized near-infrared quantum dots for in vivo dual modal (fluorescence/magnetic resonance) imaging**. *Chem Commun* 2008, **44**:5764-5766.

88. Gerion D, Herberg J, Bok R, Gjersing E, Ramon E, Maxwell R, Kurhanewicz J, Budinger TF, Gray JW, Shuman MA, Chen FF: **Paramagnetic silica-coated nanocrystals as an advanced MRI contrast agent**. *J Phys Chem* 2007, **111**:12542-12551.

89. Prinzen L, Miserus RJJHM, Dirksen A, Hackeng TM, Deckers N, Bitsch NJ, Megens RTA, Douma K, Heemskerk JW, Kooi ME, Frederik PM, Slaaf DW, van Zandvoort MA, Reutelingsperger CP: **Optical and magnetic resonance imaging of cell death and platelet activation using annexin A5-functionalized quantum dots**. *Nano Lett* 2007, **7**:93-100.

90. Erogbogbo F, Chang C-W, May JL, Liu L, Kumar R, Law W-C, Ding H, Yong KT, Roy I, Sheshadri M, Swihart MT, Prasad PN: **Bioconjugation of luminescent silicon quantum dots to gadolinium ions for bioimaging applications**. *Nanoscale* 2012, **4**:5483-5489.

91. •• Charbonniere LJ, Hildebrandt N: **Lanthanide complexes and quantum dots: a bright wedding for resonance energy transfer**. *Eur J Inorg Chem* 2008, **21**:3241-3251.

A homogeneous fluoroimmunoassay using Förster resonance energy transfer (FRET) from luminescent lanthanide complexes (LLCs – an example of a Tb complex is shown in the top right corner) to a biocompatible CdSe/ZnS quantum dot (QD) is reported. Excitation of the immunocomplex formed by the association of QD-labeled antibodies, antigen and LLC-labeled antibodies by UV light (e.g. 315 nm) led to a long-lived Tb and QD luminescence (luminescence spectra shown in the bottom right corner) due to FRET sensitization by the LLCs. This new immunoassay approach opens doors to extremely sensitive background-free fluoroimmunoassays suitable for multiplexing by using several different QDs as FRET acceptors with a single LLC donor.

92. Jimenez de Aberasturi D, Montenegro JM, Ruiz de Larramendi I, Rojo T, Klar TA, Alvarez-Puebla R, Liz-Marzán LM, Parak WJ: **Optical sensing of small ions with colloidal nanoparticles**. *Chem Mater* 2012, **24**:738-745.

93. Zhang F, Ali Z, Amin F, Feltz A, Oheim M, Parak WJ: **Ion and pH sensing with colloidal nanoparticles: influence of surface charge on sensing and colloidal properties**. *Chem Phys Chem* 2010, **11**:730-735.

94. Riedinger A, Zhang F, Dommershausen F, Röcker C, Brandholt S, Nienhaus GU, Koert U, Parak WJ: **Ratiometric optical sensing of chloride ions with organic fluorophore – gold nanoparticle hybrids: a systematic study of distance dependency and the influence of surface charge**. *Small* 2010, **6**:2590-2597.

95. Zhang F, Lees E, Amin F, Rivera_Gil P, Yang F, Mulvaney P, Parak WJ: **Polymer-coated nanoparticles: a universal tool for biolabelling experiments**. *Small* 2011, **7**:3113-3127.

96. Lin YW, Huang CC, Chang HT: **Gold nanoparticle probes for the detection of mercury, lead and copper ions**. *Analyst* 2011, **136**:863-871.

97. Kim YJ, Johnson RC, Hupp JT: **Gold nanoparticle-based sensing of "spectroscopically silent" heavy metal ions**. *Nano Lett* 2001, **1**:165-167.

98. Huang CC, Yang Z, Lee KH, Chang HT: **Synthesis of highly fluorescent gold nanoparticles for sensing Mercury(II)**. *Angew Chem Int Ed* 2007, **46**:6824-6828.

99. • Chen YF, Rosenzweig Z: **Luminescent CdS quantum dots as selective ion probes**. *Anal Chem* 2002, **74**:5132-5138.

Water-soluble luminescent CdS quantum dots (QDs) capped by polyphosphate, L-cysteine, and thioglycerol were synthesized in aqueous solution. The ligands were found to have a profound effect on the luminesence response of CdS QDs to physiologically important metal cations. The detection capability of these new ion probes, L-cysteine and thioglycerol-capped CdS QDs was demonstrated by detecting zinc and copper ions in physiological buffer samples. The detection limits were 0.8 μM for zinc (II) and 0.1 μM for copper (II) ions. The emission enhancement of the QDs by zinc (II) is attributed to activation of surface states, whereas the effective reduction of copper (II) to copper (I) may explain the emission decrease of the thioglycerol-capped CdS QDs when charged with copper ions. This was first use of luminescent semiconductor quantum dots as selective ion probes in aqueous samples.

100. Fernandez-Argüelles MT, Jin WJ, Costa-Fernandez JM, Pereiro R, Sanz-Medel A: **Surface-modified CdSe quantum dots for the sensitive and selective determination of Cu(II) in aqueous solutions by luminescent measurements**. *Anal Chim Acta* 2005, **549**:20-25.

101. Freeman R, Finder T, Willner I: **Multiplexed analysis of Hg^{2+} and Ag^{+} ions by nucleic acid functionalized CdSe/ZnS quantum dots and their use for logic gate operations**. *Angew Chem Int Ed* 2009, **48**:7818-7821.

102 • Clark HA, Barker SLR, Brasuel M, Miller MT, Monson E, Parus S, Shi ZY, Song A, Thorsrud B, Kopelman R, Ade A, Meixner W, Athey B, Hoyer M, Hill D, Lightle R, Philbert MA: **Subcellular optochemical nanobiosensors: probes encapsulated by biologically localised embedding (PEBBLEs)**. *Sens Actuators B: Chem* 1998, **51**:12-16.

The world's smallest stand-alone devices/sensors, consisting of multi-component nano-spheres with radii as small as 10 nm, have been described. Such a sensor probe encapsulated by biologically localised embedding (PEBBLE), was delivered into a cell by a variety of minimally-invasive techniques, including a pico-injector, a gene gun, liposomal incorporation and natural ingestion. These remote nano-optodes (PEBBLEs) have been prepared for pH, calcium, magnesium, potassium and oxygen. It was demonstrated that the sensor PEBBLEs can be inserted into a cell individually, in clusters (single analyte), in sets (multi-analyte) or in ensembles (single analyte, multiple locations).

103. Park EJ, Brasuel M, Behrend C, Philbert MA, Kopelman R: **Ratiometric optical PEBBLE nanosensors for real-time**

magnesium ion concentrations inside viable cells. *Anal Chem* 2003, **75**:3784-3791.

104. Clark HA, Hoyer M, Philbert MA, Kopelman R: **Optical nanosensors for chemical analysis inside single living cells. 1. Fabrication. Characterization, and methods for intracellular delivery of PEBBLE sensors**. *Anal Chem* 1999, **71**:4831-4836.

105. Sumner J, Aylott JW, Monson E, Kopelman R: **A fluorescent PEBBLE nanosensor for intracellular free zinc**. *Analyst* 2002, **127**:11-16.

106. Sumner JP, Westerberg NM, Stoddard AK, Fierke CA, Kopelman R: **Cu^{+}- and Cu^{2+}-sensitive PEBBLE fluorescent nanosensors using DsRed as the recognition element**. *Sens Actuators B: Chem* 2006, **113**:760-767.

107. Sumner JP, Kopelman R: **Alexa Fluor 488 as an iron sensing molecule and its application in PEBBLE nanosensors**. *Analyst* 2005, **130**:528-533.

108. Brasuel M, Kopelman R, Kasman I, Miller TJ, Philbert MA: **Ion concentrations in live cells from highly selective ion correlation fluorescent nano-sensors for sodium**. *Proc IEEE Sensors* 2002, **1**:288-292.

109. Brasuel M, Kopelman R, Aylott JW, Clark H, Xu H, Hoyer M, Miller TJ, Tjalkens R, Philbert MA: **Production, characteristics and applications of fluorescent PEBBLE nanosensors: potassium, oxygen, calcium and pH imaging inside live cells**. *Sens Mater* 2002, **14**:309-338.

110. Si D, Epstein T, Lee Y-EK, Kopelman R: **Nanoparticle PEBBLE sensors for quantitative nanomolar imaging of intracellular free calcium ions**. *Anal Chem* 2012, **84**:978-986.

BEILSTEIN JOURNAL OF NANOTECHNOLOGY

In vitro interaction of colloidal nanoparticles with mammalian cells: What have we learned thus far?

Moritz Nazarenus[1], Qian Zhang[1], Mahmoud G. Soliman[1], Pablo del Pino[2], Beatriz Pelaz[1], Susana Carregal-Romero[1], Joanna Rejman[1], Barbara Rothen-Rutishauser[3], Martin J. D. Clift[3], Reinhard Zellner[4], G. Ulrich Nienhaus[5,6], James B. Delehanty[7], Igor L. Medintz[7] and Wolfgang J. Parak[*1,2]

Review

Open Access

Address:
[1]Fachbereich Physik, Philipps-Universität Marburg, Renthof 7, 35037 Marburg, Germany, [2]CIC Biomagune, Paseo Miramón 182, 20009 San Sebastian, Spain, [3]BioNanomaterials, Adolphe Merkle Institute, University of Fribourg, Route de L'ancienne Papeterie CP 209, Marly 1, 1723, Fribourg, Switzerland, [4]Institute of Physical Chemistry, University of Duisburg-Essen, Universitätsstraße 5, 45141 Essen, Germany, [5]Institute of Applied Physics and Institute of Toxicology and Genetics, Karlsruhe Institute of Technology (KIT), Wolfgang-Gaede-Straße 1, 76131 Karlsruhe, Germany, [6]Department of Physics, University of Illinois at Urbana-Champaign, 1110 West Green Street, Urbana, IL 61801, USA and [7]Center for Bio/Molecular Science & Engineering, Code 6900, U.S. Naval Research Laboratory, 4555 Overlook Avenue Southwest, Washington D.C., 20375, USA

Email:
Wolfgang J. Parak[*] - wolfgang.parak@physik.uni-marburg.de

* Corresponding author

Keywords:
colloidal stability; intracellular particle distribution; nanoparticles; protein corona; toxicity of nanoparticles

Beilstein J. Nanotechnol. **2014,** *5,* 1477–1490.
doi:10.3762/bjnano.5.161

Received: 21 March 2014
Accepted: 12 August 2014
Published: 09 September 2014

This article is part of the Thematic Series "Biological responses to NPs".

Guest Editor: R. Zellner

Abstract

The interfacing of colloidal nanoparticles with mammalian cells is now well into its second decade. In this review our goal is to highlight the more generally accepted concepts that we have gleaned from nearly twenty years of research. While details of these complex interactions strongly depend, amongst others, upon the specific properties of the nanoparticles used, the cell type, and their environmental conditions, a number of fundamental principles exist, which are outlined in this review.

Introduction

There is a multitude of reports about the interaction of colloidal nanoparticles (NPs) with mammalian cells [1], as this topic is important for analyzing intended (e.g., medical applications [2-4]) and non-intended (e.g., contamination [5-7]) exposure of NPs to humans. However, there is a great number of available NPs made of many different materials [8-10] with a wide range

of different functionalities, cf. Figure 1. For a classification of NPs according to their composition, functionality, and fields of application we refer to a recent review [11]. To complicate the situation, most NPs do not consist of only one substance, but typically are hybrid materials, involving surface coatings and other modifications [12], cf. Figure 2 [13]. Even a homogeneous NP formed out of only one material will turn effectively into a hybrid NP, when it is brought into contact with any biological system (e.g., biological media) because of an organic coating that will form on the surface of the NPs [14]. This all illustrates that virtually no two types of NPs are the same and their inherent structure, properties, and constituent materials will contribute to the way in which they are taken up by cells. For example, a 20 nm diameter polymeric dendrimer may be very flexible, whereas a 20 nm metal NP may not, which leads to different interaction with cells. Furthermore, all of these different NPs can be exposed to different cells (e.g., macrophages, endothelia, and tumor cells) under different exposure scenarios (in vitro and in vivo), which as a consequence culminates in a large, but diverse body of work reported in the literature [15-17]. Due to this overwhelming amount of data, it is not easy to obtain a comprehensive overview. Many studies focus on the details of particular systems, but those can dramatically vary from case to case, and even conflicting trends are reported [17]. In addition, results will depend on the cellular test model used. In order to simplify the discussion, this review focuses on in vitro interaction of NPs with adherent, mammalian, immortalized cell lines. This avoids for example the problem of having to discuss how NPs reach and penetrate tissue, which makes in vivo scenarios more complicated than in vitro test systems. Despite these issues, it is still possible to discern some general trends, as described within this review. However, a limitation to having general trends equates to being permissive of some specific details, though common agreements reported here are clearly not trivial. It also automatically involves the possibility that studies exist, which under particular experimental conditions claim the opposite to the general statements. The most important of these trends will be discussed. In this regard, the current review will focus on physicochemically defined NPs, i.e., solutions of monodisperse NPs with a defined ligand shell attached, and without residual "left-over" impurities of the NP synthesis [13,18].

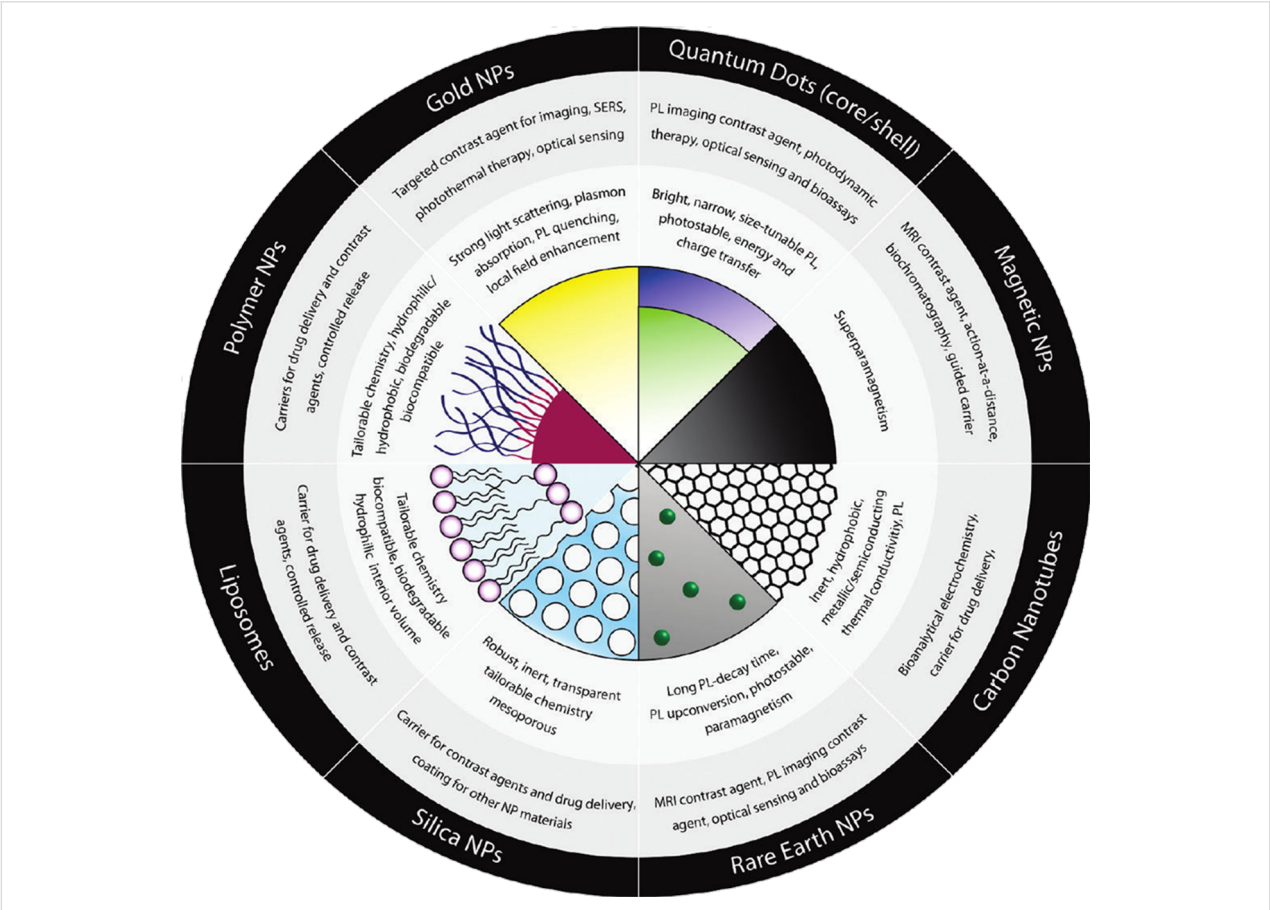

Figure 1: An overview of the "zoo" of different NPs concerning their composition, functionality, and fields of application. Reproduced with permission from [11]. Copyright (2011) American Chemical Society.

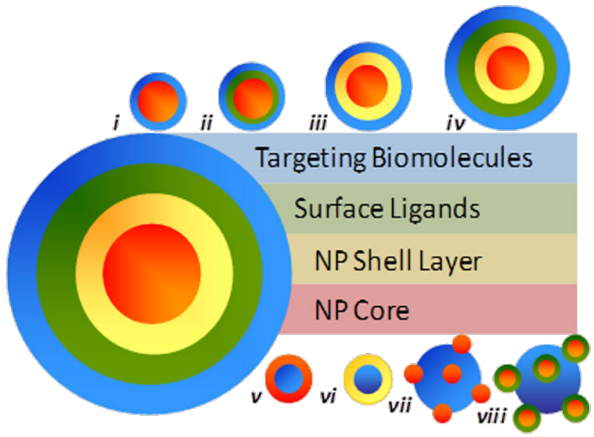

Figure 2: Hybrid nature of typical NPs, comprising different structural compartments. Reproduced with permission from [13]. Copyright (2013) American Chemical Society.

Review

How do particles enter cells and where do they go?

Virtually all cell lines internalize NPs, which are dispersed in the growth medium [19]. Uptake of different NPs by different cell lines, however, can vary significantly in biological kinetics [20-22] (this is also true for larger microparticles [23]). This is particularly important to keep in mind for specific (i.e., targeted) NP uptake, in which NPs modified by ligands (such as folic acid), which bind to appropriate receptors on the cell surface (such as folate receptors [24]), are specifically internalized [25]. Ligand-mediated uptake (which depends also on the ligand "valence", i.e., the number of ligands per NP, their density, and their orientation [26]) is faster and more efficient than non-specific (i.e., not receptor-mediated) uptake [27,28], although also plain or non-targeted NPs will be incorporated by cells. Thus, an important parameter to compare amongst studies, in which specific uptake is reported, is the time scale used within the experimental approach. While after short times of exposure huge differences in the amount of incorporated NPs can exist (e.g., between ligand-modified and plain NPs), those differences typically become less significant after longer exposure times [29], e.g., by the presence of the protein corona [30], as will be discussed later in more detail. Thus, statements which claim that only specifically modified NPs, but not non-modified NPs are taken up by cells, have to be regarded highly critically and put into the correct context of the reported time-scale. In fact, differences in uptake are not digital (i.e., "yes" or "no"), but rather are based on different kinetics. However, non-adhesive cell lines, i.e., cell suspensions, can be different and examples in which no significant internalization of NPs happened are reported [31]. Coming back to adhesive cell-lines, the first step in NP internalization obviously is the contact of the NP with the cell plasma membrane. This is a concentration-dependent process, which for high NP concentrations no longer scales linearly with concentration (i.e., saturation effects may occur). The first association of a non-targeted NP with a cell surface is usually electrostatic. Positively charged NPs are, for example, believed to interact with surface-displayed heparan sulfate proteoglycans [32,33]. As a rule of thumb, NPs which strongly interact with the cell plasma membrane, be it by ligand–receptor-mediated or by charge-mediated adhesion, are also internalized more efficiently [34]. Non-fouling polyethylene glycol (PEG)-modified NPs, for example, stick less to the cell plasma membrane and are, therefore, incorporated by cells less efficiently than other NPs [35-37] (this is also true in vivo as manifested by enhanced retention times [38]). It is clear that, while there are a number of portals through which NPs can gain entry into the cell, they all have as the common denominator the cell plasma membrane. Thus, the NP either must translocate (diffuse) directly across the cell plasma membrane entering the cytosol, or it must be internalized via any of the several routes of cellular endocytosis. While some evidence exists to support the direct membrane translocation of a select number of NP materials (typically partly hydrophobic and very small, as discussed later) the overwhelming evidence to date supports endocytosis as the common route of NP uptake. Thus, once NPs are associated to the outer cell plasma membrane they are typically internalized by endocytosis [39,40]. While a variety of different endocytotic pathways exist, which can be quite different in detail (to appreciate the complexity of endocytosis, we refer the reader to the review by Iversen et al. [41], cf. Figure 3), all of them have in common that the NPs are surrounded by membrane. Pinching-off of the membrane-surrounded NPs from the cell plasma membrane leaves the NPs incorporated into intracellular vesicles. These vesicles undergo a cascade of intracellular trafficking steps passing the NPs to more and more acidic vesicles [42,43], which also comprise enzymes specialized in digesting nutrition (and thus also parts of the NPs are digested in the lysosome [44,45]). In other words, after incorporation, the majority of NPs is not "free" in the cytosol, but inside intracellular vesicles (cf. Figure 4). Inside those intracellular vesicles the NPs are in an environment (acidic pH, enzymes) completely different from that in the cytosol (cf. Figure 5). Endocytosis and the endosomal escape dilemma have to be taken into account in particular concerning the delivery applications of NPs, in which the goal is to deliver something to the cytosol. Getting stuck inside intracellular vesicles is redundant to the purpose of these applications. However, in contrast to endocytosis as described so far, studies exist in which it is claimed that NPs can directly translocate through the cell membrane, thus indicating alternative pathways for NPs to penetrate the cell plasma membrane [46,47]. Besides other possible mechanisms, passive diffusion through (transient)

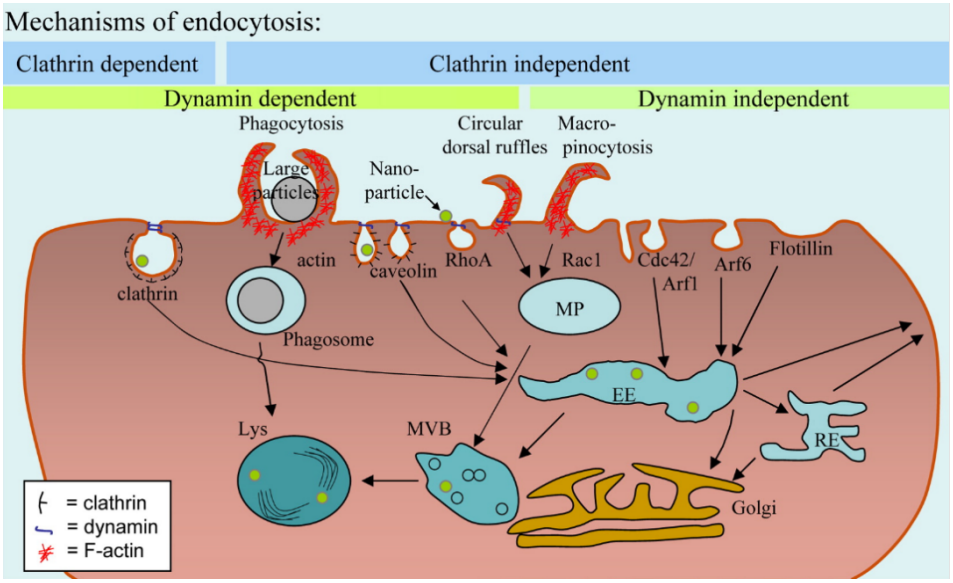

Figure 3: Scheme depicting the different mechanisms of cellular endocytosis. Reproduced with permission from [41]. Copyright (2011) Elsevier.

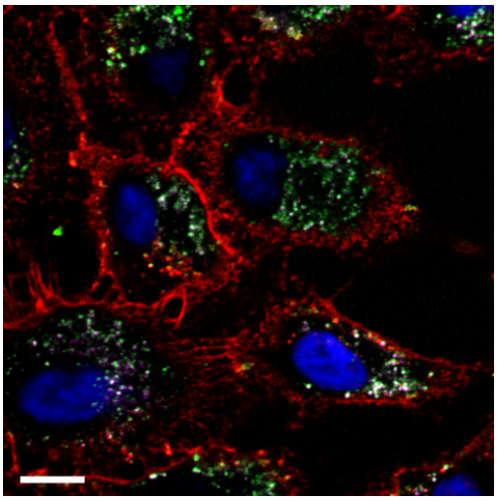

Figure 4: Fluorescence microscopy image showing the granular structure of internalized NPs inside A549 lung cancer cells (two types of iron oxide NPs with different surface chemistry, labelled with different fluorophores (green and magenta)) after 24 h of incubation at a concentration of 1 µg/mL, which are located in individual vesicles. Nuclei are stained with DAPI (blue) and the cell membrane with Wheat Germ Agglutinin (red). Note that due to limited lateral resolution of optical microscopy the spots most likely do not correspond to individual NPs, but to several NPs, which are entrapped inside intracellular vesicles. The scale bar represents 5 µm. Adopted with permission from [65] und Creative Commons Attribution 4.0 International Public License.

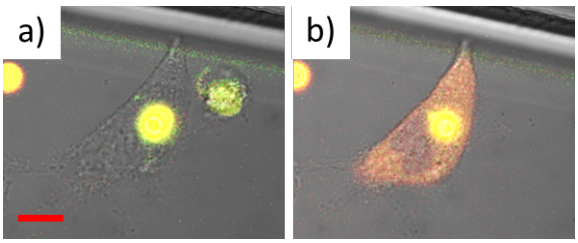

Figure 5: a) A microparticle has been internalized by an A549 lung cancer cell into an intracellular vesicle (here the lysosome [165]) and is thus clearly localized. The microparticle is filled with a pH-sensitive fluorophore (SNARF, from Invitrogen, now LifeTech) linked to dextran and the acidic pH of the lysosome is reported by the yellow fluorescence. b) After release of the pH-sensitive fluorophore linked to dextran to the cytosol (by photothermal heating), the fluorophore–dextran conjugates are freely dispersed, without any visible granular structure. Due to the neutral pH in the cytosol the fluorescence of the fluorophore–dextran conjugates has changed to red. The scale bar corresponds to 10 µm. Adopted with permission from [166]. Copyright (2012) Elsevier.

membrane pores and passive uptake by van der Waals or steric interactions (subsumed as adhesive interactions) have been suggested [48]. Still, it is always important to interpret such studies critically [49]. Most of the time studies involve an analysis of intracellular NP distributions, i.e., they rely on images showing NPs distributed in the cytosol. Additionally, these studies often rely on the observation that cellular NP entry still occurs below physiological temperatures (e.g., 4 °C), at which endocytosis and the active transport machinery are abrogated. However, without probing also for vesicular membranes around the NPs it is complicated to claim that the NPs in fact have passed the cell plasma membrane as "naked" NPs, without having ever been inside any intracellular vesicle. Clearly, there are a lot of indications (e.g., simulations) that NPs can enter cells through transient pore formation, in particular very small NPs [50,51]. Still, in many publications experiments do not

unequivocally demonstrate this pathway, though it surely exists. One possibility of experimental modification would involve, for example, pH-sensitive fluorophores (such as SNARF [52,53]) attached to the surface of the NPs, which can distinguish between the neutral cytosol and highly acidic intracellular vesicles [54]. In a similar direction the reductive capacity of glutathione (the cytosolic concentration of which is between 5 and 10 mM) may be used to displace a fluorescence resonance energy transfer (FRET) acceptor on the surface of the NP as confirmation of a successful NP localization to the cytosol [55]. Such experiments are in particular important for distinguishing between direct translocation to the cytosol versus endocytotic uptake followed by endosomal release. In fact, while there is clear experimental proof that NPs can be transported to the cytosol, the most straightforward pathway is uptake through endocytosis followed by release from the intracellular vesicles to the cytosol [56-58] (and not the diffusion through (transient) membrane pores). Endosomal release is, for example, a scenario which has been unraveled in detail for NPs coated with certain cell penetrating peptides (CPPs) [59-62]. Thus, while NPs can be free in the cytosol, this clearly does not automatically involve that they are membrane-permeable and not endocytosed. As pointed out above, observations based on merely measuring intracellular NP distributions are not sufficient for making profound statements about the uptake pathway. On the other hand it is safe to say that different intracellular locations for NPs exist. NPs have been reported in different intracellular organelles such as mitochondria, the nucleus, and free in the cytosol [63,64]. Most of the time such intracellular distributions are analyzed with transmission electron microscopy (TEM), in which also the structure of the intracellular organelles can be resolved (cf. Figure 6), or with fluorescence microscopy, in which the intracellular organelles have been co-stained with a fluorescent marker [65-67]. However, these data have to be interpreted carefully. In particular, such data should always include a quantitative distribution analysis, which is highly time-consuming. Even plain NPs without any particular surface capping can be found free in the cytosol [68], however, only to a very low extent. Thus, images in which NPs are shown in some particular intracellular organelles are only of limited value if the fraction of NPs that resides in these organelles is not quantified. Quantification, however, is not as trivial as it seems, and there is a need for better quantitative techniques for the future. While TEM offers the lateral resolution to visualize individual NPs, typically only a limited amount of cell sections (i.e., thin slices cut from cells) can be observed and thus for an absolute quantification, which is highly time-consuming, stereological tools need to be employed [68,69]. Also in case of TEM studies knowledge and understanding of cells under TEM conditions is essential. Fluorescence, on the other hand, can be recorded quantitatively by assuming that the emission intensity is proportional to the number of NPs. However, fluorescence can be partly quenched in certain organelles (for example at low pH), and it is impossible to resolve individual NPs due to the limited lateral resolution of optical microscopy [70]. In addition, as mentioned before, NPs can be partly degraded after having been internalized [71,72] and thus, in case fluorescently labeled NPs are used, it is required to prove that the fluorescence (or any other) label is still attached to the NPs inside the cells. Otherwise the recorded intracellular distribution of fluorescence may originate from detached labels and thus would not reflect the distribution of the NPs [73]. Summarizing available data suggests that, while translocation from intracellular compartments to the cytosol and from there to other cellular organelles is possible, translocation efficiencies still are moderate at best. In addition, NPs free in the cytosol may later end up again in intracellular vesicles through auto-phagocytosis [74]. Thus, for many applications, such as intracellular sensing or drug delivery, translocation of NPs to the cytosol after spontaneous endocytotic uptake remains a major challenge. External stimuli may be helpful in this direction [75]. In order to close this section it is also important to think about what happens after endocytotic uptake. It is, for instance, often overlooked that there is an eventual loss of the total NP load per cell as a result of mitotic division, NP exocytosis, and NP transcytosis [76]. This is largely due to the fact that in most experimental systems the primary issues addressed are uptake efficiency of the NPs and subsequent intracellular fate. These parameters are typically asked over the time course required for NP internalization and subcellular localization, and are not tracked over long time courses. It is generally accepted that NPs are partitioned during cell division,

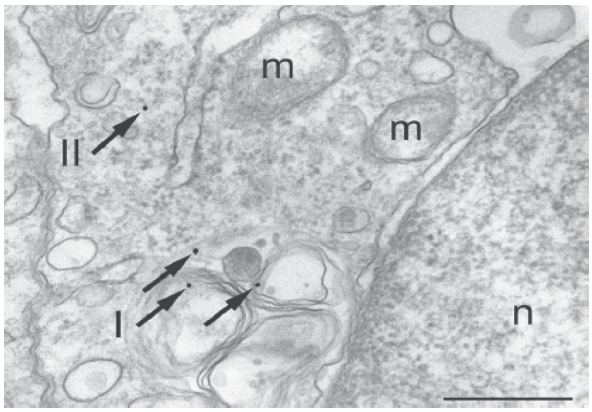

Figure 6: Intracellular compartments after internalization of PEG-coated gold NPs as visualized with TEM. The NPs (which are individually resolved due to the high lateral resolution of TEM) are located within a lysosome (arrows I) and in the cytosol (arrow II). *m* and *n* demark the nucleus and mitochondria, respectively. The scale bar corresponds to 500 nm. Adopted from with permission from [68]. Copyright 2010 Wiley-VCH Verlag GmbH & Co. KGaA, Weinheim.

in which they are passed to the daughter cells [76,77]. Such dilution effect of NP labels is in particular important for studies involving NPs as long-term tracers. Here, the relevant question arises whether upon cell division NPs are passed 50/50 to each daughter cell. Summers et al. have done both a theoretical [78] and experimental assessment [79] showing that, while partitioning of endosomes to daughter cells is symmetric, the number of NPs per endosome is a distribution and therefore NP partitioning to daughter cells is asymmetric. Thus, after several division cycles the NP distribution will not necessarily be representative for the fate of the original "mother" cells anymore. NPs also can be excreted to the extracellular medium, which represents an additional source of NP dilution effects. While endocytosis of NPs has been investigated heavily there are only a limited number of reports investigating exocytosis of NPs [80-82]. Excretion of NPs in exosomes (i.e., membrane surrounded vesicles), however, clearly affects the long-term cellular loading with NPs. In addition, for some particular cells, transcytosis has also been reported, i.e., that NPs are passed from one cell to another one [83].

What are the critical parameters involved in in vitro nanoparticle internalization?

As mentioned before, virtually all NPs are spontaneously internalized by adherent cells, mainly cell lines, that are usually grown on a certain support and covered with cell culture medium under static conditions. In this case, NPs in the medium can directly access cells, and issues like tissue penetration, which need to be considered in in vivo experiments, can be neglected. The kinetics of internalization can depend strongly on the physicochemical properties of the NPs, the type of cells, and other parameters. Cellular uptake studies of NPs require as much characterization of the NP materials as currently possible. Concerning the NPs, this is, unfortunately, hampered by our incapability to synthesize "defined" NPs. For quantitative studies NPs and their bioconjugates should be as monodisperse as possible with regard to all relevant parameters, such as charge and size, well-defined and well-characterized. Moreover, in the case of bioconjugates, the biological molecule, be it protein or drug, should be attached to the NP with control over orientation [84,85], density, affinity, and number or ratio per NP [85]. Although these goals are extremely hard to achieve, the more they can be fulfilled, the less heterogeneity is present in the NP material and the easier the results (i.e., the correlation between the properties of the NPs and the observed interaction of NPs with cells) can be interpreted [13,18,86]. With limitations, a correlation of the spontaneous endocytotic uptake of NPs to the physicochemical properties of the NPs can be found. One, however, has to be aware that many physicochemical properties of NPs, such as size, shape, charge, and colloidal stability are highly entangled [14]. The physicochemical properties are not intrinsically associated with the NPs, but result from the interaction of the NPs with the surrounding particular medium [87]. The colloidal stability is presumably the most influential parameter. NPs with low colloidal stability will agglomerate and thus, originally "small" NPs will transform into agglomerates, resulting in large particles presented to the cells (cf. Figure 7). However, "colloidal stability" is not a defined physicochemical entity such as size, but needs to be put in context with the measurement protocol, such as the tendency to agglomerate. Any correlation to the size of the NPs without any previous demonstration of colloidal stability in the incubation medium has to be seen very critically. Loss of colloidal stability during incubation also complicates dosimetry. If NPs are quantified in numbers, is an agglomerate of NPs considered to be one particle or the number of NPs in the agglomerate [14]? Agglomeration can have direct consequences on cellular uptake [62]. If the cell cultures are turned upside-down, i.e., the cells are hanging in the culture medium, NP agglomerates that have precipitated at the bottom would not reach the cells and thus the effective NP concentration would be dramatically reduced [88]. In contrast, in conventional geometry, in which the culture medium is on top of the cells, a reduced colloidal stability leads to the precipitation of NP agglomerates onto the cells and, thus, to enhanced uptake, which can influence the cell viability negatively [89]. Such different exposure scenarios are highly relevant for the prediction of NP interactions, for instance, in the human body or in ecotoxicology. Some NPs have been mistaken to elicit limited to no adverse effects upon zebrafish assays, as they had precipitated to the bottom, and thus, the fish had not been directly exposed to them. After correct solubilization, however, the same NPs turned out to be highly detrimental to zebrafish health [90]. Colloidal stability does not only interfere with size but also with other parameters such as shape. An agglomerated bundle of sharp NPs may no longer be "sharp". Thus, colloidal stability is the paramount parameter to consider for all correlations between the NP–cell interactions and the physicochemical properties of the NPs.

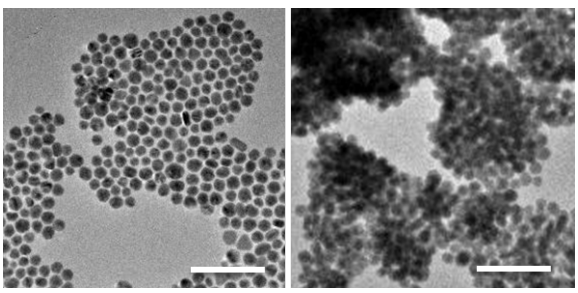

Figure 7: TEM images of a) dispersed and b) agglomerated Au NPs. The scale bars correspond to 100 nm. Adopted with permission from [30]. Copyright 2014 Royal Society of Chemistry.

Reports, in which no characterization of colloidal properties has been performed, therefore have to be regarded very critically. Unfortunately, many NPs are not colloidally stable in cell culture media [91]. The reason is that many NPs are stabilized by charge (in contrast to stabilization through steric repulsion). Salt (in particular NaCl, which always is present at high concentration) in the media screens the NP charge and thus can cause agglomeration [92]. Consequently, data which demonstrate that NPs are colloidally stable in water do not provide any proof that the same NPs also will be stable in cell culture media. Besides salt, proteins are another key compound of (serum-containing) cell media. As discussed later in more detail, proteins adsorb to the surface of NPs, forming the so-called protein corona [93,94], which in fact can increase or reduce colloidal stability [95,96]. Thus, characterization of colloidal stability and other physicochemical properties of NPs needs to be carried out under the same conditions under which later on cells are incubated with the NPs (i.e., in the respective cell culture media [86,97,98]). Obviously, NPs also should be appropriately purified [99], as otherwise effects from impurities rather than from the NPs themselves cannot be excluded. Unfortunately, for unstable NPs (e.g., for NPs to which the organic surface capping is only loosely attached) purification can trigger a loss of colloidal stability and thus agglomeration [14]. As lack of colloidal stability can overrule the other parameters, the following discussion about dependencies of other parameters is done assuming colloidally stable NPs. Uptake of NPs into the cells clearly depends on the size of the NPS. In general, smaller NPs are incorporated by cells faster than bigger ones, though there is some kind of size limit, i.e., the trend does not continue down to ultrasmall NPs [40,100]. As mentioned, upon endocytosis NPs are first wrapped by cellular membrane. Due to intrinsic stiffness and other parameters for membrane bending the radii of curvature cannot become infinitely small, and thus, there is an optimal NP size [101,102]. Excluding ultra-small NPs (smaller than 2–3 nm), smaller NP (smaller than 20–25 nm) are internalized readily in endosomes with most rapid kinetics [103]. Larger NPs (smaller than 60–70 nm) are internalized with lower kinetics to the extent that they are largely associated to the cell membrane over the time courses that see an intake of smaller NPS [62]. This has also been shown in fixed, permeabilized cells (to eliminate cell uptake machinery and pathways) to directly assess the size restrictions of plasma and intracellular membrane barriers on NP passage [104]. In contrast, ultrasmall NPs may be small enough to become membrane-permeable and thus bypass endocytotic uptake. Size-dependent uptake has also been reported for in vivo scenarios [105]. However, in particular for statements concerning size-dependent internalization, the experimental size determination of NP is important. Unfortunately, this is not a straightforward task, as different techniques measure different types of sizes. TEM only provides the geometric size of the NP core which has sufficient contrast, but organic surface cappings are typically not included [14]. In solution there is adsorption of counter ions to the NP surface [106,107] and organic surface coatings can swell, which results in hydrodynamic diameters larger than the core diameters as determined with TEM. There are several techniques for determining the hydrodynamic diameters of NPs [108], of which dynamic light scattering (DLS) might be the most common approach. All techniques have their limitations, and it is always helpful to know the measuring principle they are based on. DLS, for example, is based on calculating autocorrelation functions of the light-scattering signal of the solution. In order to obtain quantitative values, these autocorrelation data need to be fitted with a model, which is, for example, often done by assuming free diffusion of three NP species of different size. Thus, the results are based on the model (which is hidden as "black-box" in the software). To give an example, in case three species are assumed one always will obtain three peaks in the size distribution spectra, even though the sample may contain more different NP species. From the model, diffusion coefficients are yielded as fit parameters, which can be converted to hydrodynamic diameters by the Stokes–Einstein relation. As NPs of larger size also scatter light much more than smaller NPs, the results for DLS-derived size distributions also are quite different depending on whether number or intensity distributions are reported. Thus, simply taking the mean hydrodynamic diameter as displayed by commercial set-ups is prone to errors [109]. Calibration standards of NPs of known size are always a good help to benchmark size measurements and it is highly beneficial to apply several techniques in parallel [108-110]. By applying existing techniques correctly, the hydrodynamic diameters of NPs can be determined with remarkable accuracy, in particular if relative size changes are determined. Detection can be sensitive enough to resolve size-changes due to the attachment of individual macromolecules to the NPs [84,85,111,112]. Besides size, also shape has been proven to modulate the NP uptake of cells. In general, elongated, sharp NPs (i.e., NPs with a prolate spheroid shape) enter cells better than flatter NPs (i.e., NPs with an oblate spheroid shape). This however does no longer hold for very long fibers with high aspect ratios [100]. Flattening of NPs has been used, for example, to reduce NP uptake by cells in a way that flat NPs just adhere to the plasma cell membrane like a “backpack”, without being internalized, in contrast to spherical NPs that are readily incorporated [113,114]. Concerning a third parameter, charged NPs usually are internalized more efficiently than neutral ones, presumably due to enhanced charge-mediated adhesion to the outer cell membrane. Note that the charge pattern of the plasma cell membrane is patchy, and thus, while the overall net charge of cells is negative, there are plenty of positively charged domains. However, due to the overall

negative net charge, positively charged NPs are typically incorporated more efficiently by cells than negatively charged ones [65,97,115-119]. Indeed, the current consensus is that positive charges on NPs, such as those provided by the TAT peptide or surface functionalization, interact initially with the negatively charged heparan sulfate proteoglycan groups on the exterior of the cells. This allows them to then be present on the plasma cell membrane as endocytosis starts. Thus, while details may be very complex, clearly some tendencies for which physicochemical parameters enhance the spontaneous endocytosis of NPs can be given. In general, small, elongated, and positively charged NPs are incorporated preferentially to big, flat, and uncharged NPs. Dependency on other physicochemical parameters such as stiffness [120] has not been investigated extensively yet.

The role of the protein corona

In serum-containing media or inside cells all different types of biologically relevant molecules adsorb to the surface of NPs. i) Ions such as H^+, Na^+, K^+ or Ca^{2+} in the case of negatively charged NPs, or Cl^- in the case of positively charged NPs adsorb to the NPs. As a consequence of counter ion adsorption the local ion concentration around the NPs surface is different from the bulk [54,87,106,107]. ii) Also nucleic acids, such as mRNA or siRNA, which are negatively charged due to their phosphate groups attach to positively charged NPs [121,122]. iii) Lipids present in membranes or second-messenger lipids wrap around NPs driven by hydrophilic/hydrophobic interaction and often result in formation of micelles [123,124]. iv) Thiols, present in glutathione or reduced proteins bind to the surface of noble metal NPs, in particular to Au NPs [125,126]. v) Proteins, in general, tend to adsorb to surfaces, which is also true on the nanometer scale. Adsorption of albumin is, for example, an integral part of opsonization [127,128]. The proteins adsorbed to the surface of NPs are typically termed protein corona [93,94]. The protein corona has a significant impact on how NPs interact with cells and thus will be discussed in the following in more detail. NPs can, in principle, be synthesized in water without any organic surface coating, for example by laser ablation [129-131]. However, also to NPs just stabilized by their surface charge (which can be directly on the inorganic surface) proteins will adsorb in serum-containing cell media and in this way can provide additional colloidal stability [129]. Therefore, there are no "naked" NPs in serum-containing cell culture media and inorganic NP cores are always surrounded by an organic coating [14]. Adsorbed proteins can significantly alter the surface properties of NPs and are of key importance in defining the biological identity of NPs [132,133]. The corona formed around NPs is what the cell will “see” primarily, though certainly also the original properties of the underlying NPs determine interactions with the cells [97]. In general, adsorbed proteins "smear out" differences in the surface chemistry between different NPs. Thus, typically two different types of NPs show more pronounced differences in their interaction with cells in case exposure is done in serum-free media (i.e., without proteins) rather than in serum-containing media [97]. The effect of ligands immobilized on the surface of NPs designated for ligand–receptor-mediated uptake is diminished by the protein corona, which partly overcoats the ligands [134]. However, due to the fact that specific targeting still is possible [84], enough ligands still are biologically active. For highly defined NPs, such as nearly monodisperse NPs overcoated with a shell of an amphiphilic polymer [135], the corona formed by special model proteins can be surprisingly well organized. By using fluorescence correlation spectroscopy (FCS), Röcker et al. investigated the adsorption of human serum albumin onto FePt NPs and found clear evidence that the proteins formed a monolayer on the surface of the NP [136]. Additional FCS studies by using other important serum proteins invariably confirmed the formation of monolayer. The thickness of the monolayer could be related to the molecular dimensions of the adsorbed protein determined by X-ray diffraction. All proteins studied were found to adsorb in a specific orientation determined by local charge distributions on the protein surface [20,137,138]. However, adsorption of proteins to the surface of NPs is not only driven by the basic physicochemical properties of the NP such as size, shape, surface charge, but also by other parameters such as the incubation temperature [139]. While model systems involving only one type of NPs and one type of protein help to analytically quantify protein adsorption, such as by determining binding constants [30,136], the biological reality is more complex. Serum-containing cell culture media comprise hundreds of different proteins. To make it worse to analyze, protein adsorption is also a dynamic process. Thus, proteins which are initially bound to the NP surface can later be replaced by others [140,141], which also is referred to as the Vroman effect [142]. It has been shown, for example, that surfactant lipids bound on multiwall carbon nanotubes are replaced with blood plasma proteins after a subsequent incubation [143]. Mass spectrometry is an invaluable tool for quantifying the amounts of different adsorbed protein species [140,141]. The dynamic exchange of proteins, induced by their different adsorption kinetics and affinities to the NP surface is reflected in the discrimination between "soft" and "hard" corona [144,145]. The initial, soft corona is formed by the most abundant proteins, which are then replaced by the high-affinity proteins to yield the hard corona. It has been suggested that differences for different protein species can be characterized by their dissociation constants [30]. In a simple model the dissociation constant tells which protein concentration is required to saturate half of the NP surface with proteins under equilibrium conditions [30]. With simple treatments such as the Hill Model

[146] one may characterize the protein corona around NPs with only a few parameters, which would be a great help in comparing results obtained with different systems, thus allowing for a more comprehensive understanding. While the protein corona around NPs has been heavily investigated these data ultimately are only relevant for the first interaction of NPs with cells. After spontaneous endocytosis NPs are inside intracellular vesicles. This imposes a completely different environment than that of the extracellular medium, in particular low pH, presence of endo-/lysosomal enzymes, and different reducing agents [147]. Thus, after NP uptake the protein corona around NPs may change significantly. The original proteins can be displaced by other intracellular proteins, and even more severe, part of the original protein corona may be digested enzymatically [44,45,148,149]. Changes of the protein corona in turn may also alter the physicochemical properties (such as colloidal stability) of the NPs [96]. In this manner, for a full understanding of NP interaction with cells along the pathway of NP uptake the physicochemical characterization of NPs should also be done intracellularly, which, however, is complicated. This opens up a window for future research efforts.

Toxic effects of NPs

NPs clearly can trigger toxic effects in cells such as cytotoxicity, oxidative stress, (pro-)inflammation, and genotoxicity [150-152]. While again the detailed mechanisms are very complex and by far not understood in a comprehensive way, yet again there are certain characteristic features [153]. Toxic effects can result from the NPs themselves (e.g., by their catalytic surface or by their organic coating, such as in the case of cetyltrimethylammonium bromide (CTAB), a surfactant commonly used to synthesize gold nanorods) or by ions released from the NPs [154,155]. Ion release from certain materials such as Ag, ZnO, or CdSe is in particular triggered by the highly acidic pH in endo-/lysosomal compartments [156]. In both cases adverse biological effects are typically correlated with the production of reactive oxygen species (ROS) [157,158]. Also membrane damage plays a decisive role. In case of dissolvable NPs, the extent to which toxicity originates from the NPs themselves and to which extent from released ions is still subject to an intense scientific debate. Unfortunately, it is experimentally complicated to separate both effects. Even if before exposure all free ions were removed from the NP solution, inside cells new ions would be released. Thus, it is virtually impossible to have cells exposed exclusively to NPs without free ions [87]. One may argue that on the other hand cells could be exposed just to the free ions. While this is true, exposure to free ions will result in different intracellular ion distributions than the one obtained by ions which have been released from the NPs intracellularly, which again complicates direct comparison. Physicochemical properties can be, in some way, correlated with NP toxicity. In other words, reporting toxicity without accompanying in-depth NP characterization is not very useful concerning a detailed understanding of the mechanism. Surface coatings and impurities in the NPs can play an important role. Thus, also the coatings alone, as well as potential impurities need to be investigated towards potential toxic effect in control experiments. If only the physicochemical properties of "pure" NPs are considered, NPs with low colloidal stability have bigger effective sizes, thus are internalized to a larger extent, and thus typically have a greater adverse biological impact [154]. In order to account for concentration effects, it is advisable to correlate toxicity with particle internalization by using adequate methods. Enhanced uptake is one major reason (amongst others) why positively charged NPs (which are incorporated to a higher extent) elicit an increased adverse cellular effect compared to negatively charged ones [97,117,118]. This opens a dilemma. While in general, positive charge is better for enhanced uptake, too much positive charge becomes so toxic that it outweighs the added benefit of enhanced uptake. Thus, for delivery applications an optimum between both effects has to be found. This opens up another important point about the biological impact of NPs that merits discussion. There is a big difference between the use of NPs for cellular labeling or biosensing studies in research, as opposed to any therapeutic (in vivo) utility, and the two should never be thought of together or directly compared. It was, for example, recently shown that semiconductor quantum dot NPs (QDs) were unable to elicit a more negative biological effect when used for cellular labeling than a panel of dyes commonly used for the same intrinsic purposes [159]. Along with this, often transformed and immortalized cell lines are used in biological research, meaning that they are essentially cancerous. Thus, what appears to be adverse biological impact in these experiments has to be qualified with this context in mind. For cellular labeling, perhaps, there is the need for a particular experiment that should drive the issue of toxicity. If the use is specifically for in vitro labeling, tracking or sensing, there are multiple studies that have shown that over the time course required to perform such studies, the impact on cellular viability/proliferation at appropriate NP concentrations is minimal and is often comparable to or even less impactful than the use of traditional materials designed for the same purpose [159]. In this case "chronic toxicity" does not play a role, as the experiment is terminated before such an effect may occur. In contrast, for in vivo delivery one has to consider that NPs will remain in the organism over extended periods of time [160], and thus, benefits of treatment have to be weighted with long-term toxic effects [161]. Consequently, toxicity of NPs always has to be seen in the context of the applications the NPs are used for, but furthermore, the potential accidental exposure beyond the application has to be considered and its risk has to be assessed. In the

context of this review we have focused on in vitro studies. The advantage of such studies is the easy screening capability and the possibility to monitor in detail biomolecular pathways and changes in gene expression as a measure of a possible biologically adverse response. In case NP toxicity is investigated in a comprehensive study, however, involvement of in vivo experiments is crucial.

Conclusion

Due to their interesting functional properties, numerous applications of NPs exist, e.g., plasmonic NPs [2,75], magnetic NPs [162,163] or fluorescent NPs [164]. For optimizing NP properties for biological applications, an understanding of their interaction with mammalian cells needs to be gained. However, the interaction of NPs with cells is complex due to the many different types of NPs, cells, and exposure scenarios being used within the field. Still, one may make an attempt to reduce details to very general statements, in order to highlight some essential elements, which was the motivation for this review.

Endocytosis is the common route of NP uptake. NPs which strongly interact with the cell plasma membrane are also internalized more efficiently. Hereby differences in uptake are not digital (i.e., "yes" or "no"), but rather are based on different concentration-dependent kinetics. After internalization NPs inside intracellular vesicles are in an environment (acidic pH, enzymes) completely different from that in the cytosol and the extracellular space, which can modify their properties. The translocation of the NPs from these vesicles to the cytosol is a current challenge, which is referred to as endosomal escape dilemma. Uptake studies best should involve a quantitative distribution analysis. While endocytotic uptake of NPs has been extensively investigated, the eventual loss of internalized NPs as a result of mitotic division, NP exocytosis, or NP transcytosis on the other hand has not been comprehensively studied yet. Cellular uptake studies of NPs require as much characterization of the NP material as currently possible. However, many physicochemical properties of NPs such as size, shape, charge, and colloidal stability are highly entangled, which complicates analysis. Analysis of physicochemical properties should be always performed in the incubation medium in which the uptake of NPs by cells is studied. The incubation medium can for example modify the colloidal stability of the NPs. Colloidal stability does not only interfere with size but also with other parameters such as shape. In general, small, elongated, and positively charged NPs are incorporated preferentially to big, flat, and uncharged NPs.

Acknowledgements

This work and a large fraction of quoted work by WJP were supported by the German Research Foundation (DFG, SPP 1313, Project PA794/4-2) and this review represents the final report of this project. The authors are grateful to Dr. Torsten Hotopp from the DFG for managing and guiding the SPP 1313 funding initiative. BP acknowledges a fellowship from the Alexander von Humboldt Foundation. QZ acknowledges a fellowship from the Chinese Scholarship Council (CSC). MGS acknowledges a fellowship from the Youssef Jameel Foundation. JBD and ILM acknowledge the NRL NSI and DTRA for support. GUN acknowledges the DFG for support (DFG grants NI291/7 and NI291/8).

References

1. Verderio, P.; Avvakumova, S.; Alessio, G.; Bellini, M.; Colombo, M.; Galbiati, E.; Mazzucchelli, S.; Avila, J. P.; Santini, B.; Prosperi, D. *Adv. Healthcare Mater.* **2014,** *3,* 957–976. doi:10.1002/adhm.201300602
2. Sperling, R. A.; Rivera Gil, P.; Zhang, F.; Zanella, M.; Parak, W. J. *Chem. Soc. Rev.* **2008,** *37,* 1896–1908. doi:10.1039/b712170a
3. Rivera Gil, P.; Parak, W. J. *ACS Nano* **2008,** *2,* 2200–2205. doi:10.1021/nn800716j
4. Peteiro-Cartelle, J.; Rodríguez-Pedreira, M.; Zhang, F.; Rivera Gil, P.; del Mercato, L. L.; Parak, W. J. *Nanomedicine* **2009,** *4,* 967–979. doi:10.2217/nnm.09.84
5. Bar-Ilan, O.; Chuang, C. C.; Schwahn, D. J.; Yang, S.; Joshi, S.; Pedersen, J. A.; Hamers, R. J.; Peterson, R. E.; Heideman, W. *Environ. Sci. Technol.* **2013,** *47,* 4726–4733. doi:10.1021/es304514r
6. Borm, P. J. A.; Robbins, D.; Haubold, S.; Kuhlbusch, T.; Fissan, H.; Donaldson, K.; Schins, R.; Stone, V.; Kreyling, W.; Lademann, J.; Krutmann, J.; Warheit, D.; Oberdorster, E. *Part. Fibre Toxicol.* **2006,** *3,* No. 11. doi:10.1186/1743-8977-3-11
7. Lewinski, N.; Colvin, V.; Drezek, R. *Small* **2008,** *4,* 26–49. doi:10.1002/smll.200700595
8. Parak, W. J. *Science* **2011,** *334,* 1359–1360. doi:10.1126/science.1215080
9. Lin, C.-A. J.; Yang, T.-Y.; Lee, C.-H.; Huang, S. H.; Sperling, R. A.; Zanella, M.; Li, J. K.; Shen, J.-L.; Wang, H.-H.; Yeh, H.-I.; Parak, W. J.; Chang, W. H. *ACS Nano* **2009,** *3,* 395–401. doi:10.1021/nn800632j
10. Pandey, A.; Roy, M. K.; Pandey, A.; Zanella, M.; Sperling, R. A.; Parak, W. J.; Samaddar, A. B.; Verma, H. C. *IEEE Trans. NanoBiosci.* **2009,** *8,* 43–50. doi:10.1109/TNB.2009.2017316
11. Algar, W. R.; Prasuhn, D. E.; Stewart, M. H.; Jennings, T. L.; Blanco-Canosa, J. B.; Dawson, P. E.; Medintz, I. L. *Bioconjugate Chem.* **2011,** *22,* 825–858. doi:10.1021/bc200065z
12. Sperling, R. A.; Parak, W. J. *Philos. Trans. R. Soc. London, Ser. A* **2010,** *368,* 1333–1383. doi:10.1098/rsta.2009.0273
13. Sapsford, K. E.; Algar, W. R.; Berti, L.; Gemmill, K. B.; Casey, B. J.; Oh, E.; Stewart, M. H.; Medintz, I. L. *Chem. Rev.* **2013,** *113,* 1904–2074. doi:10.1021/cr300143v
14. Rivera Gil, P.; Jimenez de Aberasturi, D.; Wulf, V.; Pelaz, B.; Del Pino, P.; Zhao, Y.; De La Fuente, J. M.; Ruiz De Larramendi, I.; Rojo, T.; Liang, X.-J.; Parak, W. J. *Acc. Chem. Res.* **2013,** *46,* 743–749. doi:10.1021/ar300039j
15. Auffan, M.; Rose, J.; Bottero, J.-Y.; Lowry, G. V.; Jolivet, J.-P.; Wiesner, M. R. *Nat. Nanotechnol.* **2009,** *4,* 634–641. doi:10.1038/nnano.2009.242
16. Sardar, R.; Funston, A. M.; Mulvaney, P.; Murray, R. W. *Langmuir* **2009,** *25,* 13840–13851. doi:10.1021/la9019475

17. Goesmann, H.; Feldmann, C. *Angew. Chem., Int. Ed.* **2010,** *49,* 1362–1395. doi:10.1002/anie.200903053
18. Medintz, I. *Nat. Mater.* **2006,** *5,* 842. doi:10.1038/nmat1776
19. Treuel, L.; Jiang, X.; Nienhaus, G. U. *J. R. Soc., Interface* **2012,** *10,* 20120939. doi:10.1098/rsif.2012.0939
20. Jiang, X.; Weise, S.; Hafner, M.; Röcker, C.; Zhang, F.; Parak, W. J.; Nienhaus, G. U. *J. R. Soc., Interface* **2010,** *7* (Suppl. 1), S5–S13. doi:10.1098/rsif.2009.0272.focus
21. Doiron, A. L.; Clark, B.; Rinker, K. D. *Biotechnol. Bioeng.* **2011,** *108,* 2988–2998. doi:10.1002/bit.23253
22. Li, Y.; Yue, T.; Yang, K.; Zhang, X. *Biomaterials* **2012,** *33,* 4965–4973. doi:10.1016/j.biomaterials.2012.03.044
23. Muñoz Javier, A.; Kreft, O.; Semmling, M.; Kempter, S.; Skirtach, A. G.; Bruns, O. T.; del Pino, P.; Bedard, M. F.; Rädler, J.; Käs, J.; Plank, C.; Sukhorukov, G. B.; Parak, W. J. *Adv. Mater.* **2008,** *20,* 4281–4287. doi:10.1002/adma.200703190
24. Antony, A. C. *Annu. Rev. Nutr.* **1996,** *16,* 501–521. doi:10.1146/annurev.nu.16.070196.002441
25. Ding, H.-m.; Ma, Y.-q. *Biomaterials* **2012,** *33,* 5798–5802. doi:10.1016/j.biomaterials.2012.04.055
26. Avvakumova, S.; Colombo, M.; Tortora, P.; Prosperi, D. *Trends Biotechnol.* **2014,** *32,* 11–20. doi:10.1016/j.tibtech.2013.09.006
27. Ahrens, E. T.; Feili-Hariri, M.; Xu, H.; Genove, G.; Morel, P. A. *Magn. Reson. Med.* **2003,** *49,* 1006–1013. doi:10.1002/mrm.10465
28. Tassa, C.; Duffner, J. L.; Lewis, T. A.; Weissleder, R.; Schreiber, S. L.; Koehler, A. N.; Shaw, S. Y. *Bioconjugate Chem.* **2010,** *21,* 14–19. doi:10.1021/bc900438a
29. Muñoz Javier, A.; Kreft, O.; Piera Alberola, A.; Kirchner, C.; Zebli, B.; Susha, A. S.; Horn, E.; Kempter, S.; Skirtach, A. G.; Rogach, A. L.; Rädler, J.; Sukhorukov, G. B.; Benoit, M.; Parak, W. J. *Small* **2006,** *2,* 394–400. doi:10.1002/smll.200500282
30. del Pino, P.; Pelaz, B.; Zhang, Q.; Maffre, P.; Nienhaus, G. U.; Parak, W. J. *Mater. Horiz.* **2014,** *1,* 301–313. doi:10.1039/C3MH00106G
31. Lin, J.; Yu, Y.; Li, B.; Huang, H.; Lin, S.; Li, C.; Su, Y.; Feng, S.; Chen, G.; Li, Y.; Huang, Z.; Zeng, H.; Chen, R. *Laser Phys. Lett.* **2012,** *9,* 240–246. doi:10.1002/lapl.201110125
32. Orr, G.; Panther, D. J.; Cassens, K. J.; Phillips, J. L.; Tarasevich, B. J.; Pounds, J. G. *Toxicol. Appl. Pharmacol.* **2009,** *236,* 210–220. doi:10.1016/j.taap.2009.01.022
33. Zhang, H.; Xia, T.; Meng, H.; Xue, M.; George, S.; Ji, Z.; Wang, X.; Liu, R.; Wang, M.; France, B.; Rallo, R.; Damoiseaux, R.; Cohen, Y.; Bradley, K. A.; Zink, J. I.; Nel, A. E. *ACS Nano* **2011,** *5,* 2756–2769. doi:10.1021/nn200328m
34. Verma, A.; Stellacci, F. *Small* **2010,** *6,* 12–21. doi:10.1002/smll.200901158
35. Xiao, Y.; Forry, S. P.; Gao, X.; Holbrook, R. D.; Telford, W. G.; Tona, A. *J. Nanobiotechnol.* **2010,** *8,* No. 13. doi:10.1186/1477-3155-8-13
36. Clift, M. J. D.; Rothen-Rutishauser, B.; Brown, D. M.; Duffin, R.; Donaldson, K.; Proudfoot, L.; Guy, K.; Stone, V. *Toxicol. Appl. Pharmacol.* **2008,** *232,* 418–427. doi:10.1016/j.taap.2008.06.009
37. Soenen, S. J.; Manshian, B. B.; Abdelmonem, A. M.; Montenegro, J.-M.; Tan, S.; Balcaen, L.; Vanhaecke, F.; Brisson, A. R.; Parak, W. J.; De Smedt, S. C.; Braeckmans, K. *Part. Part. Syst. Charact.* **2014,** *31,* 794–800. doi:10.1002/ppsc.201300357
38. Lipka, M.; Semmler-Behnke, M.; Sperling, R. A.; Wenk, A.; Takenaka, S.; Schleh, C.; Kissel, T.; Parak, W. J.; Kreyling, W. G. *Biomaterials* **2010,** *31,* 6574–6581. doi:10.1016/j.biomaterials.2010.05.009
39. Gratton, S. E. A.; Ropp, P. A.; Pohlhaus, P. D.; Luft, J. C.; Madden, V. J.; Napier, M. E.; DeSimone, J. M. *Proc. Natl. Acad. Sci. U. S. A.* **2008,** *105,* 11613–11618. doi:10.1073/pnas.0801763105
40. Chithrani, B. D.; Chan, W. C. W. *Nano Lett.* **2007,** *7,* 1542–1550. doi:10.1021/nl070363y
41. Iversen, T.-G.; Skotland, T.; Sandvig, K. *Nano Today* **2011,** *6,* 176–185. doi:10.1016/j.nantod.2011.02.003
42. Grant, B. D.; Donaldson, J. G. *Nat. Rev. Mol. Cell Biol.* **2009,** *10,* 597–608. doi:10.1038/nrm2755
43. Saftig, P.; Klumperman, J. *Nat. Rev. Mol. Cell Biol.* **2009,** *10,* 623–635. doi:10.1038/nrm2745
44. Rivera-Gil, P.; De Koker, S.; De Geest, B. G.; Parak, W. J. *Nano Lett.* **2009,** *9,* 4398–4402. doi:10.1021/nl902697j
45. Chanana, M.; Rivera Gil, P.; Correa-Duarte, M. A.; Liz-Marzán, L. M.; Parak, W. J. *Angew. Chem., Int. Ed.* **2013,** *52,* 4179–4183. doi:10.1002/anie.201208019
46. Geiser, M.; Rothen-Rutishauser, B.; Kapp, N.; Schürch, S.; Kreyling, W.; Schulz, H.; Semmler, M.; Im Hof, V.; Heyder, J.; Gehr, P. *Environ. Health Perspect.* **2005,** *113,* 1555–1560. doi:10.1289/ehp.8006
47. Rothen-Rutishauser, B. M.; Schürch, S.; Haenni, B.; Kapp, N.; Gehr, P. *Environ. Sci. Technol.* **2006,** *40,* 4353–4359. doi:10.1021/es0522635
48. Rothen-Rutishauser, B.; Blank, F.; Mühlfeld, C.; Gehr, P. *Nanoparticle-Cell Membrane Interactions,* 2nd ed.; Informa Healthcare: New York, USA, 2009; pp 226–242.
49. Luccardini, C.; Yakovlev, A.; Gaillard, S.; van't Hoff, M.; Alberola, A. P.; Mallet, J.-M.; Parak, W. J.; Feltz, A.; Oheim, M. *J. Biomed. Biotechnol.* **2007,** No. 68963. doi:10.1155/2007/68963
50. Lin, J.; Alexander-Katz, A. *ACS Nano* **2013,** *7,* 10799–10808. doi:10.1021/nn4040553
51. Wang, T.; Bai, J.; Jiang, X.; Nienhaus, G. U. *ACS Nano* **2012,** *6,* 1251–1259. doi:10.1021/nn203892h
52. Semmling, M.; Kreft, O.; Muñoz Javier, A.; Sukhorukov, G. B.; Käs, J.; Parak, W. J. *Small* **2008,** *4,* 1763–1768. doi:10.1002/smll.200800596
53. Rivera Gil, P.; Nazarenus, M.; Ashraf, S.; Parak, W. J. *Small* **2012,** *8,* 943–948. doi:10.1002/smll.201101780
54. Zhang, F.; Lees, E.; Amin, F.; Rivera Gil, P.; Yang, F.; Mulvaney, P.; Parak, W. J. *Small* **2011,** *7,* 3113–3127. doi:10.1002/smll.201100608
55. Mitra, R. N.; Doshi, M.; Zhang, X.; Tyus, J. C.; Bengtsson, N.; Fletcher, S.; Page, B. D. G.; Turkson, J.; Gesquiere, A. J.; Gunning, P. T.; Walter, G. A.; Santra, S. *Biomaterials* **2012,** *33,* 1500–1508. doi:10.1016/j.biomaterials.2011.10.068
56. Panyam, J.; Zhou, W.-Z.; Prabha, S.; Sahoo, S. K.; Labhasetwar, V. *FASEB J.* **2002,** *16,* 1217–1226. doi:10.1096/fj.02-0088com
57. Fan, Y.; Li, C.; Cao, H.; Li, F.; Chen, D. *Biomaterials* **2012,** *33,* 4220–4228. doi:10.1016/j.biomaterials.2012.02.038
58. Bayles, A. R.; Chahal, H. S.; Chahal, D. S.; Goldbeck, C. P.; Cohen, B. E.; Helms, B. A. *Nano Lett.* **2012,** *10,* 4086–4092. doi:10.1021/nl102172j

59. Boeneman, K.; Delehanty, J. B.; Blanco-Canosa, J. B.; Susumu, K.; Stewart, M. H.; Oh, E.; Huston, A. L.; Dawson, G.; Ingale, S.; Walters, R.; Domowicz, M.; Deschamps, J. R.; Algar, W. R.; DiMaggio, S.; Manono, J.; Spillmann, C. M.; Thompson, D.; Jennings, T. L.; Dawson, P. E.; Medintz, I. L. *ACS Nano* **2013,** *7,* 3778–3796. doi:10.1021/nn400702r
60. Delehanty, J. B.; Bradburne, C. E.; Boeneman, K.; Susumu, K.; Farrell, D.; Mei, B. C.; Blanco-Canosa, J. B.; Dawson, G.; Dawson, P. E.; Mattoussi, H.; Medintz, I. L. *Integr. Biol.* **2010,** *2,* 265–277. doi:10.1039/c0ib00002g
61. Medintz, I. L.; Pons, T.; Delehanty, J. B.; Susumu, K.; Brunel, F. M.; Dawson, P. E.; Mattoussi, H. *Bioconjugate Chem.* **2008,** *19,* 1785–1795. doi:10.1021/bc800089r
62. Oh, E.; Delehanty, J. B.; Sapsford, K. E.; Susumu, K.; Goswami, R.; Blanco-Canosa, J. B.; Dawson, P. E.; Granek, J.; Shoff, M.; Zhang, Q.; Goering, P. L.; Huston, A.; Medintz, I. L. *ACS Nano* **2011,** *5,* 6434–6448. doi:10.1021/nn201624c
63. Nativo, P.; Prior, I. A.; Brust, M. *ACS Nano* **2008,** *2,* 1639–1644. doi:10.1021/nn800330a
64. Yang, L.; Shang, L.; Nienhaus, G. U. *Nanoscale* **2013,** *5,* 1537–1543. doi:10.1039/c2nr33147k
65. Schweiger, C.; Hartmann, R.; Zhang, F.; Parak, W. J.; Kissel, T. H.; Rivera Gil, P. *J. Nanobiotechnol.* **2012,** *10,* No. 28. doi:10.1186/1477-3155-10-28
66. Delehanty, J. B.; Blanco-Canosa, J. B.; Bradburne, C. E.; Susumu, K.; Stewart, M. H.; Prasuhn, D. E.; Dawson, P. E.; Medintz, I. L. *Chem. Commun.* **2013,** *49,* 7878–7880. doi:10.1039/c3cc42781a
67. Lehmann, A. D.; Parak, W. J.; Zhang, F.; Ali, Z.; Röcker, C.; Nienhaus, G. U.; Gehr, P.; Rothen-Rutishauser, B. *Small* **2010,** *6,* 753–762. doi:10.1002/smll.200901770
68. Brandenberger, C.; Mühlfeld, C.; Ali, Z.; Lenz, A.-G.; Schmid, O.; Parak, W. J.; Gehr, P.; Rothen-Rutishauser, B. *Small* **2010,** *6,* 1669–1678. doi:10.1002/smll.201000528
69. Mühlfeld, C.; Mayhew, T. M.; Gehr, P.; Rothen-Rutishauser, B. *J. Aerosol Med.* **2007,** *20,* 395–407. doi:10.1089/jam.2007.0624
70. Rothen-Rutishauser, B.; Kuhn, D. A.; Ali, Z.; Gasser, M.; Amin, F.; Parak, W. J.; Vanhecke, D.; Fink, A.; Gehr, P.; Brandenberger, C. *Nanomedicine* **2014,** *9,* 607–621. doi:10.2217/nnm.13.24
71. Canton, I.; Battaglia, G. *Chem. Soc. Rev.* **2012,** *41,* 2718–2739. doi:10.1039/c2cs15309b
72. Studer, A. M.; Limbach, L. K.; Van Duc, L.; Krumeich, F.; Athanassiou, E. K.; Gerber, L. C.; Moch, H.; Stark, W. J. *Toxicol. Lett.* **2010,** *197,* 169–174. doi:10.1016/j.toxlet.2010.05.012
73. Ducongé, F.; Pons, T.; Pestourie, C.; Hérin, L.; Thézé, B.; Gombert, K.; Mahler, B.; Hinnen, F.; Kühnast, B.; Dollé, F.; Dubertret, B.; Tavitian, B. *Bioconjugate Chem.* **2008,** *19,* 1921–1926. doi:10.1021/bc800179j
74. Zhao, Y.; Howe, J. L. C.; Yu, Z.; Leong, D. T.; Chu, J. J. H.; Loo, J. S. C.; Ng, K. W. *Small* **2013,** *9,* 387–392. doi:10.1002/smll.201201363
75. Muñoz Javier, A.; del Pino, P.; Bedard, M. F.; Ho, D.; Skirtach, A. G.; Sukhorukov, G. B.; Plank, C.; Parak, W. J. *Langmuir* **2008,** *24,* 12517–12520. doi:10.1021/la802448z
76. Symens, N.; Soenen, S. J.; Rejman, J.; Braeckmans, K.; De Smedt, S. C.; Remaut, K. *Adv. Drug Delivery Rev.* **2012,** *64,* 78–94. doi:10.1016/j.addr.2011.11.012
77. Parak, W. J.; Boudreau, R.; Le Gros, M.; Gerion, D.; Zanchet, D.; Micheel, C. M.; Williams, S. C.; Alivisatos, A. P.; Larabell, C. A. *Adv. Mater.* **2002,** *14,* 882–885. doi:10.1002/1521-4095(20020618)14:12<882::AID-ADMA882>3.0.CO;2-Y
78. Summers, H. D.; Rees, P.; Holton, M. D.; Brown, M. R.; Chappell, S. C.; Smith, P. J.; Errington, R. J. *Nat. Nanotechnol.* **2011,** *6,* 170–174. doi:10.1038/nnano.2010.277
79. Summers, H. D.; Brown, M. R.; Holton, M. D.; Tonkin, J. A.; Hondow, N.; Brown, A. P.; Brydson, R.; Rees, P. *ACS Nano* **2013,** *7,* 6129–6137. doi:10.1021/nn4019619
80. Pi, Q. M.; Zhang, W. J.; Zhou, G. D.; Liu, W.; Cao, Y. *BMC Biotechnol.* **2010,** *10,* No. 36. doi:10.1186/1472-6750-10-36
81. Ruan, G.; Agrawal, A.; Marcus, A. I.; Nie, S. *J. Am. Chem. Soc.* **2007,** *129,* 14759–14766. doi:10.1021/ja074936k
82. Bartczak, D.; Nitti, S.; Millar, T. M.; Kanaras, A. G. *Nanoscale* **2012,** *4,* 4470–4472. doi:10.1039/c2nr31064c
83. Blank, F.; Wehrli, M.; Lehmann, A.; Baum, O.; Gehr, P.; von Garnier, C.; Rothen-Rutishauser, B. M. *Immunobiology* **2011,** *216,* 86–95. doi:10.1016/j.imbio.2010.02.006
84. Colombo, M.; Mazzucchelli, S.; Montenegro, J. M.; Galbiati, E.; Corsi, F.; Parak, W. J.; Prosperi, D. *Small* **2012,** *8,* 1492–1497. doi:10.1002/smll.201102284
85. Montenegro, J.-M.; Grazu, V.; Sukhanova, A.; Agarwal, S.; de la Fuente, J. M.; Nabiev, I.; Greiner, A.; Parak, W. J. *Adv. Drug Delivery Rev.* **2013,** *65,* 677–688. doi:10.1016/j.addr.2012.12.003
86. Sapsford, K. E.; Tyner, K. M.; Dair, B. J.; Deschamps, J. R.; Medintz, I. L. *Anal. Chem.* **2011,** *83,* 4453–4488. doi:10.1021/ac200853a
87. Carrillo-Carrión, C.; Nazarenus, M.; Sánchez Paradinas, S.; Carregal-Romero, S.; Almendral, M. J.; Fuentes, M.; Pelaz, B.; del Pino, P.; Hussain, I.; Clift, M. J. D.; Rothen-Rutishauser, B.; Liang, X.-J.; Parak, W. J. *Curr. Opin. Chem. Eng.* **2014,** *4,* 88–96. doi:10.1016/j.coche.2013.11.006
88. Cho, E. C.; Zhang, Q.; Xia, Y. *Nat. Nanotechnol.* **2011,** *6,* 385–391. doi:10.1038/nnano.2011.58
89. Kirchner, C.; Liedl, T.; Kudera, S.; Pellegrino, T.; Muñoz Javier, A.; Gaub, H. E.; Stölzle, S.; Fertig, N.; Parak, W. J. *Nano Lett.* **2005,** *5,* 331–338. doi:10.1021/nl047996m
90. Kim, K.-T.; Truong, L.; Wehmas, L.; Tanguay, R. L. *Nanotechnology* **2013,** *24,* 115101. doi:10.1088/0957-4484/24/11/115101
91. Izak-Nau, E.; Voetz, M.; Eiden, S.; Duschl, A.; Puntes, V. F. *Part. Fibre Toxicol.* **2013,** *10,* No. 56. doi:10.1186/1743-8977-10-56
92. Pellegrino, T.; Kudera, S.; Liedl, T.; MuñozJavier, A.; Manna, L.; Parak, W. J. *Small* **2005,** *1,* 48–63. doi:10.1002/smll.200400071
93. Cedervall, T.; Lynch, I.; Lindman, S.; Berggård, T.; Thulin, E.; Nilsson, H.; Dawson, K. A.; Linse, S. *Proc. Natl. Acad. Sci. U. S. A.* **2007,** *104,* 2050–2055. doi:10.1073/pnas.0608582104
94. Lynch, I.; Cedervall, T.; Lundqvist, M.; Cabaleiro-Lago, C.; Linse, S.; Dawson, K. A. *Adv. Colloid Interface Sci.* **2007,** *134–135,* 167–174. doi:10.1016/j.cis.2007.04.021
95. Orts-Gil, G.; Natte, K.; Thiermann, R.; Girod, M.; Rades, S.; Kalbe, H.; Thünemann, A. F.; Maskos, M.; Österle, W. *Colloids Surf., B* **2013,** *108,* 110–119. doi:10.1016/j.colsurfb.2013.02.027
96. Gebauer, J. S.; Malissek, M.; Simon, S.; Knauer, S. K.; Maskos, M.; Stauber, R. H.; Peukert, W.; Treuel, L. *Langmuir* **2012,** *28,* 9673–9679. doi:10.1021/la301104a

97. Hühn, D.; Kantner, K.; Geidel, C.; Brandholt, S.; De Cock, I.; Soenen, S. J. H.; Rivera Gil, P.; Montenegro, J.-M.; Braeckmans, K.; Müllen, K.; Nienhaus, G. U.; Klapper, M.; Parak, W. J. *ACS Nano* **2013,** *7,* 3253–3263. doi:10.1021/nn3059295
98. Maiorano, G.; Sabella, S.; Sorce, B.; Brunetti, V.; Malvindi, M. A.; Cingolani, R.; Pompa, P. P. *ACS Nano* **2010,** *4,* 7481–7491. doi:10.1021/nn101557e
99. Kinnear, C.; Dietsch, H.; Clift, M. J. D.; Endes, C.; Rothen-Rutishauser, B.; Petri-Fink, A. *Angew. Chem., Int. Ed.* **2013,** *52,* 1934–1938. doi:10.1002/anie.201208568
100. Chithrani, B. D.; Ghazan, A. A.; Chan, W. C. W. *Nano Lett.* **2006,** *6,* 662–668. doi:10.1021/nl052396o
101. Tzlil, S.; Deserno, M.; Gelbart, W. M.; Ben-Shaul, A. *Biophys. J.* **2004,** *86,* 2037–2048. doi:10.1016/S0006-3495(04)74265-4
102. Deserno, M.; Bickel, T. *Europhys. Lett.* **2003,** *62,* 767–773. doi:10.1209/epl/i2003-00438-4
103. Zhang, S.; Li, J.; Lykotrafitis, G.; Bao, G.; Suresh, S. *Adv. Mater.* **2009,** *21,* 419–424. doi:10.1002/adma.200801393
104. Williams, Y.; Sukhanova, A.; Nowostawska, M.; Davies, A. M.; Mitchell, S.; Oleinikov, V.; Gun'ko, Y.; Nabiev, I.; Kelleher, D.; Volkov, Y. *Small* **2009,** *5,* 2581–2588. doi:10.1002/smll.200900744
105. Kreyling, W. G.; Hirn, S.; Möller, W.; Schleh, C.; Wenk, A.; Celik, G.; Lipka, J.; Schäffler, M.; Haberl, N.; Johnston, B. D.; Sperling, R.; Schmid, G.; Simon, U.; Parak, W. J.; Semmler-Behnke, M. *ACS Nano* **2014,** *8,* 222–233. doi:10.1021/nn403256v
106. Zhang, F.; Ali, Z.; Amin, F.; Feltz, A.; Oheim, M.; Parak, W. J. *ChemPhysChem* **2010,** *11,* 730–735. doi:10.1002/cphc.200900849
107. Riedinger, A.; Zhang, F.; Dommershausen, F.; Röcker, C.; Brandholt, S.; Nienhaus, G. U.; Koert, U.; Parak, W. J. *Small* **2010,** *6,* 2590–2597. doi:10.1002/smll.201000868
108. Sperling, R. A.; Liedl, T.; Duhr, S.; Kudera, S.; Zanella, M.; Lin, C.-A. J.; Chang, W. H.; Braun, D.; Parak, W. J. *J. Phys. Chem. C* **2007,** *111,* 11552–11559. doi:10.1021/jp070999d
109. Hagendorfer, H.; Kaegi, R.; Parlinska, M.; Sinnet, B.; Ludwig, C.; Ulrich, A. *Anal. Chem.* **2012,** *84,* 2678–2685. doi:10.1021/ac202641d
110. Hole, P.; Sillence, K.; Hannell, C.; Maguire, C. M.; Roesslein, M.; Suarez, G.; Capracotta, S.; Magdolenova, Z.; Horev-Azaria, L.; Dybowska, A.; Cooke, L.; Haase, A.; Contal, S.; Manø, S.; Vennemann, A.; Sauvain, J.-J.; Staunton, K. C.; Anguissola, S.; Luch, A.; Dusinska, M.; Korenstein, R.; Gutleb, A. C.; Wiemann, M.; Prina-Mello, A.; Riediker, M.; Wick, P. *J. Nanopart. Res.* **2013,** *15,* No. 2101. doi:10.1007/s11051-013-2101-8
111. Pellegrino, T.; Sperling, R. A.; Alivisatos, A. P.; Parak, W. J. *J. Biomed. Biotechnol.* **2007,** 26796. doi:10.1155/2007/26796
112. Sperling, R. A.; Pellegrino, T.; Li, J. K.; Chang, W. H.; Parak, W. J. *Adv. Funct. Mater.* **2006,** *16,* 943–948. doi:10.1002/adfm.200500589
113. Swiston, A. J.; Gilbert, J. B.; Irvine, D. J.; Cohen, R. E.; Rubner, M. F. *Biomacromolecules* **2010,** *11,* 1826–1832. doi:10.1021/bm100305h
114. Stoehr, L. C.; Gonzalez, E.; Stampfl, A.; Casals, E.; Duschl, A.; Puntes, V.; Oostingh, G. J. *Part. Fibre Toxicol.* **2011,** *8,* No. 36. doi:10.1186/1743-8977-8-36
115. Jiang, X.; Dausend, J.; Hafner, M.; Musyanovych, A.; Röcker, C.; Landfester, K.; Mailänder, V.; Nienhaus, G. U. *Biomacromolecules* **2010,** *11,* 748–753. doi:10.1021/bm901348z
116. Jiang, X.; Musyanovych, A.; Röcker, C.; Landfester, K.; Mailänder, V.; Nienhaus, G. U. *Nanoscale* **2011,** *3,* 2028–2035. doi:10.1039/c0nr00944j
117. Yang, S.-H.; Heo, D.; Park, J.; Na, S.; Suh, J.-S.; Haam, S.; Park, S. W.; Huh, Y.-M.; Yang, J. *Nanotechnology* **2012,** *23,* 505702. doi:10.1088/0957-4484/23/50/505702
118. Kim, S. T.; Saha, K.; Kim, C.; Rotello, V. M. *Acc. Chem. Res.* **2013,** *46,* 681–691. doi:10.1021/ar3000647
119. Albanese, A.; Tang, P. S.; Chan, W. C. W. *The Effect of Nanoparticle Size, Shape, and Surface Chemistry on Biological Systems;* Annual Review Of Biomedical Engineering, Vol. 14; Annual Reviews: Palo Alto, USA, 2012; pp 1–16.
120. Bédard, M. F.; Munoz-Javier, A.; Mueller, R.; del Pino, P.; Fery, A.; Parak, W. J.; Skirtach, A. G.; Sukhorukov, G. B. *Soft Matter* **2009,** *5,* 148–155. doi:10.1039/b812553h
121. Xia, T.; Kovochich, M.; Liong, M.; Meng, H.; Kabehie, S.; George, S.; Zink, J. I.; Nel, A. E. *ACS Nano* **2009,** *3,* 3273–3286. doi:10.1021/nn900918w
122. Su, X.; Fricke, J.; Kavanagh, D. G.; Irvine, D. J. *Mol. Pharmaceutics* **2011,** *8,* 774–787. doi:10.1021/mp100390w
123. Yue, T.; Wang, X.; Huang, F.; Zhang, X. *Nanoscale* **2013,** *5,* 9888–9896. doi:10.1039/c3nr02683c
124. Irvine, D. J. *Nat. Mater.* **2011,** *10,* 342–343. doi:10.1038/nmat3014
125. Larsson, J. A.; Nolan, M.; Greer, J. C. *J. Phys. Chem. B* **2002,** *106,* 5931–5937. doi:10.1021/jp014483k
126. Demers, L. M.; Mirkin, C. A.; Mucic, R. C.; Reynolds, R. A., III; Letsinger, R. L.; Elghanian, R.; Viswanadham, G. *Anal. Chem.* **2000,** *72,* 5535–5541. doi:10.1021/ac0006627
127. Moghimi, S. M.; Hunter, A. C.; Andresen, T. L. *Annu. Rev. Pharmacol. Toxicol.* **2012,** *52,* 481–503. doi:10.1146/annurev-pharmtox-010611-134623
128. Karmali, P. P.; Simberg, D. *Expert Opin. Drug Delivery* **2011,** *8,* 343–357. doi:10.1517/17425247.2011.554818
129. Rehbock, C.; Merk, V.; Gamrad, L.; Streubel, R.; Barcikowski, S. *Phys. Chem. Chem. Phys.* **2013,** *15,* 3057–3067. doi:10.1039/c2cp42641b
130. Menéndez-Manjón, A.; Wagener, P.; Barcikowski, S. *J. Phys. Chem. C* **2011,** *115,* 5108–5114. doi:10.1021/jp109370q
131. Barcikowski, S.; Mafune, F. *J. Phys. Chem. C* **2011,** *115,* 4985. doi:10.1021/jp111036a
132. Fadeel, B.; Feliu, N.; Vogt, C.; Abdelmonem, A. M.; Parak, W. J. *Wiley Interdiscip. Rev.: Nanomed. Nanobiotechnol.* **2013,** *5,* 111–129. doi:10.1002/wnan.1206
133. Kittler, S.; Greulich, C.; Gebauer, J. S.; Diendorf, J.; Treuel, L.; Ruiz, L.; Gonzalez-Calbet, J. M.; Vallet-Regi, M.; Zellner, R.; Köller, M.; Epple, M. *J. Mater. Chem.* **2010,** *20,* 512–518. doi:10.1039/b914875b
134. Monopoli, M. P.; Åberg, C.; Salvati, A.; Dawson, K. A. *Nat. Nanotechnol.* **2012,** *7,* 779–786. doi:10.1038/nnano.2012.207
135. Yakovlev, A. V.; Zhang, F.; Zulqurnain, A.; Azhar-Zahoor, A.; Luccardini, C.; Gaillard, S.; Mallet, J.-M.; Tauc, P.; Brochon, J.-C.; Parak, W. J.; Feltz, A.; Oheim, M. *Langmuir* **2009,** *25,* 3232–3239. doi:10.1021/la8038347
136. Röcker, C.; Pötzl, M.; Zhang, F.; Parak, W. J.; Nienhaus, G. U. *Nat. Nanotechnol.* **2009,** *4,* 577–580. doi:10.1038/nnano.2009.195
137. Maffre, P.; Nienhaus, K.; Amin, F.; Parak, W. J.; Nienhaus, G. U. *Beilstein J. Nanotechnol.* **2011,** *2,* 374–383. doi:10.3762/bjnano.2.43
138. Treuel, L.; Brandholt, S.; Maffre, P.; Wiegele, S.; Shang, L.; Nienhaus, G. U. *ACS Nano* **2014,** *8,* 503–513. doi:10.1021/nn405019v
139. Mahmoudi, M.; Abdelmonem, A. M.; Behzadi, S.; Clement, J. H.; Dutz, S.; Ejtehadi, M. R.; Hartmann, R.; Kantner, K.; Linne, U.; Maffre, P.; Metzler, S.; Moghadam, M. K.; Pfeiffer, C.; Rezaei, M.; Ruiz-Lozano, P.; Serpooshan, V.; Shokrgozar, M. A.; Nienhaus, G. U.; Parak, W. J. *ACS Nano* **2013,** *7,* 6555–6562. doi:10.1021/nn305337c

140. Tenzer, S.; Docter, D.; Rosfa, S.; Wlodarski, A.; Kuharev, J.; Rekik, A.; Knauer, S. K.; Bantz, C.; Nawroth, T.; Bier, C.; Sirirattanapan, J.; Mann, W.; Treuel, L.; Zellner, R.; Maskos, M.; Schild, H.; Stauber, R. H. *ACS Nano* **2011,** *5,* 7155–7167. doi:10.1021/nn201950e
141. Tenzer, S.; Docter, D.; Kuharev, J.; Musyanovych, A.; Fetz, V.; Hecht, R.; Schlenk, F.; Fischer, D.; Kiouptsi, K.; Reinhardt, C.; Landfester, K.; Schild, H.; Maskos, M.; Knauer, S. K.; Stauber, R. H. *Nat. Nanotechnol.* **2013,** *8,* 772–781. doi:10.1038/nnano.2013.181
142. Vroman, L. *Nature* **1962,** *196,* 476–477. doi:10.1038/196476a0
143. Gasser, M.; Rothen-Rutishauser, B.; Krug, H. F.; Gehr, P.; Nelle, M.; Yan, B.; Wick, P. *J. Nanobiotechnol.* **2010,** *8,* No. 31. doi:10.1186/1477-3155-8-31
144. Milani, S.; Bombelli, F. B.; Pitek, A. S.; Dawson, K. A.; Rädler, J. *ACS Nano* **2012,** *6,* 2532–2541. doi:10.1021/nn204951s
145. Liu, W.; Rose, J.; Plantevin, S.; Auffan, M.; Bottero, J.-Y.; Vidaud, C. *Nanoscale* **2013,** *5,* 1658–1668. doi:10.1039/c2nr33611a
146. Hill, A. V. *J. Physiol.* **1910,** *40,* iv–vii.
147. Sasmal, P. K.; Carregal-Romero, S.; Han, A. A.; Streu, C. N.; Lin, Z.; Namikawa, K.; Elliott, S. L.; Köster, R. W.; Parak, W. J.; Meggers, E. *ChemBioChem* **2012,** *13,* 1116–1120. doi:10.1002/cbic.201100719
148. Wang, F.; Yu, L.; Monopoli, M. P.; Sandin, P.; Mahon, E.; Salvati, A.; Dawson, K. A. *Nanomedicine* **2013,** *9,* 1159–1168. doi:10.1016/j.nano.2013.04.010
149. Lunov, O.; Syrovets, T.; Röcker, C.; Tron, K.; Nienhaus, G. U.; Rasche, V.; Mailänder, V.; Landfester, K.; Simmet, T. *Biomaterials* **2010,** *31,* 9015–9022. doi:10.1016/j.biomaterials.2010.08.003
150. Oberdörster, G.; Oberdörster, E.; Oberdörster, J. *Environ. Health Perspect.* **2005,** *113,* 823–839. doi:10.1289/ehp.7339
151. Oberdörster, G.; Stone, V.; Donaldson, K. *Nanotoxicology* **2007,** *1,* 2–25. doi:10.1080/17435390701314761
152. Maynard, A. D.; Aitken, R. J.; Butz, T.; Colvin, V.; Donaldson, K.; Oberdörster, G.; Philbert, M. A.; Ryan, J.; Seaton, A.; Stone, V.; Tinkle, S. S.; Tran, L.; Walker, N. J.; Warheit, D. B. *Nature* **2006,** *444,* 267–269. doi:10.1038/444267a
153. Clift, M. J. D.; Gehr, P.; Rothen-Rutishauser, B. *Arch. Toxicol.* **2011,** *85,* 723–731. doi:10.1007/s00204-010-0560-6
154. Caballero-Díaz, E.; Pfeiffer, C.; Kastl, L.; Rivera-Gil, P.; Simonet, B.; Valcárcel, M.; Jiménez-Lamana, J.; Laborda, F.; Parak, W. J. *Part. Part. Syst. Charact.* **2013,** *30,* 1079–1085. doi:10.1002/ppsc.201300215
155. Karlsson, H. L.; Cronholm, P.; Gustafsson, J.; Möller, L. *Chem. Res. Toxicol.* **2008,** *21,* 1726–1732. doi:10.1021/tx800064j
156. Kittler, S.; Greulich, C.; Diendorf, J.; Köller, M.; Epple, M. *Chem. Mater.* **2010,** *22,* 4548–4554. doi:10.1021/cm100023p
157. Hussain, S. M.; Hess, K. L.; Gearhart, J. M.; Geiss, K. T.; Schlager, J. J. *Toxicol. in Vitro* **2005,** *19,* 975–983. doi:10.1016/j.tiv.2005.06.034
158. AshaRani, P. V.; Low Kah Mun, G.; Hande, M. P.; Valiyaveettil, S. *ACS Nano* **2009,** *3,* 279–290. doi:10.1021/nn800596w
159. Bradburne, C. E.; Delehanty, J. B.; Boeneman Gemmill, K.; Mei, B. C.; Mattoussi, H.; Susumu, K.; Blanco-Canosa, J. B.; Dawson, P. E.; Medintz, I. L. *Bioconjugate Chem.* **2013,** *24,* 1570–1583. doi:10.1021/bc4001917
160. Ballou, B.; Lagerholm, B. C.; Ernst, L. A.; Bruchez, M. P.; Waggoner, A. S. *Bioconjugate Chem.* **2004,** *15,* 79–86. doi:10.1021/bc034153y
161. Liu, J.; Erogbogbo, F.; Yong, K.-T.; Ye, L.; Liu, J.; Hu, R.; Chen, H.; Hu, Y.; Yang, Y.; Yang, J.; Roy, I.; Karker, N. A.; Swihart, M. T.; Prasad, P. N. *ACS Nano* **2013,** *7,* 7303–7310. doi:10.1021/nn4029234
162. Morales, M. P.; Bédard, M. F.; Roca, A. G.; de la Presa, P.; Hernando, A.; Zhang, F.; Zanella, M.; Zahoor, A. A.; Sukhorukov, G. B.; del Mercato, L. L.; Parak, W. J. *J. Mater. Chem.* **2009,** *19,* 6381–6386. doi:10.1039/b906455a
163. Colombo, M.; Carregal-Romero, S.; Casula, M. F.; Gutiérrez, L.; Morales, M. P.; Böhm, I. B.; Heverhagen, J. T.; Prosperi, D.; Parak, W. J. *Chem. Soc. Rev.* **2012,** *41,* 4306–4334. doi:10.1039/c2cs15337h
164. Niebling, T.; Zhang, F.; Ali, Z.; Parak, W. J.; Heimbrodt, W. *J. Appl. Phys.* **2009,** *106,* 104701. doi:10.1063/1.3253762
165. Kastl, L.; Sasse, D.; Wulf, V.; Hartmann, R.; Mircheski, J.; Ranke, C.; Carregal-Romero, S.; Martínez-López, J. A.; Fernández-Chacón, R.; Parak, W. J.; Elsasser, H.-P.; Rivera Gil, P. *ACS Nano* **2013,** *7,* 6605–6618. doi:10.1021/nn306032k
166. Carregal-Romero, S.; Ochs, M.; Rivera Gil, P.; Ganas, C.; Pavlov, A. M.; Sukhorukov, G. B.; Parak, W. J. *J. Controlled Release* **2012,** *159,* 120–127. doi:10.1016/j.jconrel.2011.12.013

License and Terms

small
NANO MICRO

Particle-Based Optical Sensing of Intracellular Ions at the Example of Calcium – What Are the Experimental Pitfalls?

*Karsten Kantner, Sumaira Ashraf, Susana Carregal-Romero, Carolina Carrillo-Carrion, Mayeul Collot, Pablo del Pino, Wolfram Heimbrodt, Dorleta Jimenez De Aberasturi, Uwe Kaiser, Lyubov I. Kazakova, Marco Lelle, Natalia Martinez de Baroja, Jose Maria Montenegro, Moritz Nazarenus, Beatriz Pelaz, Kalina Peneva, Pilar Rivera Gil, Nadeem Sabir, Lorenz Maximilian Schneider, Lyudmila I. Shabarchina, Gleb B. Sukhorukov, Margarita Vazquez, Fang Yang, and Wolfgang J. Parak**

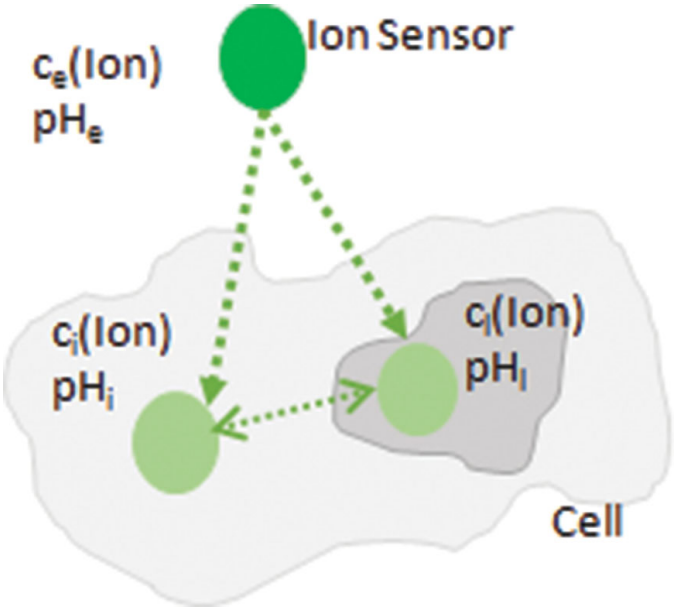

From the Contents

Colloidal particles with fluorescence read-out are commonly used as sensors for the quantitative determination of ions. Calcium, for example, is a biologically highly relevant ion in signaling, and thus knowledge of its spatio-temporal distribution inside cells would offer important experimental data. However, the use of particle-based intracellular sensors for ion detection is not straightforward. Important associated problems involve delivery and intracellular location of particle-based fluorophores, crosstalk of the fluorescence read-out with pH, and spectral overlap of the emission spectra of different fluorophores. These potential problems are outlined and discussed here with selected experimental examples. Potential solutions are discussed and form a guideline for particle-based intracellular imaging of ions.

DOI: 10.1002/smll.201402110

1. Introduction

There is a large variety of ion-sensitive fluorophores available, which change their fluorescence intensity in the presence of the respective ion.[1–7] With such fluorophores intracellular ion concentrations could, in principle, be determined, which would be an interesting tool for cell biology.[8–16] Ions play an important role in biology, for example, in signaling. This comprises signal propagation via action potentials in neurons, for example, which is governed by local switching on and off of Na^+ and K^+ currents. Another important ion related to cellular signaling is Ca^{2+}, which plays an important role in muscles. Having local ion-sensitive probes would allow the spatio-temporal observation of such signaling dynamics.

Most ion-sensitive fluorophores are based on organic molecules,[1,2,5–7] but there are also intrinsically fluorescent (nano-)particles with sensitivity to certain ionic species.[17–20] Ion-sensitive particles can be composed of a carrier particle functionalized with ion-sensitive organic fluorophores. The particle acts as a carrier for a read-out in the form of (organic) ion-sensitive fluorophores. This is possible by embedding the organic fluorophores in the volume of a porous particle matrix,[21–23] by encapsulating them in a porous particle shell,[24–26] or by linking them to the particle surface.[27–29] Ideally, the carrier particle would not interfere with the photophysical properties of the attached fluorophore. However, in the case of metal particles, quenching effects of the fluorescence of organic fluorophores close to the particle surface are possible. Also in case of very high packing densities of the fluorophores on the particle surface, self-quenching effects may occur. In some scenarios as, for example, for fluorescence resonance energy transfer (FRET), interactions of the organic fluorophore with the particle carrier is wanted in order to tune the photophysical properties of the attached fluorophores, which will be described below. Alternatively, intrinsically ion-sensitive fluorescent particles such as quantum dots (QDs) can be sensitive to ions.[102] In this case, the particle has a double function, acting as sensitive fluorophore and a carrier at the same time. In the following sections, all of these different geometries will be referred to simply as particles. These particles can range from the nanometer to the micrometer scale.[30] Besides acting as carriers, charged particles can intentionally or unintentionally modify the ion response, as their typically charged surface forms a nano-environment in the proximity of the particle surface that is different from the bulk.[27,31–34]

A particulate form of ion-sensitive fluorescence sensor offers several potential advantages. Concerning the signal-to-noise-ratio of the read-out, the emission intensity of ion-sensitive particles can be very high (in the case of intrinsically fluorescent particles such as QDs, this is due to their high absorption cross-section;[35,36] in the case of organic fluorophores, it is due to the linkage of several fluorophores per particle).[37–39] Next, the interaction with their environment, such as with cells, is predominantly governed by the physico-chemical properties of the particle surface. As particles sensitive to different ions can have the same physico-chemical properties, they also will have the same interaction with cells. In contrast, as organic fluorophores sensitive to different ions typically

Wolfgang Parak studied physics at the Technische Universität München, and made his PhD thesis in the group of Prof. Hermann Gaub at the Ludwig Maximilians Universität München, Germany. After his postdoctoral studies in the group of Prof. Paul Alivisatos at the University of California, Berkely, USA, he returned to the Ludwig Maximilians Universität as Assistant and later Associate Professor. Since 2007, Wolfgang Parak has been a Full Professor at the Philipps Universität Marburg, Germany, and since 2013 also group leader at CIC Biomagune in Spain.

Karsten Kantner studied physics in Marburg and is currently working on his PhD thesis in the group of Prof. Parak at the Philipps University of Marburg.

K. Kantner, Dr. S. Ashraf, Dr. S. Carregal-Romero, Dr. C. Carrillo-Carrion, Prof. W. Heimbrodt, Dr. D. J. De Aberasturi, U. Kaiser, Dr. J. M. Montenegro,[+] M. Nazarenus, Dr. B. Pelaz, Dr. P. Rivera Gil, N. Sabir, L. M. Schneider, M. Vazquez, F. Yang, Prof. W. J. Parak
Fachbereich Physik, Philipps- Universität Marburg
Marburg, Germany
E-mail: wolfgang.parak@physik.uni-marburg.de

Dr. S. Carregal-Romero, Dr. P. del Pino, Dr. D. J. de Aberasturi, Dr. N. M. de Baroja, Prof. W. J. Parak
CIC BiomaGUNE
San Sebastian, Spain

Dr. M. Collot
Ecole Normale Supérieure, CNRS
Paris, France

Dr. L. I. Kazakova, Dr. L. I. Shabarchina
Institute of Theoretical and Experimental Biophysics
Russian Academy of Science
Pushchino, Russian Federation

Dr. M. Lelle, Dr. K. Peneva
Max Planck Institute for Polymer Research
Mainz, Germany

Prof. G. B. Sukhorukov
School of Engineering and Materials Science
Queen Mary University of London
London, UK

M. Vazquez
Inorganic Chemistry Department
Faculty of Pharmacy
University of Santiago de Compostela
Santiago de Compostela, Spain

[+]*Present Address*: Central Research Services, University of Malaga, Bulevar Louis Pasteur 33, 29071 Málaga, Spain

DOI: 10.1002/smll.201402110

have very different molecular structures and thus different physico-chemical properties (their polarity can range from hydrophilic to hydrophobic, for example), they will interact differently with cells. The pathway of cellular uptake of fluorescent particles can therefore be quite different from plain organic fluorophores. Playing with the size of the particle that acts as the carrier (nano- or microparticles), the location of the sensor inside the cells can be designed and thus information about the ion concentrations in different cellular regions can be obtained. While nanoparticles are preferentially located in endolysosomal compartments, microparticles can also be found in phagolysosomal vesicles, which allows the design of ion-sensitive particles depending on the location of the ion of interest. Due to potentially different intracellular locations and also because of the protection by the particle, particulate fluorophores may be less degraded by intracellular enzymes, and also cause less toxic intracellular effects (in particular when their sensing part is directly located on the particle surface). Concerning multiplexed sensing, the possibility of working with detection schemes involving temporal or spatial discrimination can circumvent the problem of spectral overlap and, thus, different ion-sensitive fluorophores can be detected in parallel.[40,41] Naturally, besides these advantages there are also problems associated with particle-based intracellular ion-sensing, which will be highlighted in the following sections based on experimental examples. While the given analysis holds true in a general way for small biologically relevant ions such as Na^+, K^+, Cl^-, H^+, the statements above are illustrated by selected experimental data. For reasons of homogeneity, the experimental data are presented for the case of Ca^{2+}-sensing, though results would be similar for other ions. The technical details for the experiments can be found in the Supporting Information.

2. Upon Cellular Internalization, Particle-Based Sensors are Typically Located Inside Intracellular Acidic Vesicles

The classical entry of particles into cells is via endocytosis. While endocytosis can involve a lot of different pathways,[42–45] it results in a localization of the particles in acidic intracellular vesicles (endosomes, lysosomes).[25,46–49] In such a scenario, the particles would sense the ion concentrations inside these vesicles, but not in the cellular cytosol.[8,50] For many applications, sensing of ion concentrations in the cytosol would be favorable. Administration of particles by microinjection or electroporation allows the placing of particles in the cytosol, though these techniques are clearly invasive and would have severe limitations for in vivo applications. However, there is also clear evidence that certain particle geometry scenarios exist in which particles can be delivered to the cytosol upon spontaneous cellular uptake.[51,52] In the case of delivery to the cytosol, the particles can be either first endocytosed and then released from the intracellular vesicles ("endosomal escape"),[53–55] or they can directly traverse the cell membrane (i.e., by transient poration) and thus bypass endocytotic uptake.[56] The details of such mechanisms are still under scientific discussion. For fast uptake into cells and delivery through the cell membrane to the cytosol, a common functionalization of the particle surface involves specific peptide sequences, e.g., cell-penetrating peptides (CPPs),[57–59] which usually are derived from viruses. The data shown in **Figure 1** demonstrate an example, in which polyethylene glycol (PEG)-modified particles bearing CPPs at the termini of the PEG molecules were internalized in vitro by HeLa cells to a higher extent than similar particles without CPP functionalization. Quantification of particle internalization can be done via different techniques, such as transmission electron microscopy (TEM),[60–62] fluorescence microscopy,[63–65] flow cytometry,[47,50] and inductively coupled plasma mass spectrometry (ICP-MS).[66,67] As flow cytometry and ICP-MS do not possess direct lateral resolution at a subcellular level, these techniques do not allow one to distinguish between internalized particles which are free in the cytosol from those which are localized inside intracellular vesicles. Even worse, these methods do not allow intracellular particles to be distinguished from particles just sticking to the outer cell membrane. However, this limitation has been overcome using protocols for removing particles attached to the surface based on iodide etching[68] or, in the case of flow cytometry, by using the local pH around the particles as a discriminator between internalized (acidic pH) and extracellular (neutral pH) particles.[69] In contrast, fluorescence microscopy, when applied together with appropriate immunostaining methods, and in particular TEM, due to its high spatial resolution, can demonstrate particle internalization, and can in principle also indicate whether internalized particles are inside intracellular vesicles or not.[47,49,52] However, in many cases, uptake studies are based on fluorescence microscopy images without staining of intravesicular membranes (cf. Figure 1), with the consequence that, from such images, no conclusion about the intracellular localization of the particles can be drawn. In fact, it is important to be highly critical about the possible delivery of particles to the cytosol. Just the presence of CPPs on the particle surface does not automatically mean their delivery to the cytosol. This is illustrated in the example shown in Figure 1, which is based on two CPPs that both are rich in NH_2 groups. In these data, one can see a clear indication of enhanced cellular uptake (cf. the ICP-MS data), but neither a reliable quantification nor the intracellular location of the particles can be derived. Even if the same CPPs have been demonstrated in the literature for one particle system resulting in delivery to the cytosol, without experimental verification it must not be assumed that the same CPPs will also work for other systems in the same manner. Depending on the respective particle geometry (surface chemistry, density of CPPs, size of particles, distance of CPPs to the particle core, etc.), the effects of attached CPPs, as well as the physico-chemical properties of the particles themselves may be quite different. In the case of the example presented in Figure 1, one has to take into account that PEG molecules are partly coiled and, in this way, the CPPs at the terminal ends do not always point towards the solution, but may be buried in the PEG shell instead. Also, the density of the CPPs may play a role. Thus, without experimental proof concerning the characterization of the used particle system as well as the chosen cell system, one should not assume the presence of particles in the cytosol.

DOI: 10.1002/smll.201402110

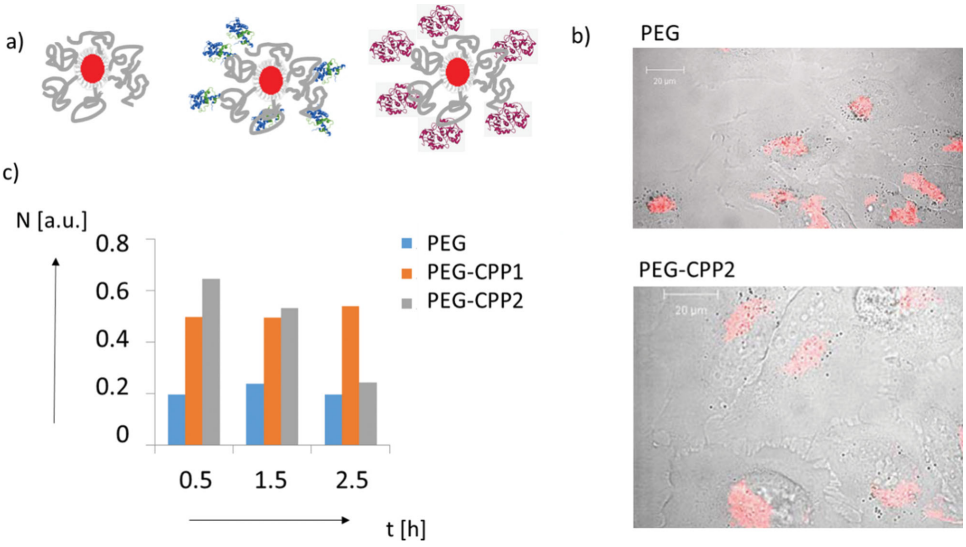

Figure 1. HeLa cells were incubated with polymer-coated Au nanoparticles (core diameter $d_c \approx 4.6$ nm) with the red fluorophore Cresyl violet (CV) integrated in their polymer shell.[70] The surface of these nanoparticles was modified with PEG of molecular weight $M_w = 3000$ Da.[71] For some particles, the terminal end of each PEG molecule was conjugated with cell-penetrating peptides (CPPs) rich in NH_2 groups. Two different CPPs were used as random examples. a) Sketch of the three different particles, with PEG, PEG-CPP1, and PEG-CPP2 surfaces. b) Overlay of the bright-field and red fluorescence images of HeLa cells after 6 h of incubation with the particles. The scale bars correspond to 20 µm. c) The amount of internalized particles *N* (as quantified by the atomic gold content inside cells) was determined with ICP-MS after t = 0.5, 1.5, and 2.5 h of incubation. The decrease in *N* for PEG-CPP2 was most likely due to the death of some cells. In both cases, the presence of CPPs enhanced uptake of particles by cells. The presented data here do not allow for any conclusion about the intracellular location of the internalized particles. Note that the fluorescence images shown in (b) are overexposed, and thus no accurate and precise quantitative data about differences in uptake between the different particles can be derived. This "homogeneous" distribution of fluorescence along the cell must in particular not be mistaken as proof for delivery to the cytosol. The granular structure of the intracellular vesicles in which the particles are embedded can be seen in cases where appropriate particle concentrations and imaging parameters are used.[46,72,73]

There is no easy solution to the "endosomal escape dilemma". It is most important to be aware of this potential problem. Most uptake studies, without a proper colocalization study, are not able to distinguish between particles free in the cytosol and particles embedded in intracellular vesicles. As mentioned above, the standard route of particle internalization by cells is endocytosis.[62] Thus, unless proven differently,[51,53] particles should be assumed to be in acidic intracellular vesicles, and thus the read-out of such ion-sensitive particles would determine the ion concentrations inside the endosomes/lysosomes,[8,74] and not the ion concentrations in the cellular cytosol. In this way, particle-based ion-sensitive particles are ideal for sensing inside endosomes/lysosomes, and one smart strategy would be to look for potential applications in this direction, e.g., sensing related to lysosomal storage diseases, instead of targeting the cytosol. Otherwise, in cases where applications definitely require sensing in other intracellular compartments, sensing methodologies need to be accompanied by profound localization studies providing information about the particle localization.

3. Many Ion-Sensitive Fluorophores Have Massive Crosstalk with pH

As pointed out previously, unless special surface coatings and very small particles are used, internalized particles are typically located in acidic intracellular vesicles, i.e., in an environment with low pH. Unfortunately, many ion-sensitive fluorophores have significant crosstalk with pH, as shown in the examples given in **Figure 2**. Thus, without knowledge of the local pH value of the particle environment, the concentration of the respective ions cannot be determined. Besides pH, many ion-sensitive fluorophores also have crosstalk with other ions. For example, potassium-sensitive fluorophores have crosstalk with sodium, and vice versa.[41]

Crosstalk with pH is a severe problem for intracellular (in vitro) ion sensing. On their standard internalization pathway from the typical slightly alkaline extracellular medium, particles are located in subsequently more and more acidic intracellular vesicles. In this way, the internalization of particles involves massive changes in pH.[8,24] Thus, in the case of a particulate ion-sensitive fluorophore which not only responds to its target ion but also to pH, it is not straightforward to interpret changes in fluorescence intensity, as they may reflect changes in target ion concentration or in pH. This is demonstrated in **Figure 3**, where particles, here micrometer-sized multilayer capsules with integrated calcium-sensitive fluorophores (Calcium Green-1 linked to dextran), were added to cells and their fluorescence was recorded for extracellular as well as for internalized particles. For the calcium-sensitive fluorophore, it is not clear whether the change in fluorescence emission upon cellular internalization, leading to localization in the lysosome,[49] is due to changes in Ca^{2+} or in pH. Thus, with this particle-based calcium sensor, it is not possible in a straightforward way to determine lysosomal calcium concentrations.

Again, there is no easy solution concerning avoiding crosstalk of ion-sensitive fluorophores with pH. Being aware of the

small 2014,
DOI: 10.1002/smll.201402110

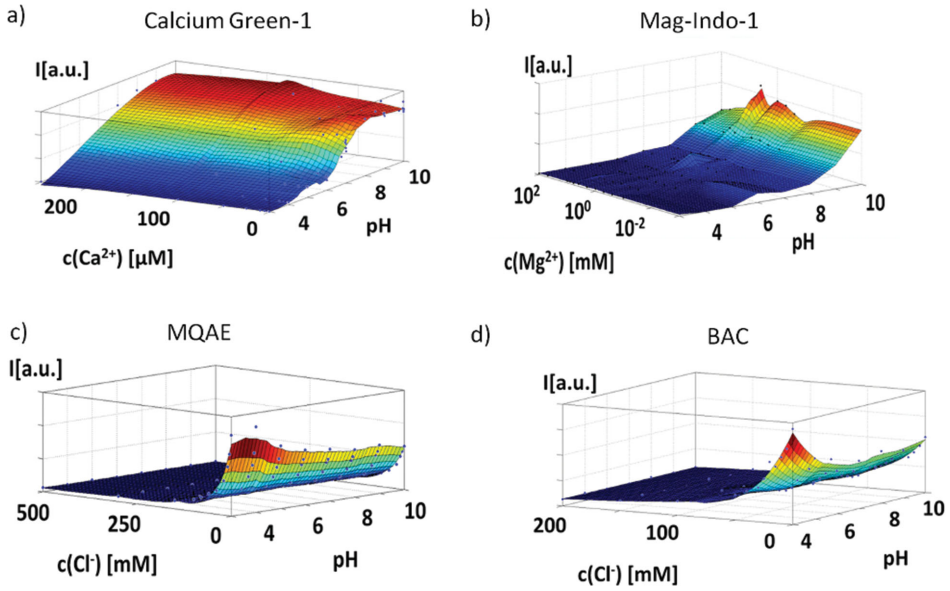

Figure 2. Different sensitive fluorophores were added to solutions in which the concentration *c* of one ionic specie as well as pH were varied, and their fluorescence intensity *I* was measured. a) *N*-[2-[2-[2-[bis(carboxymethyl)amino]-5-[[2′,7′-dichloro-3′,6′-dihydroxy-3-oxospiro[isobenzofuran-1(3H),9′-[9H]xanthene)-5-yl]carbonyl]amino]phenoxy]ethoxy]phenyl]-*N*-(carboxymethyl) (Calcium-Green-1) specific for calcium.[75] b) 1H-Indole-6-carboxylic acid, 2-[3-[2-[(acetyloxy)methoxy]-2-oxoethoxy]-4-[bis[2-[(acetyloxy)methoxy]-2-oxoethyl]amino]phenyl], (acetyloxy)methyl ester (Mag-Indo-1) specific for magnesium.[76] c) *N*-(Ethoxycarbonylmethyl)-6-methoxyquinolinium bromide (MQAE) specific for chloride.[77] d) 10,10′-Bis[3-carboxypropyl]-9,9′-acridiniumdinitrate (BAC) specific for chloride.[78] In all cases the emission intensity I of the fluorophore does not only respond to changes in the concentration of the target ions, but also to changes in pH.

problem is clearly only the first step. Naturally one may think of developing ion-sensitive fluorophores which do not respond to pH. Alternatively, in case one needs to rely on existing particle-based fluorophores that are affected by crosstalk with pH, one can think of a multiplexed read-out of several fluorophores, as will be discussed below. Here, the advantage of the "particle" character comes into play: As two particle-based fluorophores with the same surface chemistry/dimensions will have the same uptake pathway and intracellular location, several particle-based fluorophores selective to different ions could be applied and read-out at the same time. In case two Ca^{2+}-sensitive fluorophores show different crosstalk to pH, a 2D calibration curve could be obtained. By reading out the values of different Ca^{2+}-sensitive fluorophores in parallel, the Ca^{2+} concentration could be determined even without knowledge of the local pH. In a similar way, a Ca^{2+}-sensitive fluorophore could be combined with a pH-sensitive fluorophore. Again, a 2D calibration curve correlating the read-out of both fluorophores would allow determination of both the pH and the Ca^{2+} concentration. In this way, however, two different fluorophores need to be read-out simultaneously which, due to spectral overlap of fluorescence emission, can be challenging, as will be explained in detail in the following section.

4. Multiplexed Detection of Several Fluorophores Based on Different Fluorescence Lifetimes

For many applications it would be desirable to determine the intracellular concentration of several ions in parallel. This is the case if there is, for example, crosstalk between different fluorophores, and calibration curves correlating the read-out of different fluorophores are required (see above). Such a case is shown in **Figure 4**, where the read-out of a Ca^{2+}-sensitive fluorophore depends on both the Ca^{2+} concentration and also the pH. In this way, it would be desirable to combine the Ca^{2+}-sensitive fluorophore (which has crosstalk with pH) with a pH-sensitive fluorophore. However, the emission spectra of many ion-sensitive fluorophores unfortunately overlap, and thus the number of fluorophores that can be spectrally resolved and independently detected in parallel is limited.[40,80,81] The fluorescence spectrum of the Ca^{2+}-sensitive fluorophore shown in Figure 4 is relatively broad, and thus it would be complicated to find a pH-sensitive fluorophore emitting in a very different spectral range.

One solution to circumvent this problem is to use multiplexed detection techniques which are not based on spectral resolution. Besides distinguishing different fluorophores from separate emission peaks (i.e., spectral resolution), other ways of discrimination are possible. If the fluorophore-carrying particles are big enough to be optically resolved (i.e., sized above the optical resolution limit due to refraction), individual particles can be laterally resolved and identified by respective barcodes (i.e., lateral resolution).[40,41,82–84] While this is not possible for smaller particles, they still can be resolved by different fluorescence lifetimes (i.e. temporal resolution).[40] If two different fluorophores possess different lifetimes, their emission can be distinguished with time-resolved fluorescence spectroscopy. This also offers the advantage that no absolute intensity information is required, which depends on the number of particles inside each cell. This principle

DOI: 10.1002/smll.201402110

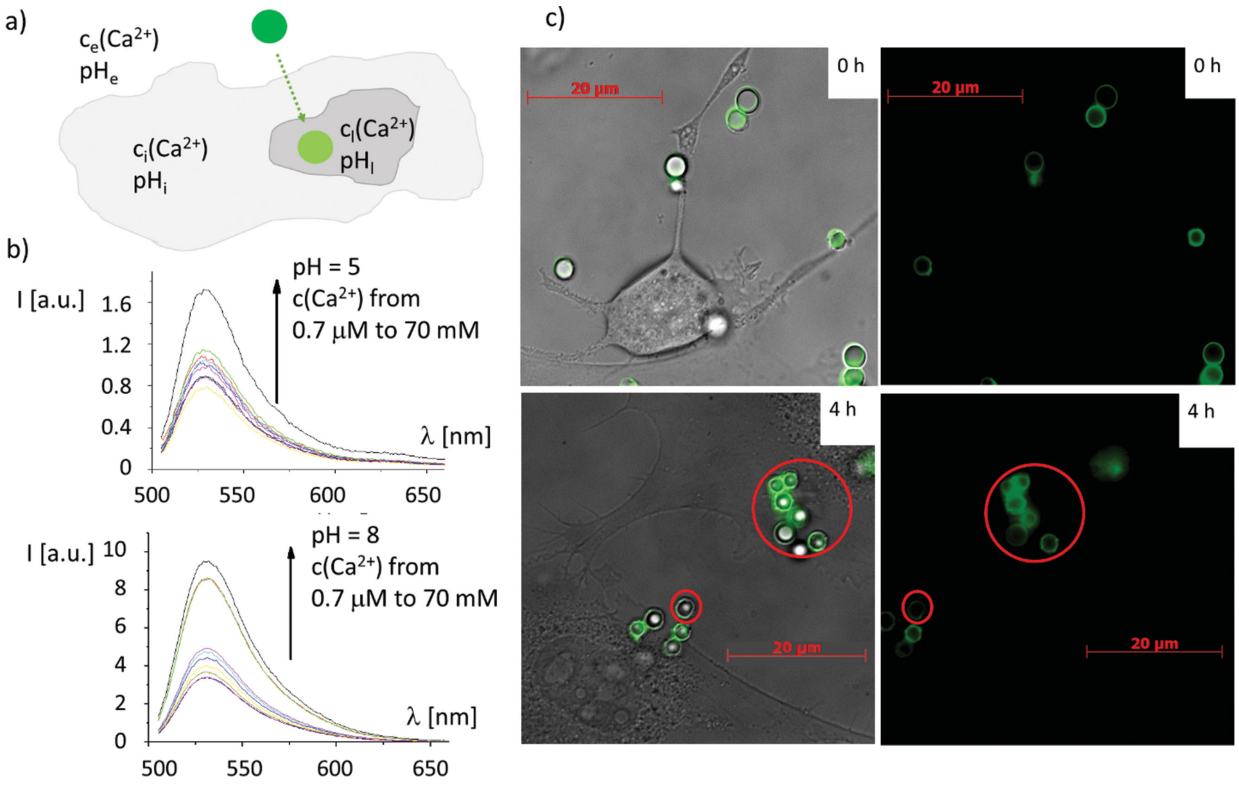

Figure 3. Micrometer-sized particles as synthesized by layer-by-layer assembly were loaded with the Ca^{2+}-sensitive fluorophore Calcium Green-1 linked to dextran.[26,79] a) One has to differentiate between different local concentrations: extracellular calcium and pH, $c_e(Ca^{2+})$ and pH_e, intracellular calcium and pH in the cytosol, $c_i(Ca^{2+})$ and pH_i, and calcium and pH inside lysosomes, $c_l(Ca^{2+})$ and pH_l. Upon internalization the particles undergo several acidification steps in their local environment, from the extracellular space to their final localization inside lysosomes.[49] b) Fluorescence emission spectra $I(\lambda)$ of Calcium Green-1 loaded particles depend on calcium, but also on pH. Changes in pH infer crosstalk with the Ca^{2+}-sensitive read-out. c) Ca^{2+}-sensitive particles were added to cells and microscopy images were recorded. Fluorescence images, together with an overlay with bright-field images, are shown. The scale bars correspond to 20 µm. After 4 h of incubation, some particles were internalized (the ones in the big red circle), whereas other particles were located outside cells (the one in the small red circle). However, due to crosstalk, changes in emission intensity between extracellular particles and particles inside the lysosome cannot be unequivocally correlated with changes in calcium concentration. Reduction in fluorescence can be caused by lowering of the calcium concentration, but also by lowering in pH. Therefore, if the local pH is unknown, the calcium concentration cannot be determined.

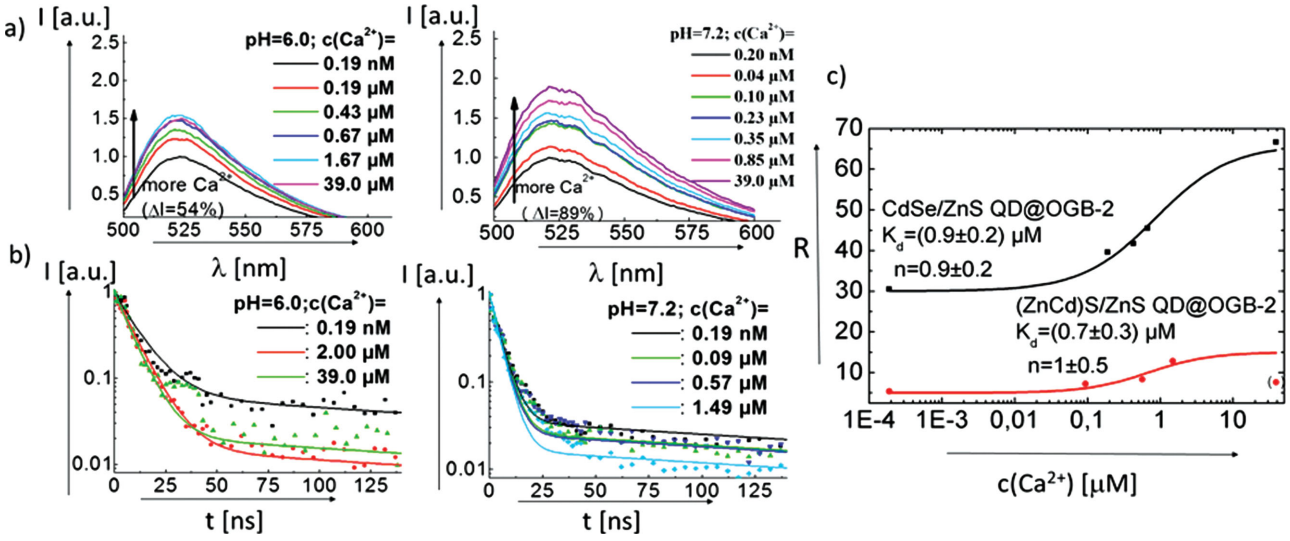

Figure 4. a) The fluorescence emission of OGB-2 depends on the Ca^{2+} concentration as well as on pH (recorded at 350 nm excitation wavelength). b) OGB-2 had been linked closely to the surface of $(Zn_xCd_{1-x})S/ZnS$ QDs and time resolved fluorescence (at the OGB-2 emission wavelength) was recorded. Decay times depend on Ca^{2+} and pH. c) From the different decay times, a resulting response curve $R(c(Ca^{2+}))$ can be derived, which is shown here for OGB-2 coupled to $(Zn_xCd_{1-x})S/ZnS$ and to CdSe/ZnS QDs at pH 7.2. From these curves, dissociation constants K_d can be obtained (for details, refer to the Supporting Information).

small 2014,
DOI: 10.1002/smll.201402110

has already been applied for ion-sensitive fluorophores.[85–87] While many organic fluorophores have similar lifetimes of a few nanoseconds, fluorescent nanoparticles such as QDs can have much longer photoluminescence lifetimes which, by using doping, can reach even milliseconds.[88] If fluorophores are coupled closely to the surface of QDs, and the emission spectrum of the QDs overlaps with the excitation spectrum of the fluorophores, FRET occurs.[89–92] Upon FRET from the QD to the fluorophores, the effective fluorescence lifetime of the fluorophores is increased towards the fluorescence lifetime of the QDs.[93,94] In this way, the detection of ions could be carried out upon linkage of ion-sensitive fluorophores to the surface of QDs. The optical changes induced by ion complexation produce changes in the FRET process and, consequently, in the fluorophore lifetime that can be determined in time-resolved fluorescence measurements.[95] The principle of time-resolved fluorescence measurements and ion-concentration determination via fluorescence lifetimes is illustrated in Figure 4, with the example of the Ca^{2+}-sensitive fluorophore Oregon Green Bapta-2 (OGB-2),[96,97] which was coupled to the surface of $(Zn_xCd_{1-x})S/ZnS$ and CdSe/ZnS (Lumidot 480 bought from Sigma Aldrich) QDs.[98,99] The fluorescence spectra of OGB-2 depend on the calcium concentration but, as mentioned above, like many organic fluorophores, also on pH. The Ca^{2+}- and pH-dependence can also be seen in time resolved fluorescence, also when OGB-2 is coupled to the surface of QDs and excited via FRET. The time resolved fluorescence curves can be fitted with a simple kinetic model, which provides the relevant lifetimes.[93] While the lifetimes themselves depend on the calcium concentration, they can be combined to a resulting response curve R, which is derived from all fit parameters. Assuming a linear increase of the FRET rate as calcium binds to OGB-2, the dissociation constants of Ca^{2+} binding to OGB-2 can be determined from this Ca^{2+}-dependent response curve (cf. Figure 4). In this way, instead of quantifying Ca^{2+} via intensity changes at a certain emission wavelength, it can be carried out via changes in fluorescence lifetime. This offers the possibility for temporally resolved multiplexed measurements of multiple ion concentrations in parallel.[40]

5. Discussion

The examples shown in this review indicate that particle-based intracellular ion-sensing is by far not trivial and involves several pitfalls. From the point of view of the sensor itself, one should be aware of the fact that the presence of the particles can change the fluorescence response, as particles impose a different nano-environment, which changes ion concentrations as compared to the bulk.[27,31,32] Another important drawback in the development of particle-based ion sensors originates from the few commercially available ion-sensitive fluorophores with enough specificity. To get a wide range of selective ion-sensitive fluorophores towards different target cations and anions of interest is a big challenge that needs to be addressed in order to advance fluorescence-based intracellular ion sensing. There are also several important points to take into account when ion-sensitive particles are used for sensing ion concentration in cells: First, the location of the particle sensors needs to be experimentally determined and, unless experimentally proven otherwise, they should be assumed to be inside highly acidic intracellular vesicles and not free in the cytosol or other cellular organelles. Thus, in the most straightforward way, applications which involve irregularities in ion concentrations inside endosomes/lysosomes could be investigated, such as lysosomal storage diseases. Localization of the sensor particles in endosomes/lysosomes involves massive changes in the pH surrounding the particles upon their internalization by cells. Transitions occur from the slightly alkaline/neutral extracellular medium to the acidic environment of endosomes/lysosomes. Due to crosstalk of many ion-sensitive fluorophores with pH, this affects the ion-sensitive fluorescence read-out. Thus, for most intracellular ion-sensing experiments, knowledge of the local pH around the particle sensors would be needed, which could be achieved by additionally using pH-sensitive sensor particles. The effect of pH might also impose limits on sensors which involve enzymes as recognition elements, such as urease,[100] glucose oxidase, or lactate oxidase to convert the analyte (urea, glucose, or lactate) into H^+,[101] which then is measured as a pH-dependent fluorescence signal. Therefore, in biological media such as the interior of cells, these sensors might give signal changes which would be problematic to interpret. Multiplexed sensing of several ions (or other relevant molecules) in parallel would offer a solution, not only to crosstalk with pH but also in the case of interference with other molecules. Thus, a reasonable strategy would involve determining the fluorescence read-out of different ion-sensitive fluorophores (or pH) in parallel. However, spectral overlap of different fluorophores sensitive to different ions/molecules imposes a severe limit, and hampers detection of several fluorophores in parallel. One solution is to resolve different fluorophores not spectrally, but in different modes. Discrimination can, for example, be achieved via determination of fluorescence lifetimes.

Supporting Information

Supporting Information is available from the Wiley Online Library or from the author.

Acknowledgements

The authors are grateful to Dr. Joana Rejman for helpful technical discussions. This work was supported by DFG GRK 1782 (grants to WJP and WH) and in part by Ministry of Education and Science of the Russian Federation, contracts 02.740.11.5226, 14.740.11.1363 and Russian Foundation for Basic Research 13–04–01507 A. SA, BP, and CCC are grateful to the Alexander von Humboldt Foundation for postdoctoral fellowships. NS is grateful to DAAD and HEC for a PhD fellowship.

DOI: 10.1002/smll.201402110

[1] R. D. Carpenter, A. S. Verkman, *Org Lett* **2010**, *12*(6), 1160–1163.
[2] X. Xie, Y. Qin, *Sens. Actuat. B* **2011**, *156*(1), 213–217.
[3] M. J. Ruedas-Rama, A. Orte, E. A. H. Hall, J. M. Alvarez-Pez, E. M. Talavera, *Analyst* **2012**, *137*(6), 1500–1508.
[4] N. Wanichacheva, K. Setthakarn, N. Prapawattanapol, O. Hanmeng, V. S. Lee, K. Grudpan, *J. Luminescence* **2012**, *132*(1), 35–40.
[5] W. Jiang, Q. Q. Fu, H. Y. Fan, W. Wang, *Chem. Commun.* **2008**, (2), 259–261.
[6] V. V. Martin, A. Rothe, Z. Diwu, K. R. Gee, *Bioorg. Medicinal Chem. Lett.* **2004**, *14*(21), 5313–5316.
[7] P. Nandhikonda, M. P. Begaye, M. D. Heagy, *Tetrahedron Lett.* **2009**, *50*(21), 2459–2461.
[8] P. Rivera Gil, M. Nazarenus, S. Ashraf, W. J. Parak, *Small* **2012**, *8*(6), 943–948.
[9] T. Mistri, M. Dolai, D. Chakraborty, A. R. Khuda-Bukhsh, K. K. Das, M. Ali, *Org. Biomolec. Chem.* **2012**, *10*(12), 2380–2384.
[10] E. Arunkumar, A. Ajayaghosh, J. Daub, *J. Am. Chem. Soc.* **2005**, *127*(9), 3156–3164.
[11] L. Zeng, E. W. Miller, A. Pralle, E. Y. Isacoff, C. J. Chang, *J. Am. Chem. Soc.* **2006**, *128*(1), 10–11.
[12] L. Xue, C. Liu, H. Jiang, *Chem. Commun.* **2009**, (9), 1061–1063.
[13] X. J. Peng, J. J. Du, J. L. Fan, J. Y. Wang, Y. K. Wu, J. Z. Zhao, S. G. Sun, T. Xu, *J. Am. Chem. Soc.* **2007**, *129*(6), 1500.
[14] D. W. Domaille, E. L. Que, C. J. Chang, *Nat. Chem. Biol.* **2008**, *4*(3), 168–175.
[15] X. A. Zhang, D. Hayes, S. J. Smith, S. Friedle, S. J. Lippard, *J. Am. Chem. Soc.* **2008**, *130*(47), 15788–15789.
[16] K. Komatsu, Y. Urano, H. Kojima, T. Nagano, *J. Am. Chem. Soc.* **2007**, *129*(44), 13447–13454.
[17] Y. F. Chen, Z. Rosenzweig, *Analyt. Chem.* **2002**, *74*(19), 5132–5138.
[18] W. J. Jin, M. T. Fernandez-Argüelles, J. M. Costa-Fernandez, R. Pereiro, A. Sanz-Medel, *Chem. Commun.* **2005**, *2005*, 883–885.
[19] M. T. Fernandez-Argüelles, W. J. Jin, J. M. Costa-Fernandez, R. Pereiro, A. Sanz-Medel, *Analyt. Chim. Acta* **2005**, *549*, 20–25.
[20] A. S. Susha, A. Munoz_Javier, W. J. Parak, A. L. Rogach, *Colloids Surf. A* **2006**, *281*, 40–43.
[21] H. A. Clark, S. L. R. Barker, M. Brasuel, M. T. Miller, E. Monson, S. Parus, Z. Y. Shi, A. Song, B. Thorsrud, R. Kopelman, A. Ade, W. Meixner, B. Athey, M. Hoyer, D. Hill, R. Lightle, M. A. Philbert, *Sens. Actuat. B* **1998**, *51*(1–3), 12–16.
[22] H. A. Clark, M. Hoyer, S. Parus, M. A. Philbert, R. Kopelman, *Microchimica Acta* **1999**, *131*(1–2), 121–128.
[23] M. Brasuel, R. Kopelman, T. J. Miller, R. Tjalkens, M. A. Philbert, *Analyt. Chem.* **2001**, *73*(10), 2221–2228.
[24] O. Kreft, A. Muñoz Javier, G. B. Sukhorukov, W. J. Parak, *Journal Of Materials Chemistry* **2007**, *17*, 4471–4476.
[25] U. Reibetanz, D. Halozan, M. Brumen, E. Donath, *Biomacromolecules* **2007**, *8*, 1928–1933.
[26] L. L. del Mercato, A. Z. Abbasi, W. J. Parak, *Small* **2011**, *7*, 351–363.
[27] F. Zhang, Z. Ali, F. Amin, A. Feltz, M. Oheim, W. J. Parak, *ChemPhysChem* **2010**, *11*, 730–735.
[28] J. Isaad, A. El Achari, *Tetrahedron* **2013**, *69*(24), 4866–4874.
[29] M. J. Ruedas-Rama, E. A. H. Hall, *Analyt. Chem.* **2008**, *80*(21), 8260–8268.
[30] S. Carregal-Romero, J.-M. Montenegro, W. J. Parak, P. Rivera_Gil, *Frontiers Pharmacol.* **2012**, *3*, 70.
[31] A. Riedinger, F. Zhang, F. Dommershausen, C. Röcker, S. Brandholt, G. U. Nienhaus, U. Koert, W. J. Parak, *Small* **2010**, *6*(22), 2590–2597.
[32] F. Zhang, E. Lees, F. Amin, P. Rivera_Gil, F. Yang, P. Mulvaney, W. J. Parak, *Small* **2011**, *7*, 3113–3127.
[33] C. Carrillo-Carrion, M. Nazarenus, S. Sánchez Paradinas, S. Carregal-Romero, M. J. Almendral, M. Fuentes, B. Pelaz, P. del Pino, I. Hussain, M. J. D. Clift, B. Rothen-Rutishauser, X.-J. Liang, W. J. Parak, *Curr. Op. Chem. Engineer.* **2014**, *4*, 88–96.
[34] C. Pfeiffer, C. Rehbock, D. Hühn, C. Carrillo-Carrion, D. J. d. AberasturiV. Merk, S. Barcikowski, W. J. Parak, *J. R. Soc., Interface* **2014**, *11*, 20130931.
[35] C. A. Leatherdale, W.-K. Woo, F. V. Mikulec, M. G. Bawendi, *J. Phys. Chem. B* **2002**, *106*(31), 7619–7622.
[36] S. Pu, M. Yang, C. Hsu, C. Lai, C. Hsieh, S. Lin, Y. Cheng, P. Chou, *Small* **2006**, *2*(11), 1308–1313.
[37] A. Huber, T. Behnke, C. Würth, C. Jaeger, U. Resch-Genger, *Analyt. Chem.* **2012**, *84*(8), 3654.
[38] D. G. Mullen, M. Fang, A. Desai, J. R. Baker, B. G. Orr, M. M. Banaszak Holl, *ACS Nano* **2010**, *4*(2), 657–670.
[39] D. G. Mullen, A. M. Desai, J. N. Waddell, X. M. Cheng, C. V. Kelly, D. Q. McNerny, I. J. Majoros, J. R. Baker, L. M. Sander, B. G. Orr, M. M. B. Holl, *Bioconjug. Chem.* **2008**, *19*(9), 1748–1752.
[40] A. Z. Abbasi, F. Amin, T. Niebling, S. Friede, M. Ochs, S. Carregal-Romero, J. M. M. Martos, P. Rivera_Gil, W. Heimbrodt, W. J. Parak, *ACS Nano* **2011**, *5*, 21–25.
[41] L. L. del Mercato, A. Z. Abbasi, M. Ochs, W. J. Parak, *ACS Nano* **2011**, *5*(12), 9668–9674.
[42] L. Shang, K. Nienhaus, G. U. Nienhaus, *J. Nanobiotechnol.* **2014**, *12*, 5.
[43] S. Xu, B. Z. Olenyuk, C. T. Okamoto, S. F. Hamm-Alvarez, *Adv. Drug Deliv. Rev.* **2013**, *65*(1), 121–138.
[44] T. G. Iversen, T. Skotland, K. Sandvig, *Nano Today* **2011**, *6*(2), 176–185.
[45] G. Sahay, D. Y. Alakhova, A. V. Kabanov, *J. Controlled Release* **2010**, *145*(3), 182–195.
[46] W. J. Parak, R. Boudreau, M. L. Gros, D. Gerion, D. Zanchet, C. M. Micheel, S. C. Williams, A. P. Alivisatos, C. A. Larabell, *Adv. Mater.* **2002**, *14*(12), 882–885.
[47] C. Schweiger, R. Hartmann, F. Zhang, W. J. Parak, T. Kissel, P. Rivera Gil, *J. Nanobiotechnol.* **2012**, *10*(1), 28.
[48] S. De Koker, B. G. De Geest, C. Cuvelier, L. Ferdinande, W. Deckers, W. E. Hennink, S. De Smedt, N. Mertens, *Adv. Funct. Mater.* **2007**, *17*(18), 3754–3763.
[49] L. Kastl, D. Sasse, V. Wulf, R. Hartmann, J. Mircheski, C. Ranke, S. Carregal-Romero, J. A. Martínez-López, R. Fernández-Chacón, W. J. Parak, H.-P. Elsaesser, P. Rivera Gil, *ACS Nano* **2013**, *7*(8), 6605–6618.
[50] M. Semmling, O. Kreft, A. Muñoz Javier, G. B. Sukhorukov, J. Käs, W. J. Parak, *Small* **2008**, *4*(10), 1763–1768.
[51] P. Nativo, I. A. Prior, M. Brust, *ACS Nano* **2008**, *2*(8), 1639–1644.
[52] C. Brandenberger, C. Mühlfeld, Z. Ali, A.-G. Lenz, O. Schmid, W. J. Parak, P. Gehr, B. Rothen-Rutishauser, *Small* **2010**, *6*, 1669–1678.
[53] K. Boeneman, J. B. Delehanty, J. B. Blanco-Canosa, K. Susumu, M. H. Stewart, E. Oh, A. L. Huston, G. Dawson, S. Ingale, R. Walters, M. Domowicz, J. R. Deschamps, W. R. Algar, S. DiMaggio, J. Manono, C. M. Spillmann, D. Thompson, T. L. Jennings, P. E. Dawson, I. L. Medintz, *ACS Nano* **2013**, *7*, 3778–3796.
[54] J. B. Delehanty, C. E. Bradburne, K. Boeneman, K. Susumu, D. Farrell, B. C. Mei, J. B. Blanco-Canosa, G. Dawson, P. E. Dawson, H. Mattoussi, I. L. Medintz, *Integrative Biology* **2010**, *2*(5–6), 265–277.
[55] H. Mattoussi, G. Palui, H. B. Na, *Adv. Drug Deliv. Rev.* **2012**, *64*(2), 138–166.
[56] A. Verma, O. Uzun, Y. H. Hu, Y. Hu, H. S. Han, N. Watson, S. L. Chen, D. J. Irvine, F. Stellacci, *Nat. Mater.* **2008**, *7*(7), 588–595.

small 2014,
DOI: 10.1002/smll.201402110

[57] H. W. Child, P. A. Del Pino, J. M. De La Fuente, A. S. Hursthouse, D. Stirling, M. Mullen, G. M. McPhee, C. Nixon, V. Jayawarna, C. C. Berry, *ACS Nano* **2011**, *5*(10), 7910–7919.
[58] T. Dejardin, J. de la Fuente, P. Del Pino, E. P. Furlani, M. Mullin, C. A. Smith, C. C. Berry, *Nanomedicine* **2011**, *6*(10), 1719–1731.
[59] J. M. de la Fuente, C. C. Berry, *Bioconjug. Chem.* **2005**, *16*(5), 1176–1180.
[60] B. D. Chithrani, A. A. Ghazan, C. W. Chan, *Nano Lett.* **2006**, *6*(4), 662–668.
[61] D. B. Peckys, N. de Jonge, *Nano Lett.* **2011**, *11*(4), 1733–1738.
[62] M. Nazarenus, Q. Zhang, M. G. Soliman, P. del Pino, B. Pelaz, S. Carregal_Romero, J. Rejman, B. Rothen-Ruthishauser, M. J. D. Clift, R. Zellner, G. U. Nienhaus, J. B. Delehanty, I. L. Medinez, W. J. Parak, *Beilstein J Nanotechnol.* **2014**, DOI: 10.3762/bjnano.5.161.
[63] D. Hühn, K. Kantner, C. Geidel, S. Brandholt, I. De Cock, S. J. H. Soenen, P. Rivera Gil, J.-M. Montenegro, K. Braeckmans, K. Müllen, G. U. Nienhaus, M. Klapper, W. J. Parak, *ACS Nano* **2013**, *7*(4), 3253–3263.
[64] A. Muñoz Javier, O. Kreft, A. Piera Alberola, C. Kirchner, B. Zebli, A. S. Susha, E. Horn, S. Kempter, A. G. Skirtach, A. L. Rogach, J. Rädler, G. B. Sukhorukov, M. Benoit, W. J. Parak, *Small* **2006**, *2*(3), 394–400.
[65] M. Mahmoudi, A. M. Abdelmonem, S. Behzadi, J. H. Clement, S. Dutz, M. R. Ejtehadi, R. Hartmann, K. Kantner, U. Linne, P. Maffre, S. Metzler, M. K. Moghadam, C. Pfeiffer, M. Rezaei, P. Ruiz-Lozano, V. Serpooshan, M. A. Shokrgozar, G. U. Nienhaus, W. J. Parak, *ACS Nano* **2013**, *7*(8), 6555–6562.
[66] A. M. Alkilany, P. K. Nagaria, C. R. Hexel, T. J. Shaw, C. J. Murphy, M. D. Wyatt, *Small* **2009**, *5*(6), 701–708.
[67] P.-H. Yang, X. Sun, J.-F. Chiu, H. Sun, Q.-Y. He, *Bioconjug. Chem.* **2005**, *16*(3), 494–496.
[68] E. C. Cho, J. W. Xie, P. A. Wurm, Y. Xia, *Nano Lett.* **2009**, *9*, 1080.
[69] M. Semmling, O. Kreft, A. M. Javier, G. B. Sukhorukov, J. Käs, W. J. Parak, *Small* **2008**, *4*(10) 1763.
[70] C.-A. J. Lin, R. A. Sperling, J. K. Li, T.-Y. Yang, P.-Y. Li, M. Zanella, W. H. Chang, W. J. Parak, *Small* **2008**, *4*(3), 334–341.
[71] R. A. Sperling, T. Pellegrino, J. K. Li, W. H. Chang, W. J. Parak, *Adv. Funct. Mater.* **2006**, *16*(7), 943–948.
[72] M. Dahan, T. Laurence, F. Pinaud, D. S. Chemla, A. P. Alivisatos, M. Sauer, S. Weiss, *Optics Lett.* **2001**, *26*(11), 825–827.
[73] P. Rivera_Gil, S. D. Koker, B. G. De_Geest, W. J. Parak, *Nano Lett.* **2009**, *9*(12), 4398–4402.
[74] P. Rivera_Gil, C. V. Vazquez, V. Giannini, M. P. Callao, W. J. Parak, M. A. C. Duarte, R. A. Alvarez-Puebla, *Angew. Chem.* **2013**, *52*, 13694–13698.
[75] M. Eberhard, P. Erne, *Biochem. Biophys. Res. Commun.* **1991**, *180*(1), 209–215.
[76] G. A. Rutter, N. J. Osbaldeston, J. G. McCormack, R. M. Denton, *Biochem. J.* **1990**, *271*(3), 627–634.
[77] A. S. Verkman, M. C. Sellers, A. C. Chao, T. Leung, R. Ketcham, *Analyt. Biochem.* **1989**, *178*(2), 355–361.
[78] N. D. Sonawane, J. R. Thiagarajah, A. S. Verkman, *J. Biological Chem.* **2002**, *277*(7), 5506–5513.
[79] N. Antipina Maria, B. Sukhorukov Gleb, *Adv. Drug Deliv. Rev.* **2011**, *63*(9), 716–729.
[80] H. Arya, Z. Kaul, R. Wadhwa, K. Taira, T. Hirano, S. C. Kaul, *Biochem. Biophys. Res. Commun.* **2005**, *329*(4), 1173–1177.
[81] P. K. Chattopadhyay, D. A. Price, T. F. Harper, M. R. Betts, J. Yu, E. Gostick, S. P. Perfetto, P. Goepfert, R. A. Koup, S. C. De Rosa, M. P. Bruchez, M. Roederer, *Nat. Med.* **2006**, *12*(8), 972.
[82] H. Xu, M. Y. Sha, E. Y. Wong, J. Uphoff, Y. Xu, J. A. Treadway, A. Truong, E. O'Brien, S. Asquith, M. Stubbins, N. K. Spurr, E. H. Lai, W. Mahoney, *Nucleic Acids Res.* **2003**, *31*(8), e42.
[83] X. Gao, S. Nie, *Anal. Chem.* **2004**, *76*(8), 2406–2410.
[84] J. A. Lee, S. Mardyani, A. Hung, A. Rhee, J. Klostranec, Y. Mu, D. Li, W. C. W. Chan, *Adv. Mater.* **2007**, *19*(20), 3113.
[85] U. Lieberwirth, J. Arden-Jacob, K. H. Drexhage, D. P. Herten, R. Müller, M. Neumann, A. Schulz, S. Siebert, G. Sagner, S. Klingel, M. Sauer, J. Wolfrum, *Analyt. Chem.* **1998**, *70*, 4771–4779.
[86] S. H. Minhindukulasuriya, T. K. Morcone, L. B. McGown, *Electrophoresis* **2003**, *24*, 20–25.
[87] K. Hoffmann, T. Behnke, D. Drescher, J. Kneip, U. Resch-Genger, *ACS Nano* **2013**, *7*, 6674–6684.
[88] C. Gan, Y. Zhang, D. Battaglia, X. Peng, M. Xiao, *Appl. Phys. Lett.* **2008**, *92*(2411111).
[89] T. Förster, *Annalen der Physik* **1948**, *437*(1–2), 55–75.
[90] I. L. Medintz, A. R. Clapp, H. Mattoussi, E. R. Goldman, B. Fisher, J. M. Mauro, *Nat. Mater.* **2003**, *2*, 630–638.
[91] R. Freeman, L. Bahshi, T. Finder, R. Gill, I. Willner, *Chem. Commun.* **2009**, (7), 764–766.
[92] A. V. Yakovlev, F. Zhang, A. Zulqurnain, A. Azhar-Zahoor, C. Luccardini, S. Gaillard, J. M. Mallet, P. Tauc, J. C. Brochon, W. J. Parak, A. Feltz, M. Oheim, *Langmuir* **2009**, *25*(5), 3232–3239.
[93] T. Niebling, F. Zhang, Z. Ali, W. J. Parak, W. Heimbrodt, *J. Appl. Phys.* **2009**, *106*, 104701.
[94] J. S. Kang, g. Piszczek, J. R. Lakowicz, *J. Fluorescence* **2002**, *12*, 97–103.
[95] U. Kaiser, D. J. d. Aberasturi, R. Malinowski, F. Amin, W. J. Parak, W. Heimbrodt, *Appl. Phys. Lett.* **2014**, *104*, 041901.
[96] A. V. Agronskaia, L. Tertoolen, H. C. Gerritsen, *J. Biomed. Optics* **2004**, *9*, 1230–1237.
[97] R. Y. Tsien, *Biochemistry* **1980**, *19*, 2396–2404.
[98] W. K. Bae, M. K. Nam, K. Char, S. Lee, *Chem. Mater.* **2008**, *20*, 5307–5313.
[99] B. O. Dabbousi, J. Rodriguez-Viejo, F. V. Mikulec, J. R. Heine, H. Mattoussi, R. Ober, K. F. Jensen, M. G. Bawendi, *J. Phys. Chem. B* **1997**, *101*(46), 9463–9475.
[100] L. I. Kazakova, L. I. Shabarchina, G. B. Sukhorukov, *Phys. Chem. Chem. Phys.* **2011**, *13*(23), 11110.
[101] O. Y. Kochetkova, L. I. Kazakova, D. A. Moshkov, M. G. Vinokurov, L. I. Shabarchina, *Russian J. Bioorg. Chem.* **2013**, *39*(5), 504–509.
[102] A. S. Susha, A. M. Javier, W. J. Parak, A. L. Rogach, *Colloids Surf. A* **2006**, *281*, 40.

Received: July 17, 2014
Revised: September 24, 2014
Published online:

Particle & Particle Systems Characterization
www.particle-journal.com

Future Perspectives Towards the Use of Nanomaterials for Smart Food Packaging and Quality Control

Xingyu Jiang, Daniel Valdeperez, Moritz Nazarenus, Zhuo Wang, Francesco Stellacci, Wolfgang J. Parak, and Pablo del Pino**

In this Progress Report some recent trends and future perspectives towards the use of nanomaterials for smart food packaging and quality control of food are given. The examples and discussion are meant to illustrate the potential use of nanotechnology for food sustainability rather than to review the state of the art of nanomaterials in this area, which although expected to have a groundbreaking impact on food sustainability is still on an early stage.

1. Food Sustainability

The true challenge for our generation is that of sustainability. The world population keeps increasing at a rapid pace. We are currently close to 7.5 billion and will be close to 10 billion in 2050, which is only 35 years from now.[1] This large world population will need energy, materials, and importantly food for itself and for generations to come. At present there are no solutions on how to feed 10 billion people. This is quite obviously an important problem that has to be rapidly addressed. While in this short position paper we cannot address all aspects of food sustainability, we will rather focus on one important part of it. Despite feeding ~6 of the 7.5 billion people in the world, we waste ~30% of the total world food production. This means that yearly 1.3 billion tons of food are wasted. If we could avoid this waste, the world would make a giant leap towards feeding everybody and allowing for true food sustainability. Among the many steps needed to address this problem, we need to have a better control of food quality, and we need to have intelligent food packaging that slows the degradation process, but also determines when the food is truly rotten based on real data. Besides these global issues, also in so-called developed countries quality control during food processing, packaging and storage is paramount, as potentially the health of consumers may be endangered. This has lead already to legislation guidelines.[2] Politics and industry have developed systems to prevent food with undesirable conditions (microbiological, chemical or physical) from reaching the final consumer. The most practical approach hereby is a label on most products in which a theoretical "expiration date" is detailed. While this drastically reduces the risk that food in unacceptable conditions may mistakenly be sold, this approach is, however, some kind of "over-protective", i.e. often impeccable food will be disposed, just because the expiration date has passed. Unfortunately, it is impossible to precisely calculate expiration dates, as these depend on a number of external parameters, which cannot always be controlled individually. More individual markers, i.e. indicators of spoilage, instead of general "expiration dates" might be an interesting and useful alternative to optimize the product shelf life. Naturally, they would need to be harmless, without any risk of food contamination, cheap, and consumer-friendly. For the interested reader regarding smart packaging for monitoring of food quality, we refer to the review article by Kuswandi et al. in which the state of the art in this field was reviewed with a strong focus on commercially available time-temperature indicators (TTIs) and radio frequency identification (RFID) tags.[3] As already acknowledged by Kuswandi et al., the potential of nanotechnology to enhance current smart packaging systems or to motivate new approaches is impressive.

Prof. X. Jiang, Dr. Z. Wang
Beijing Engineering Research Center for BioNanotechnology and Key Laboratory for Biologhical Effects of Nanomaterials and Nanosafety
National Center for NanoScience and Technology
Beijing, China
E-mail: xingyujiang@nanoctr.cn
Prof. W. J. Parak, Dr. Pablo del Pino
CIC BiomaGUNE
San Sebastian, Spain
E-mail: pdelpino@cicbiomagune.es
D. Valdeperez, M. Nazarenus, Prof. W. J. Parak
Fachbereich Physik
Philipps-Universität Marburg
Marburg, Germany
Prof. F. Stellacci
Institute of Materials and Integrative Food and Nutrition Center
EPFL
Lausanne, Switzerland

DOI: 10.1002/ppsc.201400192

2. Why Nanomaterials?

Nanotechnology has provided in the recent years an amazing set of new materials and devices, which nowadays are making their ways towards applications.[4] Beginning from health and energy related applications, these materials also have potential to impact everyday life consumer products, as we will describe herein in the case of food packaging/quality control. New nanomaterials certainly could provide new impact in this direction.[3,5] Many products in the supermarket are packaged in standard plastic foils. They prevent direct contact of the food with the environment, and shield in particular bacteria. We envisage "smart" plastic foils, which provide feedback about

potential undesired decomposition / contamination of the food, and thus suggest that this product does not retain its optimal conditions and therefore should not be consumed anymore. Indeed sensors for monitoring of temperature, humidity, reducing and oxidizing gases, and volatile organic compounds have been successfully integrated on plastic foil.[6] There has been an ever-growing number of reports on the integration of sensing nanostructures on flexible substrates,[7] which might have a groundbreaking impact on monitoring systems, for instance, in clothing and implants, and clearly in food industry, the topic of this report. In addition, nano-based sensors might be very useful for rapid in situ analysis of food at critical locations (e.g. customs, storage facilities, in situ control of food's transportation, etc.). Last but not least, nanomaterials might not be only useful for detecting spoilage but also for prevention. Appropriate coatings with antibacterial properties could be used, as for instance, films derivatized Ag nanoparticles (NPs).[8] Obviously, biocompatibility, long-term stability, and toxicity remain major issues, which will have to be further characterized and optimized, particularly in the case of direct contact between nanomaterials and food.[9]

In the last years the range of functions which can be performed by NPs has been greatly expanded including antimicrobial activity, sensing of biomolecules and ions, tunable optoelectronic properties, light shielding, etc. The versatility in terms of NP-based functionalities, in many cases completely novel and different from the bulk, have been achieved due to several important developments in colloidal chemistry with regards to controlling the size, shape, structure and composition, as well as suitable surface coatings.[9,10] Those functional NPs can be easily incorporated in polymer matrixes,[11] and thus could be readily integrated in plastic foils. Shoseyov et al. have made plastic foils from nanocrystalline cellulose, which in combination with integrated ZnO NPs are currently introduced as air tight food packaging, which also eliminates IR and UV exposure.[12] Appropriate surface coatings can provide these NPs the ability to sense their environment and report the results optically, for example by fluorescence,[13] or simply by changes in transmitted or reflected color,[14] or by electrical readout.[15] Thus, NPs could be used as reporters of a variety of basic parameters, which are indicators for ongoing decomposition, in particular for perishable food. More importantly, nanotechnology allows for monitoring of these parameters in real-time.

3. Sensing Spoilage

Sensing based on changes of the physicochemical properties of NPs, which are driven by target analytes, stand as one of the most widely explored applications of NPs in the context of life sciences, including sensing of ions and small molecules, and bio-sensing, that is, detection of biomolecules such as proteins and nucleic acids.[16] In those sensing nanoplatforms based on direct contact with the analyte, the surface of inorganic NPs is typically modified with organic molecules such carbohydrates,[17] nucleic acids,[18] aptamers,[15b] antibodies,[19] combinations of hydrophilic and hydrophobic linear chains,[20] etc., which have strong affinity for a target analyte.

Xingyu Jiang is a Professor at the National Center for NanoScience and Technology (NCNST), China. He obtained his B.S. at the University of Chicago (1999) and his Ph.D. at Harvard University (with Prof. George Whitesides, 2004). His research interests include surface chemistry, microfluidics, nanoparticles, antibiotics, and immunoassays.

Pablo del Pino is a researcher at CIC biomaGUNE. He obtained his Ph.D. degree from Technische Universität München, Germany, in 2007. He then joined the group of Wolfgang Parak as a postdoctoral fellow at the Ludwig-Maximilians-Universität München, Germany. From 2009 to 2013, he was a scientist at the Institute of Nanoscience of Universidad de Zaragoza (INA, Zaragoza, Spain). His current research interests focus on the development of materials for applications in life science.

The analyte's "catching" event can then lead to a change on the physicochemical properties of the NPs such as fluorescence, surface plasmon resonance, conductivity, magnetic relaxivity, etc. Indeed, choosing the right composition, size and shape of the inorganic core, and the surface functionalization of the NPs allows for tailoring the response of nano-based sensing systems to specific stimuli and thereby, a variety of sensing nanoplatforms have been demonstrated.[10] The possibilities of such systems are manifold, ranging from ultrahigh sensitive complex approaches[21] to affordable easy-to-use alternatives, depending on the principle of detection and equipment required. Clearly, in the case of sensing spoilage, several indicators such as time-temperature, pH, a variety of volatile compounds, etc. can be monitored using such nanosystems. Yet, approaches which are simple, easy-to-use, affordable, reliable (even at the cost of sensitivity) and which provide real-time signals are required if are to be used by the food industry,[22] be it as an analytical tool for food control or as an element of the packaging.

One of the most straightforward and widely used nanosensing approach relies on the color change that solutions of metallic NPs undergo (directly or indirectly) in the presence of a particular analyte, i.e. colorimetric sensors based on plasmonic NPs. The colorimetric nanosensors are particularly appealing for sensing food spoilage because they are cost-efficient, fast and easy to use. In this direction one particularly illustrative example was reported by Zhang et al. who proposed a TTI based on the color changes of Au nanorods

Part. Part. Syst. Charact. **2014**,
DOI: 10.1002/ppsc.201400192

upon incorporation of a Ag shell.[23] The thickness of the Ag shell, which depends on the temperature, could be synchronized with the growth of bacteria. The longer a perishable product is exposed to elevated temperatures (regardless of the detailed history), the higher is the probability that it will start to spoil. This spoilage can be microbiological (among others such as oxidation and enzymatic degradation), due to the growth of mesophilic bacteria such as *Escherichia coli, Listeria monocytogenes,* or *Staphylococcus aureus*. All these bacteria cause food poisoning, since they are able to multiply in the intestine and have an optimum growth temperature around 37 °C in common, in which they start to grow more rapidly. Based on this fact Zhang et al. could correlate the change of color of core/shell Au/Ag nanorods with the growth of *Escherichia coli* (*E. coli*) bacteria. The longer these bacteria are exposed to elevated temperatures (regardless of the detailed history), the higher their growth rate becomes. Then the longer this system is exposed to elevated temperatures (again, regardless of the detailed history), the more the shell growth progresses. The growth of the silver shell is directly correlated with a change of color (i.e. blue-shift in the surface plasmon band). Thus, the longer these NPs are exposed to elevated temperatures, the more their color in solution shifts from red to green. In this way, these NPs form a chronochromic TTI, which can be directly observed by eye. The more this indicator has been shifted from red to green, the longer the embedded product has been exposed to elevated temperatures and the higher the numbers of bacteria will be.[23] A little color spot on the packaging foil, without any direct contact with the embedded food, thus could be an indirect indicator for the degree of bacterial contamination.

Besides overgrowth of Au NPs with Ag, also agglomeration of Au NPs can be easily observed by naked eye, cf. **Figure 1**. This effect is due to the plasmon coupling of the adjacent NPs and this effect has been used for decades for molecular assays.[24] In this direction plasmonic Au NPs have been applied to quantify contamination with mercury.[25] Presence of Hg^{2+} causes a specific agglomeration of modified Au NPs, as indicated by the color change of the Au NP solution from red to blue, cf. **Figure 2**. With the same concept it was also possible to control the amount of proteins in milk products, to guarantee their quality. As pointed out, color changes of these particles offer a straightforward read-out, which can be observed with the naked eye. Milk and other dairy products are vital protein sources. A quick method to quantify the amount of proteins in milk is thus very useful for consumers, as well as producers and distributors. Zhu et al. have reported a convenient system based on functionalized gold NPs combined with click chemistry.[26] The assay is based on the fact that the peptide chains of proteins can reduce Cu(II) to Cu(I), depending on the absolute quantity of the peptide bond, and Cu(I) then catalyzes the click reaction between azide-/alkyne-functionalized gold NPs, cf. **Figure 3**. Presence of proteins thus results in the aggregation of the Au NPs, leading to the typical color change from red to purple.[27] With this method, the amount of proteins can be quantified within the range from 30 to 2500 µg/mL In the same direction, Song et al. reported on a colorimetric test based on Ag NPs for the detection of melamine, an illegal toxic additive in milk.[28] The authors proposed Ag NPs functionalized with chromotropic acid, which in the presence of melamine induce NPs aggregation and thus, a color change from yellow to orange.

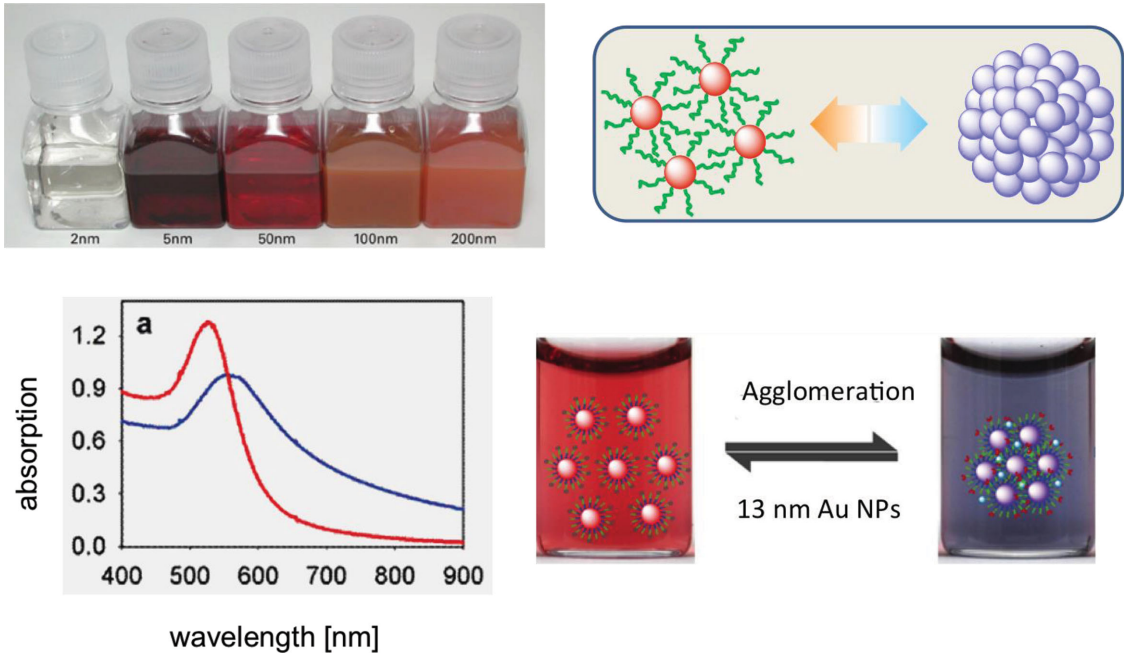

Figure 1. Dispersed gold NPs have distinct color, as shown here for solutions of colloidal gold with NPs core NP diameters of 2, 5, 50, 100, and 200 nm (from Tedpella, Inc). Their plasmon absorption peak (for Au NPs > 2 nm) lies in the green, and thus solution in reflection appear red. Upon agglomeration the plasmons of adjacent NPs couple, which shift the plasmon absorption to the red, i.e. the solution appears more bluish. Parts of this image reproduced with permission from Faraday.

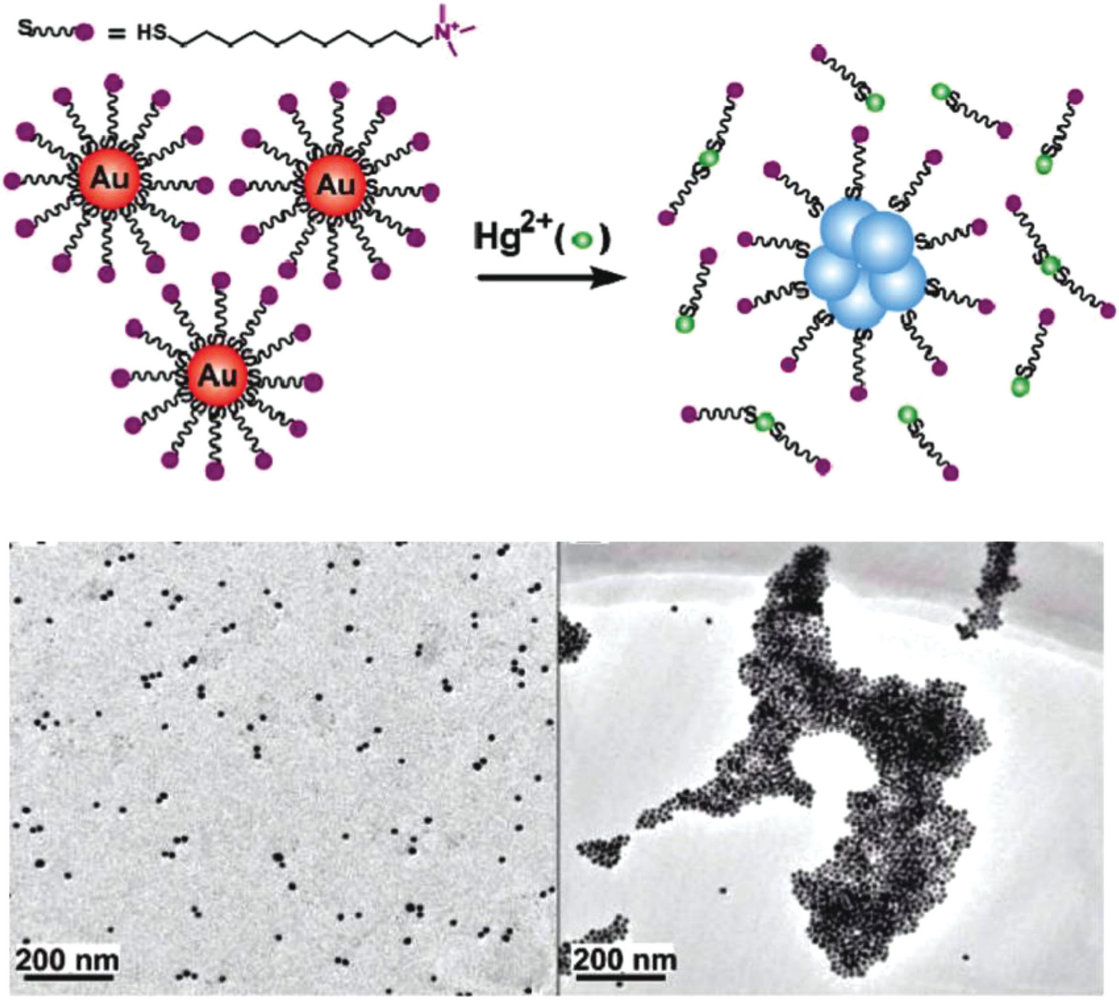

Figure 2. Highly sensitive, colorimetric detection of mercury(II). Presence of Hg^{2+} causes the specific agglomeration of Au NPs, which can be seen in the transmission electron microscopy images, as also in the change of color of the solution from red to blue. Reproduced with permission.[25] Copyright 2010, ACS.

In the same way agglomeration of Au NPs and the subsequent red-shift of their absorption can be used for detection of nucleic acids, following the classical approach by Mirkin et al.[29] As example, for the detection of pathogenic *Vibrio cholerae* (foodborne pathogens responsible for cholera, a common diarrheal illness) in food samples, Guo et al. developed a sensitive method to detect nucleic acids with the use of the target oligonucleotide-modified Au NPs, which undergo target-induced Au NP dimer formation upon presence of the target nucleotide.[18] This sensor turned out to be much more sensitive than a commonly used sensor fabricated using conventional strategies. This significant improvement in sensitivity can be largely attributed to the Y-shaped DNA duplex upon hybridization, the formation of which enables two linked Au NPs to be pulled together to a very close distance, yielding a maximum color change. The ability of the sensor to rapidly detect unamplified genomic DNA isolated from foodborne pathogens in a complex sample matrix might have important applications, in particular in the sense that this method might circumvent the need to culture bacteria before any assay. The straightforward read-out shown in these assays makes them very convenient indicators of food contamination. It has to be noted, however, that in these analytical assays (in contrast to the TTI based on Au/Ag nanorods) direct chemical contact of the sensor components (Au NPs, Ag NPs, enzymes, substrates, etc.) in solution still is necessary, and therefore requires additional steps for incorporation into food packaging.

While the so-far mentioned examples are based on direct colorimetric read-out, also fluorescence is a signal that conveniently can be detected.[30] There is a variety of potential applications for such read-out. Upon their presence specific analytes can change the color and/or intensity of fluorescence of NPs upon UV exposure, which provides and easily detectable optical signal. This principle has been used for example for the direct detection of toxins, which are excreted from bacteria.[31] Sapsford et al. modified the surface of fluorescent NPs (so-called quantum dots) with specific peptide sequences that bear an additional organic fluorophore at their free end. This fluorophore is in resonance with the quantum dot, in a process called fluorescence resonance energy transfer (FRET). Certain

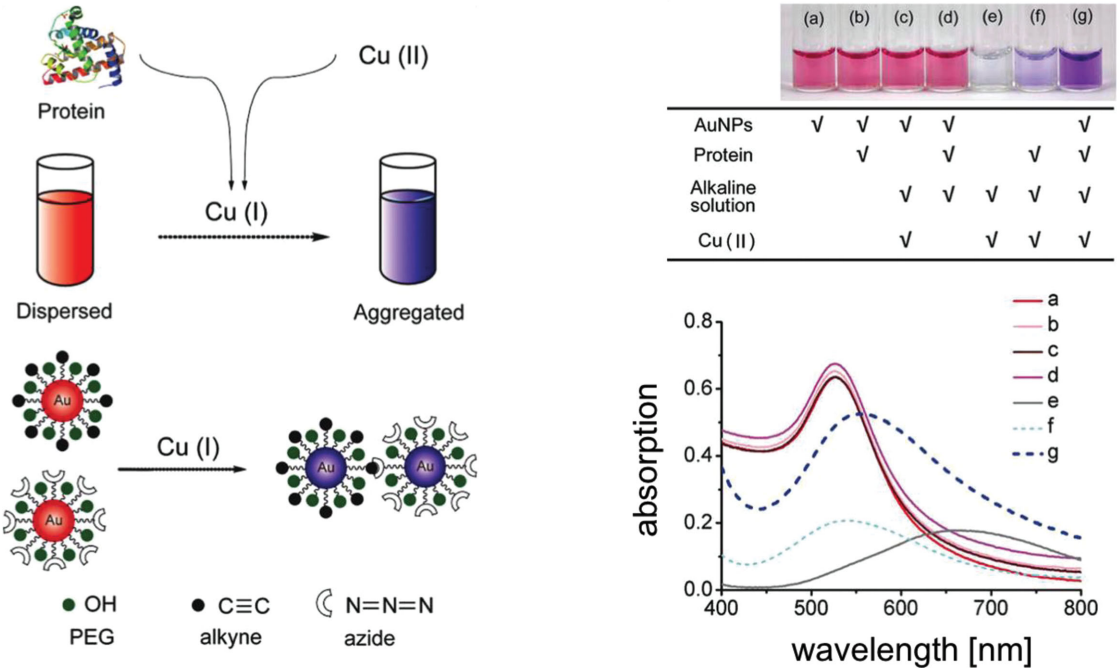

Figure 3. Click-chemistry based assay for proteins. Presence of proteins reduces copper (II) to copper (I). Cu^{+} triggers agglomeration of Au NPs which can be observed as red-shift in the absorption spectra, i.e. in a color change of the solution from red to blue. Reproduced with permission.[26] Copyright 2012, ACS.

toxins, in this case botulinum neurotoxins, specifically cut the peptides, the fragment with the organic fluorophore diffuses apart, and FRET is stopped, which can be observed as change in the fluorescence color.[31] While not as easy to observe as reflected or transmitted color, also such kind of fluorescence changes could be directly observed by a customer in a supermarket by holding the packaging foil against illumination, although again, direct contact of the sensor with the food would be required. Recently, such detection has been made possible with the camera of a smartphone.[30] Please note, while changes in intensity would be hard to quantify, the here mentioned sensors are based on spectral changes, i.e. on changes in the color of fluorescence. A variety of different surface modifications hereby allows for detection of several contaminants in parallel.[32]

In addition, combinations of both read-outs are possible as highlighted in the following example. Pesticides are widely used in the production of fruits and vegetables. They exert toxicity on human health through their residues in agricultural products and contamination of water. Organophosphorus compounds and carbamates are the pesticides most widely used in agriculture. Liu et al. developed a sensitive assay with dual read-out (colorimetric and fluorimetric) for these two classes of pesticides, which uses rhodamine B-covered gold NPs and makes use of the inhibition of acetylcholinesterase (AChE) by organophosphorus and carbamate pesticides.[33] The fluorescence of rhodamine B, which is pre-immobilized on the surface of the gold NPs, is quenched. Upon presence of AChE and acetylthiocholine (ATC) the solution turns from red (dispersed gold NPs) to blue (agglomerated gold NPs) and furthermore the green fluorescence of rhodamine B can be observed, cf. **Figure 4**. The reason is that AChE converts ATC to thiocholine, which has a higher binding affinity to the gold NPs than rhodamine B, thus releasing rhodamine B into solution, where the quenched fluorescence is recovered. Moreover, the gold NPs, now partly covered with rhodamine B and partly with thiocholine, attract each other due to the opposite charges of rhodamine B and thiocholine, leading to agglomeration and thus blue color of the solution. In presence of organophosphorus or carbamate pesticides AChE is inhibited, leading to less fluorescence and agglomeration of the gold NPs in the solution. Concentrations of the pesticides are determined using calibration curves of fluorescence and absorbance. With this method, the lowest detectable concentrations for several types of pesticides including carbaryl, diazinon, malathion, and phorate were measured to be 0.1, 0.1, 0.3, and 1 µg/L, respectively. Most importantly, this assay also allows for pesticide detection in complex samples such as agricultural products (tomatoes and cucumbers) and river water.

The advantage of using NP-based sensors as described above is the possibility for convenient direct optical read-out, either by naked eye or by very simple optical devices such as the integrated camera of a smartphone. There are, however, also several other detection schemes. Some contaminant molecules could also be detected directly, once they adsorb to the surface of gold or silver (i.e. plasmonic) NPs with an effect called surface enhanced Raman scattering (SERS).[34] For the interested reader, we refer to the review of J. Zheng and L. He about SERS for the chemical analysis of food, which covers the state of the art of SERS detection of small analytes in food, including food additives, pesticides, antibiotics and illegal drugs, melamine, illegal food dyes and small-molecule toxins.[35] While read-out of SERS signals could not be done directly by eye, portable detectors in this direction will be available in the future. Due to

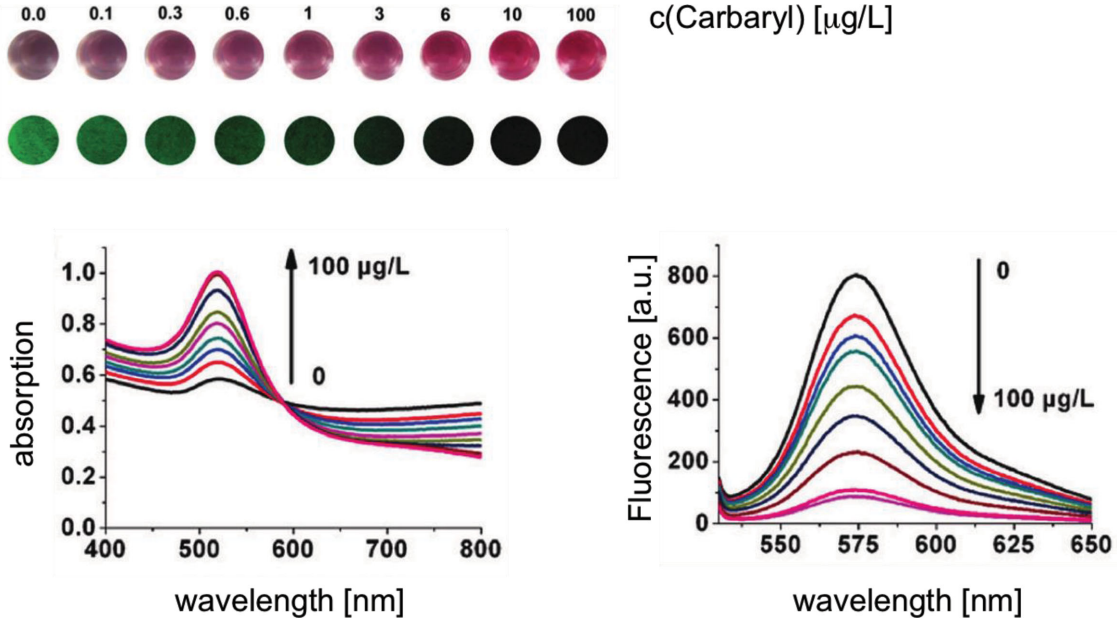

Figure 4. Highly sensitive, dual-readout assay for organophosphorus and carbamate pesticides. Reproduced with permission.[33] Copyright 2012, ACS.

the sharp Raman bands with this technique, potentially many different molecules can be detected in parallel, without the need to introduce any label.[36]

Besides optical read-out, also electrical read-out via small cost-effective devices created with printed electronics on packaging foils can be foreseen.[6] Classical routine methods for molecular analysis, such as field-effect transistors (FETs) and electrochemiluminescence are somewhat limited in their application towards the direct customer-based analysis of food-related samples. NPs, however, can drastically improve the efficiency of such methods of detection. This offers a transition from large-scale devices to much smaller detectors. This is demonstrated for example by using carbon nanotubes for the detection of bacteria.[37] Adsorption of bacteria can change the conformation and thus, electronic structure of nanomaterials, which in change can be electronically detected.[37] The NPs can also allow for a local accumulation due to specific binding of the analytes. Cho et al. have shown in this direction a simple electric readout for very low levels of toxic ions in food.[20] In order to better demonstrate the state-of-the-art of such devices two examples for quality control of mussels are given. Seafood, such as mussels, faces some serious contamination problems, such as heavy metals, toxins, etc. Mercury is one of the most common toxic heavy metals found in seafood, and its detection is important. An et al. described the fabrication and characterization of a liquid-ion gated FET-type flexible graphene aptamer-based sensor with high sensitivity and selectivity for Hg.[15b] The graphene aptamer-based sensor had excellent sensing performance down to very low concentrations of 10 pM, which has been claimed to be 2–3 orders of magnitude more sensitive than previously reported mercury sensors using standard electrochemical systems. The flexible graphene aptamer-based sensor showed a very rapid response, providing a signal in less than 1 s, when the Hg ion concentration was altered in mussel samples.[15b] Another example of improved detection efficiency is the detection of palytoxin (PITX, a very potent toxin) in seafood using electrochemiluminescence. Zamolo et al. developed an ultrasensitive electrochemiluminescence-based sensor for the detection of PITX, taking advantage of the specificity provided by anti-PlTX antibodies, the good conductive properties of carbon nanotubes, and the excellent sensitivity achieved by a luminescence-based transducer.[38] The sensor was able to produce a concentration-dependent light signal, allowing PlTX quantification in mussels, with a limit of quantification (LOQ = 2.2 μg/kg of mussel meat). This is more than 2 orders of magnitude more sensitive than that of the commonly used detection techniques, such as Liquid Chromatography Mass Spectrometry (LC-MS) or other Mass Spectrometry techniques (MS).[38] These examples demonstrate that due to the excellent transducer properties of nanomaterials smaller devices are possible.

So far we have discussed detection of "direct" contaminants, such as bacteria, toxins, heavy metal ions. However, food spoilage upon storage can be also detected by several indirect indicators. One important cause of food spoilage is the oxygen content in the package. Increase in oxygen can lead to different effects, such as the decrease of the ascorbic acid content, enzymatic browning, the possibility of growth for aerobic bacteria, and the oxidation of unsaturated fatty acids, aromas and colorants.[39] Although the food industry uses different techniques such as modified atmospheres to avoid the initial headspace content of oxygen in certain products, there is always an increase of oxygen content over time due to the permeability of the package material. In order to monitor the oxygen content in food packages, the Mills group developed a colorimetric redox dye-based indicator that gradually changes the color with small amounts of oxygen using TiO_2 NPs mixed with methylene blue in water.[40] This sensor must be activated by UV light exposition on the TiO_2 NPs to generate electron–hole pairs that oxidize the sacrificial electron donor (in this case triethanolamine), which leads to an accumulation of the photogenerated electrons

Part. Part. Syst. Charact. **2014**,
DOI: 10.1002/ppsc.201400192

on the TiO_2 NPs. These electrons finally reduce the redox dye and thus change its color. Incorporation of such oxygen sensors in food packaging would allow for on-site indication of spoiled food. Most importantly, this sensor would not require direct contact with the food and could be integrated in an oxygen-permeable compartment within the package material.

As important as the oxygen content is the moisture inside the package, which can give an idea of the freshness of a product. Luechinger et al. designed a sensor using 20–50 nm carbon-coated copper NPs dispersed on a several micrometer thick hybrid film.[41] This sensor was based on a surface plasmon resonance shift due to the water uptake of the film, affecting the membrane thickness at high relative humidity. Once this film was exposed to atmospheres with different water vapor content, it got sensitively colored with spectral shifts around 50 nm per % of relative humidity in a range of 70–80% relative humidity. At low humidity, the effect could be assigned to surface plasmon resonance shifts, whereas thin-film interference within a condensed water or solvent layer forming on top of the film accounted for the intense coloration at higher humidity. The present results suggest use of such porous hybrid metal/polymer films as an economically attractive alternative to electronic-circuit-based humidity sensing. Again, this optical humidity detection principle would not require direct contact with the food and could be integrated within a separated compartment with water-permeable enclosure. Also pH can be an important indicator for the quality state of food.[42] It can easily be detected optically with NPs, for example by changes in fluorescence color, which can be observed under UV light.[13] However, in this case contact with the food is required.

Besides oxygen, moisture and pH, several volatile compounds can be indicative of food spoilage, or even food freshness.[43] For instance, some volatile compounds are directly related to the health and nutritional value of some vegetables (e.g. tomato[44] whereas others (e.g. trimethylamine, dimethylamine, ammonia, esters, alcohols, ethylene, etc.) can be indicators of spoilage, for instance, in fish,[45] meat,[46] eggs[47] and fruits.[48] As previously stated, nanotechnology and new printing technologies allows for integration of multiple gas sensors on plastic and flexible substrates, thereby providing the foundations for cost-efficient sensors, which could be used for real-time monitoring of several volatile indicators of food spoilage as well as temperature and humidity in parallel.[6] In this direction, Pandey et al. reported on a flexible resistive nano-based sensor for ultrasensitive detection of ammonia,[49] one of the common volatiles resulting from microbial degradation of food.[45] The sensor relies on current changes upon adsorption of ammonia on films of nanocomposites formed by Ag NPs and guar gum, a type of polysaccharide. Indeed, an optical sensor for ammonia based on this nanocomposite has been also demonstrated, though in this case in solution.[50] In contrast to other common gas sensors which require high temperature operation, the ammonia nanocomposite based sensor proposed operates at room temperature and furthermore, it presents fast response/recovery. Such a flexible film ammonia sensor could be readily integrated on food packaging. Given the state of the art of printing & organic electronics, we envisage "smart" labels on food packaging, which by multiple nano-based sensors (temperature, humidity, and volatiles) can warn consumers, producers and distributors of potential food spoilage.

4. Preventing Spoilage

Nanomaterials may help not only to detect contamination, but also to reduce it, which will be explained for the cases of bacteria, heavy metal ions, and oxygen as examples. While silver NPs with their antibacterial properties[51] might not be wanted for food packaging due to potential cytotoxic effects by release of Ag^+ ions (though they might be negligible), also other antibacterial NPs are known, which are made from more biocompatible materials. Zhao et al. showed that also gold NPs can be potent antibiotics, particularly for multi-drug resistant bacteria.[52] While they have not demonstrated their use in the food industry yet, it can be envisioned that using gold-based materials for killing germs in food might be safer than silver, as small amounts of gold are already approved and consumed as food in the form of gold foil. The group of Aaron Gedanken has pioneered the use of zinc oxide and titanium oxide NPs as antibacterial agents,[53] which have been used in many consumer products over years. While so far mainly used for textiles,[54] this group has demonstrated that these NPs can be incorporated without problems in synthetic polymer films. In order to minimize any potential contamination of food, the packaging foil also could be built in double-layer geometry, thus preventing any direct contact of the sensor/antibacterial coating with the food. In the same direction, nanomaterials could also be used to (partly) remove toxic substances. For this, specific recognition leading to binding of the toxic molecules and thus to their removal is required. Due to their high surface-to-volume ratio, nanomaterials here offer clear advantages over bulk material. An example in this direction was given by Ojea-Jimenez et al., who used NPs to remove toxic ions from water.[55] Also oxygen can be removed by oxygen scavengers, which is already used for food preservation.[56] One of the most traditionally used oxygen scavengers is iron powder, which is separately packaged in small sachets in order to avoid direct contact with the food. Oxygen reduction is based on the oxidation of the iron.[57] For the same purpose, iron NPs have been used as oxygen scavengers, in this case attached to one of the inner permeable polymer layers of the multilayered package, again in a way which prevents direct contact with the product.[58] These Fe NPs were attached in kaolinite forming micrometric structures, leading to the formation of active nanocomposites that act as passive barriers avoiding gas diffusion through the membrane and as reductants due to the reactivity of the Fe NPs. In this case the big surface-to-volume ratio of the NPs is the key point.[58]

Last in this section, we want to acknowledge the presence in food industry of several products based on nanoclays (i.e. naturally occurring nanoparticles of layered aluminium silicates),[59] which are already commercially available, such as Imperm, Aegis, and Durethan.[60] In these products, nanoclays are incorporated into plastics, which are used to produce bottles, providing improved barrier properties for retaining CO_2 and keeping out O_2 (keeping beverages fresher and extending shelf life) and improved stiffness (nanoclays reinforcement).

5. Perspective

While the above mentioned examples clearly need to be seen as examples to illustrate a field still in its infancy, we believe that smart nanomaterials offer the potential for many disruptive technologies to be widely used in the future for food packaging applications. Compared to existing methods, which are usually dependent on bulky instruments, and are thus not suitable for on-site detection, the illustrated approaches allow convenient protocols and straightforward read-outs. Read-outs of NPs, in particular optical read-out, which relates molecular events to colorimetric and fluorimetric signals,[61] can be possible with the naked eye or simple tools such as standard digital cameras. This, together with the fact that nanomaterials can be integrated into standard matrixes, in particular in the detection schemes where no direct chemical contact with the food sample is required,[23] will allow for small and reasonably inexpensive integrated sensor devices. While nowadays customers upon inspecting a product in the supermarket look on the expiration date, in the future this might be a small and easily to understand sensor integrated into the packaging foil, which by means of a color code indicates onset of decomposition or contamination. Clearly, smart nano-based packaging systems have a long way ahead in order to be incorporated by the food industry. Issues such as nanoparticle toxicity (e.g. release of toxic metal ions), nanoparticle ecotoxicity, recycling (e.g. plastic foils which contain NPs) and regulation of the use of NPs in food, are still to be addressed. As the population grows and food becomes increasingly more precious and sustainability becomes more accepted, maybe in the future intelligent web-connected packagings will be used to detect the onset of degradation and prevent waste of edible food.

Acknowledgements

Part of this work was supported by the European Commission (project FutureNanoNeeds) and the CAS/SAFEA International Partnership Program for Creative Research Teams, Beijing Natural Science Foundation (grant 2122058).

Received: September 6, 2014
Published online:

[1] U. Nations, (Ed.: D. o. E. a. S. A. P. Division), United Nations. Working Paper No. ESA/P/WP.235., New York, **2014**.
[2] a) European Food Safety Authority, *EFSA supporting publication* **2013**, *EN-531*, 58 pp; b) European Commission, in *COM(2008) 366 final. Brussels, Belgium: European Commission; 2008*, COM(2008) 366 final. Brussels, Belgium: European Commission, **2008**.
[3] B. Kuswandi, Y. Wicaksono, Jayus, A. Abdullah, L. Heng, M. Ahmad, *Sens. Instrumen. Food Qual.* **2011**, *5*, 137.
[4] B. Pelaz, S. Jaber, D. Jimenez de Aberasturi, V. Wulf, J. M. de la Fuente, J. Feldmann, H. E. Gaub, L. Josephson, C. R. Kagan, N. A. Kotov, L. Liz-Marzán, H. Mattoussi, P. Mulvaney, C. B. Murray, A. L. Rogach, P. S. Weiss, I. Willner, W. J. Parak, *ACS Nano* **2012**, *6*, 8468.
[5] a) R. H. Farahi, A. Passian, L. Tetard, T. Thundat, *ACS Nano* **2012**, *6*, 4548; b) M. Valdés, A. Valdés González, J. García Calzón, M. Díaz-García, *Microchim. Acta* **2009**, *166*, 1.
[6] D. Briand, A. Oprea, J. Courbat, N. Bârsan, *Mater. Today* **2011**, *14*, 416.
[7] a) M. C. McAlpine, H. Ahmad, D. Wang, J. R. Heath, *Nat. Mater.* **2007**, *6*, 379; b) K. Takei, T. Takahashi, J. C. Ho, H. Ko, A. G. Gillies, P. W. Leu, R. S. Fearing, A. Javey, *Nat Mater* **2010**, *9*, 821; c) Q. Cao, H.-s. Kim, N. Pimparkar, J. P. Kulkarni, C. Wang, M. Shim, K. Roy, M. A. Alam, J. A. Rogers, *Nature* **2008**, *454*, 495; d) M. D. Angione, R. Pilolli, S. Cotrone, M. Magliulo, A. Mallardi, G. Palazzo, L. Sabbatini, D. Fine, A. Dodabalapur, N. Cioffi, L. Torsi, *Mater. Today* **2011**, *14*, 424.
[8] E. Fortunati, I. Armentano, Q. Zhou, A. Iannoni, E. Saino, L. Visai, L. A. Berglund, J. M. Kenny, *Carbohydrate Polym.* **2012**, *87*, 1596.
[9] B. Pelaz, G. Charron, C. Pfeiffer, Y. Zhao, J. M. de la Fuente, X.-J. Liang, W. J. Parak, P. del Pino, *Small* **2013**, *9*, 1573.
[10] P. del Pino, *BIOMEDO* **2014**, *19*, 101507.
[11] G.-M. Kim, A. Wutzler, H.-J. Radusch, G. H. Michler, P. Simon, R. A. Sperling, W. J. Parak, *Chem. Mater.* **2005**, *17*, 4949.
[12] O. Shoseyov, Y. Paltiel, S. Yochelis, S. Baruch-Sharon, Y. Nevo, *PCT/IL2013/050205* **2013**.
[13] F. Zhang, E. Lees, F. Amin, P. Rivera Gil, F. Yang, P. Mulvaney, W. J. Parak, *Small* **2011**, *7*, 3113.
[14] Y. W. Lin, C. C. Huang, H. T. Chang, *Analyst* **2011**, *136*, 863.
[15] a) S. J. Park, O. S. Kwon, S. H. Lee, H. S. Song, T. H. Park, J. Jang, *Nano Lett.* **2012**, *12*, 5082; b) J. An, S. Park, O. Kwon, J. Bae, J. Jang, *ACS Nano* **2013**, *7*, 10563.
[16] a) C. Carrillo-Carrión, M. Nazarenus, S. S. Paradinas, S. Carregal-Romero, M. J. Almendral, M. Fuentes, B. Pelaz, P. del Pino, I. Hussain, M. J. D. Clift, B. Rothen-Rutishauser, X.-J. Liang, W. J. Parak, *Curr. Opin. Chem. Eng.* **2014**, *4*, 88; b) E. Polo, P. del Pino, B. Pelaz, V. Grazu, J. M. de la Fuente, *Chem. Commun.* **2013**, *49*, 3676; c) F. Xia, X. Zuo, R. Yang, Y. Xiao, D. Kang, A. Vallée-Bélisle, X. Gong, J. D. Yuen, B. B. Y. Hsu, A. J. Heeger, K. W. Plaxco, *Prco. Natl. Acad. Sci. USA* **2010**, *107*, 10837; d) R. Elghanian, J. J. Storhoff, R. C. Mucic, R. L. Letsinger, C. A. Mirkin, *Science* **1997**, *277*, 1078; e) E. S. Cho, J. Kim, B. Tejerina, T. M. Hermans, H. Jiang, H. Nakanishi, M. Yu, A. Z. Patashinski, S. C. Glotzer, F. Stellacci, B. A. Grzybowski, *Nat. Mater.* **2012**, *11*, 978.
[17] M. Moros, B. Pelaz, P. Lopez-Larrubia, M. L. Garcia-Martin, V. Grazu, J. M. de la Fuente, *Nanoscale* **2010**, *2*, 1746.
[18] L. Guo, Y. Xu, A. Ferhan, G. Chen, D. Kim, *J. Am. Chem. Soc.* **2013**, *135*, 12338.
[19] S. Puertas, P. Batalla, M. Moros, E. Polo, P. del Pino, J. M. Guisán, V. Grazú, J. M. de la Fuente, *ACS Nano* **2011**, *5*, 4521.
[20] E. S. Cho, J. Kim, B. Tejerina, T. M. Hermans, H. Jiang, H. Nakanishi, M. Yu, A. Z. Patashinski, S. C. Glotzer, F. Stellacci, B. A. Grzybowski, *Nat. Mater.* **2012,** *11*, 978.
[21] D.-K. Lim, K.-S. Jeon, H. M. Kim, J.-M. Nam, Y. D. Suh, *Nat Mater* **2010**, *9*, 60.
[22] B. Veigas, J. M. Jacob, M. N. Costa, D. S. Santos, M. Viveiros, J. Inacio, R. Martins, P. Barquinha, E. Fortunato, P. V. Baptista, *Lab Chip* **2012**, *12*, 4802.
[23] C. Zhang, A. X. Yin, R. Jiang, J. Rong, L. Dong, T. Zhao, L. D. Sun, J. Wang, X. Chen, C. H. Yan, *ACS Nano* **2013**, *7*, 4561.
[24] a) J. H. W. Leuvering, P. J. H. M. Thal, M. v. d. Waart, A. H. W. M. Schuurs, *Fresenius J. Anal. Chem.* **1980**, *301*, 132; b) J. H. W. Leuvering, P. Thal, M. Vanderwaart, A. Schuurs, *J. Immunol. Methods* **1981**, *45*, 183; c) B. C. Goverde, J. H. W. Leuvering, P. Thal, J. C. M. Scherders, A. Schuurs, *Fresenius Z. Anal. Chem.* **1982**, *311*, 361.
[25] D. Liu, W. Qu, W. Chen, W. Zhang, Z. Wang, X. Jiang, *Anal. Chem.* **2010**, *82*, 9606.
[26] K. Zhu, Y. Zhang, S. He, W. Chen, J. Shen, Z. Wang, X. Jiang, *Anal. Chem.* **2012**, *84*, 4267.
[27] J. J. Storhoff, R. Elghanian, R. C. Mucic, C. A. Mirkin, R. L. Letsinger, *J. Am. Chem. Soc.* **1998**, *120*, 1959.
[28] J. Song, F. Wu, Y. Wan, L.-H. Ma, *Microchim. Acta* **2014**, *181*, 1267.

[29] R. A. Reynolds, C. A. Mirkin, R. L. Letsinger, *J. Am. Chem. Soc.* **2000**, *122*, 3795.
[30] E. Petryayeva, W. R. Algar, *Anal. Chem.* **2013**, *85*, 8817.
[31] K. E. Sapsford, J. Granek, J. R. Deschamps, K. Boeneman, J. B. Blanco-Canosa, P. E. Dawson, K. Susumu, M. H. Stewart, I. L. Medintz, *ACS Nano* **2011**, *5*, 2687.
[32] E. R. Goldman, A. R. Clapp, G. P. Anderson, H. T. Uyeda, J. M. Mauro, I. L. Medintz, H. Mattoussi, *Anal. Chem.* **2004**, *76*, 684.
[33] D. Liu, W. Chen, J. Wei, X. Li, Z. Wang, X. Jiang, *Anal. Chem.* **2012**, *84*, 4185.
[34] B. Peng, G. Li, D. Li, S. Dodson, Q. Zhang, J. Zhang, Y. H. Lee, H. V. Demir, X. Yi Ling, Q. Xiong, *ACS Nano* **2013**, *7*, 5993.
[35] J. Zheng, L. He, *Compr. Rev. Food Sci. Food Saf.* **2014**, *13*, 317.
[36] R. A. Alvarez-Puebla, L. M. Liz-Marzan, *Chem. Soc. Rev.* **2012**, *41*, 43.
[37] G. A. Zelada-Guillen, J. Riu, A. Duzgun, F. X. Rius, *Angew. Chem. Int. Ed. Engl.* **2009**, *48*, 7334.
[38] V. Zamolo, G. Valenti, E. Venturelli, O. Chaloin, M. Marcaccio, S. Boscolo, V. Castagnola, S. Sosa, F. Berti, G. Fontanive, M. Poli, A. Tubaro, A. Bianco, F. Paolucci, M. Prato, *ACS Nano* **2012**, *6*, 7989.
[39] a) E. Choe, D. Min, *Crit. Rev. Food Sci.* **2006**, *46*, 1; b) M. Eskin, F. Shahidi, *Biochemistry of Foods*, 3rd ed., Elsevier, London, UK, London, UK **2013**.
[40] a) T. Duncan, *J. Colloid Interf. Sci.* **2011**, *363*, 1; b) A. Mills, *Chem. Soc. Rev.* **2005**, *34*, 1003.
[41] N. Luechinger, S. Loher, E. Athanassiou, R. Grass, W. Stark, *Langmuir* **2007**, *23*, 3473.
[42] a) L. Gil, J. M. Barat, D. Baigts, R. Martínez-Máñez, J. Soto, E. Garcia-Breijo, M. C. Aristoy, F. Toldrá, E. Llobet, *Food Chem.* **2011**, *126*, 1261; b) L. Byrne, K. T. Lau, D. Diamond, *Ir. J. Agric. Food Res.* **2003**, *42*, 119.
[43] H. Kwon, F. Samain, E. T. Kool, *Chem. Sci.* **2012**, *3*, 2542.
[44] S. A. Goff, H. J. Klee, *Science* **2006**, *311*, 815.
[45] B. Kuswandi, Jayus, A. Restyana, A. Abdullah, L. Y. Heng, M. Ahmad, *Food Control* **2012**, *25*, 184.
[46] D. Mayr, R. Margesin, E. Klingsbichel, E. Hartungen, D. Jenewein, F. Schinner, T. D. Mark, *Appl. Environ. Microbiol.* **2003**, *69*, 4697.
[47] P. Liu, K. Tu, *Food Control* **2012**, *23*, 177.
[48] D. Dong, C. Zhao, W. Zheng, W. Wang, X. Zhao, L. Jiao, *Sci. Rep.* **2013**, *3*.
[49] S. Pandey, G. K. Goswami, K. K. Nanda, *Sci. Rep.* **2013**, *3*.
[50] S. Pandey, G. K. Goswami, K. K. Nanda, *Int. J. Biol. Macromol.* **2012**, *51*, 583.
[51] a) M. J. Hajipour, K. M. Fromm, A. A. Ashkarran, D. J. d. Aberasturi, I. R. d. Larramendi, T. Rojo, V. Serpooshan, W. J. Parak, M. Mahmoudi, *Trends Biotechnol.* **2012**, *30*, 499; b) S. Chernousova, M. Epple, *Angew. Chem. Int. Ed.* **2013**, *52*, 1636.
[52] a) Y. Y. Zhao, Z. L. Chen, Y. F. Chen, J. Xu, J. H. Li, X. Y. Jiang, *J. Am. Chem. Soc.* **2013**, *135*, 12940; b) Y. Zhao, Y. Tian, Y. Cui, W. Liu, W. Ma, X. Jiang, *J. Am. Chem. Soc.* **2010**, *132*, 12349; c) Y. Cui, Y. Y. Zhao, Y. Tian, W. Zhang, X. Y. Lu, X. Y. Jiang, *Biomaterials* **2012**, *33*, 2327.
[53] a) I. Perelshtein, G. Applerot, N. Perkas, E. Wehrschetz-Sigl, A. Hasmann, G. M. Guebitz, A. Gedanken, *ACS Appl. Mater. Interfaces* **2009**, *1*, 363; b) I. Perelshtein, G. Applerot, N. Perkas, J. Grinblat, A. Gedanken, *Chem.-Eur. J.* **2012**, *18*, 4575.
[54] O. V. Abramov, A. Gedanken, Y. Koltypin, N. Perkas, I. Perelshtein, E. Joyce, T. J. Mason, *Surf. Coatings Technol.* **2009**, *204*, 718.
[55] I. Ojea-Jimenez, X. Lopez, J. Arbiol, V. Puntes, *ACS Nano* **2012**, *6*, 2253.
[56] F. Tian, E. A. Decker, J. M. Goddard, *Food Function* **2013**, *4*, 669.
[57] L. Vermeiren, L. Heirlings, F. Devlieghere, J. Debevere, in *Novel Food Packaging Techniques*, Department of Food Safety and Food Quality, U. Ghent, **2003**, p. 22.
[58] M. A. Busolo, J. M. Lagaron, *Innov. Food Sci. Emerg. Technol.* **2012**, *16*, 211.
[59] H. Patel, R. Somani, H. Bajaj, R. Jasra, *Bull. Mater. Sci.* **2006**, *29*, 133.
[60] S. Ranjan, N. Dasgupta, A. Chakraborty, S. Melvin Samuel, C. Ramalingam, R. Shanker, A. Kumar, *J. Nanopart. Res.* **2014**, *16*, 1.
[61] D. Jimenez de Aberasturi, J. M. Montenegro, I. Ruiz de Larramendi, T. Rojo, T. A. Klar, R. Alvarez-Puebla, L. M. Liz-Marzán, W. J. Parak, *Chem. Mater.* **2012**, *24*, 738.

3
Composite Colloidal Nanosystems for Targeted Delivery and Sensing[1]

Pilar Rivera Gil, Moritz Nazarenus, and Wolfgang J. Parak

3.1
Introduction

Therapeutic bio(macro)molecules like antibodies, antigens, nucleic acids, or (poly)peptides have gained in the past years a great biotechnological development relevant to their clinical use. The production of these drugs is often still very tedious and costly so that normally, small amounts of materials are obtained. More importantly, most of these new pharmaceuticals, although other old formulations too, are very sensitive for degradation on administration, which often results in the drug not effectively achieving its target. Reduced plasma doses and difficulties in adjusting the dose to be administered as well as possible immunogenic effects are also derived by a premature degradation of the therapeutics. In order to save the material during technological processes as well as to preserve the bioavailability of the drug by protecting it from degradation and clearance and to assist the drug to reach its target, novel and smart formulations are required [1]. The two most common forms of pharmaceuticals are tablets and capsules (or encapsulated forms being the bioactive molecule surrounded by a shell), the latter being considered the most efficient method of taking a medication. Common "encapsulating" formulations like soft- and hard-shell capsules, solid lipid particles, liposomes, polymeric conjugates, and so on, are "mono- or bi-functional" meaning being able to offer only one or two functionalities: often protection and/or increased intracellular doses (as in the last case). However, for advanced formulations, "multifunctional" carriers that aim at protection, targeting, delivery, responsiveness, and site-specific manipulation are of paramount importance. Nanotechnology can contribute to the development of novel formulations by fabricating functional hybrid materials composed of nanoscaled building blocks. These multifunctional platforms [2, 3] combine a variety of properties allowing for the simultaneous or sequential performance of multiple functions in single cells, including enzymatic catalysis,

1) This work is based on the "Habilitationsschrift" of PRG at the Philipps Universität Marburg.

Bioinspired and Biomimetic Systems for Drug and Gene Delivery, First Edition. Edited by Zhongwei Gu.

Published 2015 by Wiley-VCH Verlag GmbH & Co. KGaA.

controlled release, directed cargo (e.g., drug) delivery, and sensing. Relevant requirements of a multifunctional system include (i) physiological *stability*, (ii) *protection* of cargo, (iii) *targeting* via nonspecific and specific strategies, (iv) stimuli sensitivity and *responsiveness* to the local environment (pH, temperature) or to an external applied trigger (e.g., light, ultrasound, magnetic field), (v) enhanced intracellular *delivery* of different types of cargo, and (vi) different *labeling* for characterization (imaging) or if required, for *multiplexing* of analytes.

Combining biological principles with physicochemical procedures, novel, smart, and multifunctional materials can be developed to fulfill the aforementioned requirements.

3.1.1 Working Toolkit

The tools or functionalities needed include the presence of a carrier vessel and responsive elements for remote control, labeling, and sensing.

Nanomaterials (colloids) in a submicron size range from a few to a few hundreds of nanometers (nm) and possess unique physicochemical and thus medical properties that differ from their macroscopic counterparts. Organic platforms including polymeric nanoparticles (NPs), dendrimers, liposomes, and other lipid assemblies, and engineered viral NPs mostly for drug/gene delivery [4] are currently the most common nanopharmaceutical forms used, where the nanomaterial plays the pivotal therapeutic role or adds additional functionality to the active compound [5]. Nevertheless, the development of inorganic nanosystems is opening the pharmaceutical nanotechnology novel horizons for diagnosis, imaging, and therapy, mainly because of their size in the nanometer range, their high surface area to volume ratios – which allow for specific functions that are not possible in the macroscopic scale – and, distinctly, their superior colloidal stability and well-defined physicochemical properties [6, 7].

Inorganic colloidal NPs are commonly composed of an inorganic core and a biocompatible surface coating that provides chemical stability under physiological conditions, dispersibility in aqueous solution, and reduced toxicity. The inorganic cores are crystalline clusters of a few hundred up to a few thousands of atoms, which can be prepared from many different materials to exhibit different properties proper from their colloidal state. For example, semiconductor materials containing cadmium possess special optical properties, NPs composed of cobalt or iron oxide show paramagnetic characteristics, and metal NPs made of gold exhibit unique photothermal performances. The most common synthesis route is at high temperatures in the presence of organic surfactants, which are crucial for the controlled growth, shape, and stability of the NPs. The polar head groups of the surfactant molecules are bound to the surface of each NP, while leaving the hydrophobic tails to the outer environment. The presence of this stable, organic, charged coating prevents the agglomeration of neighboring NPs, thus resulting in a solution of well-dispersed particles [8].

The resulting particles are hydrophobic and need to be transferred to water solutions. By wrapping an amphiphilic polymer around the particles, the NPs become hydrophilic and maintain their colloidal stability via electrostatic repulsions forces [9]. Furthermore, this surrounding organic shell of stabilizing molecules also acts as an anchor for further functionalization on attachment of biomolecules [10].

Different applications within the health care include the use of inorganic NPs (i) as active pharmaceutical ingredient, where the main role is played by the nanomaterial, that is, for the purpose of therapy, diagnostics, imaging and (ii) as vectors (a solid carrier that introduces the active ingredient into a recipient or host organism) or with an enabling function. In the latest application, the NPs add a new functionality to the preexisting product, for example, NPs for target delivery or as biomaterials [5].

The fabrication of organic hollow microcapsules via layer-by-layer (LbL) assembly [11] offers an interesting platform for the assembly of multifunctional carrier systems. Polyelectrolyte multilayer (PEM) capsules are fabricated through stepwise adsorption of PEs (polyelectrolytes) using electrostatics (mostly used), H-bonding or covalent chemistry as driving forces, followed by the chemical dissolution of the core template [12, 13]. The resulting hollow capsules usually have a wall thickness of between a few tens and several hundreds of nanometers and a diameter ranging from tens of nanometers to several micrometers (μm), depending on the size of the original core. The technique is highly versatile as different materials can be used to construct the shell or can be used as templates. The nature of the components used for the fabrication of these capsules determines their mechanical/physicochemical properties. For example, by using templates of different diameter (from 60 to 10 mm), the size of the resulting capsules can be tuned [14–16], whereas by using different types of component layers, such as synthetic PEs [17], charged and noncharged biopolymers [18–20], the chemical properties of the multilayer shell can be tailored.

The toolkit presented here comprises materials with different physicochemical properties, for example, surface chemistry (organic, inorganic, and hybrid), charge, size as well as with different functionalities.

3.1.2 Engineering a Multifunctional Carrier

There is no single material that fulfills all the requirements to be the "perfect" carrier mentioned before. Multifunctionality requires the coordinated assembly of building blocks with different functionalities into one single system to a resulting composite object. By using a carrier, the performances of all single materials are comprised within it and cargo molecules (therapeutics or bioactive molecules) can be additionally integrated for theragnostic approaches.

The use of PEM capsules as *theragnostic vehicles* presents several advantages: (i) PEM capsules can easily be administered and are easily internalized by different types of cells [21–23]; (ii) they are mechanically highly stable [24]; and (iii) they

possess two distinct compartments (shell and cavity) that can be functionalized with different building blocks. The cavity of the capsules represents the main volume and encapsulates the therapeutic or active molecules, offering at the same time protection to the cargo. Because of the big volume of the cavity, great quantities of cargo can be loaded within one single capsule. In this way, the number of administered capsules necessary to reach effective concentrations can be reduced; (iv) they are relatively easily engineered for a sustained release of their cargo at their target site, though only after the appliance of a specific physicochemical stimulus or after the power-on of an external trigger [25, 26].

As mentioned before, the distinct advantage of this carrier is the ability to be engineered with different *building blocks* to combine all the functionalities in one unique system (Figure 3.1).

NPs with different physicochemical properties can be easily incorporated *within the shell* of the capsules through the use of electrostatic interactions to impart optical, magnetic, and photothermal properties to microcapsules. By adding colloidal luminescent semiconductor NPs such as CdSe/ZnS quantum dots (QDs) [27, 28], the capsules can be easily detected by measuring their fluorescence signal with noninvasive optical techniques. The use of fluorescent NPs as fluorophores for labeling applications presents two main advantages compared with commercial organic fluorophores. Firstly, they are characterized by nearly continuous excitation spectra with narrow emission bands, located at different wavelengths depending on the NP size [29, 30]. This allows for simultaneous excitation of probes of different colors by light of a single wavelength [31]. Secondly, their reduced photobleaching makes them suitable for measurements over long periods of time [32, 33]. On the other hand, the Cd-based QDs, which are still most frequently used, can cause cytotoxic effects by releasing Cd ions

Color Fig.: **3.1**

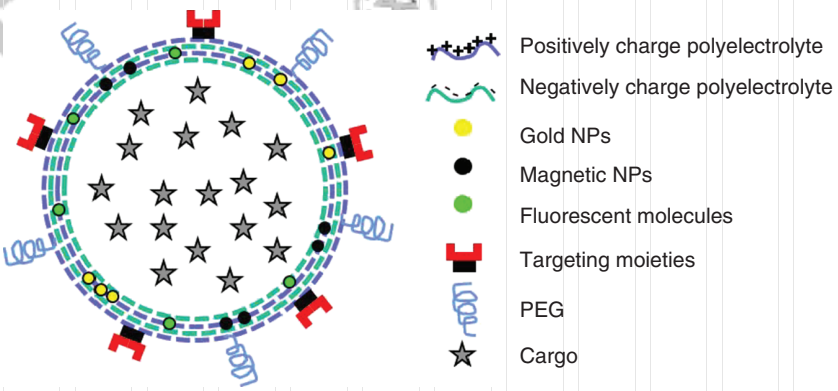

Figure 3.1 Schema of a multifunctional carrier vessel. The surface chemistry of the carrier is characterized by a stealth coating and cell-recognition molecules. The shell is decorated with different NPs to add functionalities like responsiveness, labeling, or targeting. The cavity contains the cargo to be delivered.

[34, 35]. However, with an appropriate coating that avoids ions leaking from the surface of the NP, toxic effects can be acutely neglected *in vitro*. By embedding superparamagnetic iron oxide based NPs (SPIONs) into the capsule walls, the movement of capsules toward a desired direction can be controlled by applying an external magnetic field gradient [36–38]. In addition, heating of the NPs on application of radiofrequency fields increases the permeability of the capsule walls [39]. Noble metal NPs such as gold (Au) and silver (Ag) are known to strongly absorb light. On irradiation, the major part of the absorbed light energy by each NP is transformed into heat. The collective effect of several NPs within the capsule shells serves to amplify the heating effect and the resulting increase in temperature in the surrounding areas [40–42]. In this way, by embedding metal NPs into the walls of the capsules, the integrity/permeability of the wall of individual capsules can be selectively perturbed [43–46]. Furthermore, Au NPs are electron dense and therefore very suitable for characterization techniques like electron microscopy.

Another possibility for the functionalization of PEM capsule is through conjugation of biological molecules (e.g., PEG, antibodies, streptavidin) to their *walls*. Biomolecules can be added to the outermost layer of the capsule walls by electrostatic adsorption or covalent binding, depending on their charge features. The addition of low-fouling polymers that possess protein-repellent qualities is required besides targeting features toward the design of novel vehicles for targeted delivery *in vivo*. For instance, microcapsules coated with a layer of PEG-grafted PEs have been shown to escape clearance by the mononuclear phagocyte system [47–49]. Such biofunctionalized capsules might fully mimic the features of bioactive molecules, thus improving the biocompatibility and physiological stability of the capsules as well as adding molecular recognition properties [50–52].

The *cavity* of the PEM capsules can also be loaded with different cargo molecules including the aforementioned functionalitites. More meaningful for pharmaceutical/medical applications is the encapsulation of biotherapeutics (e.g., nucleic acid, drugs, vaccines, or peptides). Especially, hydrophobic drugs [53] or extremely costly biomolecules can be efficiently entrapped within the container. Because of the big size of the cavity, higher amounts of material can be loaded and the dose of capsules to be administered to perform its action can be minimized. Because of the high versatility of the technique that allows to encapsulate different types of cargo molecules, the LbL approach appears nowadays to be useful in a wide range of applications including cancer, antisense or hormone-substitution therapies [20, 54–58], vaccination [22, 59], and diagnosis [60].

The shell modification with different types of NPs combined with an efficient loading of the cavity of these capsules allows for addressing important functions such as labeling, targeting, and the controlled opening of the capsules together with cargo delivery and protection. Those are essential features for using these vessels as theragnostic vehicles.

3.2 Objective

The objective of this work is to present a novel multifunctional carrier system with different abilities:

- Tracking following the presence of different labels, for example, fluorescent QDs, electron dense Au NPs, organic dyes.
- Manipulation of the carrier with NPs responsive to light (Au NPs) or to a magnetic field (SPIONs) for a controlled opening and/or targeting, respectively.
- Encapsulation and delivery of active compounds, for example, therapeutic biomacromolecules (nucleic acids, peptides, antigens, drugs, and sensors).
- Sensing, for example, optical readout of local analytes to get a feedback of the environment of the carrier.

To achieve this objective, materials are developed according to different approaches, and chemical modifications are performed to make these materials suitable for living organisms. This work is focused on materials for pharmacy and medicine. Therefore a good *in vitro* characterization of the interactions of these materials with living cells needs to be performed.

3.3 Cellular Behavior of the Carrier

3.3.1 Intracellular Fate

Cells can incorporate objects ranging from the molecular up to the micrometer scale by numerous processes. Extensive studies with NPs show that NPs with different physicochemical properties have different mechanisms of internalization and different intracellular distribution patterns. For example, *surface chemistry* plays a key role as the surface of the NPs can be modified with specific molecules either to increase or to reduce uptake. Ligands like transferrin increase the rate of internalization via receptor mediated endocytosis; however, if the particles are conjugated with PEG molecules, the uptake is decreased [61]. This is especially important for *in vivo* application. By reducing uptake from the mononuclear phagocyte system, particles can, for example, after an i.v. injection, circulate in the blood for longer periods of time and can reach the target organ at the desired concentration. Charge also plays an important role in the internalization pattern of particles. A positive overall charge ensures faster internalization rates than a negative charge because of electrostatic interaction with the negatively charged glycocalyx of the cells. However, the observed increase in the internalization rate of positively charged NPs is strongly dependent on membrane accumulation and thus directly related to a specific NP concentration [62, 63]. I thus hypothesized an NP-concentration threshold responsible for the fast internalization rates of

positively charged NPs. *Size* appears to be a limiting factor. Both positive and negative charged NPs are internalized via clathrin- or caveloae-mediated endocytosis depending on their surface chemistry and charge [64, 65]. However, NPs with a size between 500 and 1000 nm are rather caveolae internalized compared to smaller particles (<200 nm) that are endocytosed via clathrin-coated vesicles [66]. Other mechanisms like macropinocytosis and phagocytosis have been described for the engulfment of solutes and bigger particles (>1 μm), respectively, whereas signal-mediated transport via pores occurs when the size is less than 0.1 μm [67].

PEM capsules of different sizes (from nanometers to micrometers) are taken up by living cells. Despite their "big" size (normally around 2 μm) PEM capsules are easily incorporated not only by phagocytic cells (macrophages) but also by a great variety of different cells (e.g., embryonic fibroblasts, neuro- and glioblastoma cells, and epithelial cancer cells) including primary cells (e.g., cortical neurons, monocyte-derived dendritic cells). The incorporation of the capsules occurs spontaneously and is noncell specific. Therefore, special attention should be kept on improving the molecular recognition properties of the capsules. In general, the internalization of capsules by cells appears to be a highly energy-consuming, actin-mediated process that depends on microcapsule intrinsic factors like size and composition rather than on cell type.

Although the exact mechanism of cellular uptake is still largely unknown, some important parameters that regulate this process have recently been elucidated. For instance, the overall charge of capsules has been demonstrated to play a role for capsule uptake. As for smaller colloidal NPs, charged capsules are ingested faster than uncharged ones, and positively charged capsules are found to be engulfed more than negatively charged ones [68]. At any rate, adsorption of cell medium proteins to the capsule surface tends to smear out differences in surface chemistry for long incubation times. Atomic force microscopy measurements of adhesive forces between capsules and cell membranes show that the uptake of PEM capsules strongly correlates with the adhesion of capsules to the outer cell membrane [68]. These results have also been confirmed by Confocal Laser Scanning Microscopy (CLSM) and by Transmission Electron Microscopy (TEM) (unpublished data). Using CLSM membrane ruffling and redistribution of the actin cytoskeleton to form large cytoplasmatic protrusions to engulf the PEM capsules was observed (Figure 3.2a). Incubation of the cells with Cytochalasin D clearly disturbed the internalization of the capsules. Although attachment to the plasma membrane and an attempt of internalization was visible with the CLSM and with the TEM (Figure 3.2c,d), the actin cytoskeleton was not able to reorganize properly and invagination of the vesicles into the cytosolic side of the cells was not completed. Mostly all uptake processes, except caveolae-mediated, macropinocytosis, and phagocytosis appear to be enhanced by, although are not strictly dependent on, a functional actin cytoskeleton. Labeling of cellular structures with different markers clearly revealed an initial colocalization of the capsules with lipid rafts, which are membrane microdomains enriched in cholesterol, specific proteins, and glycosphingolipids, the last being stained

Color Fig.: **3.2**

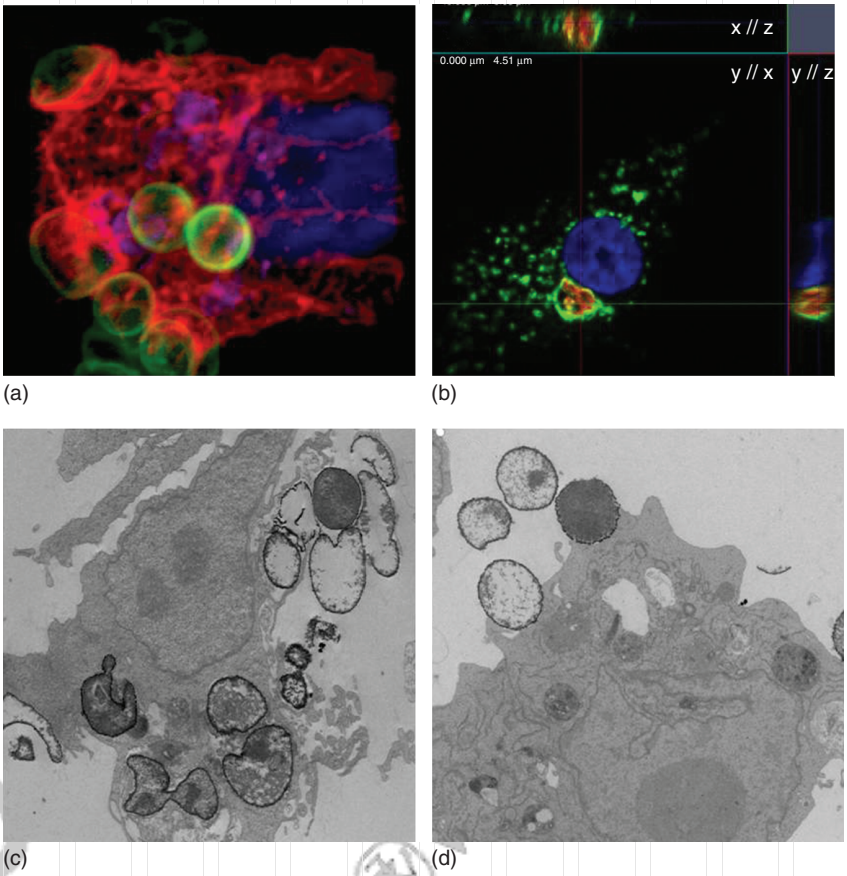

Figure 3.2 Characterization of the internalization of PEM capsules via CLSM (upper images) and TEM (lower images). For this purposes, capsules were synthesized hollow to carry fluorescent molecules (FITC (a) and red QDs (b)) together with Au NPs within their shells to allow their visualization with CLSM and TEM, respectively. (a) Actin reorganization (red) of the cytoskeleton to engulf a PEM capsule (green) in a sort of phagocytic cup and (b) final localization of capsules (red) in (phago)lysosomal structures (green). (c–d) TEM pictographs of cells incubated with capsules for 4 h in the absence (c) or presence (d) of cytochalasin d.

by Cholera toxin B1 [69] and a final colocalization with structures containing LAMP1, that is, (phago)lysosomes (Figure 3.2b).

On the one hand, the uptake of the capsules after 4 h was completely abolished by methyl-β-cyclodextrin that removes cholesterol from cultured cells thus inhibiting uptake-associated processes like macropinocytosis and lipid rafts. However, as cholesterol is a common component of the plasma membrane and the engulfment of capsules involves large parts of the plasma membrane, phagocytosis cannot really be excluded. Caveolin-dependent and -independent

lipid rafts can be excluded as internalization route because the markers used did not stain caveosomes. Furthermore, caveosomes have a different pH (neutral) and a different content compared to endosomes (acid) and do not end up fusing the lysosomes [70, 71]. Whereas the vesicles involved in the internalization of the capsules are clearly acidic [72] and possess lysosomal markers (unpublished results). In addition, caveosomes are transported within the cell along microtubules, and inhibition of microtubule formation with Nocodazole had no effect on the internalization of capsules. On the other hand, cellular incubation with Bafilomycin A disturbed the uptake of the capsules in a concentration-dependent manner. Bafilomycin is a specific inhibitor of the vacuolar type H^+-ATPase that prevents reacidification of the lysosome [60] and is required for the maturation of the phagosomes. Although the exact mechanism of internalization of the capsules cannot be elucidated yet, these unpublished results demonstrate a primary localization in plasma membrane invaginations (enriched in cholesterol and glycosphingolipids) and a final localization in (phago)lysosomes located in the perinuclear region. This would point out to phagocytosis as a predominant route of internalization. Nevertheless, different mechanisms could be sequentially involved. For example, first of all, adsorptive mechanisms, because of the electrostatic interactions, are responsible for the primary cell-capsule contact. Once the capsules are attached to the cellular membrane, there is a local accumulation of glycosphingolipids and cholesterol, which might form a sort of microdomains as the lipid rafts do. Strong actin reorganization occurs then to form long protrusions (not lipid rafts) to engulf the "big" capsules similar to by phagocytic processes. Finally, the capsules are transported to the perinuclear region of the cell and remain in acidic (phago)lysosomes.

3.3.2 Biocompatibility

Regarding the cytotoxicity of the capsules, although not yet well studied, the main sources for toxicity come obviously from the PEs composing the wall as well as from the functionalities embedded in the cavity and/or in the wall. Initial studies have suggested that capsules alone do not exhibit acute cytotoxic damage on cell cultures, but rather the NPs with which the capsules are functionalized are potentially cytotoxic, as, for example, when Cd-based semiconductor NPs embedded in the capsule walls corrode and release toxic cadmium ions [73]. On the other hand, both magnetic and Au NPs are relatively harmless to the cells [74, 75].

The magnitude of the cytotoxic effect of the capsules is primarily concentration- and time-dependent [23, 73]. In addition, the intrinsic chemical properties of the positively charged PE (polycation) turned out to make polycations effective triggers of mitochondrial-mediated cell death (apoptosis/necrosis) [76, 77]. Because of their positive charge, polycations cause cellular membrane damage with subsequent activation of signaling pathways that end up with mitochondrial depolarization and generation of reactive oxygen species resulting in cell death. In this

regard, together with the molecular weights, the cationic charge density of the polycations are key parameters for the interaction with cell membrane and cell damage [78, 79]. Furthermore, polycations containing polyamine functionalities may result in an increased interaction with anionic intracellular components that also lead to oxygen-independent cell death [80]. In this regard, a reduction of the cytotoxicity could be obtained by using alternative materials (to polyamines) that mimic natural cell components [81]. Interestingly, when the polycation is complexed with the polyanion as in the case of supramolecular structures like the PEM capsules, a strong reduction or even disappearance of toxicity was observed (Figure 3.3).

Cytotoxicity assays *in vitro* have been employed to confirm the innocuousness of PE-based systems [82]. In general, the internalization of several capsules *in vitro* neither interferes with the regular cell cycle nor with the viability of the cells. Life imaging of cultured cells in the presence of PEM capsules showed how cells move toward the capsules, engulf them, and continue their movement. Furthermore, cells pass their internalized capsules to daughter cells on cellular division and continue their proliferation to mature cells [26]. Nevertheless, more advanced studies involving animal tissue demonstrate that plain unfunctionalized PEM capsules can transiently cause local inflammations after subcutaneous injection [23]. Despite the impact this would have on medical applications, the cytotoxicity effects of capsules *in vivo* have not yet been fully investigated.

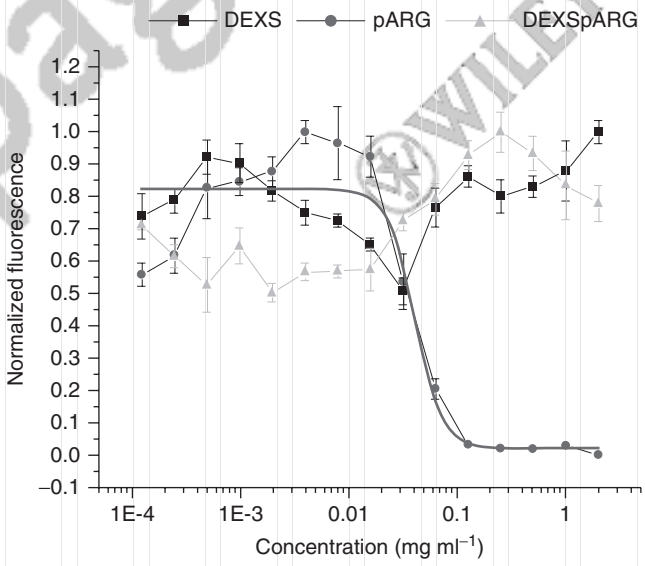

Figure 3.3 Citotoxicity derived by the PEs. In this case the toxicity of the two PEs (DEXS, dextran sulfate and pARG, poly arginine) commonly used for the synthesis of biodegradable PEM capsules was compared. Each PE either alone or conjugated (as in the capsules) was tested for viability. High fluorescent values correspond to viable cells whereas low values are characteristics of death cells.

3.4 Applications

As mentioned before, the use of PEM capsules as carriers have found different applications in clinics including therapy and diagnosis. However, the main goal is to present PEM capsules as a multifunctional carrier system, which is able to perform both actions. Therefore, the main applications studied were PEM capsules for targeted delivery of biotherapeutics and for sensing of analytes, the last being additionally used to get a feedback from the environment of the carrier. To proof the effectiveness and the versatility of these carriers, the geometry of the carrier was varied depending on the problem addressed, that is, different cargos (e.g., siRNA, drugs, proteins, and sensors) as well as different wall constituent were used to synthesize and functionalize the capsules for different purposes.

3.4.1 Delivery with Multifunctional PEM Capsules

Delivery systems have to fulfill some basic physicochemical requirements. They have to be biocompatible and able to navigate within living organisms using remote guidance. They have to be able to entrap efficiently different molecules with different sizes, which can be hydrophobic or hydrophilic, and have to protect the entrapped molecule from undesired degradation thus providing improved cargo stability, sustained and controlled release rates, and increased bioavailability. For targeted release, the cargo must not leak out from the carrier system before it reaches its target. Once there, the cargo should not leave the carrier uncontrollably but rather on controlled release, that is, by the manipulation of the carrier. To the best of my knowledge a system that combines all these functionalities into one single structure has not been developed yet despite great efforts, probably because colloidal engineering is being extremely challenged to fulfill all these conditions.

3.4.1.1 Magnetic Targeting and Magnetofection

Targeting is a must-have. Targeted delivery technologies are especially crucial for most drugs either because their designated site of action is difficult to reach or because cytotoxic side effects have to be minimized. There is currently no applied pharmaceutical treatment available that can be applied locally in a controlled way, thereby shielding healthy cells from drug interaction.

Magnetic drug targeting has been suggested as a method to locally accumulate drugs. It has recently been shown *in vivo* that it is possible to direct drugs bound to magnetic NPs to tumor tissue using magnetic field gradients [83, 84]. The same concept can be applied for PEM capsules whose walls are functionalized with magnetic NPs [38]. Naturally, the classical concept of targeted drug delivery via receptor–ligand interaction can also be applied to the capsules. For this purpose, molecules with molecular recognition properties, for example, antibodies, growth factors, and so on, can be immobilized on the capsule surface, resulting in

an increase in the uptake rate of capsules by target cells compared with surrounding cells [85].

Delivery systems carrying nucleic acids that shells are functionalized with magnetic NPs, that is, SPIONs, allows for magnetic force-assisted transfection (magnetofection) as well as magnetic targeting in both static and fluidic conditions mimicking the blood stream [86, 87].

Antisense therapies are very promising tools against diseases like cancer; however, the administration of genetic materials is subject to important restrictions like rapid clearance or fast degradation by nucleases [88]. Many carrier systems, that is, viral and nonviral have been developed [89–93]. The transfection efficiency using viral vectors is significantly higher than using nonviral vectors but their application in human raises many safety concerns [94]. Many efforts are being directed in creating nonviral carriers with comparable transfection efficiency but less immunological responses [95]. In this sense, PEM capsules appear as ideal carriers to improve the efficiency of nonviral vectors. The capsules are biocompatible and are easily incorporated by the cells. Furthermore, the wall can be functionalized with targeting moieties, for example, with SPIONs to approach high local accumulation of the carriers by applying a magnetic field, thus increasing the number of capsules in the cell area. PEM capsules can deliver great quantities of material because of the big size of their cavities, which at the same time offer protection to the cargo. All this should allow for an increased transfection efficiency compared to polymeric/lipid complexes.

Although the use of PEM capsules as nonviral vectors for genetic material has not been well studied yet, I would like to point out that my research outlook next focuses on this direction as it appears very promising to me.

Some previous works support this assumption. Zebli *et al.* already described the functionalization of PEM capsules with SPIONs to target the capsules to desired cell culture areas. By applying a magnetic field, capsules moved toward a permanent magnet that was located in a specific cell area. The magnetic force gradient surely caused local accumulation of the magnetic capsules at the outer membrane of the target cells increasing in this way the internalization of the capsules by those cells [96]. Planck *et al.* [97] have intensively researched lipospheres tagged with siRNA to try to improve the transfection efficiency of nonviral vectors by adding a second driving force that is magnetic targeting as described before. These magnetic acoustically active lipospheres appeared to be quite safe and achieved a down regulation of reporter gene expression even at very low concentration of siRNA [98].

Both systems used a flow channel system for modeling the bloodstream in the circulatory system thus proving the feasibility of magnetic assisted transfection *in vivo*.

Although focussing magnetic field gradients do not work on a single cell level, at least two parallel ways of targeting can be achieved by PEM capsules: (i) local accumulation of capsules near the target tissue by attraction of magnetic NPs in the capsule walls with magnetic field gradients and (ii) enhanced uptake by target cells because of cell-specific molecules attached to the surface of the capsule

walls. In this way, the combination of two strategies within one carrier system is expected to lead to improved targeting and thus less unwanted delivery of drugs to the surrounding tissue.

3.4.1.2 Strategies for Controlled Opening

Targeted cargo delivery can be combined with remotely controlled cargo release. Remote activation is based on the manipulation of the carrier if necessary, with help from an external physical stimulus (i.e., trigger) that acts on the carrier to enable the release of the cargo from the cavity to the cellular environment. There are several strategies to achieve this performance. Some carriers are designed to disintegrate on changes in the conditions of the environment, for example, pH, temperature, solvent. A quick release is observed when the carrier breaks on contact with a surface or specifically when it encounters a protein/enzyme. In this sense, PEM capsules composed of biodegradable PEs such as polypeptides and polysaccharides have a great potential for the delivery of therapeutics [19]. These systems retain their structural integrity before cellular uptake but get rapidly degraded on enzymatic cleavage after internalization. To prove the ability of these systems to trigger release and activation of cargo, polyarginine/dextran sulfate biodegradable capsules filled with a model for a prodrug – a self-quenched (nonactive) fluorescence-labeled protein – were synthesized (Figure 3.4). In this way, the cavity of the capsules was additionally used for a spatially confined reaction, that is, activation of the prodrug after its enzymatic hydrolysis. Furthermore, the release of the active drug occurred exclusively intracellularly [26].

Nevertheless any of the strategies mentioned before can be controlled. Manipulation of the carrier to temporarily and spatially control its opening is of paramount importance and inorganic NP-modified PEM capsules are ideally carriers to fulfill this work. Depending on the nature of the NPs present in the wall of the capsules, different stimulus such as light [43], oscillating magnetic fields, ultrasound [99], or radio frequency [100] can be applied to achieve a controlled rupturing/permeation of the walls of the capsules so that the cargo is released from the cavity to the cellular environment whenever and wherever is required. For example, light-responsive capsules can be synthesized by functionalizing the shell of the capsules with metal NPs, for example, Au [101, 102]. Agglomerates of Au NPs have been used to efficiently open the wall of the capsules through plasmon-assisted photothermal processes [103]. Au NPs are able to strongly absorb light if the corresponding frequency matches with their surface plasmon resonance frequency [104]. Au-NPs-based formulations make use of different forms of laser excitation (near infrared, NIR, or visible light) to cause a light-to-heat energy conversion [105, 106]. In case the Au NPs are agglomerated (as in the case of the capsule shell), their plasmon peak is moved to higher wavelengths and can be efficiently illuminated with near-infrared light thus making use of the optical transparent window of biological tissues. Nevertheless, when using this trigger, the limitation of light to penetrate deep in the tissue is to be kept in mind. Optical excitation and light absorption of Au NPs produce a heat dissipation and subsequent local increase in the temperature [107] as well as the local

Color Fig.: **3.4**

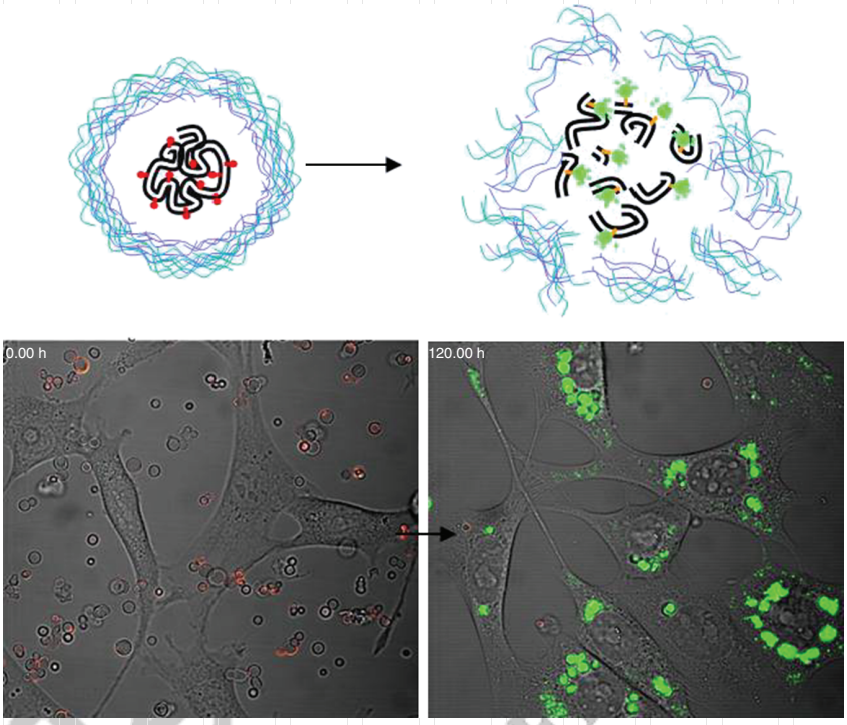

Figure 3.4 Release and cargo activation mediated by biodegradable PEM capsules. Capsules were synthesized with biodegradable polymers. On cellular internalization, the capsule wall was degraded and the cargo (a fluorogenic substrates for enzymes) was available for activation. In this case the selected cargo acted as a model for a prodrug that needs to be cleavage ("activated") into its functional form. When the cargo was structurally intact, the fluorescence was quenched. However, when the capsule wall was degraded and enzymes could reach the cargo, the fluorescence was dequenched and a visible green signal was detected. (Image taken from Ref. [26].)

destruction of the capsules shell mediated by disintegration/fragmentation of the Au NP clusters [108]. Those are competing mechanisms that rule the capsule opening and the cargo release on switching on/off the external trigger (i.e., light). Furthermore, sequential light illumination of individual capsules allows for subsequent release of cargo to the cytosol of the cells interfering neither with the integrity of the cargo [46] nor with the viability of the cells [109].

Other external triggers used to open NP-modified PEM capsules through mechanical disintegration of their walls include sonication, ultrasound, and radio frequency [101, 110]. However they can penetrate the tissue well, they are complicated to focus.

Several key advances for controlled release using PEM capsules were then demonstrated: manipulation of the carrier for a controlled opening, delivery of cargo to the cytosol of the cell, and maintenance of the functionality of the cargo.

3.4.2 Intracellular Ion Sensing

Besides the potential use of PEM capsules as carriers for targeted and controlled release of cargo, capsules can also be designed for diagnostic applications. In this sense, the capsules carry sensor molecules that allow the transduction of chemical concentration information into optical signals. Fluorescent indicators are a class of fluorophores whose spectral properties are sensitive to a substance (the analyte) of interest. Numerous indicators are commercially available for a variety of analytes, including Ca^{2+}, Mg^{2+}, Cl^{-}, H^{+}, Na^{+}, and O_2 [111]. This represents an interesting research line as the control of intracellular ion homeostasis is essential for all cellular organisms. At physiological condition ions like K^{+} or H^{+} are found at high concentrations inside the cells whereas ions like Na^{+}, Ca^{2+}, or Cl^{-} are rather found extracellularly [112]. Many pathological situations like liver insufficiency, diabetic ketoacidosis, hypercatabolism, fibrosing disorders, sickle cell anemia, infection [112], cystic fibrosis [113–115], or intoxication with metals [116] are associated with a defective regulation of the ion concentrations.

So far, most of the techniques employed to measure ion concentrations make use of electrodes [117] or fiber-based optodes [118, 119]. These systems work well for solutions but in general not for cellular organism, as they are too big to enter the cells over extended periods of time. There are other techniques like microanalysis that can measure intracellular analyte concentrations. However, they are destructive for the biological sample [120]. For subcellular (intracellular) analyte detection, smaller noninvasive sensors are required, especially if long-term measurements in live cells are envisaged. One possibility toward this direction is the use of particles as carrier matrix/container for analyte-sensitive molecules. Examples of such nano/micrometer-sized containers include solid particle matrices [121, 122], liposomes [123], hollow fiber membranes [124], vesicles [125], inorganic NPs [126, 127], and PEM capsules [72, 128].

Carriers must be designed in a way that ions or molecules are able to freely diffuse to the location of the sensor. The biggest advantage of using micrometer-sized carriers is the great capacity for loading, which can be enhanced by filling the whole volume with analyte-sensitive molecules. Compared to other micrometer-sized carriers, PEM capsules offer the distinct and novel advantage of multiplexing. This is based on the fact that capsules can be functionalized with fluorescent molecules at two distinct positions, in their walls and in their cavities. Following this concept, fluorophores sensitive to different analytes (e.g., H^{+}, Na^{+}, K^{+}, and Cl^{-}) are loaded into the cavities of different capsules [129] and the walls of each capsules are fluorescently labeled with barcodes [130]. The color of the capsule wall would allow for the identification of each capsule, thus providing the information for which analyte this particular capsule is sensitive to.

The lysomotropy showed by the capsules can be used to measure changes in the concentration of lysosomal ions, for example, H^{+} *in situ* over long periods of time [60]. Because of the continuous readout provided by the capsules, dynamic measurements of changes in the lysosomal pH can be performed (Figure 3.5). In

Color Fig.: **3.5**

Figure 3.5 PEM capsules for sensing applications. pH sensitive capsules were synthesized to locally measure the concentration of H^+ on disruption of ion homeostasis. (a) Schema of the process. Capsules in the slightly alkaline extracellular medium are more fluorescent in red, whereas capsules inside the acidic lysosome are more fluorescent in yellow. In this way, changes in the ratio red-to-yellow can be correlated to changes in the pH. If an agent that increases the pH in the lysosome is added, changes in the capsule fluorescence from yellow to red can be detected. (b) Micrographs of cells incubated with pH-sensitive capsules before and after disruption of the lysosomal pH (in this case with chloroquine). (c) The kinetic of lysosomal alkalinization produced by chloroquine (green line) was followed over time and was compared to changes in the pH of capsules located extracellularly (red line). (Figure taken from Ref. [60].)

this way, differences in the mechanism of action of agents disturbing the lysosomal acidification could be elucidated [60].

In conclusion, the presented sensor based microcapsules offer a great possibility to engineer multidetection systems in which several ions in parallel could be sensed. The presented sensing abilities can be combined with targeted delivery to create multifunctional systems that strongly interact with their (cellular) environment thus giving us crucial information.

3.5 Conclusions

Multifunctional PEM capsules fabricated by the LbL assembly technique possess remarkable properties. In particular, this very general assembly mechanism allows for the integration of virtually all different types of nanoscale objects into and on top of their walls. These building blocks introduces functionality (such as fluorophores, magnetic particles, and local heat sources) and specificity (such as molecular recognition ligands). The cavity of the capsules can be filled with cargo, which is to be released at designated targets or with active molecules, as, for example, for multiplexed sensing. Compared with other carrier systems, capsules can be functionalized at two distinct compartments, walls and cavities, introducing in this way flexibility for the interference-free assembly of multiple functionalities.

Nowadays several *in vitro* [20, 24, 131–133] and *in vivo* studies [20, 134] have established the use of these capsules as carriers in living systems. Notably, capsules with different physicochemical properties have been produced for different applications ranging from simultaneous imaging and delivery of biologically active molecules [27, 135, 136] to intracellular sensing and bioreactors [72, 137–140].

In the context of this work, I presented clear proofs of how to design multifunctional carriers. I could demonstrate that tuning the physicochemical properties of the materials used to build up the carrier, functionalities like biocompatibility, targeted delivery, controlled release of cargo, and sensing can be efficiently performed.

Abbreviations

μm	Micrometer
CLSM	Confocal laser scanning microscopy
LAMP1	Lysosomal-associated membrane protein 1
LbL	Layer-by-layer
nm	Nanometer
NPs	Nanoparticles
PEM	Polyelectrolyte multilayer
PEs	Polyelectrolytes

QDs	Quantum dots
siRNA	Small (or short) interfering ribonucleic acid
SPIONs	Superparamagnetic iron oxide nanoparticles
TEM	Transmission electron microscopy

References

1. LaVan, D.A., McGuire, T., and Langer, R. (2003) Small-scale systems for in vivo drug delivery. *Nat. Biotechnol.*, **21**, 1184–1191.
2. Peteiro-Cartelle, J. *et al.* (2009) One example on how colloidal nano- and microparticles could contribute to medicine. *Nanomedicine*, **4**, 967–979.
3. Tasciotti, E. *et al.* (2008) Mesoporous silicon particles as a multistage delivery system for imaging and therapeutic applications. *Nat. Nanotechnol.*, **3**, 151–157.
4. Cho, K., Wang, X., Nie, S., Chen, Z.G., and Shin, D.M. (2008) Therapeutic nanoparticles for drug delivery in cancer. *Clin. Cancer Res.*, **14**, 1310–1316.
5. Rivera Gil, P., Hühn, D., del Mercato, L.L., Sasse, D., and Parak, W.J. (2010) Nanopharmacy: inorganic nanoscale devices as vectors and active compounds. *Pharmacol. Res.*, **62**, 115–125.
6. Nie, S.M., Xing, Y., Kim, G.J., and Simons, J.W. (2007) Nanotechnology applications in cancer. *Annu. Rev. Biomed. Eng.*, **9**, 257–288.
7. Zhang, F. *et al.* (2010) Ion and pH sensing with colloidal nanoparticles: influence of surface charge on sensing and colloidal properties. *ChemPhysChem*, **11**, 730–735.
8. Hyeon, T. (2003) Chemical synthesis of magnetic nanoparticles. *Chem. Commun.*, **8**, 927–934.
9. Pellegrino, T. *et al.* (2004) Hydrophobic nanocrystals coated with an amphiphilic polymer shell: a general route to water soluble nanocrystals. *Nano Lett.*, **4**, 703–707.
10. Lin, C.-A.J. *et al.* (2008) Design of an amphiphilic polymer for nanoparticle coating and functionalization. *Small*, **4**, 334–341.
11. Decher, G. (1997) Fuzzy nanoassemblies: toward layered polymeric multicomposites. *Science*, **277**, 1232–1237.
12. Donath, E., Sukhorukov, G.B., Caruso, F., Davis, S.A., and Möhwald, H. (1998) Novel hollow polymer shells by colloid-templated assembly of polyelectrolytes. *Angew. Chem. Int. Ed.*, **37**, 2202–2205.
13. Sukhorukov, G.B. *et al.* (1998) Layer-by-layer self assembly of polyelectrolytes on colloidal particles. *Colloids Surf. A*, **137**, 253–266.
14. Peyratout, C.S. and Dähne, L. (2004) Tailor-made polyelectrolyte microcapsules: from multilayers to smart containers. *Angew. Chem. Int. Ed.*, **43**, 3762–3783.
15. Sukhorukov, G.B. *et al.* (2004) Porous calcium carbonate microparticles as templates for encapsulation of bioactive compounds. *J. Mater. Chem.*, **14**, 2073–2081.
16. Yu, A.M., Wang, Y.J., Barlow, E., and Caruso, F. (2005) Mesoporous silica particles as templates for preparing enzyme-loaded biocompatible microcapsules. *Adv. Mater.*, **17**, 1737.
17. Tong, W.J. and Gao, C.Y. (2005) Stable microcapsules assembled stepwise from weak polyelectrolytes followed by thermal crosslinking. *Polym. Adv. Technol.*, **16**, 827–833.
18. Berth, G., Voigt, A., Dautzenberg, H., Donath, E., and Mohwald, H. (2002) Polyelectrolyte complexes and layer-by-layer capsules from chitosan/chitosan sulfate. *Biomacromolecules*, **3**, 579–590.
19. De Geest, B.G. *et al.* (2006) Intracellularly degradable polyelectrolyte microcapsules. *Adv. Mater.*, **18**, 1005–1009.
20. Zhao, Q. *et al.* (2007) Hollow chitosan-alginate multilayer microcapsules as drug delivery vehicle: doxorubicin loading and in vitro and in vivo studies. *Nanomedicine*, **3**, 63–74.

21. Lomas, H. *et al.* (2011) Polymersome-loaded capsules for controlled release of DNA. *Small*, **7**, 2109–2119.
22. Sexton, A. *et al.* (2009) A protective vaccine delivery system for in vivo T cell stimulation using nanoengineered polymer hydrogel capsules. *ACS Nano*, **3**, 3391.
23. De Koker, S. *et al.* (2007) In vivo cellular uptake, degradation, and biocompatibility of polyelectrolyte microcapsules. *Adv. Funct. Mater.*, **17**, 3754–3763.
24. Muñoz Javier, A. *et al.* (2008) Uptake of colloidal polyelectrolyte coated particles and polyelectrolyte multilayer capsules by living cells. *Adv. Mater.*, **20**, 4281–4287.
25. Bedard, M.F., Braun, D., Sukhorukov, G.B., and Skirtach, A.G. (2008) Toward self-assembly of nanoparticles on polymeric microshells: near-IR release and permeability. *ACS Nano*, **2**, 1807–1816.
26. Rivera Gil, P., Koker, S.D., De Geest, B.G., and Parak, W.J. (2009) Intracellular processing of proteins mediated by biodegradable polyelectrolyte capsules. *Nano Lett.*, **9**, 4398–4402.
27. Rogach, A. *et al.* (2000) Nano- and microengineering: 3-D colloidal photonic crystals prepared from sub-μ-sized polystyrene latex spheres pre-coated with luminescent polyelectrolyte/nanocrystal shells. *Adv. Mater.*, **12**, 333–337.
28. Wang, D., Rogach, A.L., and Caruso, F. (2002) Semiconductor quantum dot-labeled microsphere bioconjugates prepared by stepwise self-assembly. *Nanoletters*, **2**, 857–861.
29. Bruchez, M.J., Moronne, M., Gin, P., Weiss, S., and Alivisatos, A.P. (1998) Semiconductor nanocrystals as fluorescent biological labels. *Science*, **281**, 2013–2016.
30. Chan, W.C. and Nie, S. (1998) Quantum dot bioconjugates for ultrasensitive nonisotopic detection. *Science*, **281**, 2016–2018.
31. Han, M., Gao, X., Su, J.Z., and Nie, S. (2001) Quantum-dot-tagged microbeads for multiplexed optical coding of biomolecules. *Nat. Biotechnol.*, **19**, 631–635.
32. Gerion, D. *et al.* (2001) Synthesis and properties of biocompatible water-soluble silica-coated cdse/zns semiconductor quantum dots. *J. Phys. Chem. B*, **105**, 8861–8871.
33. Dahan, M. *et al.* (2003) Diffusion dynamics of glycine receptors revealed by single –quantum dot tracking. *Science*, **302**, 442–445.
34. Derfus, A.M., Chan, W.C.W., and Bhatia, S.N. (2004) Probing the cytotoxicity of semiconductor quantum dots. *NanoLetters*, **4**, 11–18.
35. Kirchner, C. *et al.* (2005) Cytotoxicity of colloidal CdSe and CdSe/ZnS nanoparticles. *Nano Lett.*, **5**, 331–338.
36. Caruso, F., Spasova, M., Susha, A., Giersig, M., and Caruso, R.A. (2001) Magnetic nanocomposite particles and hollow spheres constructed by a sequential layering approach. *Chem. Mater.*, **13**, 109–116.
37. Gaponik, N., Radtchenko, I.L., Sukhorukov, G.B., and Rogach, A.L. (2004) Luminescent polymer microcapsules addressable by a magnetic field. *Langmuir*, **20**, 1449–1452.
38. Abbasi, A.Z. *et al.* (2011) Magnetic capsules for NMR imaging: effect of magnetic nanoparticles spatial distribution and aggregation. *J. Phys. Chem. C*, **115**, 6257–6264.
39. Katagiri, K., Nakamura, M., and Koumoto, K. (2010) Magnetoresponsive smart capsules formed with polyelectrolytes, lipid bilayers and magnetic nanoparticles. *ACS Appl. Mater. Interfaces*, **2**, 768–773.
40. Govorov, A.O. and Richardson, H.H. (2007) Generating heat with metal nanoparticles. *Nano Today*, **2**, 30–38.
41. Hrelescu, C. *et al.* (2010) DNA melting in gold nanostove clusters. *J. Phys. Chem. C*, **114**, 7401–7411.
42. Hühn, D., Govorov, A., Gil, P.R., and Parak, W.J. (2012) Photostimulated Au nanoheaters in polymer and biological media: characterization of mechanical destruction and boiling. *Adv. Funct. Mater.*, **22**, 294–303.
43. Radt, B., Smith, T.A., and Caruso, F. (2004) Optically addressable nanostructured capsules. *Adv. Mater.*, **16**, 2184–2189.

44. Skirtach, A.G. *et al.* (2005) The role of metal nanoparticles in remote release of encapsulated materials. *Nanoletters*, **5**, 1371–1377.
45. Skorb, E.V., Skirtach, A.G., Sviridov, D.V., Shchukin, D.G., and Mohwald, H. (2009) Laser-controllable coatings for corrosion protection. *ACS Nano*, **3**, 1753–1760.
46. Carregal-Romero, S. *et al.* (2012) NIR-light triggered delivery of macromolecules into the cytosol. *J. Control. Release*, **159**, 120–127. doi: 10.1016/j.jconrel.2011.12.013
47. Heuberger, R., Sukhorukov, G., Vörös, J., Textor, M., and Möhwald, H. (2005) Biofunctional polyelectrolyte multilayers and microcapsules: control of non-specific and bio-specific protein adsorption. *Adv. Funct. Mater.*, **15**, 357–366.
48. Wattendorf, U., Kreft, O., Textor, M., Sukhorukov, G.B., and Merkle, H.P. (2008) Stable stealth function for hollow polyelectrolyte microcapsules through a poly(ethylene glycol) grafted polyelectrolyte adlayer. *Biomacromolecules*, **9**, 100–108.
49. Ochs, C.J., Such, G.K., Stadler, B., and Caruso, F. (2008) Low-fouling, biofunctionalized, and biodegradable click capsules. *Biomacromolecules*, **9**, 3389–3396.
50. Cortez, C. *et al.* (2006) Targeting and uptake of multilayered particles to colorectal cancer cells. *Adv. Mater.*, **18**, 1998–2003.
51. Cortez, C. *et al.* (2007) Influence of size, surface, cell line, and kinetic properties on the specific binding of A33 antigen-targeted multilayered particles and capsules to colorectal cancer cells. *ACS Nano*, **1**, 93–102.
52. Zhang, F. *et al.* (2006) Bioactive galactose-branched polyelectrolyte multilayers and microcapsules: self-assembly, characterization, and biospecific lectin adsorption. *Langmuir*, **22**, 8458–8464.
53. Wang, K. *et al.* (2007) Encapsulated photosensitive drugs by biodegradable microcapsules to incapacitate cancer cells{. *J. Mater. Chem.*, **17**, 4018–4021.
54. Reibetanz, U., Claus, C., Typlt, E., and Donath, J.H. (2006) Defoliation and plasmid delivery with layer-by-layer coated colloids. *Macromol. Biosci.*, **6**, 153–160.
55. Reibetanz, U. *et al.* (2010) Colloidal DNA carriers for direct localization in cell compartments by pH sensoring. *Biomacromolecules*, **11**, 1779.
56. Itoh, Y., Matsusaki, M., Kida, T., and Akashi, M. (2008) Locally controlled release of basic fibroblast growth factor from multilayered capsules. *Biomacromolecules*, **9**, 2202–2206.
57. Facca, S. *et al.* (2010) Active multilayered capsules for in vivo bone formation. *Proc. Natl. Acad. Sci. U.S.A.*, **107**, 3406–3411.
58. Zhang, X. *et al.* (2010) Poly(L-lysine) nanostructured particles for gene delivery and hormone stimulation. *Biomaterials*, **31**, 1699–1706.
59. De Geest, B.G., McShane, M.J., Demeester, J., De Smedt, S.C., and Hennink, W.E. (2008) Microcapsules ejecting nanosized species into the environment. *J. Am. Chem. Soc.*, **130**, 14480–14482.
60. Rivera Gil, P., Nazarenus, M., Ashraf, S., and Parak, W.J. (2012) pH sensitive capsules as intracellular optical reporters for monitoring lysosomal pH changes upon stimulation. *Small*, **8**, 943–948. doi: 10.1002/smll.201101780
61. Van Hoecke, K. *et al.* (2011) In vitro ecotoxicity and uptake of polymer coated gold nanoparticles. *Nanotoxicology* (Epub ahead of print).• Q3
62. Schweiger, C. *et al.* (2012) The internalization patterns of superparamagnetic iron oxide nanoparticles quantitatively depend on their charge. *J. Nanobiotechnol.*, submitted to.• Q4
63. Hühn, D. *et al.* (2012) Charge dependent protein corona and cellular uptake of polymer-coated colloidal nanoparticles. , to be submitted.• Q5
64. Jiang, X., Röcker, C., Hafner, M., and Nienhaus, G.U. (2010) Endo- and exocytosis of zwitterionic quantum dot nanoparticles by living cells. *ACS Nano Under Rev.*, **23**, 6787–6797.
65. Jiang, X.E. *et al.* (2010) Specific effects of surface amines on polystyrene

nanoparticles in their interactions with mesenchymal stem cells. *Biomacromolecules*, **11**, 748–753.

66. Rejman, J., Oberle, V., Zuhorn, I.S., and Hoekstra, D. (2004) Size-dependent internalization of particles via the pathways of clathrin- and caveolae-mediated endocytosis. *Biochem. J.*, **377**, 159–169.
67. Geiser, M. *et al.* (2005) Ultrafine particles cross cellular membranes by nonphagocytic mechanisms in lungs and in cultured cells. *Environ. Health Perspect.*, **113**, 1555–1560.
68. Muñoz Javier, A. *et al.* (2006) Combined atomic force microscopy and optical microscopy measurements as a method to investigate particle uptake by cells. *Small*, **2**, 394–400.
69. Kenworthy, A.K., Petranova, N., and Edidin, M. (2000) High-resolution FRET microscopy of cholera toxin B-subunit and GPI-anchored proteins in cell plasma membranes. *Mol. Biol. Cell*, **11**, 1645–1655.
70. Pelkmans, L. and Helenius, A. (2002) Endocytosis via caveolae. *Traffic*, **3**, 311–320.
71. Pelkmans, L., Puntener, D., and Helenius, A. (2002) Local actin polymerization and dynamin recruitment in SV40-induced internalization of caveolae. *Science*, **296**, 535–539.
72. Kreft, O., Muñoz Javier, A., Sukhorukov, G.B., and Parak, W.J. (2007) Polymer microcapsules as mobile local pH-sensors. *J. Mater. Chem.*, **17**, 4471–4476.
73. Kirchner, C. *et al.* (2005) Cytotoxicity of nanoparticle-loaded polymer capsules. *Talanta*, **67**, 486–491.
74. Weissleder, R. *et al.* (1989) Superparamagnetic iron-oxide – pharmacokinetics and toxicity. *Am. J. Roentgenol.*, **152**, 167–173.
75. Shukla, R. *et al.* (2005) Biocompatibility of gold nanoparticles and their endocytotic fate inside the cellular compartment: a microscopic overview. *Langmuir*, **21**, 10644–10654.
76. Hunter, A.C. (2006) Molecular hurdles in polyfectin design and mechanistic background to polycation induced cytotoxicity. *Adv. Drug Deliv. Rev.*, **58**, 1523–1531.
77. Fischer, D., Li, Y.X., Ahlemeyer, B., Krieglstein, J., and Kissel, T. (2003) In vitro cytotoxicity testing of polycations: influence of polymer structure on cell viability and hemolysis. *Biomaterials*, **24**, 1121–1131.
78. Bieber, T., Meissner, W., Kostin, S., Niemann, A., and Elsasser, H.P. (2002) Intracellular route and transcriptional competence of polyethylenimine-DNA complexes. *J. Control. Release*, **82**, 441–454.
79. Godbey, W.T., Wu, K.K., and Mikos, A.G. (1999) Size matters: molecular weight affects the efficiency of poly(ethylenimine) as a gene delivery vehicle. *J. Biomed. Mater. Res.*, **45**, 268–275.
80. Seiler, N. and Raul, F. (2005) Polyamines and apoptosis. *J. Cell. Mol. Med.*, **9**, 623–642.
81. Kolbe, A. *et al.* (2011) De Novo design of supercharged, unfolded protein polymers, and their assembly into supramolecular aggregates. *Macromol. Rapid Commun.*, **32**, 186–190.
82. Hartig, S.M., Greene, R.R., Dikov, M.M., Prokop, A., and Davidson, J.M. (2007) Multifunctional nanoparticulate polyelectrolyte complexes. *Pharm. Res.*, **24**, 2353–2369.
83. Alexiou, C. *et al.* (2003) Magnetic drug targeting-biodistribution of the magnetic carrier and the chemotherapeutic agent mitoxantrone after locoregional cancer treatment. *J. Drug Targeting*, **11**, 139–149.
84. Alexiou, C. *et al.* (2005) In vitro and in vivo investigations of targeted chemotherapy with magnetic nanoparticles. *J. Magn. Magn. Mater.*, **293**, 389–393.
85. De Koker, S. *et al.* (2011) Polymeric multilayer capsules delivering biotherapeutics. *Adv. Drug Deliv. Rev.*, **63**, 748–761.
86. Holzbach, T. *et al.* (2010) Non-viral VEGF(165) gene therapy – magnetofection of acoustically active magnetic lipospheres ('magneto-bubbles') increases tissue survival in an

oversized skin flap model. *J. Cell. Mol. Med.*, **14**, 587–599.

87. Mykhaylyk, O. *et al.* (2010) Engineering magnetic nanoparticles and formulations for gene delivery. *J. Control. Release*, **148**, E63–E64.
88. Bertrand, J.R. *et al.* (2002) Comparison of antisense oligonucleotides and siRNAs in cell culture and in vivo. *Biochem. Biophys. Res. Commun.*, **296**, 1000–1004.
89. Santel, A. *et al.* (2006) A novel siRNA-lipoplex technology for RNA interference in the mouse vascular endothelium. *Gene Ther.*, **13**, 1222–1234.
90. Schaffert, D. and Wagner, E. (2008) Gene therapy progress and prospects: synthetic polymer-based systems. *Gene Ther.*, **15**, 1131–1138.
91. Zhou, J.H. *et al.* (2006) PAMAM dendrimers for efficient siRNA delivery and potent gene silencing. *Chem. Commun.*, **22**, 2362–2364.
92. Giljohann, D.A., Seferos, D.S., Prigodich, A.E., Patel, P.C., and Mirkin, C.A. (2009) Gene regulation with polyvalent siRNA-nanoparticle conjugates. *J. Am. Chem. Soc.*, **131**, 2072–2073.
93. Kunath, K. *et al.* (2003) Low-molecular-weight polyethylenimine as a non-viral vector for DNA delivery: comparison of physicochemical properties, transfection efficiency and in vivo distribution with high-molecular-weight polyethylenimine. *J. Controlled Release*, **89**, 113–125.
94. Pike-Overzet, K., van der Burg, M., Wagemaker, G., van Dongen, J.J., and Staal, F.J. (2007) New insights and unresolved issues regarding Insertional mutagenesis in x-linked SCID gene therapy. *Mol. Ther.*, **15**, 1910–1916.
95. Li, S.D. and Huang, L. (2006) Gene therapy progress and prospects: non-viral gene therapy by systemic delivery. *Gene Ther.*, **13**, 1313–1319.
96. Zebli, B., Susha, A.S., Sukhorukov, G.B., Rogach, A.L., and Parak, W.J. (2005) Magnetic targeting and cellular uptake of polymer microcapsules simultaneously functionalized with magnetic and luminescent nanocrystals. *Langmuir*, **21**, 4262–4265.
97. Vlaskou, D. *et al.* (2010) Magnetic and acoustically active lipospheres for magnetically targeted nucleic acid delivery. *Adv. Funct. Mater.*, **20**, 3881–3894.
98. del Pino, P. *et al.* (2010) Gene silencing mediated by magnetic lipospheres tagged with small interfering RNA. *Nano Lett.*, **10**, 3914–3921.
99. Skirtach, A.G. *et al.* (2007) Ultrasound stimulated release and catalysis using polyelectrolyte multilayer capsules. *J. Mater. Chem.*, **17**, 1050–1054.
100. Pankhurst, Q.A., Connolly, J., Jones, S.K., and Dobson, J. (2003) Applications of magnetic nanoparticles in biomedicine. *J. Phys. D: Appl. Phys.*, **36**, R167–R181.
101. Skirtach, A.G., Antipov, A.A., Shchukin, D.G., and Sukhorukov, G.B. (2004) Remote activation of capsules containing Ag nanoparticles and IR dye by laser light. *Langmuir*, **20**, 6988–6992.
102. Angelatos, A.S., Radt, B., and Caruso, F. (2005) Light-responsive polyelectrolyte/gold nanoparticle microcapsules. *J. Phys. Chem. B*, **109**, 3071–3076.
103. Bedard, M., De Geest, B., Skirtach, A., Mohwald, H., and Sukhorukov, G. (2010) Polymeric microcapsules with light responsive properties for encapsulation and release. *Adv. Colloid Interface Sci.*, **158**, 2–14.
104. Urban, A.S. *et al.* (2009) Controlled nanometric phase transitions of phospholipid membranes by plasmonic heating of single gold nanoparticles. *Nano Lett.*, **9**, 2903–2908.
105. Hirsch, L.R. *et al.* (2003) Nanoshell-mediated near-infrared thermal therapy of tumors under magnetic resonance guidance. *Proc. Natl. Acad. Sci. U.S.A.*, **100**, 13549–13554.
106. Schwartz, J.A. *et al.* (2009) Feasibility study of particle-assisted laser ablation of brain tumors in orthotopic canine model. *Cancer Res.*, **69**, 1659–1667.
107. Baffou, G., Quidant, R., and de Abajo, F. (2010) Nanoscale control of optical heating in complex plasmonic systems. *ACS Nano*, **4**, 709–716.
108. Hühn, D., Govorov, A., Rivera Gil, P., and Parak, W.J. (2011) Photo-stimulated

Au nanoheaters in polymer and biological media: Characterization of mechanical destruction and boiling. *Adv. Funct. Mater.*, published online.

109. Muñoz Javier, A. *et al.* (2009) Photoactivated release of cargo from the cavity of polyelectrolye capsules to the cytosol of cells. *Langmuir*, **24**, 12517–12520.

110. del Mercato, L.L., Gonzalez, E., Abbasi, A.Z., Parak, W.J., and Puntes, V. (2011) Synthesis and evaluation of gold nanoparticle-modified polyelectrolyte capsules under microwave irradiation for remotely controlled release for cargo. *J. Mater. Chem.*, **21**, 11468–11471.

111. Mc Shane, M.J., Brown, J.Q., Guice, K.B., and Lvov, Y.M. (2002) Polyelectrolyte microshells as carriers for fluorescent sensors: loading and sensing properties of a ruthenium-based oxygen indicator. *J. Nanosci. Nanotechnol.*, **2**, 411–416.

112. Lang, F. (2007) Mechanisms and significance of cell volume regulation. *J. Am. Coll. Nutr.*, **26**, 613S–623S.

113. Matsui, H. *et al.* (1998) Evidence for periciliary liquid layer depletion, not abnormal ion composition, in the pathogenesis of cystic fibrosis airways disease. *Cell*, **95**, 1005–1015.

114. Mall, M., Hipper, A., Greger, R., and Kunzelmann, K. (1996) Wild type but not delta F508 CFTR inhibits Na^+ conductance when coexpressed in Xenopus oocytes. *FEBS Lett.*, **381**, 47–52.

115. Stutts, M.J. *et al.* (1995) Cftr as a camp-dependent regulator of sodium-channels. *Science*, **269**, 847–850.

116. Darbha, G.K., Ray, A., and Ray, P.C. (2007) Gold nanoparticle-based miniaturized nanomaterial surface energy transfer probe for rapid and ultrasensitive detection of mercury in soil, water, and fish. *ACS Nano*, **1**, 208–214.

117. Bakker, E., Buhlmann, P., and Pretsch, E. (1997) Carrier-based ion-selective electrodes and bulk optodes. 1. General characteristics. *Chem. Rev.*, **97**, 3083–3132.

118. Tan, W.H., Shi, Z.Y., Smith, S., Birnbaum, D., and Kopelman, R. (1992) Submicrometer intracellular chemical optical fiber sensors. *Science*, **258**, 778–781.

119. Buhlmann, P., Pretsch, E., and Bakker, E. (1998) Carrier-based ion-selective electrodes and bulk optodes. 2. Ionophores for potentiometric and optical sensors. *Chem. Rev.*, **98**, 1593–1687.

120. Cameron, I.L., Smith, N.K.R., Pool, T.B., and Sparks, R.L. (1980) Intracellular concentration of sodium and other elements as related to mitogenesis and oncogenesis invivo. *Cancer Res.*, **40**, 1493–1500.

121. Burns, A., Sengupta, P., Zedayko, T., Baird, B., and Wiesner, U. (2006) Core/shell fluorescent silica nanoparticles for chemical sensing: towards single-particle laboratories. *Small*, **2**, 723–726.

122. Hidalgo, G. *et al.* (2009) Functional tomographic fluorescence imaging of pH microenvironments in microbial biofilms by use of silica nanoparticle sensors. *Appl. Environ. Microbiol.*, **75**, 7426–7435.

123. Nguyen, T. and Rosenzweig, Z. (2002) Calcium ion fluorescence detection using liposomes containing alexa-labeled calmodulin. *Anal. Bioanal. Chem.*, **374**, 69–74.

124. Ballerstadt, R. and Schultz, J. (2000) A fluorescence affinity hollow fiber sensor for continuous transdermal glucose monitoring. *Anal. Chem.*, **72**, 4185–4192.

125. Dimosthenis, L.G. and Athanasios, G.V. (2011) Synthetic membranes (vesicles) in inorganic ion analysis: a review. *Anal. Chim. Acta*, **683**, 156–169.

126. Zhang, F. *et al.* (2011) Polymer-coated nanoparticles: a universal tool for biolabelling experiments. *Small*, **7**, 3113–3127.

127. Clark, H.A., Hoyer, M., Philbert, M.A., and Kopelman, R. (1999) Optical nanosensors for chemical analysis inside single living cells. 1. Fabrication, characterization, and methods for intracellular delivery of PEBBLE sensors. *Anal. Chem.*, **71**, 4831–4836.

128. Delcea, M. *et al.* (2010) Multicompartmental micro- and nanocapsules:

hierarchy and applications in biosciences. *Macromol. Biosci.*, **10**, 465.

129. del Mercato, L.L., Abbasi, A.Z., and Parak, W.J. (2011) Synthesis and characterization of ratiometric ion-sensitive polyelectrolyte capsules. *Small*, **7**, 351–363.

130. del Mercato, L.L., Abbasi, A.Z., Ochs, M., and Parak, W.J. (2011) Multiplexed sensing of ions with barcoded polyelectrolyte capsules. *ACS Nano*, **5**, 9668–9674.

131. Wang, Y.J., Bansal, V., Zelikin, A.N., and Caruso, F. (2008) Templated synthesis of single-component polymer capsules and their application in drug delivery. *Nano Lett.*, **8**, 1741–1745.

132. An, Z., Kavanoor, K., Choy, M.L., and Kaufman, L.J. (2009) Polyelectrolyte microcapsule interactions with cells in two- and three-dimensional culture. *Colloids Surf. B Biointerfaces*, **70**, 114–123.

133. Semmling, M. *et al.* (2008) A novel flow-cytometry-based assay for cellular uptake studies of polyelectrolyte microcapsules. *Small*, **4**, 1763–1768.

134. Lu, Z.S. *et al.* (2008) Mechanism of antimicrobial activity of CdTe quantum dots. *Langmuir*, **24**, 5445–5452.

135. Gaponik, N. *et al.* (2003) Labeling of biocompatible polymer microcapsules with near-infrared emitting nanocrystals. *Nano Lett.*, **3**, 369–372.

136. Gaponik, N., Radtchenko, I.L., Sukhorukov, G.B., Weller, H., and Rogach, A.L. (2002) Toward encoding combinatorial libraries: charge-driven microencapsulation of semiconductor nanocrystals luminescing in the visible and near IR. *Adv. Mater.*, **14**, 879–882.

137. Dähne, L., Leporatti, S., Donath, E., and Mohwald, H. (2001) Fabrication of micro reaction cages with tailored properties. *J. Am. Chem. Soc.*, **123**, 5431–5436.

138. Shchukin, D.G. and Sukhorukov, G.B. (2004) Nanoparticle synthesis in engineered organic nanoscale reactors. *Adv. Mater.*, **16**, 671–682.

139. Qi, W. *et al.* (2009) Glucose-sensitive microcapsules from glutaraldehyde cross-linked hemoglobin and glucose oxidase. *Biomacromolecules*, **10**, 1212–1216.

140. Reibetanz, U., Halozan, D., Brumen, M., and Donath, E. (2007) Flow cytometry of HEK 293 T cells interacting with polyelectrolyte multilayer capsules containing fluorescein-labeled poly(acrylic acid) as a pH sensor. *Biomacromolecules*, **8**, 1928–1933.

"keywords/abstract

Dear Author,

Keywords and abstracts will not be included in the print version of your chapter but only in the online version.

Thank you!"

Abstract

The availability of different materials with well-defined and tunable physicochemical properties, for example, surface chemistry, size, or charge significantly increases the probability to design multifunctional systems with real possibilities of success in clinical translation. In this work, different materials with different functionalities for targeting, delivery, sensing, and site-specific manipulation are integrated in a common carrier. The carriers are organic, three-dimensional hollow microstructures that can be modified at two distinct positions, the cavity, and the shell. The different materials (i.e., building blocks) that are incorporated range from inorganic nanoparticles to molecules or more complex structures. Depending on the building block selected different functionalities can be integrated within the carrier. For example, the incorporation of gold, iron oxide, or semiconductor nanoparticles within the shell of the capsules gives the carrier responsiveness to light and magnetic fields. On the one hand, the capsules can be efficiently tracked by embedding semiconductor nanoparticles. On the other hand, stimuli–responsive capsules can also be obtained. Modification with gold nanoparticles controls the opening of individual capsules on light absorption whereas the presence of iron oxide nanoparticles targets the capsules to the cells on activation with a magnet. By attaching molecules with molecular recognition properties, the capsules can be targeted to specific cells. Furthermore, the cavity can be efficiently loaded with bioactive molecules with different lyotropy, for example, hydrophobic/hydrophilic drugs, vaccines, hormones, enzymes, or sensors. Entrapment of these molecules impart cargo protection increasing its bioavailability and reducing side effects.

Indeed, different materials with different properties for different purposes are integrated within the carrier. More interestingly, the physicochemical properties of the carrier can also be tuned. Different constituents for the layer as well as for the cores can be used in order to get, for example, mechanical highly stable versus degradable capsules or smaller versus bigger capsules, and so on. I would also like to point out that these sophisticated materials with novel properties are always tried to get adjusted to the requirements/demands of clinicians. These multifunctional systems are biocompatible, are easily incorporated by numerous types of cells, and are able to interact with the cellular environment. In this sense, the targeting and the spatially and temporally resolved, controlled release of

several types of cargoes is demonstrated. Neither the viability of the cells nor the integrity of the cargo is impaired. Furthermore, because of the multiplexing abilities of barcoded capsules modified with sensor molecules, different information, for example, concentration of different ions can be obtained in parallel.

In summary, a multifunctional delivery system that offers cargo protection as well as efficient and sufficient loading capacity is created. This biocompatible carrier possesses the distinct ability of multiplexing, that is, the ability of performing different inputs/outputs (targeting, controlled release, and sensing), during a single application.

Keywords

Affiliation for the Authors: Pilar Rivera Gil,
Moritz Nazarenus,
Wolfgang Parak
Philipps University of Marburg, Department of Biophotonics, Institute of Physics, Renthof 7, 35037 Marburg Germany

Queries in Chapter 3

Q1. Please confirm if these abbreviations 'PEG, NIR, and FITC' need to be spelt out. If yes, please provide the expansions.

Q2. We have changed the bold and underline text to italics text. Please chck and confirm the edit made.

Q3. Please clarify if this article has since been published. If so, please provide the volume number and page range for Reference 61.

Q4. Please clarify if this article has since been published. If so, please provide the volume number and page range for Reference 62.

Q5. Please clarify if this article has since been published. If so, please provide the volume number, journal title and page range for Reference 63.

small NANO MICRO

Sensors

pH-Sensitive Capsules as Intracellular Optical Reporters for Monitoring Lysosomal pH Changes Upon Stimulation

*Pilar Rivera_Gil, Moritz Nazarenus, Sumaira Ashraf, and Wolfgang J. Parak**

The concept of a long-term sensor for ion changes in the lysosome is presented. The sensor is made by layer-by-layer assembly of oppositely charged polyelectrolytes around ion-sensitive fluorophores, in this case for protons. The sensor is spontaneously incorporated by cells and resides over days in the lysosome. Intracellular changes of the concentration of protons upon cellular stimulation with pH-active agents are monitored by read-out of the sensor fluorescence at real time. With help of this sensor concept it is demonstrated that the different agents used (Monensin, Chloroquine, Bafilomycin A1, Amiloride) possessed different kinetics and mechanisms of action in affecting the intracellular pH values.

1. Introduction

Public media have long since envisioned miniaturized " submarines", such as devices to be injected into human bodies where they could diagnose and treat diseases (e.g., the novel *Fantastic Voyage* by Issac Asimov). Though such devices are science fiction, in particular the idea of down scaling functional objects to the nano- and microscale, smart materials could nevertheless go in a direction to fulfill part of these visions.[1] Concerning diagnosis an observed object would be needed which could reside non-invasively inside cells, and which would continuously report data about its local environment to the outside. In this work we want to demonstrate one prototype device towards this goal, which fulfills the basic requirements, though arguably with limitations. We chose pH as parameter to detect. Protons are heavily involved in biological processes on all levels and irregularities in their concentration are also associated with diseases.[2] As carrier vessel polyelectrolyte capsules fabricated with layer-by-layer assembly[3] were used. These capsules have a semipermeable wall, which confines big molecules to their cavity, whereas small molecules like protons can diffuse through the wall.[4] It was recently demonstrated that pH-sensitive fluorophores can be loaded to the cavity of such capsules and that changes in pH can be observed by reading out the fluorescence originating from the capsule cavity.[5,6] These pH sensitive capsules are spontaneously incorporated by living cells,[7] are finally localized in the lysosome,[6,8] and do not exhibit acute cytotoxicity.[9] The transition from the slightly alkaline cell medium to the acidic lysosome can be followed by reading out changes in fluorescence of the capsules.[5,10] For intracellular sensing clearly translocation to the cytosol would be desirable. However, this has not been achieved so far, though some ideas have been reported.[11] On the other hand, this obstacle can be turned into an advantage. As the capsules are trapped in the lysosome their location is exactly defined. The capsules reside over long time (weeks) in the lysosome, whereby they are passed to the daughter cells upon cellular division.[12] There is no acute cytotoxicity.[9,13] In this way the capsules are reporters which can stay at one defined location over long periods of time and which report the local analyte concentration (in this case of local pH) via fluorescence to the outside. We need to state that the present work is dealing with in vitro experiments involving cell cultures, and thus the present system certainly can't be directly transferred to an in vivo "submarine" - like device, though it nevertheless presents a first step in this direction.

Dr. P. Rivera_Gil, M. Nazarenus
S. Ashraf,[+] Prof. W. J. Parak
Fachbereich Physik and WZMW
Philipps Universität Marburg
Renthof 7, D-35037, Marburg, Germany
E-mail: wolfgang.parak@physik.uni-marburg

[+] Present address: National Institute for Biotechnology and Genetic Engineering, Jhang Road Faisalabad, Pakistan

DOI: 10.1002/smll.201101780

A variety of other fluorescence-based particle reporters for intracellular sensing have already been described in literature.[14] However, most of these reporters allow rather for static instead of dynamic measurements, i.e. the change in fluorescence intensity of the reporter after addition of the agent is recorded only once. The capsule system presented here on the other hand facilitates continuous read-out of the local analyte (in this case H^+) concentration. This is mainly attributed to the microscopic size of the capsules (in our case around 2.5 μm, though capsules smaller than 1 μm can easily be made), which allows for optical addressing of individual capsules. Most analyte sensitive fluorophores change their fluorescence intensity (at fixed wavelength) upon presence of the specific analyte.[15] In this way, absolute fluorescence intensities (at the respective wavelength) originating from the reporters inside the cells have to be recorded. Obviously the more reporters are present in one cell, the higher the fluorescence intensity originating from this cell will be. As there is no way to fix the number of reporters inside each cell to a desired value (as uptake by cells happens statistically) absolute fluorescence intensities will vary significantly between different cells. This is further enhanced due to dilution of the reporters, as upon cell division they are (statistically) divided between the daughter cells. Thus, due to variation in reporter density in time and per cell continuous detection of analyte concentrations via absolute fluorescence intensity read-out is complicated. On the other hand, if the reporters are big enough to be individually resolved by optical microscopy this problem is circumvented. Under these circumstances the number of reporters in each cell is precisely known at each point of time (simply by counting the number of the analyte-sensitive particles) and as fluorescence can be traced back to each individual particle absolute intensity measurements are possible. Photobleaching involves another complication for absolute intensity detection. However, effects of photobleaching can be partially overcome by ratiometric measurements, in which the fluorescence intensity of an analyte-sensitive fluorophore (at one wavelength) is compared to the intensity of a reference fluorophore (at another wavelength). Due to the big cavity of polyelectrolyte capsules mixtures of different fluorophores can easily be embedded, thus allowing for relative, ratiometric, instead of absolute fluorescence detection.[16] Ratiometric measurements allow for compensation of inhomogeneities in capsule loading with the fluorophores and size distribution of capsules[16].

2. Results and Discussion

In our study we used a commercial pH-sensitive fluorophore from the seminaphthorhodafluors (SNARF) class of indicators. In order to increase its molecular weight (thus allowing to retain the SNARF inside the cavity of the capsules) we conjugated SNARF to amino-dextran (M_W = 500 kDa).[16] $CaCO_3$ particles filled with SNARF-dextran were produced via coprecipitation by $CaCl_2$, Na_2CO_3, and SNARF-dextran.[16] These particles were used as template cores for subsequent deposition of poly(styrenesulfonate) (PSS, M_W = 70 kDa) and poly(allylamine hydrochloride) (PAH, M_W = 70 kDa), leading to the final architecture of $(PSS, PAH)_5$ (for more information the reader is referred to the supporting information, §1.1). The template cores were finally dissolved with ethylenediaminetetraacetic acid (EDTA), leading to capsules with SNARF-dextran in their cavity.[16] Due to the embedded SNARF the color of fluorescence originating from the cavity of the capsules depended on the surrounding pH, leading to more yellow fluorescence (λ = 580 nm) at acidic pH and to more red fluorescence (λ = 640 nm) at alkaline pH, cf. **Figure 1**b (see SI §1.2 for a detailed information about the sensitivity of the sensors). When these capsules were added to cultured cells their ability to sense local pH could be directly seen. After spontaneous incorporation capsules residing in the lysosome were more fluorescent in the yellow, whereas capsules remaining in the slightly alkaline cell medium were fluorescent more in the red, cf. Figure 1a,c.[5] As outlined above the internalized capsules can be regarded as intracellular long term reporters for lysosomal pH.

In order to demonstrate the reporting principle we were looking for agents which are related to lysosomal acidification. (i) Chloroquine is a weak base that accumulates in and neutralizes the lysosome.[17] In its non-protonated form Chloroquine passes through cellular membranes. However, upon lowering of environmental pH Chloroquine becomes protonated and remains entrapped in the acidic vesicles (i.e. the lysosome). In this way the pH of the lysosome in the presence of this lysosomotropic substance increases. (ii) Bafilomycin A1 is a well known inhibitor of the activity of the vacuolar (V) proton pump ATPase (V-type ATPase)[18] which is present in cellular membranes (plasma membrane as well as intracellular membranes).[19] The vacuolar ATPases hydrolyse ATP, generating a proton gradient which is used for acidification of compartments within cells. Upon addition of Bafilomycin A1 this effect is blocked and an increase in the pH is observed. (iii) Amiloride is an inhibitor of the sodium-proton exchange (NPE). The NPE is present in the membrane of cells and catalyses the electroneutral exchange of sodium ions for protons. The different isoforms of NPE are involved in the regulation of the pH within the cytosol and within organelles of the endocytic pathway.[20] NPEs exclude protons from and take up sodium ions into the cells. When Amiloride is added to the cells, the Na^+/H^+ flux is reverted thus causing alkalinisation. (iv) Monensin is an exogenous Na^+/H^+ exchanging ionophore[21] with antiporter properties. Monensin disrupts intracellular Na^+ and H^+ gradients leading to alkalinisation of the media. Extracellular Na^+ ions are exchanged by intracellular H^+ ions, thus decreasing the concentration of H^+ available.

Data resulting from one typical challenge of cells to one of the above mentioned agents are shown in Figure 1d. First, cells were incubated with pH-sensitive capsules for 24 hours (≈30 capsules added to the medium per cell) (see SI §2 for the cell culture procedures). After this period most cells had at least one capsule incorporated, while other capsules still remained in the extracellular medium. The cell culture dishes containing the cells were mounted in an incubator on top of a fluorescence microscope and phase contrast and fluorescence images (yellow and red channel) were recorded in intervals

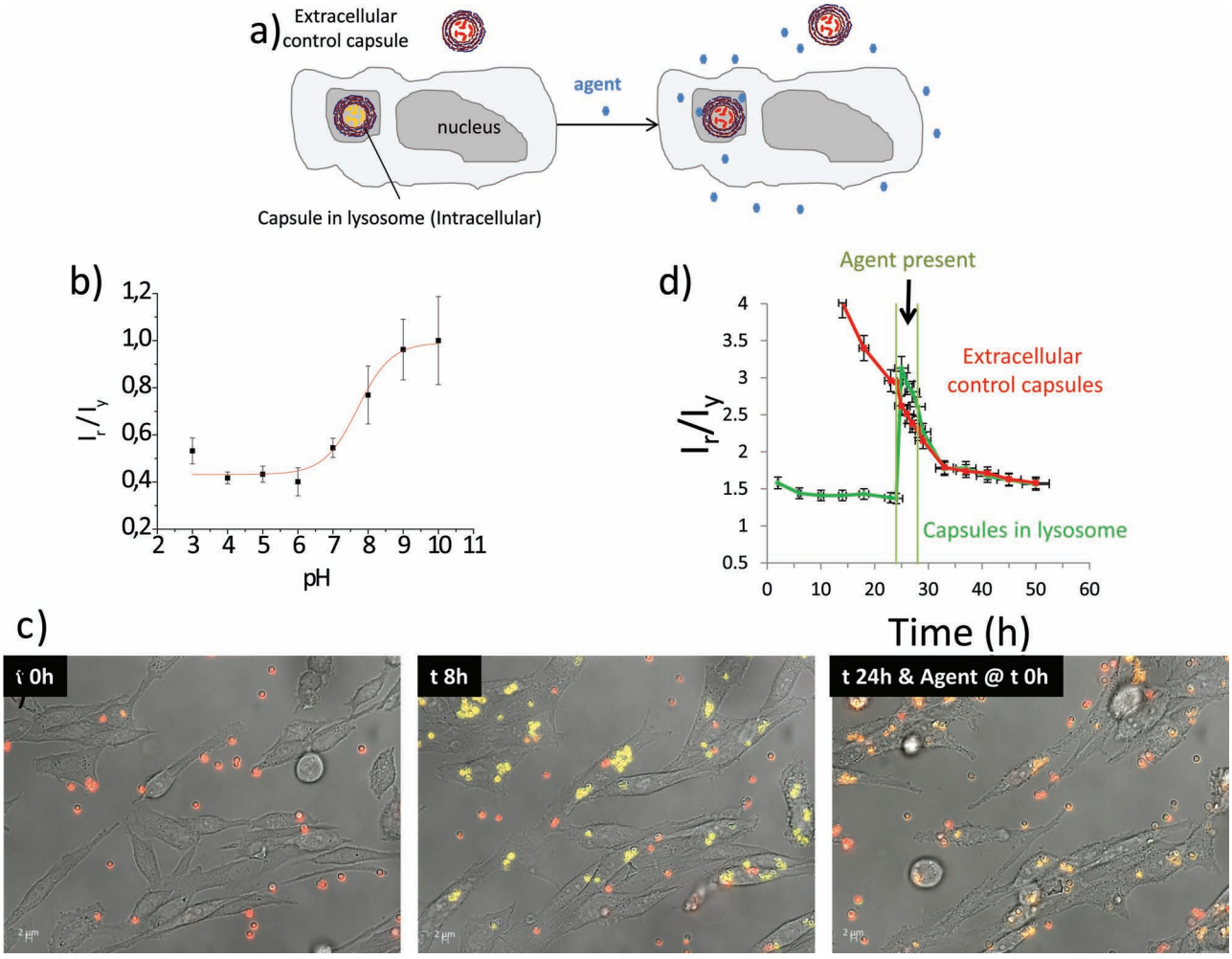

Figure 1. a) Cells have been incubated with pH-sensitive polyelectrolyte capsules. Some of the capsules are spontaneously incorporated by the cells and are transported to the lysosome. b) The ratio of red to yellow fluorescence (I_r/I_y) of the capsules depends on the surrounding pH. Capsules in the slightly alkaline extracellular medium are more fluorescent in the red, whereas capsules inside the acidic lysosome are more fluorescent in the yellow. If an agent which increases the pH in the lysosome is added changes in the capsule fluorescence from yellow to red can be detected. c) Overlay of microscopy images (phase contrast, yellow fluorescence, red fluorescence) before and after addition of an agent (in this case the agent was Chloroquine) which increases the pH inside the lysosome. The change of the fluorescence of internalized capsules from yellow to red reports the pH change in the lysosome, whereas control capsules in the extracellular medium retain their red fluorescence. d) The ratio of red to yellow fluorescence is plotted over time for capsules inside lysosomes versus control capsules located in the extracellular medium. The points of time when the agent was added and rinsed out are indicated. Note that the I_r/I_y ratio diminishes over time due to photobleaching over time. For this reason the I_r/I_y ratio of capsules inside the lysosome needs to be compared with control capsules in the extracellular medium that serve as reference.

ranging from a few minutes to 70 hours, cf. Figure 1d. From each cell in each image the absolute (background-corrected) yellow (I_y) and red (I_r) fluorescence intensities originating from the respective incorporated capsules were determined (see SI §3 for a detailed information about image processing and data evaluation). The mean values of different cells and images of the I_r/I_y ratio were then plotted versus time, cf. Figure 1d. During experiments the agent whose effect on the lysosomal pH was to be probed was added at fixed time and rinsed out after a defined incubation time, cf. Figure 1d. A series of dose-dependent viability experiments was performed in order to choose appropriate concentrations of the added agents, at which no cytotoxic effects happened (see SI §6).

In **Figure 2**e the red-to-yellow ratio of internalized capsules is plotted versus incubation time. The I_r/I_y values close at the beginning indicate the acidic environment of the internalize capsules in the lysosome (cf. Figure 1d). However, the I_r/I_y values slightly decay over time, although no stimulus was applied. We ascribe this effect to photobleaching (see SI §5), which changes the I_r/I_y ratio and thus the I_r/I_y versus pH calibration curve over time.[5] As a control capsules outside cells which were remaining in the extracellular medium were concomitantly analyzed. Also for extracellular capsules initial high I_r/I_y values correctly indicated a slightly alkaline pH of the cell medium, and also I_r/I_y values decayed over time (cf. Figure 2e). This behavior was clearly not associated with changes in pH, as the pH of the cell medium was checked to

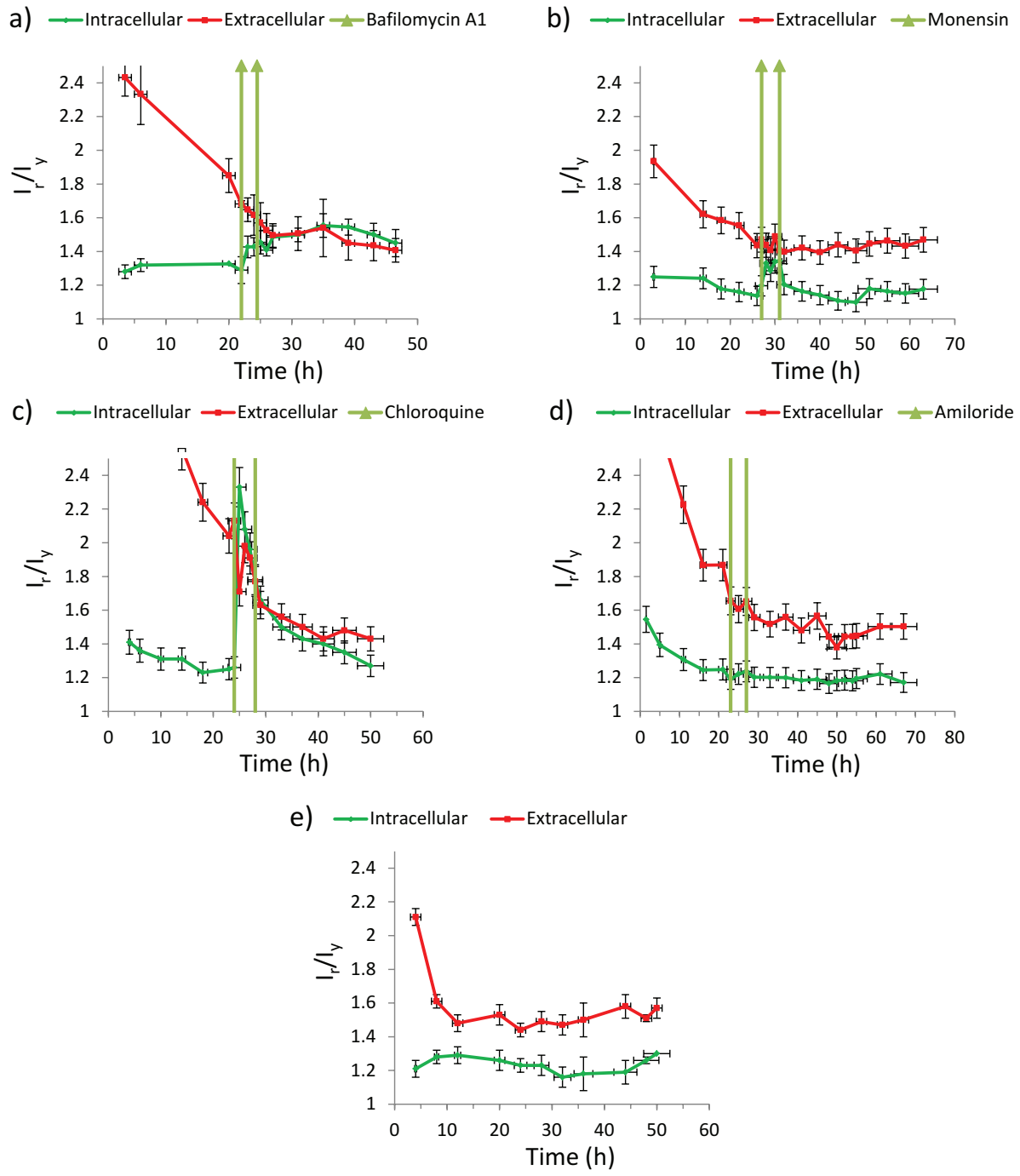

Figure 2. Cells have been incubated with pH-sensitive capsules as shown in Figure 1. Different agents were added and rinsed out: a) Bafilomycin A1 (600 nM), b) Monensin (20 μM), c) Chloroquine (100 μM), d) Amiloride (1 mM). In an additional control experiment e) no agent was added. The ratios of red to yellow fluorescence (I_r/I_y) originating from capsules inside the lysosome (drawn in green) and from control capsules in the extracellular medium (drawn in red) are plotted versus time. The data show the average ratios I_r/I_y as detected on typically >40 internalized capsules and >25 control capsules and the corresponding standard deviations as error bars.

be constant at different incubation times with an electrode based pH meter (SI §5.1). In this way one has to keep in mind that photobleaching changes the I_r/I_y versus pH calibration curve over time. However, control experiments as shown in Figure 2e allow in principle for the recording of time-dependent calibration curves, which in principle would need to be recorded also at different pH values, as photo-bleaching might depend on the pH. However, more pragmatic, changes in intracellular pH can be compared to external control capsules, cf. Figure 2. In this way imaging was always performed as well on internalized capsules as on control capsules outside cells. The I_r/I_y values of internalized capsules thus always were referred to the I_r/I_y values of extracellular capsules, which form the baseline for the slightly alkaline pH of the

cell medium. The possibility to use extracellular control capsules is one conceptual advantage of our system, which helps reducing effects due to photobleaching and substituting absolute by relative measurements.

Typical results of lysosomal pH responses to different stimulating agents are shown in Figure 2. Additionally all the results of the different experiments performed for all pH active agents are presented in the SI §4. Upon addition of Bafilomycin A1 the lysosomal pH raised to the extracellular pH. The elevated pH level remained even after rinsing out of Bafilomycin A1 (Figure 2a). The presence of Monensin also increased the lysosomal pH to the extracellular one. However, the lysosomal pH went back to its acidic value after Monensin had been rinsed out (Figure 2b). The effect of Monensin on the intracellular pH has been extensively studied; however, to our knowledge no data exist regarding the effect on the intra-lysosomal pH. Monensin increases the intracellular Na^+ ion concentrations by decreasing the H^+ concentrations. In our study Monensin also exhibited a clear lysosomal alkalinisation. Increase in the intracellular Na^+ concentration normally induces an activation of the Na^+/Ca^{++} exchanger to restore the normally low intracellular Na^+ values. Since the effect of Monensin is Na^+ dependent and the intracellular Na^+ concentration is prone to be maintained low, as soon as Monensin is rinsed the normal pH values can be restored. The response to Chloroquine was phenomenologically similar to that of Bafilomycin A1 (Figure 2c). In the case of stimulation with Amiloride no change in lysosomal pH was observed (Figure 2d). In changing the lysosomal pH, the different agents showed a different mechanism of action. Whereas Chloroquine as well as Monensin induced a rapid increase in the pH the removal of the ionophore led to a rapid recovery of the regular lysosomal pH. On the other hand, removal of the weak base from the cell medium had no effect on the acidification of the lysosome. The intra-lysosomal pH values were still comparable to the extracellular control capsules after 50 h. This effect was also visible in case of Bafilomycin A1. Inhibition of the V-ATPase with Bafilomycin A1, induced an irreversible change of the lysosomal pH (at least during our time lapse, i.e., 50–70 h). These results indicate that both the H^+ availability as well as the V-ATPase are crucial mechanisms of long term regulation of the intra-lysosomal pH. No neutralization in the pH of the lysosome was observed by the presence of Amiloride, an inhibitor of NPE. Therefore, if the antiporter is regulating the pH within the organelles involved in the endocytic processes then the Na^+/H^+ pump involved must be Amiloride-insensitive. It is well known that there are different NPE isoforms with different sensitivity to Amiloride.[22] However, their intracellular or tissue distribution is not totally clarified yet. Furthermore, it could also be possible that the binding-site for Amiloride was not available due to our experimental conditions. This means, Amiloride was added once the capsule sensors have already been internalized whereas the NPE responsible for acidification of the intracellular vesicles is believed to be present in the extracellular site of the NPE.[23]

The data presented in Figure 2 demonstrate that in fact our capsule system can be used for real-time monitoring of the lysosomal pH over days. During this period the method is virtually non-invasive. The capsules act as intracellular reporters at defined location, the lysosome, and time-dependent changes in lysosomal pH upon stimulation can be observed. A key feature of our system is the relatively large size of the capsules. This may impose limitations for sensing in other compartment and inside the cytosol, but for sensing in the lysosome reporters with the size of a few μm do not challenge cells. Size could be decreased to a few 100 nm, though it needs to be bigger that the optical resolution limit, as our technique is based on identifying individual capsules. By putting a barcode on the surface of the capsules reporters for different ions and small molecules could be created and ultimately allow for multiplexed imaging.[5,24] Due to the universal construction, in principle cavities could also be loaded with analyte-sensitive molecules which are not detected with fluorescence but for example with SERS.[25] Though continuous multiplexed intracellular reporting of analyte concentrations even in vitro still is far from route we think that the system here describes a significant step towards this direction.

Supporting Information

Supporting Information is available from the WIley Online Library or from the author.

Acknowledgements

This work was supported in part by the BMBF (ERANET Nanosyn grant to WJP) and the DFG (SPP 1313 grant PA794/4-2 to WJP and PRG). The authors are grateful to Dr. Irshad Hussain for stimulation discussions and for supervising SA. SA is grateful to Higher Education Commission Pakistan (HEC) for a fellowship. Dr. Loretta del Mercato, Dr. Abbasi Azhar, and Dr. Susana Carregal helped with the initial capsule production.

[1] J. Peteiro-Cartelle, M. Rodríguez-Pedreira, F. Zhang, P. Rivera_Gil, L. L. del_Mercato, W. J. Parak, *Nanomedicine* **2009**, *4*, 967.

[2] F. Lang, *J. Am. College Nutrition* **2007**, *26*, 613S; H. Matsui, B. R. Grubb, R. Tarran, S. H. Randell, J. T. Gatzy, C. W. Davis, R. C. Boucher, *Cell* **1998**, *95*, 1005; M. Mall, A. Hipper, R. Greger, K. Kunzelmann, *FEBS Lett.* **1996**, *381*, 47; M. J. Stutts, C. M. Canessa, J. C. Olsen, M. Hamrick, J. A. Cohn, B. C. Rossier, R. C. Boucher, *Science* **1995**, *269*, 847; G. K. Darbha, A. Ray, P. C. Ray, *ACS Nano* **2007**, *1*, 208.

[3] G. Decher, *Science* **1997**, *277*, 1232; G. B. Sukhorukov, E. Donath, H. Lichtenfeld, E. Knippel, M. Knippel, A. Budde, H. Mohwald, *Colloids Surf. A* **1998**, *137*, 253; G. B. Sukhorukov, E. Donath, S. Davis, H. Lichtenfeld, F. Caruso, V. I. Popov, H. Möhwald, *Polym. Adv. Technol.* **1998**, *9*, 759; E. Donath, G. B. Sukhorukov, F. Caruso, S. A. Davis, H. Möhwald, *Angew. Chem. Int. Ed.* **1998**, *37*, 2202.

[4] G. B. Sukhorukov, M. Brumen, E. Donath, H. Mohwald, *J. Phys. Chem. B* **1999**, *103*, 6434; W. F. Dong, J. K. Ferri, T. Adalsteinsson, M. Schonhoff, G. B. Sukhorukov, H. Mohwald, *Chem. Mater.* **2005**, *17*, 2603; T. Adalsteinsson, W.-F. Dong, M. Schönhoff,

J. Phys. Chem. **2004**, *108*, 20056; D. Halozan, U. Riebentanz, M. Brumen, E. Donath, *Colloids Surf. A* **2009**, *342*, 115.
[5] O. Kreft, A. Muñoz_Javier, G. B. Sukhorukov, W. J. Parak, *J. Mater. Chem.* **2007**, *17*, 4471.
[6] U. Reibetanz, D. Halozan, M. Brumen, E. Donath, *Biomacromolecules* **2007**, *8*, 1928.
[7] G. B. Sukhorukov, A. L. Rogach, B. Zebli, T. Liedl, A. G. Skirtach, K. Köhler, A. A. Antipov, N. Gaponik, A. S. Susha, M. Winterhalter, W. J. Parak, *Small* **2005**, *1*, 194; U. Reibetanz, M. H. A. Chen, S. Mutukumaraswamy, Z. Y. Liaw, B. H. L. Oh, S. Venkatraman, E. Donath, B. r. Neu, *Biomacromolecules* **2010**, *11*, 1779; P. Rivera_Gil, S. D. Koker, B. G. De_Geest, W. J. Parak, *Nano Lett.* **2009**, *9*, 4398; A. Muñoz_Javier, O. Kreft, M. Semmling, S. Kempter, A. G. Skirtach, O. Bruns, P. d. Pino, M. F. Bedard, J. Rädler, J. Käs, C. Plank, G. Sukhorukov, W. J. Parak, *Adv. Mater.* **2008**, *20*, 4281.
[8] S. De Koker, B. G. De Geest, S. K. Singh, R. De Rycke, T. Naessens, Y. Van Kooyk, J. Demeester, S. C. De Smedt, J. Grooten, *Angew. Chem. Int. Ed.* **2009**, *48*, 8485.
[9] C. Kirchner, A. M. Javier, A. S. Susha, A. L. Rogach, O. Kreft, G. B. Sukhorukov, W. J. Parak, *Talanta* **2005**, *67*, 486.
[10] M. Semmling, O. Kreft, A. Muñoz_Javier, G. B. Sukhorukov, J. Käs, W. J. Parak, *Small***2008**, *4*, 1763.
[11] P. Rivera Gil, L. L. del Mercato, P. del-Pino, A. Munoz-Javier, W. J. Parak, *Nano Today* **2008**, *3*, 12.
[12] A. Muñoz_Javier, O. Kreft, A. P. Alberola, C. Kirchner, B. Zebli, A. S. Susha, E. Horn, S. Kempter, A. G. Skirtach, A. L. Rogach, J. Rädler, G. B. Sukhorukov, M. Benoit, W. J. Parak, *Small* **2006**, *2*, 394.
[13] C. R. Kinnane, G. K. Such, G. Antequera-Garcia, Y. Yan, S. J. Dodds, L. M. Liz-Marzan, F. Caruso, *Biomacromolecules* **2009**, *10*, 2839; A. Kolbe, L. L. del Mercato, A. Z. Abassi, P. Rivera_Gil, S. J. Gorzini, W. H. C. Huibers, B. Poolman, W. J. Parak, A. Herrmann, *Macromol. Rapid Commun.* **2011**, *32*, 186; S. De_Koker, B. G. De_Geest, C. Cuvelier, L. Ferdinande, W. Deckers, W. E. Hennink, S. De_Smedt, N. Mertens, *Adv. Funct. Mater.* **2007**, *17*, 3754.
[14] L. Bahshi, R. Freeman, R. Gill, I. Willner, *Small* **2009**, *5*, 676; A. Burns, P. Sengupta, T. Zedayko, B. Baird, U. Wiesner, *Small* **2006**, *2*, 723; F. Zhang, E. Lees, F. Amin, P. Rivera_Gil, F. Yang, P. Mulvaney, W. J. Parak, *Small* **2011**, *7*, 3113; H. Xu, J. W. Aylott, R. Kopelman, T. J. Miller, M. A. Philbert, *Anal. Chem.* **2001**, *73*, 4124.
[15] J. E. Whitaker, R. P. Haugland, F. G. Prendergast, *Anal. Biochem.* **1991**, *194*, 330.
[16] L. L. del_Mercato, A. Z. Abbasi, W. J. Parak, *Small* **2011**, *7*, 351.
[17] P. O. Seglen, B. Grinde, A. E. Solheim, *Eur. J. Biochem.* **1979**, *95*, 215.
[18] T. Yoshimori, A. Yamamoto, Y. Moriyama, M. Futai, Y. Tashiro, *J. Biol. Chem.* **1991**, *266*, 17707.
[19] H. Tapper, R. Sundler, *J. Cell Physiol.* **1995**, *163*, 137.
[20] S. C. D. van IJzendoorn, R. Ohgaki, M. Matsushita, H. Kanazawa, S. Ogihara, D. Hoekstra, *Mol. Biol. Cell* **2010**, *21*, 1293.
[21] H. H. Mollenhauer, D. J. Morré, L. D. Rowe, *Biochim. Biophys. Acta.* **1990**, *1031*, 225.
[22] B. Masereel, L. Pochet, D. Laeckmann, *Eur. J. Med. Chem.* **2003**, *38*, 547.
[23] D. J. Hackam, O. D. Rotstein, W. J. Zhang, N. Demaurex, M. Woodside, O. Tsai, S. Grinstein, *J. Biol. Chem.* **1997**, *272*, 29810.
[24] A. Z. Abbasi, F. Amin, T. Niebling, S. Friede, M. Ochs, S. C. Romero, J. M. M. Martos, P. Rivera_Gil, W. Heimbrodt, W. J. Parak, *ACS Nano* **2011**, *5*, 21; L. L. del_Mercato, A. Z. Abbasi, M. Ochs, W. J. Parak, *ACS Nano* **2011**, in press.
[25] J. Kneipp, H. Kneipp, B. Wittig, K. Kneipp, *J. Phys. Chem. C* **2010**, *114*, 7421; M. Sanles-Sobrido, W. Exner, L. Rodriguez-Lorenzo, B. Rodriguez-Gonzalez, M. A. Correa-Duarte, R. A. Alvarez-Puebla, L. M. Liz-Marzan, *J. Am. Chem. Soc.* **2009**, *131*, 2699.

Received: November 3, 2011
Published online: February 8, 2012

Journal of Controlled Release 196 (2014) 132–138

Contents lists available at ScienceDirect

Journal of Controlled Release

journal homepage: www.elsevier.com/locate/jconrel

Biodegradable capsules as non-viral vectors for *in vitro* delivery of PEI/siRNA polyplexes for efficient gene silencing

Carolin Ganas [a,1], Annika Weiß [a,1], Moritz Nazarenus [a], Susanne Rösler [b], Thomas Kissel [b], Pilar Rivera_Gil [a,*], Wolfgang J. Parak [a,c,**]

[a] Fachbereich Physik, Philipps-Universität Marburg, 35037 Marburg, Germany
[b] Fachbereich Pharmazie, Philipps-Universität Marburg, 35037 Marburg, Germany
[c] CIC Biomagune, 20009 Donostia-San Sebastián, Spain

ARTICLE INFO

Article history:
Received 6 June 2014
Accepted 3 October 2014
Available online 14 October 2014

Chemical compounds studied in this article:
Polyethylenimine (PubChem CID: 9033)
Poly-L-arginine (PubChem CID: 6322)
Dextran sulfate (PubChem SID: 57288723)
Polyallylamine (Pub Chem CID: 7853)
Polystyrene sulfonate (Pub Chem CID: 75905)

Keywords:
Transfection
Gene silencing
Non-viral vectors
siRNA
Polyplexes
Microcapsules

ABSTRACT

The efficiency of siRNA delivery is demonstrated to be improved by encapsulating the siRNA within a non-viral carrier based on layer-by-layer assembly of oppositely charged biodegradable and biocompatible polyelectrolytes. In comparison to other non-viral delivery vehicles such as polycation-based complexes, a smaller amount of siRNA was necessary to produce *in vitro* gene silencing as early as 20–30 h after incubation. Colloidal carriers based on assembled biodegradable polyelectrolytes offer several advantages, such as efficient intracellular delivery after endocytosis followed by release to the cytosol, as well as protection of the siRNA, which is crucial for its therapeutic activity.

1. Introduction

Gene transfer technologies are an important biological research tool to investigate gene expression and function. Concerning *in vitro* application, this technology allows, for example, the identification of genes involved in cellular processes. By modification of genes, the behavior of cells can be controlled by modifying the particular composition of proteins they express. Also *in vivo* application is envisaged. In the future, gene therapy might develop into a molecular medicine that provides new treatment possibilities for several pathophysiological states. In many cancers and inherited diseases, genes are altered or damaged, so that the encoded proteins are no longer functional. Defect genes might then be substituted by healthy ones (gene therapy). It also occurs that genes are regulated incorrectly, such that proteins involved in the disease process are over-expressed. Thus, expression of the genes could be blocked (antisense therapy). The aim of such inhibitory antisense therapy is to use synthetic oligonucleotides (ONTs), *i.e.* short fragments of nucleic acids, such as double-stranded oligodeoxynucleotides (dsODNs) and small hairpin RNA (shRNA) or small interfering RNA (siRNA) to block the expression of proteins involved in the disease. This can occur at different levels of the gene expression process, *i.e.* during transcription or translation. The development of antisense technologies as therapeutic agents has led to numerous clinical trials. However, a limitation of the silencing approach is toxicity upon transfection of cells and its suspected effect on the expression of other genes or proteins (off-target effects). Therefore, safe transfection procedures with controlled release kinetics are highly desirable.

For many *in vivo* applications, a carrier is strongly required to deliver and protect the genetic material. In general, the ideal delivery method for therapeutic genetic materials needs to fulfill three major criteria. It should (i) impart protection in intercellular matrices (*i.e.* biological fluids and the intracellular space) against nucleases, (ii) perform

* Correspondence to: P. Rivera Gil, Department of Physical and Inorganic Chemistry, Rovira i Virgili University and the Chemistry Technology Center of Catalonia (CTQC), 43007 Tarragona, Spain.
** Correspondence to: W.J. Parak, Fachbereich Physik, Philipps-Universität Marburg, 35037 Marburg, Germany.
E-mail addresses: pilar.rivera@urv.cat (P. Rivera_Gil), wolfgang.parak@physik.uni-marburg.de (W.J. Parak).
[1] Both authors contributed equally to this manuscript.

http://dx.doi.org/10.1016/j.jconrel.2014.10.006
0168-3659/

transport across biological barriers, *e.g.* the plasma membrane, in order to reach its action site, and (iii) exclude toxic or off-target effects. Viral platforms are probably the most efficient method of getting foreign genetic material into large numbers of cells with high possibility of long-term inhibition. They are, however, associated to high host immunogenicity and mutagenesis [1]. This has raised serious safety concerns. Thus, although the great potential of gene or antisense therapy for some diseases is already demonstrated, viral vectors are still not authorized for gene or antisense therapy in Europe. Therefore, there is a strong necessity to develop alternative non-viral carriers with comparable transfection efficiencies and low host immunogenicity. Frequently used non-viral carriers include lipoplexes and polyplexes. Furthermore, there are commercial transfection agents based on different cationic lipids, which allow transfecting cells with plasmid DNA, siRNA, miRNA, *etc.* [2]. Typically used cationic polymers involve polyethylenimine (PEI), chitosan (CS), poly(L-lysine) (PLL), and poly(allylamine) (PAA) [3,4]. Carriers usually enter cells *via* endocytic pathways, and genetic material (DNA/RNA) is then translocated from endocytic vesicles to the cytosol. The exact mechanism of translocation to the cytosol is still under debate, though buffering of vesicular pH due to the cationic polymers (proton sponge effect) which cause influx and accumulation of Cl^- ions, and thus swelling and lysis of the vesicles, is likely to play a role [5,6]. While needed for translocation to the cytosol, cationic polymers are in general toxic, in particular those of high molecular weight [7,8]. Thus, the amount of cationic polymers in the polyplexes has to be chosen carefully in order to maximize transfection efficiency while minimizing cytotoxicity.

Apart from lipoplexes and polyplexes, colloids, such as nanoparticles [9,10], liposphere [11,12], and polymeric capsules [13,14] are currently being discussed as non-viral carriers for the delivery of genetic material. Polymeric capsules can be synthesized under mild conditions by a multilayer assembly of oppositely charged polyelectrolytes. These capsules possess tunable physicochemical properties that strongly depend on the material used for their synthesis. They can also be functionalized at two distinct positions, their wall and their cavity, with additional building blocks, such as inorganic nanoparticles, antibodies, drugs, analyte-sensitive fluorophores, *etc.* to create a multifunctional delivery system [15–17], and they are steadily internalized by mammalian cells *via* phagocytosis and lipid-raft-mediated macropinocytosis [18,19]. Polymeric capsules have already been used for several sensing and drug delivery applications [20–22] including DNA delivery [23,24]. However, there are only few reports on siRNA delivery [25,26]. The biggest advantage of these capsules compared to other non-viral carriers is their superior colloidal stability over time, loading capacity, and good biocompatibility [27]. Nevertheless, as for other carriers, off-target effects dependent on the capsules themselves cannot be excluded [25]. In addition, one general obstacle is that after uptake by cells capsules are located in the lysosome [19], and thus the delivered cargo is not readily available for cytosolic targets. Translocation of capsule-delivered cargo from the lysosomal compartments to the cytosol can either be achieved by biodegradable capsules [28] or by local heating which transiently opens the capsules and the surrounding lysosomal membranes [22,24,29]. In case of biodegradable capsules, translocation efficiency is not very high and in the case of local heating, relatively complicated set-ups are required, which in fact also reduce the percentage of successful translocation events.

In this study we thus attempted to combine the advantages of polyplexes and polyelectrolyte capsules for siRNA delivery. For this purpose, polyplexes formed by siRNA and PEI were encapsulated within multilayers of biodegradable polymers. By encapsulating PEI with the siRNA (in the form of polyplexes) several advantageous properties can be obtained: (i) reduction of the toxicity of PEI during transfection, as it is encapsulated until the walls of the capsules are degraded; (ii) facilitation of the lysosomal escape of the siRNA due to the proton sponge effect of PEI; (iii) inhibition of siRNA leakage from the capsule cavity as siRNA itself is a small molecule and could escape through the permeable walls, in contrast to the bigger PEI/siRNA complexes; (iv) increased stability of the polyplexes. By encapsulating the siRNA within the cavity of capsules it is protected from metabolizing enzymes, thus increasing its bioavailability and reducing the quantity needed to be administered. By using biodegradable polyelectrolytes for the capsules, a release of the siRNA is obtained inside the cells upon digestion of the capsule walls [28]. Taken together, the main idea is that the capsules add a controlled shield to the siRNA and the rather cytotoxic PEI. Outside the cells the PEI is encapsulated and thus assumed to be less toxic. Inside the cells, the PEI becomes effective in mediating endosomal escape once the capsule shell has been digested, thus favoring translocation of the siRNA to the cytosol. This concept is investigated in the present study. Within this work we show a systematic investigation involving quantification of siRNA loading of biodegradable capsules, the efficiency of *in vitro* intracellular delivery and release, and the cellular effect of siRNA. Transfection efficiency of the encapsulated polyplexes is compared to that of standard polyplexes.

2. Materials and methods

2.1. Fluorescent labeling and concentration determination of polyethylenimine (PEI)

The red fluorophore DY-651 (Dyomics, $\lambda_{excitation} = 656$ nm, $\lambda_{emission} = 678$ nm) or the green fluorophore fluorescein isothiocyanate (FITC, Sigma-Aldrich, $\lambda_{excitation} = 492$ nm, $\lambda_{emission} = 518$ nm) were linked as fluorescent labels to PEI (branched, 25 kDa, Sigma-Aldrich). All details can be found in the supporting information (SI). The PEI:dye ratio of the purified labeled PEI was determined *via* UV–Vis absorption spectroscopy. For Dy-651 we found a molar labeling ratio of PEI:Dy-651 = 1:10 and for FITC a ratio of PEI:FITC = 1:25. This ratio was found to be an optimal compromise between complexation of DNA/siRNA by PEI, fluorescence signal for tracking, and for the quantification of PEI. PEI quantification was achieved by using the ability of (primary) amino functionalities to form tetra-amino copper(II) complexes upon mixture with an aqueous $CuSO_4$ solution [30,31] (*cf.* SI).

2.2. Synthesis of PEI/siRNA and PEI/DNA polyplexes

siRNA (sequence: 5′- GAA CUU CAG GGU CAG CUU GCC G -3′) fluorescently labeled with Alexa Fluor-546 (AF-546, custom special order from Qiagen, $\lambda_{excitation} = 554$ nm, $\lambda_{emission} = 570$ nm) against the expression of GFP in GFP-expressing HeLa cells was complexed with PEI to form polyplexes. 40 μg/mL siRNA and 25 kDa PEI at a fixed nitrogen-to-phosphor-ratio (N/P-ratio) of 10 were mixed in an isotonic NaCl solution. After gently mixing, the solution was stored for 10–15 min at room temperature, before using the freshly prepared polyplexes in cell experiments [32]. As a model system for initial uptake studies, single-stranded DNA labeled with Cy5 with a random sequence of comparable length to siRNA was used to form PEI/DNA polyplexes. For all details we refer to the SI.

2.3. Synthesis of biodegradable capsules filled with polyplexes

Biodegradable capsules were fabricated by Layer-by-Layer (LbL) adsorption of the biodegradable polyelectrolytes dextran sulfate (DexS) and poly-L-arginine (pArg) onto spherical templates (Fig. 1) as published before [33]. Hereby, the $CaCO_3$ templates with PEI were precipitated from solutions of calcium chloride ($CaCl_2$) and sodium carbonate (Na_2CO_3) in the presence of PEI under vigorous stirring, leading to spherical $CaCO_3$ particles with an average diameter of 3.5 μm measured by an optical microscopy. Afterwards, siRNA (or ssDNA (30 bp)) was adsorbed on the PEI-filled $CaCO_3$ cores. Then, the $CaCO_3$ particles were coated by multiple LbL assembly of DexS and pArg in 0.5 M NaCl solutions with extensive washing in between the formation of the different layers. In this way, five polyelectrolyte

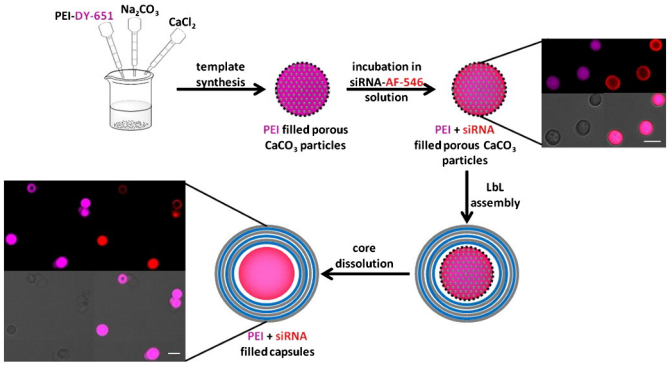

Fig. 1. Schematic representation of the synthesis of biodegradable capsules filled with PEI-DY-651 and siRNA-AF-546. The insets correspond to confocal laser scanning microscope images of the $CaCO_3$ loaded templates and the prepared biodegradable capsules comprising five double layers $(DexS/pArg)_5$ with encapsulated DY-651-labeled PEI and AF-546-labeled siRNA. The images correspond to the fluorescent signals of PEI (violet) and siRNA (red), the transmission channel, and the overlay of all channels. The scale bars represents 5 μm. The schematic representation is not drawn to scale.

bilayers were adsorbed on the PEI/siRNA-loaded $CaCO_3$ particles. Finally, the $CaCO_3$ template cores were removed by complexation of Ca^{2+} with ethylenediaminetetraacetic acid (EDTA) solution (0.2 M, pH 7), leaving the PEI and the siRNA inside the hollow polyelectrolyte walls. Afterwards, the PEI- and siRNA- (or DNA-) filled capsules were washed three times with Milli-Q water by repetitive centrifugation and sedimentation at 1100 rpm for 8 min. The resulting encapsulated polyplexes were stored as suspension in Milli-Q water at 4 °C. We assume an overall size of 3.5 μm as the polyelectrolyte layers do not significantly increase the size of the capsules [33]. The number of capsules per volume was determined by counting the capsules in a defined volume with a hemocytometer chamber under a microscope. Typically obtained amounts of capsules from one synthesis were around 10^8 capsules. For more details we refer to the SI. As control non-degradable capsules made of poly(sodium 4-styrenesulfonate) (PSS) and poly(allylamine hydrochloride) (PAH) were synthesized.

2.4. Determination of the amount of encapsulated PEI/siRNA and PEI/DNA per polymer capsule

UV–Vis absorption spectroscopy could not be used to quantify the amount of encapsulated PEI/siRNA and PEI/DNA due to the intrinsic scattering and absorption of the polymer capsules, which turned out to be much larger than the absorption originating from the fluorescently labeled PEI and fluorescently labeled siRNA. Therefore, the fluorescence emission of the labels of PEI and siRNA in the capsules was measured instead. Quantification was done based on previously recorded calibration curves, relating the fluorescence of DY-651 or FITC to the amount of PEI, and the fluorescence of AF-546 to the amount of siRNA (and the fluorescence of Cy5 to the amount of DNA). In order to make the obtained calibration universal, *i.e.* independent of the excitation intensity, the settings of the fluorescence spectrometer, *etc.*, all spectra were normalized to the Raman scattering peak of water, to so-called "raman units" [34]. The amount of capsules in solution was determined as described above by counting. More details are given in the SI.

2.5. Cell culture

GFP-expressing HeLa cells (HeLa-GFP, human cervical epithelial adenocarcinoma cells stably expressing the green fluorescent protein (GFP) [12]) were cultured at 37 °C in 5% CO_2 atmosphere. Cells were supplied with Eagle's Minimum Essential Medium (EMEM), supplemented with 10% fetal bovine serum (FBS) and 1% penicillin/streptomycin as additives. For transfection experiments with siRNA a total amount of $2 \cdot 10^4$ HeLa-GFP cells per cm^2 was seeded in 8-well μ-slide culture dishes purchased from Ibidi. Each well had an area of 1 cm^2 and was filled with 300 μL of medium. After seeding, the cells were stored in the incubator until adhesion (around 24 h for the used HeLa cells). For transfection with encapsulated polyplexes, the cells were incubated with 20 capsules per seeded cell. For transfection with plain PEI/siRNA polyplexes, the culture medium was first exchanged (after cell adhesion) for medium without FBS, followed by a subsequent exchange with complete growth medium again after 22 h. This step was done according to standard transfection protocols. In a control experiment (*cf.*SI) it is demonstrated that the presence or absence of serum had no effect on the release and effect of PEI/siRNA in the case of encapsulated PEI/siRNA polyplexes. Thus, transfection with encapsulated polyplexes and plain polyplexes could be directly compared according to the amount of PEI/siRNA added to the cells. The used concentrations are enlisted in Table 1. For uptake studies of PEI/DNA polyplexes (plain and encapsulated), non-transfected MDA-MB-231 cells were used. We refer to the SI for all details. Cytotoxicity assays were performed with HeLa-GFP cells using a standard resazurin assay (details can be found in the SI).

2.6. Quantification of the intracellular siRNA delivery and GFP silencing

After incubation with polyplexes or encapsulated polyplexes, the cells were imaged either with a confocal laser scanning microscope (CLSM; LSM 510 Meta, Zeiss) or with a fluorescence widefield microscope (Axiovert 200 M, Zeiss). Images were taken at different points in time from 0 to 50–70 h and the integrated fluorescence intensity was measured, *i.e.* the area of the cells times the mean fluorescence intensity. In delivery studies, the amount of released PEI/DNA from polyplexes and encapsulated polyplexes was compared in terms of DNA fluorescence (Cy5 label of DNA). In GFP-silencing studies, the reduction in GFP fluorescence intensity upon delivery of PEI/siRNA by polyplexes or encapsulated polyplexes was compared in terms of GFP fluorescence. Details can be found in the SI.

3. Results and discussion

3.1. Determination of polyplex concentrations

PEI/siRNA and PEI/DNA polyplexes were efficiently synthesized according to previously published protocols [35]. The polyplexes were used as prepared or were encapsulated within polyelectrolyte multilayer capsules by use of the LbL technique. Some loss of PEI and siRNA (or DNA) had to be accounted for during the LbL assembly procedure and in particular upon dissolution of the template core. Furthermore, depending on the polymer used for the formation of the capsule walls, the porosity changes [36] and thus, additional loss of PEI and siRNA (or DNA) is likely to occur. Leaching of cargo is a general problem of LbL encapsulation, as has been reported also for other cargo [37]. While for many applications the amount of encapsulated cargo is not crucial, here the amount of encapsulated PEI and siRNA (or DNA) needs to be known exactly, as otherwise delivery of plain *versus* encapsulated PEI/DNA polyplexes, and therefore gene silencing by plain *versus* encapsulated PEI/siRNA polyplexes, cannot be compared. In other words, because in transfection experiments the amount of delivered material is crucial for estimation of the transfection efficiency, the concentrations of encapsulated material must be determined precisely [30]. Often, the amount of encapsulated cargo is determined by subtracting the amount of cargo found in the supernatant after the encapsulation from the amount of cargo, which had been added initially [37]. However, this method can be quite inaccurate, in particular because pooled supernatants from all purification steps need to be considered. An alternative method frequently used in literature is concentration determination *via* UV–Vis absorption spectroscopy. As PEI does not have a distinct intrinsic absorption peak, a characteristic peak can be generated by the formation of PEI–copper-complexes mediated

Table 1
Amounts and concentrations of siRNA and PEI. M_w is the molecular weight, and m_{caps} and m_{dish} the mass of siRNA or PEI per capsule and per culture dish (well), respectively. Hereby, 20 capsules were added per cell and $2 \cdot 10^4$ cells had been seeded per dish: $m_{dish} = m_{caps} \times 40 \times 2 \times 10^4$. Note that rounded values are given. V_{dish} is the volume of the cell culture medium in each culture dish. Thus, the concentration of siRNA and PEI in solution is $c_{dish} = \frac{m_{dish}}{M_W \cdot V_{dish}}$.

	M_w (g/mol)	m_{caps} [pg] (*per* capsule)	m_{dish} [ng] (*per* culture dish)	V_{dish} [μL]	c_{dish} [nM]
siRNA	8187	0.016	6.4	300	2.60
PEI	25,000	6.250	25	300	3.33

by the amino groups of PEI [31]. However, this method bears some limitations; upon encapsulation of polyplexes, scattering and absorption of the capsule walls dominate, and thus make the identification of the PEI–copper-complex absorption peaks complicated. Furthermore, due to the use of pArg, the walls of the capsules contain amino groups as well, and thus also provide a signal at the PEI–copper-complex absorption peak. PEI/siRNA polyplexes are often quantified in terms of (N/P)-ratios, where the nitrogen and phosphor concentration corresponds to the amount of PEI (which contains amino groups) and the amount of siRNA (which contains phosphor in the phosphate group of its backbone), respectively. However, as also the walls of the capsules contain nitrogen due to the amino groups of pArg, this method is not well suited for determining the amount of encapsulated polyplexes. To this end, we used fluorescently labeled PEI (FITC or DY-651) and fluorescently labeled siRNA (AF-546) or DNA (Cy5). The amount of fluorophore per PEI was determined *via* UV–Vis absorption spectroscopy with PEI-copper-complexes (*cf.* the SI). siRNA and DNA were purchased with fluorescent label and we assume 100% labeling efficiency, *i.e.* one fluorophore *per* siRNA and DNA molecule, respectively. As the autofluorescence of the capsule walls in the spectral range from green to red is much lower than that of the fluorescent labels FITC, AF-546, DY-651, and Cy5 fluorescence of the capsule walls can be neglected. Therefore, fluorescence measurements allow direct concentration determination both for PEI and siRNA (or DNA). As concentration determination is paramount but error-prone, as described above, all experimental details, such as the used calibration curves are provided in the SI. At any rate, absolute concentrations always have to be considered with care, which often is not done critically enough. Our data yielded an average mass of $1.6 \cdot 10^{-8}$ μg siRNA and $625 \cdot 10^{-8}$ μg of PEI *per* capsule (*cf.* Table 1).

3.2. Quantification of PEI/DNA delivery to cells in free and encapsulated form

Fluorescent labels of the cargo (PEI, DNA or siRNA) allowed us not only to quantify the amount of PEI and DNA (or siRNA) in each pharmaceutical form but also to quantify its release within the cells. First, the kinetics of cellular uptake and release were evaluated. A comparative study of free DNA, PEI/DNA polyplexes, PEI/DNA polyplexes encapsulated in biodegradable $(DexS/pArg)_5$ capsules, and PEI/DNA polyplexes encapsulated in non-degradable $(PSS/PAH)_5$ capsules was done. It is worth noting that the uptake of these capsules by a huge variety of eukaryotic cells has been extensively demonstrated [19,20,26]. DNA was used instead of siRNA for these experiments as only delivery and not transfection was investigated here and DNA is cheaper and easier to handle than siRNA. For this reason, no transfected cells were required for these experiments and thus a standard cell line used in our laboratory, MDA-MB-231, was used. The experiments were done both with serum-free (following standard transfection protocols) and serum-supplemented medium. Images were taken after different incubation times (Fig. 2). The amount of PEI and DNA released to the cytosol was then determined. Cargo remaining trapped in the capsules was not considered for this evaluation (details can be found in the SI). The integrated fluorescence intensities I(t) after different times of incubation, which are assumed to be proportional to the amount of PEI or DNA released to the cytosol, are presented in Fig. 3.

As can be seen from Figs. 2 and 3, no DNA could be detected inside the cytosol in case of administration of free DNA or PEI/DNA polyplexes at the used concentrations. Capsules, in contrast, were clearly incorporated by cells. Both for the biodegradable and the non-degradable capsules some release of PEI to the cytosol could be observed. The release of DNA from the capsules to the cytosol was only significant for the biodegradable capsules, *cf.* Figs. 2 and 3, which is in line with previous observations for the delivery of other types of cargo [28]. In this cited work the use of biodegradable capsules to release cargo to the cytosol, while maintaining cell viability and cargo integrity, and the kinetics of release were shown. The incubation was first performed in absence of serum following standard transfection protocols. This, however, is a limitation as the cells suffer from stress when incubated under serum-free conditions. In order to see if our carrier could help overcoming this limitation, we also performed the experiments under normal physiological conditions, *i.e.* in the presence of serum (10% FBS). As seen in Fig. 3, the release from biodegradable capsules is even higher with serum compared to serum-free conditions. Thus, our data indicate that by using biodegradable capsules as carriers for the polyplexes an effective DNA release can be achieved even in the presence of serum and the carrier protects the genetic material against possible degradation. In particular, more DNA was released to the cytosol from encapsulated PEI/DNA polyplexes (biodegradable polyelectrolytes) compared to free PEI/DNA polyplexes. Furthermore, the release occurs relatively fast, within less than one day of incubation.

3.3. Quantification of gene silencing upon delivery of PEI/siRNA in free and encapsulated form

While encapsulation of polyplexes in biodegradable polyelectrolyte shells improved the delivery efficiency of oligonucleotides to the cytosol (*cf.* Fig. 3), these data do not give any information about the biological activity of the delivered oligonucleotides. We thus used, in a next step, siRNA instead of DNA and stably GFP-transfected HeLa cells. Biological activity of the chosen siRNA sequence was demonstrated by GFP

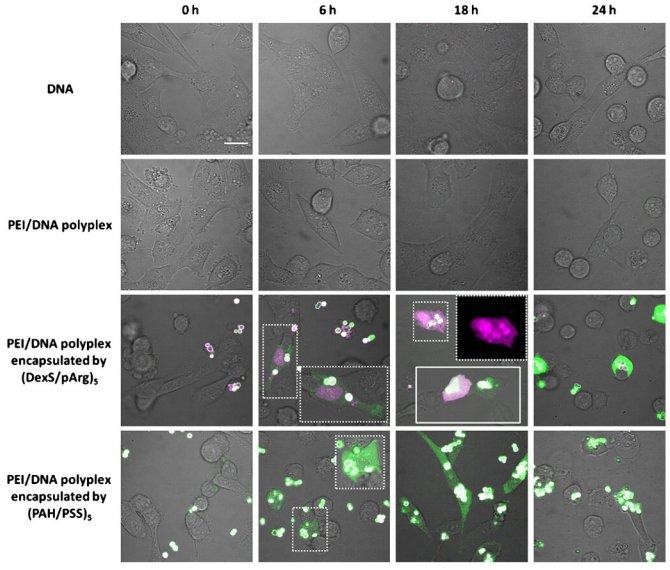

Fig. 2. MDA-MB-231 cells were incubated with free DNA, DNA/PEI polyplexes, biodegradable $(DexS/pArg)_5$ capsules with embedded PEI/DNA, and non-degradable $(PSS/PAH)_5$ capsules with embedded PEI/DNA at equal concentrations of genetic material. After different incubation times t, as indicated in the top panel, cells were imaged. The transmission channel shows the cells, and the green and violet (false color) channels show the emission of the FITC labels and Cy5 labels of PEI and DNA, respectively. Insets with dashed outlines show the release profile of DNA or PEI mediated by the capsules. Images from serum-free experiments are shown. The scale bar corresponds to 20 μm.

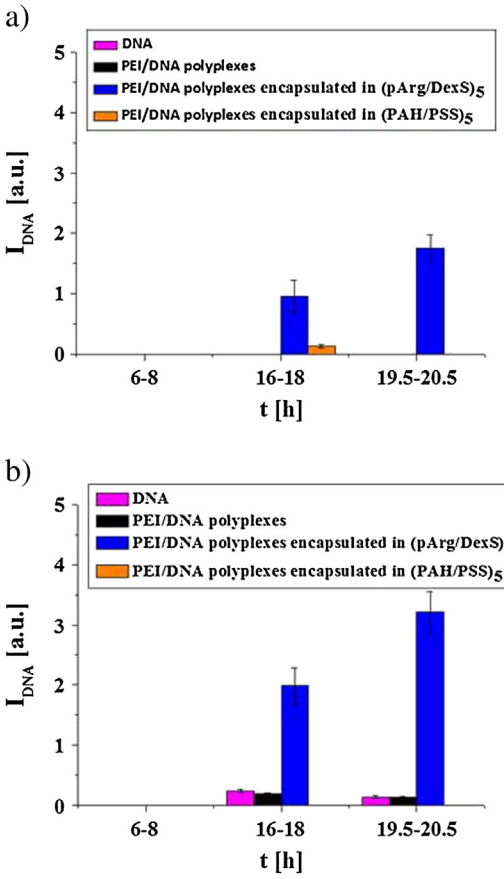

Fig. 3. From the microscopy data, as presented in Fig. 2, for each cell in each recorded image the integrated fluorescence intensity I_{DNA} was determined. The integrated fluorescence intensity corresponds to the area of the cell (determined from the transmission channel) times the mean fluorescence intensity from the Cy5 (DNA) channel in that area. Note, that fluorescence originating from the capsules was not considered, but only fluorescence located in the cytosol. The mean fluorescence intensities, as observed for the different means of delivery, are displayed for incubation in a) serum-free and in b) serum-containing media together with the corresponding standard deviations. For each data point at least 30 cells were analyzed.

silencing. Besides transmission, three fluorescence channels were recorded (false colors: green: GFP, red: AF-546 label of siRNA, violet: DY-651 label of PEI), *cf.* Fig. 4. Incubation of cells was done with $6.4 \cdot 10^{-3}$ μg of siRNA and $25 \cdot 10^{-3}$ μg of PEI for capsules and $10 \cdot 10^{-3}$ μg of siRNA and $12.5 \cdot 10^{-3}$ μg of PEI for polyplexes. In Fig. 4 no reduction of GFP fluorescence can be observed upon addition of PEI/siRNA polyplexes, though an effect was observed at higher polyplex concentrations (data can be found in the SI). In contrast, a reduction of GFP fluorescence could be observed upon incubation with encapsulated PEI/siRNA (biodegradable polymers) (see cells labeled with an asterisk in Fig. 4).

Quantitative evaluation turned out to be complicated due to the fact that cells are "individuals". Though stably transfected, the GFP fluorescence intensity was in general significantly different for each cell within one cell culture (more examples in the SI). However, the fluorescence intensity did not fluctuate within the same cell over time, though naturally after cell division the fluorescence was slightly altered in a cell-dependent manner. In order to obtain a quantitative analysis, the effect of siRNA on the GFP expression was quantified on the level of individual cells and not as average over the cell culture. This way of analysis decreased the statistics, as fewer cells could be evaluated, but it increased the reliability of the results, as they were no longer susceptible to intrinsic fluctuations. Quantitative analysis in the form of integrated fluorescence intensities I_{GFP} of expressed GFP demonstrated that polyplexes encapsulated within biodegradable polymers effectively

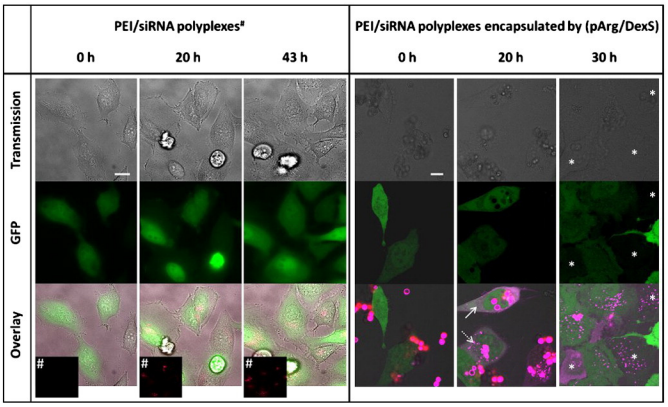

Fig. 4. GFP expressing HeLa cells were incubated with free (left column) and encapsulated ($(DexS/pArg)_5$, right column) PEI/siRNA polyplexes. Live images of the same cells were taken over time t. Besides the transmission channel showing the cells, also GFP (green), AF-546 labeled siRNA (red), and DY-651 labeled PEI (violet) are displayed in false colors. The straight arrow indicates a homogenous cytosolic distribution of PEI, whereas the dashed arrow shows a punctuate distribution. Cells marked with asterisks (*) have clearly lost their GFP fluorescence. The insets (#) correspond to images of the polyplexes. For clarity these insets were enhanced in contrast in order to show the presence of the siRNA inside the cells. The scale bars correspond to 10 μm.

knocked down the GFP expression in a time-dependent manner, *cf.* Fig. 5. The inhibition of GFP expression hereby showed a kind of sigmoidal time dependence (*cf.* Fig. 5) in contrast to other carriers that show a more linear effect [12] or polyplexes containing a higher amount of siRNA (*cf.* SI). These results indicate that inhibition by siRNA encapsulated within polyelectrolyte capsules is dependent on the carrier, as it clearly influences the mechanism of release of the siRNA cargo and its availability to the cell.

Within the first day, I_{GFP} remained unaffected, but after one day of incubation the GFP expression was significantly blocked and I_{GFP} decreased rapidly, reaching a level of minimum GFP expression. These results indicate that the released siRNA from encapsulated polyplexes could perform its action, *i.e.* interaction with the mRNA and inhibition of translation, already after 30 h, which is remarkably fast in comparison to the effect caused by plain polyplexes or other common methods that require around 48 h to make the siRNA available to perform its action [12,38] (*cf.* SI). This is in line with the work of others [25]. The total amount of siRNA delivered to the cells with biodegradable capsules necessary to cause down regulation of protein expression is clearly below the total required amount of siRNA delivered to the cells when using

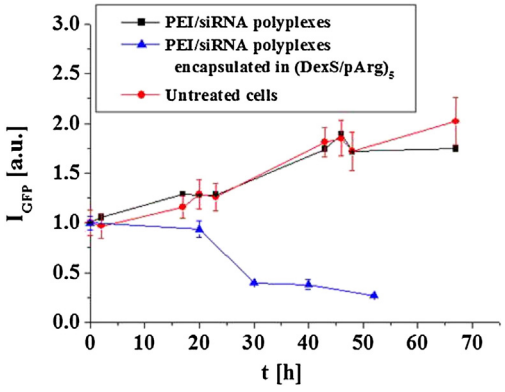

Fig. 5. GFP-expressing HeLa cells were incubated with free (black squares) or encapsulated (within biodegradable capsules; blue triangles) PEI/siRNA polyplexes. The total amount of siRNA and PEI was $6.4 \cdot 10^{-3}$ μg and $25 \cdot 10^{-3}$ μg for capsules and $10 \cdot 10^{-3}$ μg and $12.5 \cdot 10^{-3}$ μg for polyplexes, respectively. Images were taken at different points in time t (*cf.* Fig. 4) and the mean integrated fluorescence density of GFP, *i.e.* the area of each cell times its mean fluorescence intensity, is displayed. Error bars represent standard deviations of the mean.

commercial transfection agents. In our study we needed 2.6 nM siRNA (*cf.* Table 1), whereas the amount required for successful transfection with one of these agents lies around 100 nM [39].

3.4. Quantification of induced toxicity of free versus encapsulated PEI

Due to the concentration-dependent toxicity reported for PEI in polyplexes [40], the amount of PEI has to be controlled carefully to avoid harmful effects. The idea therefore was to protect the cells from the toxic effects of PEI by encapsulation. To test this hypothesis, a resazurin-based viability assay was used. In Fig. 6 concentration-dependent cytotoxic effects of free and encapsulated PEI are compared.

For free PEI the LD_{50} value was (0.80 ± 0.02) μg. When PEI was encapsulated in biodegradable capsules, the viability of the cells was far less affected than by non-encapsulated PEI. 20 capsules per cell, which was the amount added for experiments (*cf.* Fig. 4) corresponds to a value of $0.188 \cdot 10^{-3}$ μg PEI, which is in the non-toxic range. Note that this number is different from the one in Table 1 as for cytotoxicity studies 15,000 instead of 20,000 cells were seeded in each well. Thus, by encapsulating the PEI/siRNA polyplexes within the cavity of polyelectrolyte capsules, the viability of the cells was preserved while allowing an efficient delivery and cellular action. This was probably due to the fact that upon encapsulation much less PEI and siRNA had to be used to achieve transfection.

4. Conclusions

We demonstrate that PEI/siRNA polyplexes can be encapsulated within biodegradable polymer capsules and that due to encapsulation release inside cells and *in vitro* transfection efficiencies of siRNA are higher compared to non-encapsulated polyplexes. The stability of the PEI/siRNA polyplexes against undesired degradation and the viability of the cells are preserved by adding a physical barrier in form of the capsules in between the cells and the cargo. Since this polymeric barrier is degraded only in the lysosomes of the cells, an effective cargo release is ensured. Delivery works both for serum-containing and serum-free cell culture conditions. Cytosolic release of cargo mediated by these capsules without an external trigger could be proven. The biodegradable capsule shell and the PEI made the siRNA to be released to the cytosol. Indeed, the efficacy of siRNA was increased (gene silencing was observed already after 20 h) while PEI-derived toxicity was reduced. Thus, we demonstrated that biodegradable capsules with integrated PEI constitute an alternative to viral carriers for efficient delivery and *in vitro* transfection of genetic material.

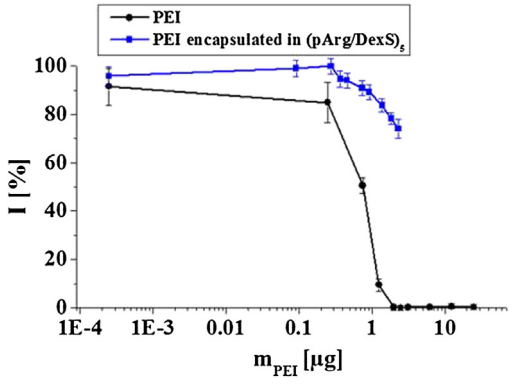

Fig. 6. Reduction of cell viability caused by encapsulated and non-encapsulated PEI. The normalized cell viability in terms of resazurin fluorescence intensity I *versus* the amount of added PEI m_{PEI} is displayed. The average of six (PEI capsules) and three (PEI solution) independent measurements is displayed. Higher amounts of encapsulated PEI could not be measured due to the impossibility to obtain a more saturated capsule solution. Furthermore, there is a threshold at which the capsules themselves can induce toxicity if added in too high quantities to the cells [27]. Error bars represent standard deviations of the mean.

Acknowledgments

GFP-expressing HeLa cells were a gift of Dr. Christian Plank and are described in previous publications [12]. This work was supported by LOEWE (grant Synbiochem to WJP).

Appendix A. Supplementary data

Supplementary data to this article can be found online at http://dx.doi.org/10.1016/j.jconrel.2014.10.006.

References

[1] S. Han, R.I. Mahato, Y.K. Sung, S.W. Kim, Development of biomaterials for gene therapy, Mol. Ther. 2 (2000) 302–317.
[2] D. Liu, T. Ren, X. Gao, Cationic transfection lipids, Curr. Med. Chem. 10 (2003) 1307–1315.
[3] A. Zintchenko, A. Philipp, A. Dehshahri, E. Wagner, Simple modifications of branched PEI lead to highly efficient siRNA carriers with low toxicity, Bioconjug. Chem. 19 (2008) 1448–1455.
[4] P. Pereira, A.F. Jorge, R. Martins, A. Pais, F. Sousa, A. Figueiras, Characterization of polyplexes involving small RNA, J. Colloid Interface Sci. 387 (2012) 84–94.
[5] A. Akinc, M. Thomas, A.M. Klibanov, R. Langer, Exploring polyethylenimine-mediated DNA transfection and the proton sponge hypothesis, J. Gene Med. 7 (2005) 657–663.
[6] G. Creusat, A.S. Rinaldi, E. Weiss, R. Elbaghdadi, J.S. Remy, R. Mulherkar, G. Zuber, Proton sponge trick for pH-sensitive disassembly of polyethylenimine-based siRNA delivery systems, Bioconjug. Chem. 21 (2010) 994–1002.
[7] M. Breunig, U. Lungwitz, J. Klar, A. Kurtz, T. Blunk, A. Goepferich, Polyplexes of polyethylenimine and per-N-methylated polyethylenimine-cytotoxicity and transfection efficiency, J. Nanosci. Nanotechnol. 4 (2004) 512–520.
[8] A.C. Hunter, S.M. Moghimi, Cationic carriers of genetic material and cell death: a mitochondrial tale, BBA Bioenerg. 1797 (2010) 1203–1209.
[9] J. Conde, A. Ambrosone, V. Sanz, Y. Hernandez, V. Marchesano, F.R. Tian, H. Child, C.C. Berry, M.R. Ibarra, P.V. Baptista, C. Tortiglione, J.M. de la Fuente, Design of multifunctional gold nanoparticles for *in vitro* and *in vivo* gene silencing, ACS Nano 6 (2012) 8316–8324.
[10] N. Nafee, S. Taetz, M. Schneider, U.F. Schaefer, C.M. Lehr, Chitosan-coated PLGA nanoparticles for DNA/RNA delivery: effect of the formulation parameters on complexation and transfection of antisense oligonucleotides, Nanomedicine 3 (2007) 173–183.
[11] D. Vlaskou, O. Mykhaylyk, F. Krotz, N. Hellwig, R. Renner, U. Schillinger, B. Gleich, A. Heidsieck, G. Schmitz, K. Hensel, C. Plank, Magnetic and acoustically active lipospheres for magnetically targeted nucleic acid delivery, Adv. Funct. Mater. 20 (2010) 3881–3894.
[12] P. del Pino, A. Munoz-Javier, D. Vlaskou, P. Rivera Gil, C. Plank, W.J. Parak, Gene silencing mediated by magnetic lipospheres tagged with small interfering RNA, Nano Lett. 10 (2010) 3914–3921.
[13] A.N. Zelikin, A.L. Becker, A.P.R. Johnston, K.L. Wark, F. Turatti, F. Caruso, A general approach for DNA encapsulation in degradable polymer microcapsules, ACS Nano 1 (2007) 63–69.
[14] A.P.R. Johnston, G.K. Such, S.L. Ng, F. Caruso, Challenges facing colloidal delivery systems: from synthesis to the clinic, Curr. Opin. Colloid Interface Sci. 16 (2011) 171–181.
[15] P. Rivera Gil, L.L. del Mercato, P. del Pino, A. Muñoz-Javier, W.J. Parak, Nanoparticle-modified polyelectrolyte capsules, Nano Today 3 (2008) 12–21.
[16] L.L. del Mercato, P. Rivera Gil, A.Z. Abbasi, M. Ochs, C. Ganas, I. Zins, C. Sönnichsen, W.J. Parak, LbL multilayer capsules: recent progress and future outlook for their use in life sciences, Nanoscale 2 (2010) 458–467.
[17] M.L. De Temmerman, J. Demeester, S. De Smedt, I. Rejman, Tailoring layer-by-layer capsules for biomedical applications, Nanomedicine (UK) 7 (2012) 771–788.
[18] A. Muñoz Javier, O. Kreft, M. Semmling, S. Kempter, A.G. Skirtach, O. Bruns, P.d. Pino, M.F. Bedard, J. Rädler, J. Käs, C. Plank, G. Sukhorukov, W.J. Parak, Uptake of colloidal polyelectrolyte coated particles and polyelectrolyte multilayer capsules by living cells, Adv. Mater. 20 (2008) 4281–4287.
[19] L. Kastl, D. Sasse, V. Wulf, R. Hartmann, J. Mircheski, C. Ranke, S. Carregal-Romero, J.A. Martínez-López, R. Fernández-Chacón, W.J. Parak, H.-P. Elsaesser, P. Rivera Gil, Multiple internalization pathways of polyelectrolyte multilayer capsules into mammalian cells, ACS Nano 7 (2013) 6605–6618.
[20] S. De Koker, B.G. De Geest, S.K. Singh, R. De Rycke, T. Naessens, Y. Van Kooyk, J. Demeester, S.C. De Smedt, J. Grooten, Polyelectrolyte microcapsules as antigen delivery vehicles to dendritic cells: uptake, processing, and cross-presentation of encapsulated antigens, Angew. Chem. Int. Ed. 48 (2009) 8485–8489.
[21] P. Rivera Gil, M. Nazarenus, S. Ashraf, W.J. Parak, pH sensitive capsules as intracellular optical reporters for monitoring lysosomal pH changes upon stimulation, Small 8 (2012) 943–948.
[22] S. Carregal-Romero, M. Ochs, P. Rivera Gil, C. Ganas, A.M. Pavlov, G.B. Sukhorukov, W.J. Parak, NIR-light triggered delivery of macromolecules into the cytosol, J. Control. Release 159 (2012) 120–127.
[23] H. Lomas, A.P.R. Johnston, G.K. Such, Z.Y. Zhu, K. Liang, M.P. van Koeverden, S. Alongkornchotikul, F. Caruso, Polymersome-loaded capsules for controlled release of DNA, Small 7 (2011) 2109–2119.

[24] M. Ochs, S. Carregal-Romero, J. Rejman, K. Braeckmans, S.C. De Smedt, W.J. Parak, Light-addressable capsules as caged compound matrix for controlled *in vitro* release, Angew. Chem. Int. Ed. 52 (2013) 695–699.
[25] A.L. Becker, N.I. Orlotti, M. Folini, F. Cavalieri, A.N. Zelikin, A.P.R. Johnston, N. Zaffaroni, F. Caruso, Redox-active polymer microcapsules for the delivery of a survivin-specific siRNA in prostate cancer cells, ACS Nano 5 (2011) 1335–1344.
[26] J. Ruesing, O. Rotan, Gross-Heitfeld, C. Mayer, M. Epple, Nanocapsules of a cationic polyelectrolyte and nucleic acid for efficient cellular uptake and gene transfer, J. Mater. Chem. B 2 (2014) 4625–4630.
[27] C. Kirchner, A.M. Javier, A.S. Susha, A.L. Rogach, O. Kreft, G.B. Sukhorukov, W.J. Parak, Cytotoxicity of nanoparticle-loaded polymer capsules, Talanta 67 (2005) 486–491.
[28] P. Rivera_Gil, S.D. Koker, B.G. De Geest, W.J. Parak, Intracellular processing of proteins mediated by biodegradable polyelectrolyte capsules, Nano Lett. 9 (2009) 4398–4402.
[29] R. Palankar, A.G. Skirtach, O. Kreft, M. Bedard, M. Garstka, K. Gould, H. Mohwald, G.B. Sukhorukov, M. Winterhalter, S. Springer, Controlled intracellular release of peptides from microcapsules enhances antigen presentation on MHC class I molecules, Small 5 (2009) 2168–2176.
[30] F. Ungaro, G. De Rosa, A. Miro, F. Quaglia, Spectrophotometric determination of polyethylenimine in the presence of an oligonucleotide for the characterization of controlled release formulations, J. Pharm. Biomed. Anal. 31 (1967) 143–149.
[31] T.D. Perrine, W.R. Landis, Analysis of polyethylenimine by spectrophotometry of its copper chelate, J. Polym. Sci. A1 5 (1967) 1993–2003.
[32] O.M. Merkel, A. Beyerle, D. Librizzi, A. Pfestroff, T.M. Behr, B. Sproat, P.J. Barth, T. Kissel, Nonviral siRNA delivery to the lung: investigation of PEG–PEI polyplexes and their *in vivo* performance, Mol. Pharm. 6 (2009) 1246–1260.
[33] G.B. Sukhorukov, E. Donath, S. Davis, H. Lichtenfeld, F. Caruso, V.I. Popov, H. Möhwald, Stepwise polyelectrolyte assembly on particle surfaces: a novel approach to colloid design, Polym. Adv. Technol. 9 (1998) 759–767.
[34] A.J. Lawaetz, C.A. Stedmon, Fluorescence intensity calibration using the Raman scatter peak of water, Appl. Spectrosc. 63 (2009) 936–940.
[35] A. Beyerle, A. Braun, O. Merkel, F. Koch, T. Kissel, T. Stoeger, Comparative *in vivo* study of poly(ethylene imine)/siRNA complexes for pulmonary delivery in mice, J. Control. Release 151 (2011) 51–56.
[36] A. Kolbe, L.L. del Mercato, A.Z. Abassi, P. Rivera Gil, S.J. Gorzini, W.H.C. Huibers, B. Poolman, W.J. Parak, A. Herrmann, De novo design of supercharged, unfolded protein polymers, and their assembly into supramolecular aggregates, Macromol. Rapid Commun. 32 (2011) 186–190.
[37] L.L. del Mercato, A.Z. Abbasi, W.J. Parak, Synthesis and characterization of ratiometric ion-sensitive polyelectrolyte capsules, Small 7 (2011) 351–363.
[38] X.P. Liu, G.S. Wang, Z.C. You, P. Qian, H.P. Chen, Y. Dou, Z.H. Wei, Y. Chen, C.D. Mao, J.X. Zhang, Inhibition of hypoxia-induced proliferation of pulmonary arterial smooth muscle cells by a mTOR siRNA-loaded cyclodextrin nanovector, Biomaterials 35 (2014) 4401–4416.
[39] Invitrogen, Stealth™/siRNA Transfection Protocol Lipofectamine® 2000, http://www.lifetechnologies.com/de/de/home/references/protocols/cell-culture/transfection-protocol/stealth-sirna-transfection-lipofectamine.html 2006 (last accessed 08 May 2014).
[40] O.M. Merkel, A. Beyerle, B.M. Beckmann, M.Y. Zheng, R.K. Hartmann, T. Stoger, T.H. Kissel, Polymer-related off-target effects in non-viral siRNA delivery, Biomaterials 32 (2011) 2388–2398.

Polymer capsules as theragnostic delivery and analysis vehicle for universal *in vitro* screening assays in the case of lysosomal storage diseases

Moritz Nazarenus[1], Maria-Eugenia López Sánchez[2], Natalia García Aranda[2], Ibane Abasolo[2], Joanna Rejman[1], Pilar Rivera Gil[1#], Wolfgang J. Parak[1,3#]

[1]Fachbereich Physik, Philipps-Universität Marburg, Marburg, Germany
[2]Institut de Recerca, Vall d'Hebron Hospital, Barcelona, Spain
[3]CIC Biomagune, San Sebastian, Spain
[#]corresponding authors: pilar.rivera@urv.cat, wolfgang.parak@physik.uni-marburg.de

Abstract:

Lysosomal storage disorders are diseases where proteins in the lysosomes of certain cells are not sufficiently expressed due to a gene defect. The defect leads to accumulation of toxic metabolites in the cells. Here, we take advantage of the natural endocytotic uptake route of polymer capsules, which are finally localized inside the lysosomes. For diagnostics, we monitored the lysosomal pH with polymer capsules in oligodendritic cells upon accumulation of the metabolite psychosine. We found different results for cells expressing the enzyme and knockout cells deficient of the enzyme. For therapy, we utilized biodegradable capsules to deliver the missing enzyme to the lysosomes of the cells and found that the adverse effects of psychosine could be prevented in enzyme-deficient cells. In a cell model for Fabry disease, we used biodegradable capsules to deliver the deficient enzyme to the cells and determined the intracellular efficacy based on the degradation of a fluorescently labeled substrate of the enzyme.

Introduction:

Particulate delivery vehicles such as colloidal nano- and microparticles offer the possibility to combine different functionalities within one vehicle [1-4]. Concerning theragnostics, this allows for example combining delivery with sensing in one single carrier. Sensing is meant as *in situ* analysis of the local effect of the delivered molecules, and thus immediate feedback of the caused action upon delivery would be obtained. However, one general problem with particle-based delivery vehicles is their biodistribution. In case of intravenous injection, like most pharmaceutical agents, a large fraction of the particles end up in the liver [5] and show the general problems of specific targeting. Nevertheless, a significant difference exists concerning intracellular distribution. While some classical pharmaceutical agents can diffuse through the plasma membrane of cells, particles are in general internalized *via* endocytosis, and subsequently are located in endosomal / lysosomal compartments rather than the cytosol [6]. In case delivery to the cytosol is required, methods for translocation of particles from endosomal / lysosomal compartments to the cytosol exist [7, 8]. Unfortunately, in most cases such translocation suffers either from relatively low yields, or involves cytotoxic effects. In contrast, one may think of applications, in which delivery of particles to the endosome or the lysosome would be beneficial.

Lysosomal storage disorders are caused by malfunctions of lysosomal proteins, typically enzymes, which result in lysosomal accumulation of undegraded metabolites [9, 10]. This class of diseases involves, for example, sphingolipidoses [9], in which missing enzymes cause

increased levels of sphingolipids, such as psychosine or globotriaosylceramide, as those are not sufficiently catabolized [11]. Sphingolipids are expressed in the membrane of cells for the purpose of stabilization, protection, and recognition sites for specific chemicals, as well as for signaling purposes. In order to regulate their concentration, catabolizing enzymes exist. They typically remove sugar molecules from the lipid part upon hydrolyzation. Galactocerebrosidase (galactosylceramidase, GALC), for example, is an enzyme which cleaves galactose from psychosine (galactosylphingosine), leading to sphingosine (2-amino-4-octadecene-1,3-diol), *cf.* Figure 1a. Insufficient levels of GALC are associated with Krabbe disease. As another example, α-galactosidase A (GLA) cleaves galactose from globotriaosylceramide (ceramide trihexoside, CD77, Gb3) leading to lactosylceramide, *cf.* Figure 1b. Lack of GLA has been associated with Fabry disease. The enzymes (*e.g.* GALC, GLA) hereby are located in the cellular lysosome, as otherwise they could digest the important sphingolipids in an uncontrolled way. As pointed out, if these enzymes are not sufficiently present in the lysosome, or in case they are defective, which is often associated with genetic mutation, the concentration of certain sphingolipids rises to harmful levels, ultimately leading to sphingolipidoses, *e.g.* Krabbe or Fabry disease. One possibility to treat such diseases is enzyme replacement therapy [12], which involves the delivery of the defective enzymes to the lysosome [13]. GLA, for example, can be brought to the lysosome directly *via* endocytotic uptake [14, 15], or by gene therapy *via* a viral vector encoding for GLA [16].

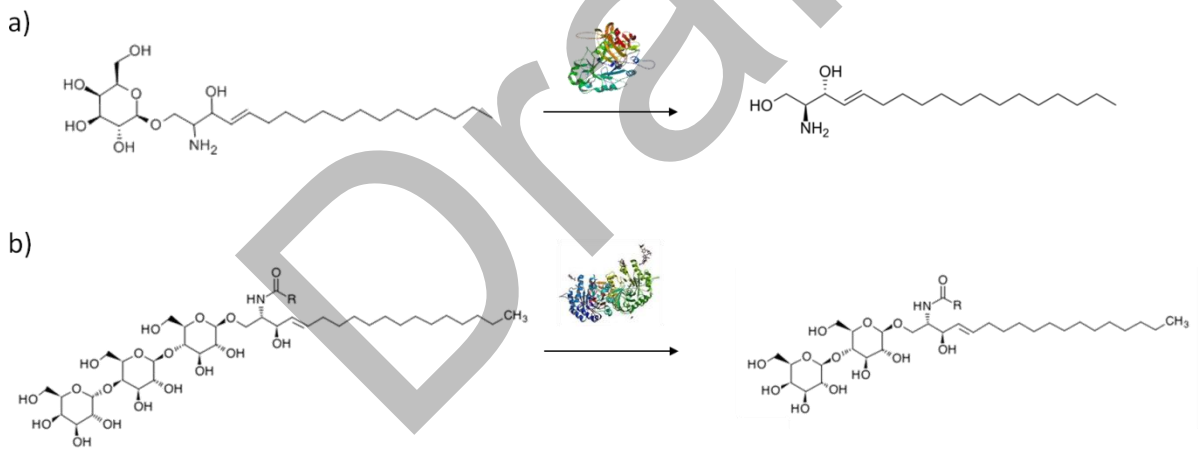

Figure 1: a) Galactocerebrosidase converts psychosine to sphingosine. b) α-galactosidase A converts globotriaosylceramide to lactosylceramide.

Particle-based delivery of enzymes may in particular be interesting in the case of lysosomal storage diseases as they naturally target the lysosome and allow for combination with other functionalities, such as in the context of sensing. In this work, polyelectrolyte capsules are discussed in this context. Such capsules posses the geometry of ping-pong balls, with a large cavity in the size of microns, and very thin polymer walls (a few nanometer), which are synthesized by layer-by-layer assembly [17]. The cavity can be used as reservoir for delivery of different types of molecules [18], such as proteins [19]. In *in vitro* models, capsules are readily endocytosed by many cell lines [20, 21], and are ultimately located in the cellular lysosome [22]. In case of protein delivery by biodegradable capsules [23, 24], the proteins will be directly present in the lysosome after endocytotic uptake and degradation of the capsules in the lysosome. It is important to be aware that the lysosome is filled with proteases, which can

digest certain proteins enzymatically [24]. In addition to using capsules as delivery vehicle of proteins to the lysosomes, they also can be used as platforms for optical sensing. Ion-sensitive fluorophores integrated into non-degradable capsules allow for monitoring lysosomal concentrations of specific ions [25]. Detection of local pH values is an important example in this direction [26, 27]. Impairment of cellular viability upon exposure to toxic substances, for example, can lead to loss of the acidic conditions in the lysosome, which can be monitored by continuous optical read-out of lysosomal pH [28]. Most importantly, capsules allow for integration of different functionalities within one carrier. Functionalities can be either added to the cavity of their shells [29], or even to multiple compartments in core-shell [25, 30] and other geometries [31].

Materials and Methods:

Fabrication of pH-sensitive capsules: Template particles of 2-3 µm in diameter as determined by light microscopy were obtained by coprecipitation of SNARF-dextran (Lifetech, D-3304) with $CaCO_3$ from solutions of $CaCl_2$ (0.33 M) and Na_2CO_3 (0.33 M) in NaCl (0.5 M). 615 µL of $CaCl_2$ were mixed with 770 µL SNARF-dextran (1mg/mL in DMSO) for 30 seconds prior to adding of 615 µL of Na_2CO_3 and subsequent vigorous mixing for 30 seconds at room temperature (RT). The particles were left for 2 minutes at RT, then centrifuged at 150 g to sediment them, and washed twice with Milli-Q water. Two bilayers of polystyrene sulfonate (PSS, pH 6.5 in 0.5 M NaCl) and polyallylamine hydrochloride (PAH, pH 6.5 in 0.5 M NaCl) were adsorbed to the particles, starting with PSS. In between each step, the particles were washed twice with Milli-Q water. Afterwards, the core was removed with ethylendiaminetetraacetic acid (EDTA, 0.2 M, pH 5), and the resulting SNARF-filled capsules were washed three times and stored in Milli-Q water at 4 °C until use in experiments. The concentration of the capsules was determined using a hemocytometer.

Fabrication of enzyme-filled capsules: Template particles of 3-5 µm in diameter as determined by light microscopy were obtained from coprecipitation of enzyme (GALC, R&D Systems, 7310-GH-005, or GLA (Replagal® from Shire)) with $CaCO_3$ as above. Here, however, the volumes of enzyme, $CaCl_2$, and Na_2CO_3 solutions were equal (1 mL in case of GLA, c = 1mg/mL, 50 µL in case of GALC, c = 0.05 mg/mL), and the enzyme was mixed first with Na_2CO_3 and precipitated by adding $CaCl_2$. The particles were left for 2 minutes at RT, then centrifuged at 150 g to sediment them, and washed twice with Milli-Q water. Two bilayers of dextran sulfate (DexS, 2 mg/mL, pH 6.5 in 0.5 M NaCl) and poly-L-arginine (pArg, 1 or 2 mg/mL, pH 6.5 in 0.5 M NaCl) were deposited onto the particles starting with DexS. The core was dissolved as above and the capsules were stored at 4 °C until use.

Cell culture: MO3.13 (both WT and KO) cells were cultured in DMEM supplemented with 10 % FBS, 1 % L-glutamine, and 1 % penicillin-streptomycin and kept at 37 °C and 5 % CO_2 atmosphere. MO3.13 KO cells were stably transfected cells with knocked out GALC. Mouse aorta endothelial cells (MAEC) were obtained from sacrificed mice according to Shu *et al.* [32] and cultured in RPMI medium (HyClone) supplemented with 1 % L-glutamine (Lonza, 17-605E), 1 % antibiotic-antimicotic (Lifetech, 15240-096), 1 % non-essential amino acids (Lonza, 13-114E), 0.5 mg/mL endothelial cell growth supplement (Becton Dickinson, 356006), 0.1 mg/mL heparin (Sigma-Aldrich, H3149), and 0.001 mg/mL hydrocortisone (Sigma-Aldrich, H0888). The FBS content depended on the passage: for passage 1 and 2, 20 % heat-inactivated FBS (hiFBS) was added, for passage 3 and 4, 15 % hiFBS, and for passage 5 or higher, 10 % hiFBS.

pH-sensing experiments: 1.5 x 10^4 *per* cm^2 MO3.13 cells (WT or KO) were seeded in cell culture dishes and incubated for 24 h. The medium was exchanged for "starvation medium", *i.e.* DMEM supplemented with 0.2 % FBS, 1 % L-glutamine, and 1 % penicillin-streptomycin, and the cells were incubated for 24 h to provoke differentiation. Simultaneously, 5 pH-sensitive capsules *per* seeded cell were added to the cells. For imaging, the cells were mounted on a CLSM (Zeiss Meta 510) and the medium was changed for "starvation medium" supplemented with psychosine (Santa Cruz Technology, sc-202781) at a concentration of 2 or 10 µM. The cells were imaged for up to 24 h every 10 or 15 minutes.

MTT viability test: 5000 MO3.13 (WT and KO) cells were seeded in 96-well plates in DMEM supplemented with 10 % FBS, 1 % L-glutamine, and 1% penicillin-streptomycin for 24 h. Then, the medium was exchanged for "starvation medium" and GALC-filled capsules were added at a concentration of 5 or 10 capsules *per* seeded cell. In KO cells, also empty capsules were tested at a concentration of 5 capsules *per* seeded cell. 24 h later, the medium was exchanged for "starvation medium" containing psychosine at different concentrations and the cells were incubated for another 24 h. For the MTT assay (Roche, 11465007001), the cells were washed with PBS and medium containing 10 % MTT-1 solution was added for 4 h. Subsequently, solubilization solution (MTT-2) was added and the cells were incubated for 12 h. The absorption maximum at 590 nm was measured by UV-vis. The absorption for cells not treated with psychosine was set to represent 100 % viability and all values of one experiment were normalized by this absorption value.

GLA delivery: 10^5 MAEC were seeded in 24-well plates in 0.5 mL growth medium appropriate for the cell passage and incubated for 24 h. The medium was exchanged for NBD-Gb3-supplemented medium and either GLA or GLA-filled capsules at various concentrations. The preparation of the NBD-Gb3 medium can be found in the SI. The cells were incubated for another 48 h. Then, the cells were rinsed with PBS, trypsinized, centrifuged, and kept in ice-cold PBS until use in flow cytometry. Approximately 10^4 cells were examined per sample. Details can be found in the SI.

Results and Discussion:

Response of lysosomal pH upon stimulation of GALC-deficient cells with psychosine: First, the effect of psychosine on WT and KO cells was examined. In order to observe the effect, cells were incubated with pH sensitive non-degradable capsules, which reside inside the lysosome as local fluorescent pH reporters [28], *cf.* Figure 2.

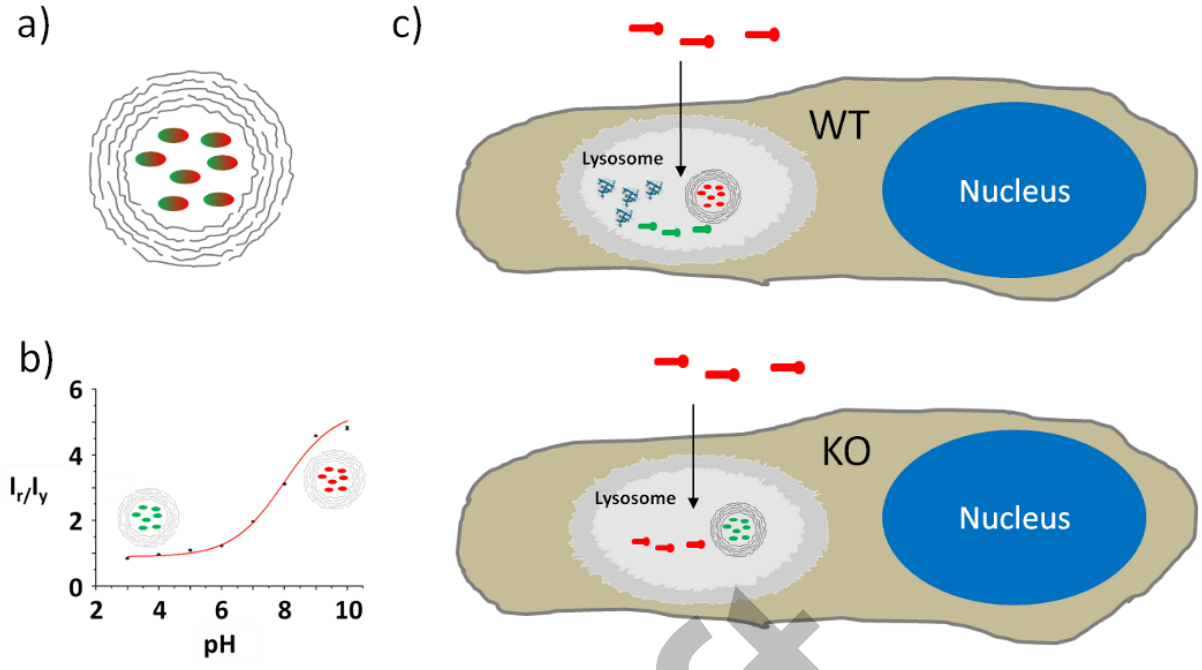

Figure 2: a) pH-sensitive capsules comprise pH-sensitive fluorophores in their cavities, surrounded by polyelectrolyte walls permeable to H^+ [27]. b) Local pH around the capsules is indicated by ratiometric emission, in which intensity in the red (I_r) is smaller than intensity in the yellow (I_y) at acidic conditions [27]. The intensity ratio I_r/I_y of both emission peaks is a measure for the local pH. Emission in the yellow is depicted in green false-color. c) After internalization by cells, capsules are located in the lysosome (depicted in gray) [28]. In case of WT cells, the enzyme GALC (depicted in blue) is present in the cellular lysosome, but not in case of KO cells. Psychosine (drawn in red) is added to cells. Only if GALC is present, psychosine can be converted to sphingosine (drawn in green). The color of the capsules indicated the local pH inside the cellular lysosome. Schemes are not drawn to scale.

In Figure 3, the development of the lysosomal pH upon exposure of WT and KO cells to psychosine at 2 µM and 10 µM concentration is shown. First, it needs to be pointed out that determination of absolute pH values is error-prone [27], for example due to variations in the I_r/I_y-pH calibration curve in-between individual capsules. For this reason, emphasis in evaluation is given to analysis of relative changes in pH. Second, in order to reduce fluctuations in read-out, a low-pass filter in the form of averaged values was applied, which limits temporal resolution of the data to tens of minutes. In KO cells, lysosomal pH remains constant upon cellular stimulation with psychosine. On the contrary, in WT cells at high concentration of psychosine, *i.e.* 10 µM, but not 2 µM, the lysosomal pH rises from the normal acidic conditions to the neutral pH of the cytosol. This is an indication for cellular impairments. A possible explanation may be that proton pumps localized in the cellular membrane, which typically warrant acidic lysosomal pH, had been deactivated. In this way, pH-sensitive capsules can be used as lysosomal reporters for probing effects of cellular stimulation.

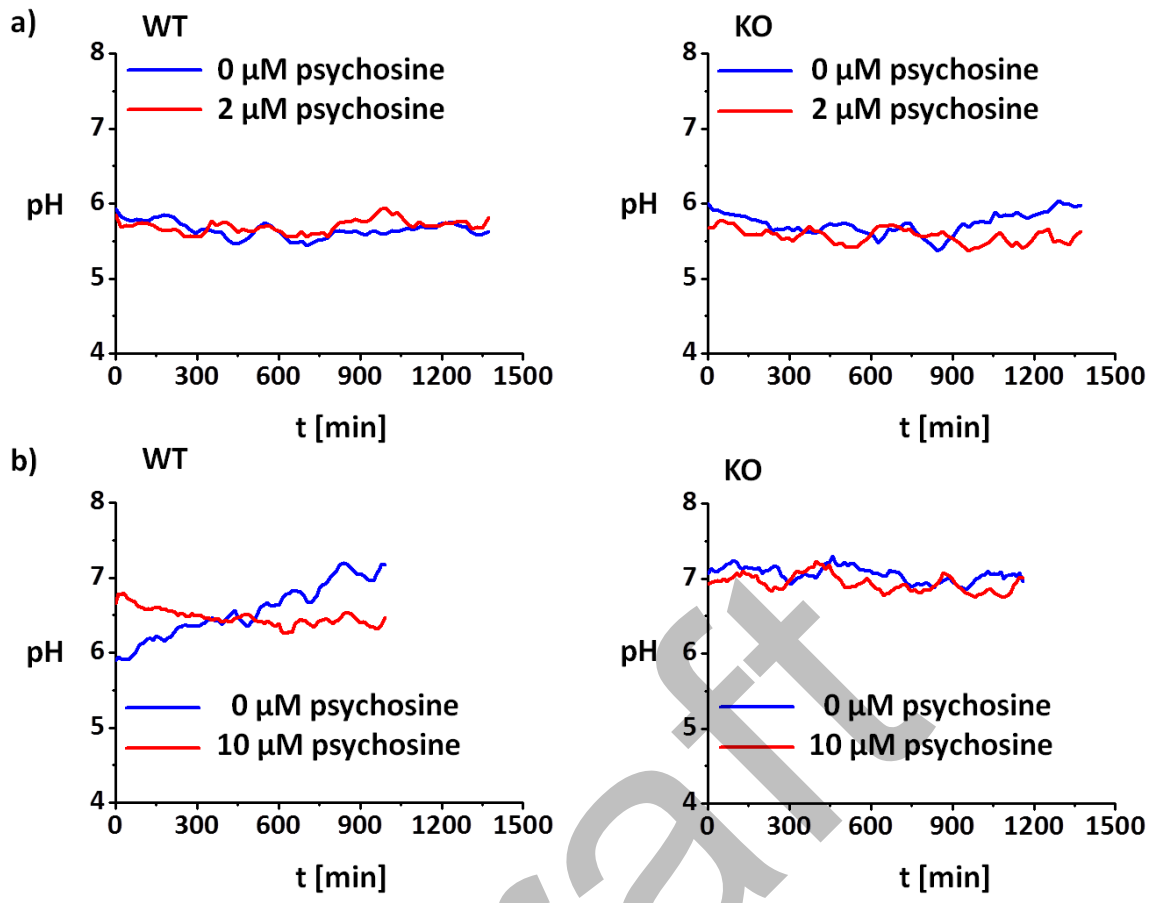

Figure 3: Intracellular pH as determined from the I_r/I_y signal from pH-sensitve capsules which are localized in the lysosome of WT or KO cells, as sketched in Figure 2. Changes in lysosomal pH upon stimulations of cells with psychosine at t = 0 are reported, together with the controls (c(psychosine) = 0).

Capsule-based delivery of GALC to GALC-deficient cells: In a second set of experiments, biodegradable capsules loaded with GALC were added to KO cells, *cf.* Figure 4. Effect of delivery was probed by exposure of the cells to psychosine and a subsequent test of cellular viability.

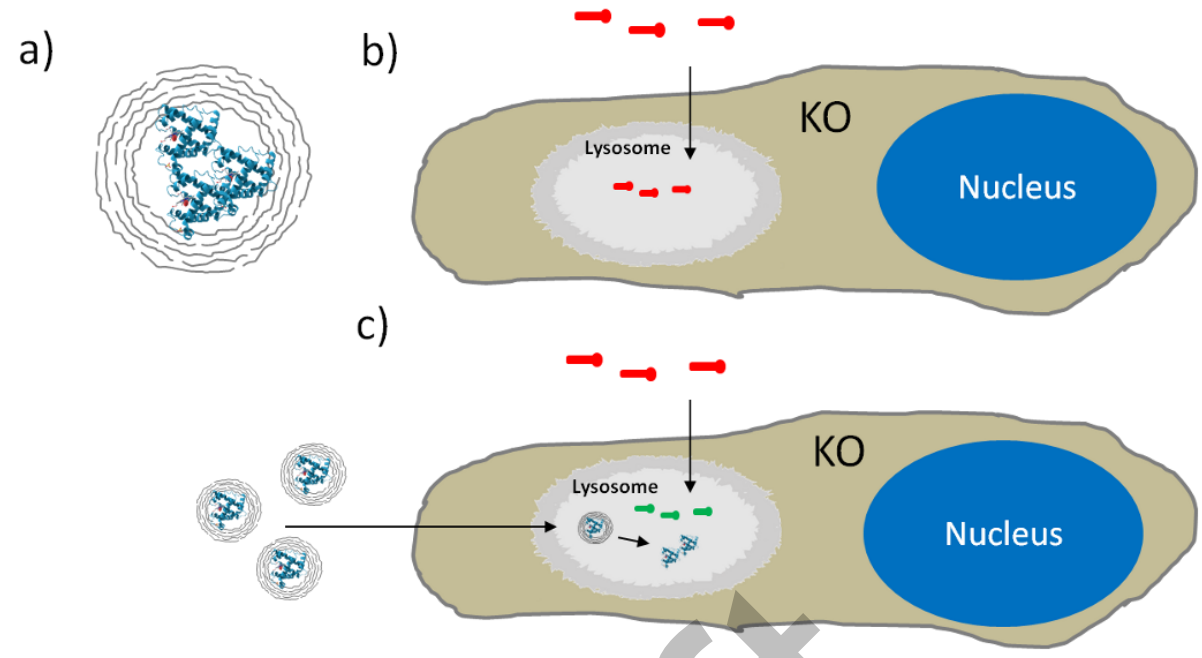

Figure 4: a) GALC was encapsulated within the cavity of biodegradable capsules. b) KO cells were stimulated with psychosine, and cellular response was probed with MTT viability assay. c) Cells were incubated with GALC-filled capsules, which were degraded in the cellular lysosome [24] and released GALC. Cells were then stimulated with psychosine and cellular response was probed *via* MTT viability assay. Schemes are not drawn to scale.

Instead of probing the effect of cellular stimulation with psychosine *via* lysosomal pH changes, also standard viability tests such as the MTT assay can be used. In Figure 5, data of cellular viability upon incubation of cells with psychosine are presented. In case of WT cells, stimulation of cells with psychosine did not reduce cellular viability (Figure 5a). In case cells were pre-incubated with encapsulated GALC, there was some reduction of cellular viability at high psychosine doses. In contrast, in the case of KO cells, stimulation with psychosine drastically reduced cellular viability (Figure 5b). In case GALC was delivered to the cellular lysosomes in encapsulated form, reduction of cellular viability upon psychosine exposure could be omitted. This demonstrates that encapsulated GALC can be delivered to the lysosome, where it fulfills its function to hydrolize psychosine. The effect is clearly attributed to the encapsulated GALC, as delivery of empty capsules did not have an effect on cellular viability compared to non-treated cells (Figure 5c). While empty capsules did not cause cytotoxic effects, they also had no reducing effect on cytotoxicity upon exposure to psychosine.

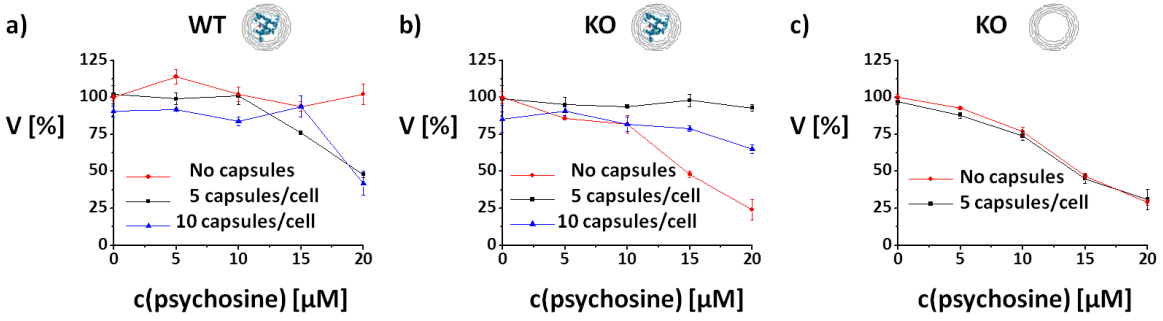

Figure 5: The normalized viability V of WT and KO cells are plotted *versus* the concentration c of added psychosine. The experimental procedure is shown in Figure 4. Cells were preloaded with either GALC-filled (a, b) or empty (c) biodegradable capsules.

Capsule-based delivery of GLA to GLA-deficient cells: In a third set of experiments, KO cells were exposed to GLA, either as free protein or in encapsulated form inside the cavity of biodegradable capsules, *cf.* Figure 6. Cells were exposed to globotriaosylceramide (Gb3) with attached fluorophore (N-[7-(4-nitrobenzo-2-oxa-1,3-diazole)]-aminocaproyl; NBD), *cf.* Figure 6. Digestion of Gb3 by GLA to lactosylceramide, involving cleavage of NBD from the sphingolipid, was probed by flow cytometry.

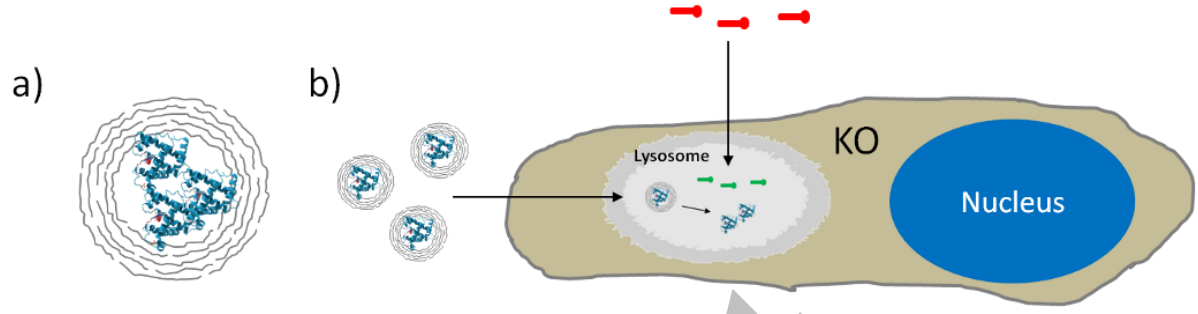

Figure 6: a) GLA was encapsulated. b) Cells with knocked-out GLA were incubated either with native (not shown) or with encapsulated GLA. In both forms of administration, GLA is endocytosed and delivered to the cellular lysosome. Cells were then stimulated with NBD-labeled Gb3 (drawn in red), which in case of presence of GLA in the lysosome was degraded to lactosylceramide (drawn in green) under release of a non-fluorescent derivative of NBD. Loss in fluorescence was probed by flow cytometry. Schemes are not drawn to scale.

In order to verify that lysosomal enzymes can be delivered to enzyme-deficient cells by capsules as shown in Figure 6, we demonstrated this effect with another enzymatic system. In Figure 7, the effect of delivery of free and encapsulated GLA to KO cells deficient in lysosomal GLA is shown. Free and encapsulated form was compared according to the amount of GLA added to the cells. Cellular effect upon exposure of cells to fluorescently labeled Gb3 was monitored by flow cytometry in terms of fluorescence loss inside cells. Upon hydrolysis of fluorescently labeled Gb3, the fluorophore is converted to a non-fluorescent derivative, leading to a reduction of intracellular fluorescence. The data shown in Figure 7 clearly indicate that delivery of GLA leads to hydrolysis of Gb3. However, larger effect is observed for free rather than for encapsulated GLA. As also free GLA is readily endocytosed [15] one may ask which advantage encapsulation may involve. First, biodistribution of free proteins and encapsulated proteins can be different, and by integration of targeting moieties, for example magnetic nanoparticles, specific targeting could be achieved [33]. Second, and more important, release kinetic can be changed by encapsulation; in particular slower release over extended periods of time is possible [24].

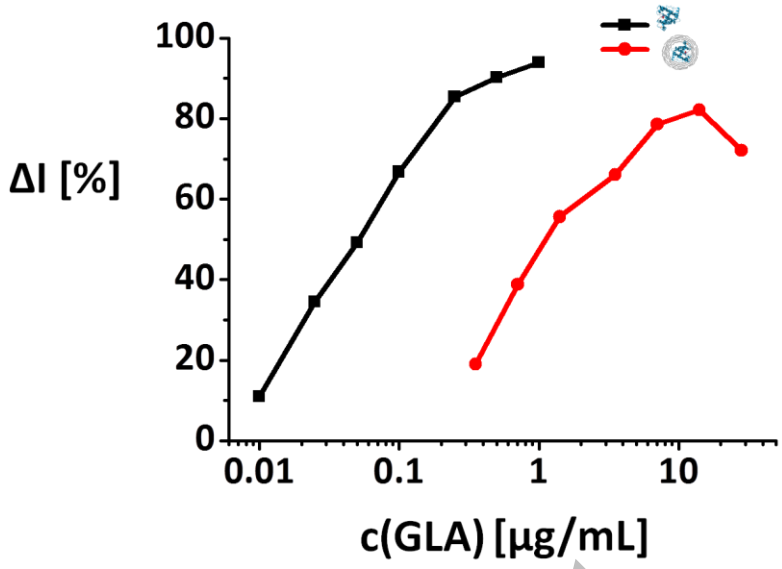

Figure 7: Fluorescently labeled Gb3 was added to cells deficient of GLA, together with GLA either as free protein or in encapsulated form in different concentrations. Upon enzymatic hydrolysis, the fluorescently labeled Gb3 was converted into non-fluorescent products (*cf.* Figure 6) and the reduction in intracellular fluorescence intensity ΔI was recorded. The fluorescence loss is plotted *versus* the amount of added GLA in either form.

Conclusion:

We demonstrated that polymer capsules are capable of both delivery of deficient enzymes and analysis of pH in cells. We oriented on cells representing lysosomal storage diseases, namely Krabbe and Fabry disease. As the capsules automatically are trafficked to the lysosome, the encapsulated enzymes directly reached their target site. We could show that the enzymatic activity is preserved by the capsules and accumulation of metabolites, psychosine in case of Krabbe, and Gb3 in case of Fabry, was prevented. In case of analysis of the lysosomal pH, we could demonstrate that high amounts of psychosine (10 µM) provoked rise of the lysosomal pH in WT cells, but not in KO cells. Low concentration of psychosine (2 µM) did not induce changes of the pH of either sort of cell. Therefore, we have shown that polymer capsules can be used as therapeutic carrier for delivery of enzymes, and as diagnostic reporters for continuous read-out of intracellular analytes such as protons.

Acknowledgements:

MO3.13 wildtype and knockout cells were a gift from Marco Cecchini from Instituto Nanoscienze in Pisa. This work was supported by LOEWE (grant SynChemBio to WJP).

References:

[1] J. Peteiro-Cartelle, M. Rodríguez-Pedreira, F. Zhang, P. Rivera_Gil, L. L. d. Mercato, W. J. Parak, *Nanomedicine* **2009**, *4*, 967.
[2] Z. Ali, A. Z. Abbasi, F. Zhang, P. Arosio, A. Lascialfari, M. F. Casula, A. Wenk, W. Kreyling, R. Plapper, M. Seidel, R. Niessner, J. Knoll, A. Seubert, W. J. Parak, *Anal. Chem.* **2011**, *83*, 2877.
[3] A. Musyanovych, K. Landfester, *Macromol. Biosci.* **2014**, *14*, 458.
[4] G. B. Sukhorukov, H. Mohwald, *Trends Biotechnol.* **2007**, *25*, 93.
[5] M. Lipka, M. Semmler-Behnke, R. A. Sperling, A. Wenk, S. Takenaka, C. Schleh, T. Kissel, W. J. Parak, W. G. Kreyling, *Biomaterials* **2010**, *31*, 6574.

[6] M. Nazarenus, Q. Zhang, M. G. Soliman, P. del Pino, B. Pelaz, S. Carregal_Romero, J. Rejman, B. Rothen-Ruthishauser, M. J. D. Clift, R. Zellner, G. U. Nienhaus, J. B. Delehanty, I. L. Medintz, W. J. Parak, *Beilstein J. Nanotechnol.* **2014**, *5*, 1477.
[7] E. Wagner, *Accounts Chem. Res.* **2012**.
[8] A. Muñoz Javier, P. del Pino, M. F. Bedard, A. G. Skirtach, D. Ho, G. B. Sukhorukov, C. Plank, W. J. Parak, *Langmuir* **2008**, *24*, 12517.
[9] A. H. Futerman, G. van Meer, *Nat. Rev. Mol. Cell Bio.* **2004**, *5*, 554.
[10] E. F. Neufeld, *Annu. Rev. Biochem.* **1991**, *60*, 257.
[11] T. D. Butters, R. A. Dwek, F. M. Platt, *Chem. Rev.* **2000**, *100*, 4683.
[12] E. F. Neufeld, in *Fabry Disease: Perspectives from 5 Years of FOS* (Eds.: A. Mehta, M. Beck, G. Sunder-Plassmann), Oxford PharmaGenesis, Oxford, **2006**.
[13] G. A. Grabowski, R. J. Hopkin, *Annu. Rev. Genomics. Hum. Genet.* **2003**, *4*, 403.
[14] L. Shu, J. A. Shayman, *J. Biol. Chem.* **2007**, *282*, 20960.
[15] J. S. Mayes, E. L. Cray, V. A. Dell, J. B. Scheerer, R. N. Sifers, *Am. J. Hum. Genet.* **1982**, *34*, 602.
[16] J. Park, G. J. Murray, A. Limaye, J. M. Quirk, M. P. Gelderman, R. O. Brady, P. Qasba, *Proc. Natl. Acad. Sci. U. S. A.* **2003**, *100*, 3450.
[17] E. Donath, G. B. Sukhorukov, F. Caruso, S. A. Davis, H. Möhwald, *Angew. Chem. Int. Edit.* **1998**, *37*, 2202.
[18] G. B. Sukhorukov, E. Donath, S. Moya, A. S. Susha, A. Voigt, J. Hartmann, H. Mohwald, *J. Microencapsulation* **2000**, *17*, 177.
[19] E. Donath, S. Moya, B. Neu, G. B. Sukhorukov, R. Georgieva, A. Voigt, H. Baumler, H. Kiesewetter, H. Mohwald, *Chem. Eur. J.* **2002**, *8*, 5481.
[20] S. De Koker, B. G. De Geest, C. Cuvelier, L. Ferdinande, W. Deckers, W. E. Hennink, S. De Smedt, N. Mertens, *Adv. Funct. Mater.* **2007**, *17*, 3754.
[21] A. Muñoz_Javier, O. Kreft, M. Semmling, S. Kempter, A. G. Skirtach, O. Bruns, P. d. Pino, M. F. Bedard, J. Rädler, J. Käs, C. Plank, G. Sukhorukov, W. J. Parak, *Adv. Mater.* **2008**, *20*, 4281.
[22] L. Kastl, D. Sasse, V. Wulf, R. Hartmann, J. Mircheski, C. Ranke, S. Carregal-Romero, J. A. Martínez-López, R. Fernández-Chacón, W. J. Parak, H.-P. Elsaesser, P. Rivera Gil, *ACS Nano* **2013**, *7*, 6605.
[23] B. G. De_Geest, W. Van Camp, F. E. Du Prez, S. C. De Smedt, J. Demeester, W. E. Hennink, *Chem. Comm.* **2008**, 190.
[24] P. Rivera_Gil, S. D. Koker, B. G. De_Geest, W. J. Parak, *Nano Lett.* **2009**, *9*, 4398.
[25] L. L. del Mercato, A. Z. Abbasi, M. Ochs, W. J. Parak, *ACS Nano* **2011**, *5*, 9668.
[26] U. Reibetanz, D. Halozan, M. Brumen, E. Donath, *Biomacromolecules* **2007**, *8*, 1928.
[27] O. Kreft, A. Muñoz Javier, G. B. Sukhorukov, W. J. Parak, *J. Mater. Chem.* **2007**, *17*, 4471.
[28] P. Rivera Gil, M. Nazarenus, S. Ashraf, W. J. Parak, *Small* **2012**, *8*, 943.
[29] G. B. Sukhorukov, A. L. Rogach, M. Garstka, S. Springer, W. J. Parak, A. Muñoz-Javier, Oliver Kreft, A. G. Skirtach, A. S. Susha, Y. Ramaye, R. Palankar, M. Winterhalter, *Small* **2007**, *3*, 944.
[30] O. Kreft, M. Prevot, H. Mohwald, G. B. Sukhorukov, *Angew. Chem. Int. Edit.* **2007**, *46*, 5605.
[31] M. Delcea, A. Yashchenok, K. Videnova, O. Kreft, H. Möhwald, A. G. Skirtach, *Macromol. Biosci.* **2010**, *10*, 465.
[32] L. M. Shu, H. S. Murphy, L. Cooling, J. A. Shayman, *J. Am. Soc. Nephrol.* **2005**, *16*, 2636.
[33] M. Ochs, S. Carregal-Romero, J. Rejman, K. Braeckmans, S. C. De Smedt, W. J. Parak, *Angew. Chem. Int. Edit.* **2013**, *52*, 695.